UNIVERSITÀ DEGLI STUDI DI ROMA
"LA SAPIENZA"

FACOLTÀ DI SCIENZE MATEMATICHE, FISICHE E NATURALI

Gravitational waves from perturbed stars

DOTTORATO DI RICERCA IN FISICA
PH.D. IN PHYSICS

XIV Ciclo – AA.AA. 1998-2001

Coordinatore: *Prof. Guido Martinelli*

Supervisor:
Prof. Valeria Ferrari

Candidate:
Dott. Emanuele Berti

We play at Paste,
Till qualified for Pearl
Then drop the Paste,
And deem ourself a fool
The Shapes - though - were similar
And our new Hands
Learned **Gem**-*Tactics*
Practicing **Sands**

E. Dickinson

Contents

Introduction

In 1969, quite ironically, Frank Zerilli stated in the introduction to his Ph. D. thesis: *"Joseph Weber at the University of Maryland has detected events which may well prove to be pulses of gravitational radiation. Dyson has proposed, probably only half seriously, that these events may be the result of encounters between stars and black holes (that is, collapsed stars)"*. Since then the situation has changed quite a lot.

Of course, today there is more than just hope in the existence of gravitational waves, which are one of the main predictions of Einstein's theory of gravity. The measurement, performed by Hulse and Taylor [42], of the decay of the orbital period of a compact binary system, PSR 1913+16, has already provided experimental evidence (though only an *indirect* one) for this crucial prediction of Einstein's theory. On the other hand, despite the initial illusions, the *direct* detection of gravitational waves has proven to be a formidable task, but finally we can confidently say, thanks to a worldwide joint experimental effort, to be really close to the goal. Resonant bars (ALLEGRO, NIOBE, EXPLORER, AURIGA and NAUTILUS) are already in operation; new resonant detectors (GRAIL, OMNI-1 and TIGA), called TIGAs (Truncated Icosahedral Gravitational Arrays), are in project; an earth-based interferometer (TAMA) is taking data, while others (LIGO, VIRGO and GEO600) will become operative very soon; the project for a space-based interferometer (LISA) has recently been approved by NASA and ESA. Earth-based detectors will be sensitive to gravitational waves in the high-frequency band ($\sim$ 1 kHz for resonant detectors, and in the region 1 Hz $\lesssim \nu \lesssim$ a few kHz for interferometers). LISA will hopefully be able to detect low-frequency waves (10^{-4} Hz $\lesssim \nu \lesssim$ 1 Hz).

Thanks to the enormous advances in observational astrophysics, the idea of "encounters between stars and black holes" is no longer regarded as a joke. Indeed, at present, binary systems composed by neutron stars and/or black holes (spiraling together to form, eventually, a new compact object) are considered one of the most interesting (if not the most promising) among sources of gravitational waves to be detected in the near future ([39], [84]).

The theoretical modeling of binary systems is the main topic of this thesis. As is well known, binaries can be modelled using various approximation schemes. The simplest approximation is the so-called *quadrupole formula*, in which the components of the binary are considered as *pointlike* particles following *Newtonian* orbits, and the emitted radiation is computed from the time variation of the quadrupole moment of the system.

A more accurate treatment can be achieved in many different ways. One of the most common approaches considers the members of the binary as point particles, but includes *Post-Newtonian* (PN) corrections to the equations of motion, i.e., basically, corrections in powers of v/c (where v is the orbital velocity), which are expected to be more and more important for compact binaries as they spiral together and finally coalesce. Taking into account the internal structure of the members of the binary system is, in general, a very difficult task. Accurate theoretical predictions for the late stages of a compact binary coalescence require the integration

of the full Einstein equations coupled to hydrodynamics in strong field situations, and this is a formidable challenge for today's computers.

The main point of this thesis is to show that relevant information on the gravitational waves emitted by binary systems can be gained using *perturbative approaches*. In this case, the key idea is that, when a component of the binary has mass much smaller than the other ($m_0 \ll M$), one can solve *exactly* the Einstein equations coupled to hydrodynamics to obtain the equilibrium structure of the larger body, and treat the small mass m_0 as inducing perturbations on the (known) geometry of space-time obtained through this procedure. We have applied this method to two classes of astrophysical binary systems: **extrasolar planetary systems** and **compact binaries**.

Extrasolar planetary systems

Before proceeding, we wish to make a point on terminology. We shall call "extrasolar planetary systems" both systems composed of a solar-type star and a planet, and systems composed of a solar-type star and a brown dwarf. In fact, in the astrophysical community, the very definition of a "planet" is still object of debate (see, e.g., [57]). Some authors *define* a planet on the basis of the *formation mechanism*. According to this point of view, planets are objects formed by coagulation of smaller, possibly rocky, bodies, orbiting a much larger star; on the other hand, stars were probably formed by fragmentation of large bodies into smaller objects. Other authors *define* a planet as an object with mass smaller then 13 Jupiter masses (the minimum mass needed to ignite deuterium in its core); similarly, brown dwarfs are often *defined* as objects that do not burn hydrogen in their core, and therefore have masses less than about 80 jovian masses. We will follow the latter definition (though it is quite a matter of convention), because the mass distribution turns out to be the distinguishing feature even adopting a definition based on the formation mechanism ([57]). In any event, since the physical distinction between planets and brown dwarfs is not so sharp, and since brown dwarfs are hardly observationally distinguishable, at present, from planets, we will loosely speak of "extrasolar planetary systems" even when dealing with systems composed of a star and a brown dwarf.

The first extrasolar planetary system (from now on, EPS) was discovered in 1992 [89]; since then a number of such systems, composed of one or more planets orbiting around a main sequence solar-type star, has been revealed (see [64] for a review), and many others will surely be observed in the near future. Some of the discovered EPS's are well characterized, since the mass and radius of the central star, the mass of the planets and their orbital parameters can be deduced from observations. With this information we have been able to give a first estimate of the characteristics of the gravitational radiation emitted by these systems, that, being at a distance of a few tens of parsecs, are very close to us. As a first step, we have selected a set of EPS's for which all needed information is available, and computed the gravitational signal emitted by each couple star-planet due to the orbital motion, using the quadrupole formalism.

Then we turned our attention on an interesting mechanism of gravitational wave emission, not so directly related to the orbital motion of the system. It is known from the theory of stellar pulsations that a star, when perturbed from its equilibrium configuration, oscillates in a set of so-called *quasi-normal modes*. These modes have complex frequencies; the imaginary part corresponds to a damping of the mechanical energy of oscillation, due to the emission of gravitational waves. The stellar quasi-normal modes are classified, following a classic paper by Cowling [23], according to the prevailing force restoring a displaced fluid element to

the equilibrium position. So we term g-modes the ones in which the prevailing force is *gravity*, and p-modes the ones in which a dispaced fluid element is restored to equilibrium mainly by *pressure gradients*. The lowest frequency p-mode is known as f-mode (for *fundamental*), since it is present also in extremely simple stellar models, such as homogeneous incompressible spheres. Typically, any given stellar model has an infinite number of g-modes and p-modes; the g-modes have decreasing oscillation frequencies, the p-modes have increasing frequencies, and the f-mode separates the two classes:

$$\ldots < \nu_{g2} < \nu_{g1} < \nu_f < \nu_{p1} < \nu_{p2} < \ldots$$

Notice, however, that a stellar model is endowed with g-modes only if the stellar structure shows the presence of entropy gradients (due either to temperature gradients or differences in chemical composition). So the simplest neutron star models we shall consider in chapter 4 (in which the star is approximated as if it were at zero-temperature) do not show the presence of g-modes, while the Newtonian, solar-like stars considered in chapter 3 do.

We mention for completeness that a new class of modes with no Newtonian analogue, essentially related to oscillations of the metric variables, has been recently shown to exist [47]. These modes have been termed w-modes, because they are intimately related with the (essentially relativistic) process of emission of gravitational *waves*.

An interesting features of the stellar quasi-normal modes is that they can be **excited** by tidal interactions with the orbiting planet. This problem has been studied in the literature for solar type stars with a planet and for neutron star-neutron star close binary systems using different approaches, based essentially on the deformation induced by the dynamical tides raised by the companion ([1], [82], [46]). In particular, the emission of gravitational waves associated with the resonant excitation of the modes of a star has been studied by Kojima [45]. He considered a small mass in circular orbit around a compact star, and integrated the equations describing the perturbation of the star excited by the small mass, in the framework of general relativity. He showed that a sharp resonance occurs if the frequency of the fundamental mode of the star is twice the keplerian frequency of the orbiting mass, and that the characteristic wave amplitude emitted at the resonant frequency can be up to ~ 100 times larger than that evaluated by the quadrupole formula. The excitation of the w-modes has later been studied by Ruoff *et al.* [73] through a time-domain evolution of the perturbation equations.

Motivated by observations, which have shown that a surprisingly large fraction of the observed planets are in close, nearly circular orbits, we have considered the possibility for a planet to get sufficiently close to the central star to excite the lowest order g-modes, and possibly the fundamental one, without being disrupted by tidal forces or melted by the central star. We have shown that for solar type stars the resonant excitation of the low-order g-modes may, in principle, be possible.

When the planet is close enough to a resonance, the power lost by the system in gravitational waves can be large, and the orbit tends to shrink more rapidly due to this energy loss. Including gravitational radiation reaction effects on the planetary orbit tells us how the orbit evolves: in this way, we have obtained typical timescales for a planet to get off-resonance.

The information on the excitation of the mode and on the timescale of the resonant process can be used to estimate how much time a given EPS can spend emitting waves of amplitude greater than a fixed threshold. The main result of our analysis is that systems composed of a solar-type star and a brown dwarf in resonant conditions could potentially be detectable by LISA.

Compact binaries

To radiate gravitational waves with large intensity and at frequencies accessible to ground-based interferometers, the members of a binary system must not only be massive: they must also orbit each other at very small separations (a few hundred kilometers or less).

According to the existing views, these massive objects can only be the end products of stellar evolution: neutron stars and black holes. Since a large fraction of all stars are in close binary systems, the dead remnants of stellar evolution may contain a significant number of binary systems whose components are neutron stars or black holes, and are close enough together to be driven into coalescence by gravitational radiation reaction in a time smaller than the age of the universe. The binary pulsar 1913+16 is an example of such a system, and will coalesce $\sim 3.5 \times 10^8$ years from now. Binaries containing two black holes or a neutron star and a black hole have not been observed yet, but we already have reliable observational data on binary neutron stars [53], which will be the main subject of this thesis. Anyway, the current theories on the formation and relative abundance of various populations of observed binaries consisting of normal stars and neutron stars predict neutron star-black hole and black hole-black hole binaries as possible outcomes [39].

By the time a binary enters the sensitivity window of ground-based interferometers (i.e., the gravitational wave frequency is larger than about 10 Hz) gravitational radiation reaction has circularized the orbit [65]; so, as the two bodies in the binary spiral together, they emit periodic gravitational waves with a frequency which is simply twice the orbital frequency. This frequency sweeps upward ("chirps") toward a maximum, which is around 1 kHz for neutron star binaries, and around $10 M_{BH}/M_\odot$ for black hole binaries when the larger black hole has mass M_{BH}. During the first part of the frequency sweep the waveform can be fairly accurately computed from the quadrupole formalism, but as the objects get closer Post-Newtonian orbital effects and effects due to the extended structure of the bodies become more and more significant. In the final, merging phase, the full equations of general relativity and detailed hydrodynamical models are definitely needed for a prediction of the gravitational wave signal we may observe. An accurate theoretical modeling of the signal is especially important, since comparison of the predicted wave forms with observed ones may well be the strongest test ever of general relativity.

We shall attempt to model the binary as a system in which one of the members is an exact solution to EInstein's equations, and the other is considered as a pointlike mass exciting perturbations in the (known) spacetime corresponding to the unperturbed object. This approach should provide hints on the nature of the true, fully general relativistic two-body problem in which both objects are extended. In particular, we want to understand the difference in the power emitted and in the waveform between a system in which the extended object is a neutron star and one in which the extended object is a black hole. For example, we may expect some of the oscillation modes of the star (especially the g-modes, which have lower frequencies) to be excited during coalescence. Even if this is not the case, the structure of the star must sooner or later play a role in the gravitational wave emission process.

Usually the theoretical modelling of compact binaries includes orbital corrections (but not corrections due to the structure) in the form of Post-Newtonian expansions of the standard, Newtonian equations of motion. In producing the theoretical templates used to extract the signal from noise in interferometers, only the phase of the wave (not the amplitude) is corrected throught the inclusion of these effects, i.e., one uses the so-called *restricted Post-Newtonian approximation* [25]. We will show that this approximation ignores a characteristic beating process

between wave components of different angular behaviour.

Depending on the stellar structure, we find that effects due to the excitation of the stellar f-mode and/or the extended structure of the star begin to show up when the test mass orbital velocity is $\sim c/4$ (where, of course, c is the speed of light). Moreover, the excitation of stellar modes in high-order multipoles ($\ell > 2$) may occur *before* the quadrupole mode is excited, and possibly play a role in the binary's evolution.

Using the test mass case as a testbed, we also argue that, especially when trying to model neutron star binaries, the use of equal-mass Post-Newtonian expansions needs to be pushed to very high order (v^6 or v^7) for the expansion to converge with sufficient accuracy; otherwise the loss in signal-to-noise ratio due to the inaccurate modeling of the system could completely destroy not only the determination of the parameters of the binary, but also the very possibility to detect the signal.

Thesis plan

The first two chapters of the thesis will be devoted to a description of the method we use to compute the gravitational wave power spectrum and the shape of the waveform from binary systems; in chapters 3 and 4 we will discuss the application of this method to extrasolar planetary systems and compact binaries, respectively.

In particular, in chapter 1 we concentrate, to have a test ground for the inclusion of structural effects in the signal, on the gravitational wave emission from binary systems in which the structure of the bodies is *not* taken into account. We start recalling briefly the standard quadrupole formalism, and recover well-known results for the shape of the spectrum emitted by a source composed of two point masses orbiting around each other according to the Newtonian laws of motion. As an original part, we show how to decompose the quadrupole wave in tensor spherical harmonics. Then we describe a slightly different approach, which we call the *semirelativistic quadrupole approximation*: we compute the radiation emitted by a test mass following geodesics in the Schwarzschild geometry (in other words, we consider the particle as moving in curved spacetime), but we compute the emitted radiation by plugging this "exact" orbital motion in the quadrupole formula. In other words, we treat the emission process as if the system were radiating in *flat* spacetime. As we shall see, this method gives some insight on the structure of the power spectrum emitted from binaries in which one of the members is actually endowed with a structure.

In chapter 2 we write down the perturbation equations for a non-rotating star. The amplitude of the perturbations in the linearized Einstein equations, of course, is not fixed if there is no source to excite the perturbations. We show how to deal with the excitation of the perturbations by a test mass $m_0 \ll M$, where M is the stellar mass, using an approach based directly on the perturbation of the metric functions (that we will term the *Zerilli* formalism). We actually computed the source term for perturbation equations in this "metric" approach only for circular orbits, since the calculation is quite involved. Later on, in chapter 4, we will introduce a different but equivalent approach, based on the Newman-Penrose perturbation technique (the *Bardeen-Press-Teukolsky* or BPT formalism), which allows to deal more easily with the general case of bound, eccentric orbits. In the zero-eccentricity limit our numerical codes yield exactly the same results using both formalisms (as they should!). This is a strong consistency check for our calculations in the non-zero-eccentricity case. Of course, the special case of circular orbits has great physical interest, since, as we stated before, radiation reaction circularizes the orbit of any

compact binary systems much before the gravitational signal emitted by the binary enters the sensitivity window of earth-based interferometers.

In chapter 3 we give estimates of the radiation emitted by extrasolar planetary systems. We list the parameters of some of the EPS's discovered up to now, as they were deduced from observations, and use them to compute the gravitational signal emitted by each couple star-planet due to the orbital motion, using the quadrupole formalism.

Then we turn our attention to the possibility of an excitation of the oscillation modes of the star by tidal interactions with the orbiting planet. Motivated by observations, which have shown that a surprisingly large fraction of the observed planets are in close, nearly circular orbits, we consider the possibility for a planet to get sufficiently close to the central star to excite the lowest order g-modes, and possibly the fundamental mode, without being disrupted by tidal forces or melted by the central star. We show that for solar type stars the resonant excitation of the low-order g-modes may, in principle, be possible.

When the planet is close enough to a resonance, the power lost by the system in gravitational waves can be large, and the orbit tends to shrink more rapidly due to this energy loss. Including gravitational radiation reaction effects (in the so-called *adiabatic approximation*) we can understand how fast the orbit evolves. In this way, we obtain typical timescales for a planet to get off-resonance, or, equivalently, estimates on how long the amplitude of the emitted wave can go beyond some fixed "observability threshold". The main result of our analysis is that systems composed of a solar-type star and a brown dwarf in resonant conditions could, at least potentially, be detectable by the spaceborn interferometer LISA, that has been approved by NASA and ESA, and should fly in a few years.

In chapter 4 we apply the perturbative approach to the gravitational wave emission from compact binary systems. We first describe the Bardeen-Press-Teukolsky formalism, and then apply the formalism to particles in closed, eccentric orbits around a star, comparing results with those obtained through the semirelativistic quadrupole formalism. We show that the stellar structure introduces qualitatively and quantitatively new effects, among which are the appearance of an axial component in the radiation and, consequently, a beating between the polar and axial components; a significant reduction in the total power radiated in $\ell = 2$; a great enhancement in the wave amplitude if the stellar quasi-normal modes are excited. Then we consider the possibility to excite quasi-normal modes in an astrophysical binary coalescence, both for neutron-star and black-hole binaries. We show that the excitation of black hole quasi-normal modes can only occur in a collapse; for neutron stars, the f-mode excitation is highly implausible unless the star is rotating. The g-modes, on the other hand, could be excited in a frequency band relevant for earth-based interferometers, and we will explore this issue in the future. Using the adiabatic approximation, we consider the orbital evolution of binary systems endowed with an eccentricity in our perturbative approach, showing that the inclusion of structural effects does not affect the commonly accepted conclusion that gravitational radiation reaction acts *circularizing* any binary system initially born with a nonzero eccentricity. Anyway, when the orbiting mass is close enough, the emission features of a system in which the central object is a star are significantly different from those of a system in which the central object is a black hole. We discuss these differences, and show how effects due to the equation of state affect the power emitted by the system in gravitational waves.

As a next step, we compare our perturbative results with those obtained in the literature using Post-Newtonian approximations, either in the test mass or in the comparable mass limit. We compute differences in the number of cycles between different stellar models and black holes, and discuss the reductions in signal-to-noise ratio due to a non-optimal modeling of the signal.

Finally, we give an argument in favour of the perturbative approximation, showing that fluid and metric perturbations remain small up to very little orbital separations. In other words, the perturbative approach seems to be surprisingly good up to very late stages of the coalescence.

Chapter 1

Gravitational wave emission due to the orbital motion

It is well known that the gravitational wave emission from coalescing binaries can be modelled using various approximation schemes. The simplest approximation is the so-called *quadrupole formalism*, in which the components of the binary are considered as *pointlike* particles following *Newtonian* orbits, and the emitted radiation is computed from the time variation of the quadrupole moments of the system. In this chapter we briefly recall some well-known results about the quadrupole formalism. Our purpose here is first of all to establish the notation, and then to set up a simple theoretical framework (in which the structure of the members of the binary is *not* taken into account) to use for comparison when, in the next chapters, we shall include in the computation effects due to the extended structure of at least one of the bodies.

We start recalling briefly, in section 1.1, the well-known quadrupole formalism; then, in section 1.2 we show how to decompose the quadrupole wave in tensor spherical harmonics (as far as we know, this has never been done in the published literature). In section 1.3 we recover well-known results for the shape of the spectrum emitted by a source composed of two point masses orbiting around each other according to the Newtonian laws of motion. In particular, we compute the power spectrum and the amplitude for general, eccentric orbits, and then we recover well-known, simple analytic formulas for the special case of circular orbits. Then, in section 1.4, we describe a slightly different approach, which we call the *semirelativistic quadrupole approximation*. In this approach we compute the radiation emitted by a test mass in the Schwarzschild geometry taking into account the *exact* geodesic motion of the mass (in other words, we consider the particle as moving in curved spacetime), but then we plug the exact orbital evolution in the quadrupole formulas (which amounts to considering the system as emitting in *flat* spacetime). We shall see that this method gives some insight on the structure of the power spectrum emitted from binaries in which one of the members is actually endowed with a structure; in particular, it shows that the spectrum is a discrete one, and that all the spectral frequencies can be expressed as linear combinations (with integer coefficients) of only two fundamental frequencies, whose meaning is clarified in section 1.4.3.

1.1 Quadrupole formalism

In the transverse-traceless gauge, the quadrupole wave is given in terms of the reduced quadrupole moments [77] by:

$$h^{TT}_{0\mu}(t,\ \mathbf{x}) = 0 \tag{1.1}$$

$$h^{TT}_{ij}(t,\ \mathbf{x}) = \frac{2G}{c^4 r}\left(P_{ik}P_{jl} - \frac{1}{2}P_{ij}P_{kl}\right)\ddot{Q}_{kl}(\tau)|_{\tau=t-\frac{r}{c}} \tag{1.2}$$

where

$$P_{hk} = \delta^h_k - n_h n_k$$

is used to project the metric perturbation in the plane orthogonal to the radial unit vector $\mathbf{n}$. Since $n_x = \sin\vartheta\cos\varphi$, $n_y = \sin\vartheta\sin\varphi$ and $n_z = \cos\vartheta$ we have:

$$P = \begin{pmatrix} 1-\sin^2\vartheta\cos^2\varphi & -\sin^2\vartheta\sin\varphi\cos\varphi & -\sin\vartheta\cos\vartheta\cos\varphi \\ -\sin^2\vartheta\sin\varphi\cos\varphi & 1-\sin^2\vartheta\sin^2\varphi & -\sin\vartheta\cos\vartheta\sin\varphi \\ -\sin\vartheta\cos\vartheta\cos\varphi & -\sin\vartheta\cos\vartheta\sin\varphi & 1-\cos^2\vartheta \end{pmatrix} \tag{1.3}$$

We can reformulate the indicial expressions in formula (1.2) in terms of matrix products and traces:

$$P_{ik}P_{jl}\ddot{Q}_{kl} = P_{ik}\ddot{Q}_{kl}P_{lj} = (P\ddot{Q}P)_{ij}$$

$$-\frac{1}{2}P_{ij}P_{kl}\ddot{Q}_{kl} = -\frac{1}{2}P_{ij}P_{kl}\ddot{Q}_{lk} = -\frac{1}{2}Tr(P\ddot{Q})P_{ij}$$

Now we can find $h^{TT}_{ij}(t,\ \mathbf{x})$ through simple matrix manipulations. Since our goal is to find the expression of the components of the metric perturbation in spherical polar coordinates, $h^{TT}_{\vartheta\vartheta}$ and $h^{TT}_{\vartheta\varphi}$, we must also perform a change of basis. Let us denote by A the matrix whose elements give the polar coordinates $x^{\alpha'}$ in terms of the cartesian ones x^β:

$$A^{\alpha'}_{\beta} = \frac{\partial x^{\alpha'}}{\partial x^\beta} \tag{1.4}$$

Consider the polar coordinate basis $\mathbf{e}_{\alpha'}$, expressed in terms of the cartesian coordinate basis $\mathbf{e}_\beta$ by the formula $\mathbf{e}_{\alpha'} = \frac{\partial x^\beta}{\partial x^{\alpha'}}\mathbf{e}_\beta$; i.e.:

$$\mathbf{e}_{\alpha'} = A^{T\,\beta}_{\alpha'}\mathbf{e}_\beta. \tag{1.5}$$

It is well known that such a coordinate basis is not orthonormal:

$$\mathbf{e}_{\alpha'}\cdot\mathbf{e}_{\beta'} = g_{\alpha'\beta'}, \tag{1.6}$$

i.e.: $\mathbf{e}_r\cdot\mathbf{e}_r = g_{rr} = 1$, $\mathbf{e}_\vartheta\cdot\mathbf{e}_\vartheta = g_{\vartheta\vartheta} = r^2$, $\mathbf{e}_\varphi\cdot\mathbf{e}_\varphi = g_{\varphi\varphi} = r^2\sin^2\vartheta$. We need to project the metric perturbation h over a (non-coordinate) *orthonormal* basis whose elements, denoted by a hat, are:

$$\mathbf{e}_{\hat{r}} = \mathbf{e}_r \tag{1.7}$$

$$\mathbf{e}_{\hat{\vartheta}} = \frac{1}{r}\mathbf{e}_\vartheta$$

$$\mathbf{e}_{\hat{\varphi}} = \frac{1}{r\sin\vartheta}\mathbf{e}_\varphi$$

Correspondingly, each row of the matrix A^T appearing in formula (1.5) has to be multiplied by a factor 1 (first row), $1/r$ (second row) or $1/r\sin\vartheta$ (third row) to give the matrix $\tilde{A}^T$ used to switch to our new, orthonormal basis. Of course, now we must project h over the vectors $\mathbf{e}_\vartheta$ and $\mathbf{e}_\varphi$:

$$P = \begin{pmatrix} 0 & 0 & 0 \\ 0 & 1 & 0 \\ 0 & 0 & 1 \end{pmatrix} \tag{1.8}$$

and $\ddot{Q}$ must be replaced by $\tilde{A}^T\ddot{Q}\tilde{A}$.

The tetrad components of the waveform, $h^{TT}_{(\vartheta)(\vartheta)}$ and $h^{TT}_{(\vartheta)(\varphi)}$, have been computed by the *Maple* program **TetradWaveform** given in Appendix H.

The explicit expressions of $h_{\vartheta\vartheta}$ and $h_{\vartheta\varphi}$ evaluated by this procedure are

$$\begin{aligned} h^{TT\ Q}_{(\vartheta)(\vartheta)} &= -h^{TT\ Q}_{(\varphi)(\varphi)} = \frac{1}{r}\left[\left(a(t)\cos^2\varphi + b(t)\sin 2\varphi\right)\left(1+\cos^2\vartheta\right) + c(t)\cos^2\vartheta + d(t)\right] \\ h^{TT\ Q}_{(\vartheta)(\varphi)} &= -\frac{1}{r}\cos\vartheta\left[a(t)\sin 2\varphi + 2b(t)\left(1-2\cos^2\varphi\right)\right] \end{aligned} \tag{1.9}$$

where the Q stands for "quadrupole", and

$$\begin{aligned} a(t) &= \ddot{Q}_{xx} - \ddot{Q}_{yy}, \quad b(t) = \ddot{Q}_{xy}, \\ c(t) &= \ddot{Q}_{yy} - \ddot{Q}_{zz}, \quad d(t) = \ddot{Q}_{zz} - \ddot{Q}_{xx}. \end{aligned}$$

The subscript indices $(\vartheta)(\vartheta)$ and $(\vartheta)(\varphi)$ indicates that the tensor has been projected onto the orthonormal basis.

1.2 Projection of the quadrupole wave on tensor harmonics

The quadrupole wave $h^{TT\ Q}_{(\mu)(\nu)}$ is a symmetric tensor, that we denote (to simplify the notation) by **h**. As any symmetric tensor, **h** can be split into an axial and a polar part,

$$\mathbf{h} = \mathbf{h^{ax}} + \mathbf{h^{pol}}, \tag{1.10}$$

and expanded in the tensor harmonics defined by Zerilli:

$$\mathbf{h^{ax}} = \sum_{\ell m}\left[Q^{(0)}_{\ell m}\mathbf{c}^{(0)}_{\ell m} + \ + Q_{\ell m}\mathbf{c}_{\ell m} + D_{\ell m}\mathbf{d}_{\ell m}\right], \tag{1.11}$$

$$\begin{aligned} \mathbf{h}^{pol} &= \sum_{\ell m}\Big[A^{(0)}_{\ell m}\mathbf{a}^{(0)}_{\ell m} + A^{(1)}_{\ell m}\mathbf{a}^{(1)}_{\ell m} + A_{\ell m}\mathbf{a}_{\ell m} + \\ &\quad + B^{(0)}_{\ell m}\mathbf{b}^{(0)}_{\ell m} + B_{\ell m}\mathbf{b}_{\ell m} + G_{\ell m}\mathbf{g}_{\ell m} + F_{\ell m}\mathbf{f}_{\ell m}\Big]. \end{aligned} \tag{1.12}$$

The coefficients of the expansion can be found as follows

$$\begin{aligned} Q_{\ell m} &= (\mathbf{c}_{\ell m}, \mathbf{h}) = \int c^*_{\ell m\mu\nu}\ h_{\lambda\rho}\ \eta^{\mu\lambda}\eta^{\nu\rho}d\Omega \\ &= \int_0^{2\pi} d\varphi \int_{-1}^{1} d\cos\vartheta\ \eta^{\mu\lambda}\eta^{\nu\rho}\ c^*_{\ell m\mu\nu}\ h_{\lambda\rho} \\ &= \int_0^{2\pi} d\varphi \int_{-1}^{1} d\cos\vartheta\ c^*_{\ell m\mu\nu}\ h^{\mu\nu} = \int_0^{2\pi} d\varphi \int_{-1}^{1} d\cos\vartheta\ c^{*\ (\alpha)(\beta)}_{\ell m}\ h_{(\alpha)(\beta)} \end{aligned} \tag{1.13}$$

However, since the harmonics $(\mathbf{a}^{(1)}_{\ell m}, \mathbf{b}^{(0)}_{\ell m}, \mathbf{c}^{(0)}_{\ell m})$, are normalized to -1, whereas all the others are normalized to 1 (see Appendix A for a proof), the coefficients $A^{(1)}_{\ell m}, B^{(0)}_{\ell m}, Q^{(0)}_{\ell m}$ will be defined with a minus sign.

We know that, for example,

$$c^{*\,(\alpha)(\beta)}_{\ell m} = e^{(\alpha)\mu} e^{(\beta)\mu} c^{*}_{\ell m\ \mu\nu} \tag{1.14}$$

and since $e^{(\alpha)\mu} e_{(\alpha)\nu} = \delta^{\mu}_{\nu}$,

$$\begin{aligned} e^{(t)\alpha} &= (1,0,0,0) \\ e^{(\varphi)\alpha} &= (0,-r\sin\vartheta,0,0) \\ e^{(r)\alpha} &= (0,0,-1,0) \\ e^{(\vartheta)\alpha} &= (0,0,0,-r)\,; \end{aligned} \tag{1.15}$$

therefore, the only nonzero elements in the tensor matrices projected onto the tetrad will be the same as those of the tensor harmonics listed in Appendix A. On the other hand, the non vanishing components of $h^{TT\ Q}_{(\mu)(\nu)}(t,r,\vartheta,\varphi)$ are only

$$h^{TT\ Q}_{(\vartheta)(\vartheta)} = -h^{TT\ Q}_{(\varphi)(\varphi)}, \qquad \text{and} \qquad h^{TT\ Q}_{(\vartheta)(\varphi)} = -h^{TT\ Q}_{(\varphi)(\vartheta)}.$$

Consequently when we take the inner product $c^{*\,(\alpha)(\beta)}_{\ell m}\ h_{(\alpha)(\beta)}$ it gives a non zero value only if the matrix $c^{*\,(\alpha)(\beta)}_{\ell m}$ has non vanishing $(\vartheta)(\vartheta)-$, $(\varphi)(\varphi)-$ or $(\vartheta)(\varphi)-$ components. This means that the axial harmonics $Q_{\ell m}, Q^{(0)}_{\ell m}$ and the polar hamonics $A^{(0)}_{\ell m}$, $A^{(1)}_{\ell m}$, $A_{\ell m}$, $B^{(0)}_{\ell m}$, $B_{\ell m}$ will automatically vanish, and the only coefficients that remain to be computed are $D_{\ell m}$ for the axial part, $G_{\ell m}$ and $F_{\ell m}$ for the polar part.

With the *Maple* program **Flm**, given in Appendix H, we find that the only nonzero coefficients (for $\ell = 2$, of course) are:

$$F_{22} = 8\sqrt{\frac{6\pi}{5}}\frac{m(\ell)}{r}(a - 2ib) \tag{1.16}$$

$$F_{2-2} = 8\sqrt{\frac{6\pi}{5}}\frac{m(\ell)}{r}(a + 2ib) = F^{*}_{22} \tag{1.17}$$

$$F_{20} = 8\sqrt{\frac{\pi}{5}}\frac{m(\ell)}{r}(3a + c + 5) \tag{1.18}$$

where we recall that

$$m(\ell) = \frac{1}{\sqrt{2\ell(\ell+1)(\ell-1)(\ell+2)}},$$

and that the functions a, b and c are related to the quadrupole moments by

$$\begin{aligned} a(t) &= \ddot{Q}_{xx} - \ddot{Q}_{yy}, \quad b(t) = \ddot{Q}_{xy} \\ c(t) &= \ddot{Q}_{yy} - \ddot{Q}_{zz}, \quad d(t) = \ddot{Q}_{zz} - \ddot{Q}_{xx}. \end{aligned}$$

In particular, this result implies that *the quadrupole wave is purely polar*, since it only involves tesor harmonic coefficients for which $\ell + m$ is *even*.

1.3 Newtonian treatment

It is known that two pointlike masses revolving around their common center of mass emit gravitational energy because of their time varying quadrupole moment. Consider first the gravitational emission by two *point masses* whose motion is described in the framework of *Newtonian gravity*. To describe their motion it is convenient to choose a coordinate system with the origin located at the center of mass of the system, the orbital plane coincident with the x-y plane and the x-axis oriented along the relative position vector, $\mathbf{X} \equiv \mathbf{x}_\star - \mathbf{x}_p$, when the mass m_0 is at the periastron. With this choice of the coordinate system we have:

$$\mathbf{x}_\star = \frac{m_0}{M+m_0}\mathbf{X}\,; \quad \mathbf{x}_p = -\frac{M}{M+m_0}\mathbf{X} \tag{1.19}$$

According to Newtonian gravity, the vector $\mathbf{X}$ describes, in general, an ellipse with semi-major axis a and eccentricity e, and its evolution is described by the parametric equations:

$$\rho = a(1 - e\cos u) \tag{1.20}$$

$$\alpha = 2\arctan\left[\left(\frac{1+e}{1-e}\right)^{1/2}\tan\frac{u}{2}\right]. \tag{1.21}$$

Here $\rho = |\mathbf{X}|$, α is the angle between $\mathbf{X}$ and the $x-$axis, and u is the eccentric anomaly, related to time by the Kepler equation:

$$\omega_k t = u - e\sin u, \tag{1.22}$$

where ω_k is the keplerian orbital frequency

$$\omega_k = \frac{2\pi}{P} = \left(\frac{GM_t}{a^3}\right)^{1/2} \to \left(\frac{GM}{a^3}\right)^{1/2}, \tag{1.23}$$

and $M_t = M + m_0$ is the total mass of the system, and the last expression refers to the test mass limit, $m_0 \ll M$. In terms of a, u and e the components of $\mathbf{X}$ are:

$$\begin{aligned} X^1 &= a(\cos u - e) \\ X^2 &= a(1-e^2)^{1/2}\sin u \\ X^3 &= 0 \end{aligned} \tag{1.24}$$

To compute the quadrupole moments we need the $T_{00}-$component of the stress-energy tensor, which is given by:

$$T_{00}(t,\,\mathbf{x}) = c^2[M\delta^{(3)}(\mathbf{x} - \mathbf{x}_\star(t)) + m_0\delta^{(3)}(\mathbf{x} - \mathbf{x}_p(t))]$$

where $\delta^{(3)}(\mathbf{z}) = \delta(z^1)\delta(z^2)\delta(z^3)$ is the 3-dimensional $\delta-$function. From the general expression for the quadrupole moment:

$$q_{kl}(t) = \frac{1}{c^2}\int T^{00}(t,\,\mathbf{y})y^k y^l d^3\mathbf{y} \tag{1.25}$$

we have then:

$$\begin{aligned} q_{kl}(t) &= \int \left[M\delta^{(3)}(\mathbf{y} - \mathbf{x}_\star(t)) + m_0\delta^{(3)}(\mathbf{y} - \mathbf{x}_p(t))\right] y^k y^l d^3\mathbf{y} = \\ &= M x_\star^k(t)x_\star^l(t) + m_0 x_p^k(t)x_p^l(t) \end{aligned} \tag{1.26}$$

or, using (1.19):

$$q_{kl} = \mu X^k X^l, \tag{1.27}$$

$\mu = m_0 M/(m_0 + M)$ being the reduced mass of the system. The reduced quadrupole moment is then given by:

$$Q_{kl} = \mu \left(X^k X^l - \frac{1}{3}\delta^k_l \left|\mathbf{X}\right|^2 \right) \tag{1.28}$$

Substituting the parametric representation (1.24) in the definition (1.28) of Q_{ij}, and using the chain rule for derivatives:

$$\frac{dx}{dt} = \frac{dx}{du} \cdot \left(\frac{dt}{du}\right)^{-1} = \frac{\omega_k}{1 - e\cos u}\frac{dx}{du} \tag{1.29}$$

we can easily obtain the second time-derivative $\ddot{Q}_{ij}$ of the reduced quadrupole moment. The result is:

$$\begin{aligned}
\ddot{Q}_{xx} &= \frac{2GM_t\mu}{3a(e\cos u - 1)^3}\left[(e^3 - 3e)\cos^3 u + (6 - 2e^2)\cos^2 u - 2e\cos u + 3e^2 - 3\right] \\
\ddot{Q}_{xy} &= -\frac{2GM_t\mu\sqrt{1-e^2}}{a(e\cos u - 1)^3}\sin u\left[e\cos^2 u - 2\cos u + e\right] \\
\ddot{Q}_{xz} &= 0 \\
\ddot{Q}_{yy} &= -\frac{2GM_t\mu}{3a(e\cos u - 1)^3}\left[(2e^3 - 3e)\cos^3 u + (6 - 4e^2)\cos^2 u - e\cos u + 3e^2 - 3\right] \\
\ddot{Q}_{yz} &= 0 \\
\ddot{Q}_{zz} &= \frac{2GM_t\mu e\cos u}{3a(e\cos u - 1)}
\end{aligned} \tag{1.30}$$

Specializing the general results (1.9) to our case, and using formulas (1.30) for the second time derivatives of the quadrupole moments, we get

$$\begin{aligned}
h^{TT\,Q}_{\vartheta\vartheta}(u, r, \vartheta, \varphi) &= \frac{2G^2 M_t\mu}{c^4 r a(1 - e\cos u)^3} \times \\
&\times \{(e^2 - 1)(1 + \cos^2\vartheta)(1 - 2\cos^2\varphi) \\
&+ \cos^2 u(e\cos u - 2)\left[(1 - e^2)(\cos^2\varphi + \cos^2\vartheta\cos^2\varphi - \cos^2\vartheta)\right. \\
&+ \left.\cos^2\varphi + \cos^2\vartheta\cos^2\varphi - 1\right] + e\cos u(\cos^2\varphi + \cos^2\vartheta\cos^2\varphi - 1) \\
&+ 2\sqrt{1 - e^2}\sin\varphi\cos\varphi(1 + \cos^2\vartheta)\sin u(e\cos^2 u - 2\cos u + e)\},
\end{aligned} \tag{1.31}$$

$$\begin{aligned}
h^{TT\,Q}_{\vartheta\varphi}(u, r, \vartheta, \varphi) &= \frac{4G^2 M_t\mu\cos\vartheta}{c^4 r a(1 - e\cos u)^3} \times \\
&\times \{\sin\varphi\cos\varphi\left[(e^2 - 2)\cos^2 u(e\cos u - 2) - e\cos u + 2(e^2 - 1)\right] \\
&+ (2\cos^2\varphi - 1)\sqrt{1 - e^2}\sin u(e\cos^2 u - 2\cos u + e)\}.
\end{aligned} \tag{1.32}$$

From these formulas one can easily check that, if the orbit is circular ($e = 0$), the radiation is emitted at twice the orbital frequency ($\omega^{GW} = 2\omega_k$). But if the orbit is eccentric, waves

will be emitted at frequencies multiple of ω_k, and the number of equally spaced spectral lines contributing to the signal will increase with the eccentricity[1].

1.3.1 Energy flux and characteristic amplitude

The energy flux emitted in gravitational waves can be evaluated in terms of the (01)-component of the stress-energy pseudotensor of the gravitational field:

$$t_{01} = \frac{dE}{dSdt} = \frac{1}{16\pi}\left\{\left[\dot{h}^{TT}_{\vartheta\vartheta}(t,r,\vartheta,\varphi)\right]^2 + \left[\dot{h}^{TT}_{\vartheta\varphi}(t,r,\vartheta,\varphi)\right]^2\right\} \tag{1.33}$$

Suppose, first of all, that our signal were not periodic. In this case we can define the Fourier transforms of the metric perturbations as:

$$\begin{aligned} h^{TT}_{\vartheta\vartheta}(\omega,r,\vartheta,\varphi) &= \frac{1}{2\pi}\int_{-\infty}^{+\infty} h^{TT}_{\vartheta\vartheta}(t,r,\vartheta,\varphi)e^{i\omega t}dt, \\ h^{TT}_{\vartheta\varphi}(\omega,r,\vartheta,\varphi) &= \frac{1}{2\pi}\int_{-\infty}^{+\infty} h^{TT}_{\vartheta\varphi}(t,r,\vartheta,\varphi)e^{i\omega t}dt, \end{aligned} \tag{1.34}$$

and use Parseval's theorem:

$$\frac{1}{2\pi}\int_{-\infty}^{+\infty}|f(t)|^2\,dt = \int_{-\infty}^{+\infty}|f(\omega)|^2\,d\omega. \tag{1.35}$$

We find from (1.33):

$$\int_{-\infty}^{+\infty}\left(\frac{dE}{dSdt}\right)dt = \frac{1}{8}\int_{-\infty}^{+\infty}\omega^2\left\{\left|h^{TT}_{\vartheta\vartheta}(\omega,r,\vartheta,\varphi)\right|^2 + \left|h^{TT}_{\vartheta\varphi}(\omega,r,\vartheta,\varphi)\right|^2\right\}d\omega. \tag{1.36}$$

Since the following relations between the one-sided spectral densities and the two-sided spectral densities hold:

$$\int_{-\infty}^{+\infty}\left(\frac{dE}{dSdt}\right)dt = \int_{-\infty}^{+\infty}\left(\frac{dE}{dSd\omega}\right)d\omega = \frac{1}{r^2}\int_{-\infty}^{+\infty}\left(\frac{dE}{d\Omega d\omega}\right)d\omega, \tag{1.37}$$

$$\left(\frac{dE}{d\Omega d\omega}\right) = \frac{1}{2\pi}\left(\frac{dE}{d\Omega d\nu}\right), \tag{1.38}$$

[1]Note that, since the geometry of the system is symmetrical for reflections with respect to the orbital plane, the metric coefficients have nice symmetry properties:

$$\begin{aligned} h_{\vartheta\vartheta}(\vartheta) &= h_{\vartheta\vartheta}(\pi-\vartheta) \\ h_{\vartheta\varphi}(\vartheta) &= -h_{\vartheta\varphi}(\pi-\vartheta) \end{aligned}$$

and the following relations hold:

$$\int_0^{\pi}\sin\vartheta d\vartheta\,|h_{\vartheta\vartheta}(\omega,r,\vartheta,\varphi)|^2 = 2\int_0^{\pi/2}\sin\vartheta d\vartheta\,|h_{\vartheta\vartheta}(\omega,r,\vartheta,\varphi)|^2$$

$$\int_0^{\pi}\sin\vartheta d\vartheta\,|h_{\vartheta\varphi}(\omega,r,\vartheta,\varphi)|^2 = 2\int_0^{\pi/2}\sin\vartheta d\vartheta\,|h_{\vartheta\varphi}(\omega,r,\vartheta,\varphi)|^2$$

we can easily read off from equation (1.36):

$$\left(\frac{dE}{d\Omega d\omega}\right) = \frac{\omega^2 r^2}{8}\left\{\left|h^{TT}_{\vartheta\vartheta}(\omega, r, \vartheta, \varphi)\right|^2 + \left|h^{TT}_{\vartheta\varphi}(\omega, r, \vartheta, \varphi)\right|^2\right\}. \tag{1.39}$$

Since our signal *is* periodic, we must use instead a Fourier-*series* version of Parseval's theorem. Our conventions on the Fourier transform will be:

$$\begin{aligned} H(\omega) &= \frac{1}{2\pi}\int_{-\infty}^{+\infty} h(t)e^{i\omega t}dt, \\ h(t) &= \int_{-\infty}^{+\infty} H(\omega)e^{-i\omega t}d\omega. \end{aligned} \tag{1.40}$$

Parseval's theorem reads then:

$$\frac{1}{2\pi}\int_{-\infty}^{+\infty} |h(t)|^2\, dt = \int_{-\infty}^{+\infty} |H(\omega)|^2\, d\omega. \tag{1.41}$$

Consider now a time-periodic signal with period $P = 1/\nu$. Such a signal can be expanded in a Fourier *series* rather than a Fourier integral,

$$h(t) = \sum_{n=-\infty}^{+\infty} H_n e^{-2n\pi i t/P}, \tag{1.42}$$

where the coefficients of the series are given by

$$H_n = \frac{1}{P}\int_0^P h(t)e^{2n\pi i t/P}dt. \tag{1.43}$$

The discrete equivalent of Parseval's theorem is:

$$\frac{1}{P}\int_0^P |h(t)|^2\, dt = \sum_{n=-\infty}^{\infty} |H_n|^2, \tag{1.44}$$

and as a consequence:

$$\frac{1}{P}\int_0^P \left|\dot{h}(t)\right|^2 dt = 2\sum_{n=0}^{\infty}\left(\frac{2\pi n}{P}\right)^2 |H_n|^2. \tag{1.45}$$

Along the lines traced for a non-periodic signal we can write:

$$\begin{aligned} \frac{1}{P}\int_0^P \frac{dE}{dSdt}dt &= \frac{c^3}{16\pi GP}\int_0^P \left\{\left[\dot{h}^{TT}_{\vartheta\vartheta}(t, r, \vartheta, \varphi)\right]^2 + \left[\dot{h}^{TT}_{\vartheta\varphi}(t, r, \vartheta, \varphi)\right]^2\right\} dt \\ &= \frac{c^3}{8\pi G}\sum_{n=0}^{\infty}\left(\frac{2\pi n}{P}\right)^2\left(\left|H_n^{\vartheta\vartheta}\right|^2 + \left|H_n^{\vartheta\varphi}\right|^2\right) \end{aligned}$$

Averaging over angles the n-th Fourier component we find the associated gravitational flux:

$$F_n = \frac{c^3(n\omega_k)^2}{8\pi G}\left[\langle\tilde{h}^{(n)}_{\vartheta\vartheta}\rangle^2 + \langle\tilde{h}^{(n)}_{\vartheta\varphi}\rangle^2\right], \tag{1.46}$$

where

$$\langle \tilde{h}^{(n)}_{\vartheta\vartheta} \rangle^2 = \frac{1}{4\pi} \int d\Omega \left| H^{\vartheta\vartheta}_n \right|^2 ,$$
$$\langle \tilde{h}^{(n)}_{\vartheta\varphi} \rangle^2 = \frac{1}{4\pi} \int d\Omega \left| H^{\vartheta\varphi}_n \right|^2 .$$

The corresponding luminosity is given by:

$$\dot{E}_n = L_n = 4\pi r^2 F_n = \frac{c^3 (n\omega_k)^2 r^2}{2G} \left[\langle \tilde{h}^{(n)}_{\vartheta\vartheta} \rangle^2 + \langle \tilde{h}^{(n)}_{\vartheta\varphi} \rangle^2 \right] . \tag{1.47}$$

Finally, we can define a characteristic gravitational-wave amplitude, according to formula (50) in reference [84], as:

$$h_c(n\omega_k, r) = \sqrt{\frac{2}{3}} \left[\langle \tilde{h}^{(n)}_{\vartheta\vartheta} \rangle^2 + \langle \tilde{h}^{(n)}_{\vartheta\varphi} \rangle^2 \right]^{1/2} , \tag{1.48}$$

where the factor $\sqrt{2/3}$ takes into account an average over orientation.

1.3.2 A special case: circular orbits

For a system in circular orbit, formulas (1.31) and (1.32) specialize to:

$$\begin{aligned} h^{TT\ Q}_{\vartheta\vartheta}(\omega_k t, r, \vartheta, \varphi) &= -\frac{2G^2 M_t \mu}{c^4 r a}(1+\cos^2\vartheta) \left\{ (2\cos^2\varphi - 1)\cos(2\omega_k t) + \sin 2\varphi \sin(2\omega_k t) \right\} \\ h^{TT\ Q}_{\vartheta\varphi}(\omega_k t, r, \vartheta, \varphi) &= \frac{4G^2 M_t \mu}{c^4 a r} \cos\vartheta \left\{ \sin 2\varphi \cos(2\omega_k t) - (2\cos^2\varphi - 1)\sin(2\omega_k t) \right\} \end{aligned}$$

and we can get an explicit expression for the Fourier coefficients of the two independent metric components:

$$\begin{aligned} H^{\vartheta\vartheta}_2 &= -\frac{G^2 M_t \mu}{c^4 a r}(1+\cos^2\vartheta) \left\{ (2\cos^2\varphi - 1) + i \sin 2\varphi \right\} \\ H^{\vartheta\varphi}_2 &= -\frac{G^2 M_t \mu}{c^4 a r} 2\cos\vartheta \left\{ -\sin 2\varphi + i(2\cos^2\varphi - 1) \right\} . \end{aligned}$$

From these formulas we obtain the angular averages

$$\begin{aligned} \langle \tilde{h}^{(2)}_{\vartheta\vartheta} \rangle^2 &= \frac{28}{15} \frac{G^4 M_t^2 \mu^2}{c^8 a^2 r^2} \\ \langle \tilde{h}^{(2)}_{\vartheta\varphi} \rangle^2 &= \frac{4}{3} \frac{G^4 M_t^2 \mu^2}{c^8 a^2 r^2}, \end{aligned}$$

and we can get the flux in closed form from (1.46):

$$F = \frac{8 G^3 M_t^2 \mu^2 \omega_k^2}{5\pi c^5 a^2 r^2}. \tag{1.49}$$

For the luminosity we get

$$\dot{E} = L = 4\pi r^2 F = \frac{32 G^4 (M m_0)^2 (M + m_0)}{5 c^5 a^5}, \tag{1.50}$$

and this result agrees with equation (16) in reference [65].

Since in following chapters we will sometimes need to compare this result with those obtained from Post-Newtonian expansions (which are basically expansions in the orbital velocity of the binary v) in the test mass case, we note that formula (1.50), when specialized to the test-mass case $m_0 \ll M$ and expressed in terms of the orbital velocity, which for test masses is related to the keplerian frequency by $v = (M\omega_k)^{1/3}$, becomes:

$$\dot{E}_N = \frac{32}{5}\frac{m_0^2}{M^2}v^{10}, \tag{1.51}$$

where we have used geometric units and we have introduced a subscript "N", meaning that the orbital evolution is described in terms of the Newtonian equations of motion. Notice also that we can recover the general formula for the energy flux from this test mass limit by a simple replacement of the particle's mass m_0 by the reduced mass μ, and of the stellar mass M by the total mass of the system $M_t \equiv M + m_0$. This remark will be relevant when, in chapter 4, we will try to extrapolate test mass results (obtained taking into account the stellar structure) to the comparable mass case.

Going back to the general case of comparable masses, and defining the quadrupole amplitude for a system in circular orbit as:

$$h_Q = h_c(2\omega_k, r), \tag{1.52}$$

we get the analytic formula:

$$h_Q = \frac{8}{\sqrt{15}}\frac{G^2 M_t \mu}{c^4 a r} = \frac{8}{\sqrt{15}}\frac{G}{c^4}\frac{\mu}{r}(\omega_k R_0)^2 \to \frac{8}{\sqrt{15}}\frac{G}{c^4}\frac{m_0}{r}(\omega_k R_0)^2, \tag{1.53}$$

where R_0 is the (constant) radius of the orbit, ω_k is the keplerian frequency of the system, and the last formula is valid in the test mass limit.

The dominant coefficients in the expansion of the quadrupole wave in tensor spherical harmonics, in the case under consideration, are given by

$$F_{22} = -\frac{8\sqrt{2\pi}}{\sqrt{5}}\frac{\mu}{r}(\omega_k R_0)^2, \qquad F_{2-2} = F_{22}. \tag{1.54}$$

Using the definitions of the spin-weighted spherical harmonics ${}_sY_{\ell m}$, given in Appendix G, it's easy to show that

$$\sum_{m=\pm 2} F_{\ell m}\hat{f}_{\ell m} = \frac{1}{\sqrt{2}}\sum_{m=\pm 2} F_{\ell m}\,{}_2Y_{\ell m}, \tag{1.55}$$

so that we can write the dominant part of the quadrupole amplitude in TT-gauge as

$$\begin{aligned} h^{TT\ Q}_{\vartheta\vartheta} + i h^{TT\ Q}_{\vartheta\varphi} &= \sum_{m=\pm 2}\left[-\frac{8\sqrt{2\pi}}{\sqrt{10}}\frac{\mu}{r}(\omega_k R_0)^2\right]\,{}_2Y_{\ell m} \to \\ &\to \sum_{m=\pm 2}\left[-\frac{8\sqrt{2\pi}}{\sqrt{10}}\frac{m_0}{r}(\omega_k R_0)^2\right]\,{}_2Y_{\ell m}, \end{aligned} \tag{1.56}$$

where (as usual) the last line refers to the test mass limit. The *Maple* code used to perform the calculations described in this section, **NewtonianQuadrupole**, is included in Appendix H.

1.4 Semirelativistic quadrupole approximation

We have seen that the amplitudes of the metric perturbations in TT-gauge are expressed in terms of the quadrupole moments as

$$\begin{aligned} h^{TT\,Q}_{\vartheta\vartheta} &= \frac{G}{c^4 r}\left\{\left[\left(\ddot{Q}_{xx}-\ddot{Q}_{yy}\right)\cos^2\varphi + 2\ddot{Q}_{xy}\sin\varphi\cos\varphi\right]\left(1+\cos^2\vartheta\right)\right. \\ &+ \left.\left[\ddot{Q}_{yy}-\ddot{Q}_{zz}\right]\cos^2\vartheta + \ddot{Q}_{zz} - \ddot{Q}_{xx}\right\}, \\ h^{TT\,Q}_{\vartheta\varphi} &= -\frac{G}{c^4 r}\left\{2\cos\vartheta\left[\left(\ddot{Q}_{xx}-\ddot{Q}_{yy}\right)\sin\varphi\cos\varphi + \ddot{Q}_{xy}\left(1-2\cos^2\varphi\right)\right]\right\}, \end{aligned} \tag{1.57}$$

and we have explicitly computed the quadrupole moments for a binary system composed of two point masses obeying *Newtonian* gravity. Now we want to assume that one of the members of the binary is a non-rotating star or a Schwarzschild black hole, while the other is a small mass following a geodesic in the background metric of the first object, and compute the gravitational radiation emitted by the mass m_0 because of its accelerated orbital motion around the central object.

We are basically using a *semi-relativistic approximation*, since we are assuming that m_0 moves along a geodesic of the curved spacetime, but radiates as if it were in flat spacetime. To compute the quadrupole moments we must briefly recall the properties of the geodesic motion of such a small mass in the Schwarzschild metric.

1.4.1 Geodesics in the Schwarzschild metric

The geodesic equations for a small mass moving in the equatorial plane in the Schwarzschild metric are

$$\frac{dr}{d\tau} \equiv \sigma\gamma = \pm\sqrt{E^2 - V(r)^2}, \qquad \frac{d\varphi}{d\tau} = \frac{L_z}{r^2}, \qquad \frac{dt}{d\tau} = \frac{E}{1-\frac{2M}{r}}, \tag{1.58}$$

where E and L_z are the (constant) energy and angular momentum of the moving body, and σ is the sign of the square root appearing in the first equation. The first equation can be written in the form

$$E^2 = \dot{r}^2 + V(r)^2, \tag{1.59}$$

where the effective potential

$$V(r) \equiv \sqrt{\left(1-\frac{2M}{r}\right)\left(1+\frac{L_z^2}{r^2}\right)}. \tag{1.60}$$

So $E \geq V(r)$, and the condition $E = V(r)$ corresponds to the orbital turning points, for which $\dot{r} = 0$.

From the geodesic equations we can also obtain the following relations:

$$\begin{aligned} \frac{dr}{dt} &= \frac{1-\frac{2M}{r}}{E}\sqrt{E^2 - V(r)^2} \\ \frac{d\varphi}{dt} &= \frac{L_z\left(1-\frac{2M}{r}\right)}{Er^2} \end{aligned}$$

$$\begin{aligned}\frac{d^2r}{dt^2} &= \frac{d}{dr}\left(\frac{dr}{dt}\right)\left(\frac{dr}{dt}\right) = \\ &= \frac{(r-2M)\left[(2ME^2-3M)r^3+(6M^2+L_z^2)r^2-7rML_z^2+10M^2L_z^2\right]}{r^6E^2} \\ \frac{d^2\varphi}{dt^2} &= \frac{d}{dr}\left(\frac{d\varphi}{dt}\right)\left(\frac{dr}{dt}\right) = -\frac{2L_z(r-3M)}{r^4E}\left(\frac{dr}{dt}\right).\end{aligned}$$

The effective potential $V(r)$ is defined for $r > 2M$, satisfies $V(2M) = 0$ and has a maximum V_{max} when

$$r = r_- = \frac{L_z}{2M}\left(L_z - \sqrt{L_z^2 - 12M^2}\right), \tag{1.61}$$

then drops to a minimum V_{min} when

$$r = r_+ = \frac{L_z}{2M}\left(L_z + \sqrt{L_z^2 - 12M^2}\right). \tag{1.62}$$

Asymptotically, $V(r \to \infty) = 1$.

When $\sqrt{12} < L_z < 4$, $V_{max} < 1$ and the condition to have closed orbits is $V_{min} < E < V_{max}$. On the other hand, if $L_z > 4$, $V_{max} > 1$, and the condition for closed orbits becomes $V_{min} < E < 1$. In the latter case, $V = 1$ when

$$r = r'_- = \frac{L_z}{4M}\left(L_z + \sqrt{L_z^2 - 16M^2}\right). \tag{1.63}$$

Notice that closed orbits in the Schwarzschild metric are *quasi-periodic*, in the sense that

$$\begin{aligned} r\left(t+\Delta t\right) &= r(t), \\ \varphi\left(t+\Delta t\right) &= \varphi(t) + \Delta\varphi, \end{aligned} \tag{1.64}$$

for some Δt. First of all, the radial motion is periodic because it is determined by the effective potential, which depends only on r: when the test mass goes back to the periastron after a proper time $\Delta\tau$ it will move outwards again with the same initial conditions, so the radial motion is exactly periodic. If we consider t and φ, on the other hand, since $\frac{dt}{d\tau}$ and $\frac{d\varphi}{d\tau}$ are functions only of r, in each period $\Delta\tau$ the particle will span the same intervals Δt, $2\pi + \Delta\varphi$. So the overall motion is *quasi-periodic*.

To perform the integration of the geodesics in the first branch (which, according to the symmetries we have just discussed, is the only one we need) we make the following change of variable:

$$r(\chi) = \frac{pM}{1 + e\cos\chi}. \tag{1.65}$$

In the previous formula, e is the orbital eccentricity and p is the orbital semi-latus rectum. These parameters are related to the periastron r_P and to the apoastron r_A by

$$e = \frac{r_A - r_P}{r_A + r_P}, \qquad p = \frac{2}{M}\frac{r_A r_P}{r_A + r_P}, \tag{1.66}$$

$$r_P = \frac{pM}{1+e}, \qquad r_A = \frac{pM}{1-e}. \tag{1.67}$$

The parameter χ ranges from 0 to 2π in a whole orbit, and from 0 to π to go from the periastron to the apoastron. The semi-latus rectum is essentially a measure of the size of the orbit, and the eccentricity is (of course) a measure of the departure of the orbit from circularity. Note that $0 \leq e < 1$.

Furthermore, the orbital energy and angular momentum can be obtained from p and e through the formulas

$$E^2 = \frac{(p-2-2e)(p-2+2e)}{p(p-3-e^2)}, \qquad L_z^2 = \frac{p^2 M^2}{p-3-e^2}. \tag{1.68}$$

Once we have fixed the mass of the central object, the orbit is determined just by two parameters. Given any couple of parameters, through the previous relations we can obtain any other couple[2].

When we switch from the proper time τ to χ, the equations to integrate become:

$$\frac{dt}{d\chi} = \frac{p^2 M (p-2-2e)^{1/2}(p-2+2e)^{1/2}}{(p-2-2e\cos\chi)(1+e\cos\chi)^2(p-6-2e\cos\chi)^{1/2}} \tag{1.70}$$

$$\frac{d\tau}{d\chi} = \frac{p^{3/2} M (p-3-e^2)^{1/2}}{(1+e\cos\chi)^2(p-6-2e\cos\chi)^{1/2}} \tag{1.71}$$

$$\frac{d\varphi}{d\chi} = \frac{p^{1/2}}{(p-6-2e\cos\chi)^{1/2}} \tag{1.72}$$

To integrate the previous equations we don't need to make any expansion close to the periastron. We just use an adaptive Runge-Kutta to step forward from $\chi = 0$ to $\chi = \pi$, and we compute $\Delta\varphi$ and Δt from:

$$\Delta t = 2\bar{t} \tag{1.73}$$

$$\Delta\varphi = 2\bar{\varphi} \tag{1.74}$$

where $\bar{t}$ and $\bar{\varphi}$ are the values of t and φ at the apoastron ($\chi = \pi$).

The geodesic equations are symmetric under the transformation $(t, \varphi) \to (-t, -\varphi)$, so we can solve the equations for just half an orbit, e.g. the one with $t \in \left[0, \frac{\Delta t}{2}\right]$: the other half, with $t \in \left[-\frac{\Delta t}{2}, 0\right]$, can be obtained from the first through a reflection.

Suppose the solution of the geodesic equations for $t \in \left[0, \frac{\Delta t}{2}\right]$ (found by integration) is

$$\begin{cases} t_0^+ = t_0(r) \\ \varphi_0^+ = \varphi_0(r) \end{cases}. \tag{1.75}$$

Then the solution for $t \in \left[-\frac{\Delta t}{2}, 0\right]$ is

$$\begin{cases} t_0^- = -t_0(r) \\ \varphi_0^- = -\varphi_0(r) \end{cases}, \tag{1.76}$$

[2]For example, we can fix e and r_P, and then obtain (e.g.) E and L_z through the following procedure:

- From the first of formulas (1.66) we get

$$r_A = r_P \frac{1+e}{1-e} \tag{1.69}$$

and the second relation fixes the semi-latus rectum p.

- Once e and p are known, we use (1.68) to find E ed L_z.

and the generic branch of the trajectory can be found from

$$\begin{cases} t_k^+(r) = t_0(r) + k\Delta t \\ \varphi_k^+(r) = \varphi_0(r) + k\Delta\varphi \\ t_k^-(r) = -t_0(r) + k\Delta t \\ \varphi_k^-(r) = -\varphi_0(r) + k\Delta\varphi \end{cases} \qquad k = -\infty, \ldots, \infty\,. \tag{1.77}$$

1.4.2 Wave amplitude and energy

The expressions of the second time-derivative of the components of Q_{kl} in terms of $r(t)$ and $\varphi(t)$ are

$$\begin{aligned} \ddot{Q}_{xx} &= m_0\left(\alpha\cos 2\varphi - \beta\sin 2\varphi + \delta/2\right), \\ \ddot{Q}_{yy} &= m_0\left(-\alpha\cos 2\varphi + \beta\sin 2\varphi + \delta/2\right), \\ \ddot{Q}_{xy} &= m_0\left(\alpha\sin 2\varphi + \beta\cos 2\varphi\right), \quad \ddot{Q}_{zz} = -m_0\delta, \end{aligned} \tag{1.78}$$

where

$$\begin{aligned} &\alpha = \dot{r}^2 + r\ddot{r} - 2r^2\dot{\varphi}^2, \\ &\beta = 4r\dot{r}\dot{\varphi} + r^2\ddot{\varphi}, \quad \delta = 2\left(\dot{r}^2 + r\ddot{r}\right)/3. \end{aligned} \tag{1.79}$$

We shall now compute the Fourier transform of the wave emitted by the pointlike particle because of its orbital motion, given in Eq. (1.57), and discuss the symmetry properties of the corresponding spectrum. The orbit is quasi-periodic in φ, but exactly periodic in $(r, \dot{r}, \ddot{r}, \dot{\varphi}, \ddot{\varphi})$ so that we can decompose the Fourier transform as a sum over periods

$$\begin{aligned} h(\omega) &= \frac{1}{2\pi}\int_{-\infty}^{\infty} h(t)e^{i\omega t}dt = \\ &= \frac{1}{2\pi}\sum_{n=-\infty}^{\infty}\int_{(n-1/2)\Delta t}^{(n+1/2)\Delta t} h(t_n = t_0 + n\Delta t, \varphi_n = \varphi_0 + n\Delta\varphi)e^{i\omega t_n}dt_n, \end{aligned} \tag{1.80}$$

where $(t_0(r), \varphi_0(r))$ indicates the branch of the trajectory which starts at the periastron ($r = r_P$) at $t = 0$ and ends at the apoastron ($r = r_A$) at $t = \frac{\Delta t}{2}$; $(-t_0(r), -\varphi_0(r))$ indicates the "mirror" branch starting at r_A and ending at r_P, with $t \in [-\frac{\Delta t}{2}, 0]$. An inspection of Eqs. (1.57) and (1.78) shows that the integrals are essentially of three types:

- 1) those containing δ, say $h_1(t)$, which do not depend on φ and therefore are exactly periodic;
- 2) those that contain a periodic term, say $h_2(t)$, times $\sin 2\varphi$, and
- 3) those that contain a periodic term, say $h_3(t)$, times $\cos 2\varphi$.

These integrals can be developed in the following way:

$$\begin{aligned} 1) \qquad &\frac{1}{2\pi}\sum_{n=-\infty}^{\infty}\int_{(n-1/2)\Delta t}^{(n+1/2)\Delta t} h_1(t_n)e^{i\omega t_n}dt_n = \frac{1}{2\pi}\int_{-\Delta t/2}^{\Delta t/2} h_1(t_0)e^{i\omega t_0}\sum_{n=-\infty}^{\infty} e^{i\omega n\Delta t}dt_0 = \\ &= \sum_{j=-\infty}^{\infty}\delta\left(\omega - \omega_{0j}\right)\left[\frac{1}{\Delta t}\int_{-\Delta t/2}^{\Delta t/2} h_1(t_0)e^{i\omega t_0}dt_0\right]. \end{aligned}$$

To obtain this result we have used the property

$$\sum_{k=-\infty}^{+\infty} e^{\mathrm{i}kX} = 2\pi \sum_{j=-\infty}^{+\infty} \delta\left(X - 2\pi j\right)$$

and we have defined

$$\omega_{mj} = \frac{2\pi j + m\Delta\varphi}{\Delta t} \equiv j\Omega_r + m\Omega_\varphi \,. \tag{1.81}$$

Notice that the following symmetry property holds:

$$\omega_{-m-j} = -\omega_{mj}. \tag{1.82}$$

Similarly we have:

$$\begin{aligned}
2) \qquad & \frac{1}{2\pi}\sum_{n=-\infty}^{\infty}\int_{(n-1/2)\Delta t}^{(n+1/2)\Delta t} h_2(t_n)\sin 2\varphi_n e^{i\omega t_n} dt_n \\
= \; & \sum_{j=-\infty}^{\infty}\left\{\delta\left(\omega-\omega_{-2j}\right)\left[\frac{1}{\Delta t}\int_{-\Delta t/2}^{\Delta t/2} h_2(t_0)\frac{e^{i(\omega t_0+2\varphi_0)}}{2i}dt_0\right]\right. \\
+ \; & \left.\delta\left(\omega-\omega_{2j}\right)\left[-\frac{1}{\Delta t}\int_{-\Delta t/2}^{\Delta t/2} h_2(t_0)\frac{e^{i(\omega t_0-2\varphi_0)}}{2i}dt_0\right]\right\}.
\end{aligned}$$

$$\begin{aligned}
3) \qquad & \frac{1}{2\pi}\sum_{n=-\infty}^{\infty}\int_{(n-1/2)\Delta t}^{(n+1/2)\Delta t} h_3(t_n)\cos 2\varphi_n e^{i\omega t_n} dt_n \\
= \; & \sum_{j=-\infty}^{\infty}\left\{\delta\left(\omega-\omega_{-2j}\right)\left[\frac{1}{\Delta t}\int_{-\Delta t/2}^{\Delta t/2} h_3(t_0)\frac{e^{i(\omega t_0+2\varphi_0)}}{2}dt_0\right]\right. \\
+ \; & \left.\delta\left(\omega-\omega_{2j}\right)\left[\frac{1}{\Delta t}\int_{-\Delta t/2}^{\Delta t/2} h_3(t_0)\frac{e^{i(\omega t_0-2\varphi_0)}}{2}dt_0\right]\right\}.
\end{aligned}$$

Proceeding along this line, we find that the wave components can be written as

$$\begin{aligned}
h^{TT}_{\vartheta\vartheta}(\omega, r, \vartheta, \varphi) &= \sum_{j=-\infty}^{\infty}\sum_{m=-2,0,2}\delta(\omega-\omega_{mj})\, H_{\vartheta\vartheta}(\omega_{mj}, \vartheta, \varphi) \\
h^{TT}_{\vartheta\varphi}(\omega, r, \vartheta, \varphi) &= -\sum_{j=-\infty}^{\infty}\sum_{m=-2,2}\delta(\omega-\omega_{mj})\, H_{\vartheta\varphi}(\omega_{mj}, \vartheta, \varphi),
\end{aligned} \tag{1.83}$$

where

$$\begin{aligned}
H_{\vartheta\vartheta}(\omega_{2j}, \vartheta, \varphi) &= \frac{m_0}{r}\left[\left(\mathcal{I}^{\alpha}_{2j} + \mathcal{I}^{\beta}_{2j}\right)(1+\cos^2\vartheta)(\cos 2\varphi + i\sin 2\varphi)\right] \\
H_{\vartheta\vartheta}(\omega_{-2j}, \vartheta, \varphi) &= \frac{m_0}{r}\left[\left(\mathcal{I}^{\alpha}_{-2j} - \mathcal{I}^{\beta}_{-2j}\right)(1+\cos^2\vartheta)(\cos 2\varphi - i\sin 2\varphi)\right] \\
H_{\vartheta\vartheta}(\omega_{0j}, \vartheta, \varphi) &= \frac{3m_0}{r}\mathcal{K}^{\delta}_{j}(\cos^2\vartheta - 1) \\
H_{\vartheta\varphi}(\omega_{2j}, \vartheta, \varphi) &= \frac{2m_0}{r}\cos\vartheta\left[\left(\mathcal{I}^{\alpha}_{2j} + \mathcal{I}^{\beta}_{2j}\right)(\sin 2\varphi - i\cos 2\varphi)\right] \\
H_{\vartheta\varphi}(\omega_{-2j}, \vartheta, \varphi) &= \frac{2m_0}{r}\cos\vartheta\left[\left(\mathcal{I}^{\alpha}_{-2j} - \mathcal{I}^{\beta}_{-2j}\right)(\sin 2\varphi + i\cos 2\varphi)\right]
\end{aligned}$$

and we have defined

$$\begin{aligned}
\mathcal{I}^{\alpha}_{\pm 2j} &= \frac{1}{\Delta t}\int_0^{\Delta t/2} \alpha\cos(\omega_{j\pm 2}t_0 \mp 2\varphi_0)dt_0 \\
\mathcal{I}^{\beta}_{\pm 2j} &= \frac{1}{\Delta t}\int_0^{\Delta t/2} \beta\sin(\omega_{j\pm 2}t_0 \mp 2\varphi_0)dt_0 \\
\mathcal{K}^{\delta}_{j} &= \frac{1}{\Delta t}\int_0^{\Delta t/2} \delta\cos(\omega_{0j}t_0)dt_0.
\end{aligned}$$

Now that we know the wave amplitude, we want to compute the time-averaged quadrupole energy flux. We recall that, according to eq. (1.33),

$$\frac{dE^{(Q)}}{dSdt} = \frac{1}{16\pi}\left\{\left|\dot{h}^{TT}_{\vartheta\vartheta}(t,r,\vartheta,\varphi)\right|^2 + \left|\dot{h}^{TT}_{\vartheta\varphi}(t,r,\vartheta,\varphi)\right|^2\right\}. \tag{1.84}$$

For our quasi-periodic signal, it follows that the average power emitted by the system is given by the limit

$$\dot{E}^{(Q)} \equiv \left\langle\frac{dE^{(Q)}}{dt}\right\rangle = \frac{r^2}{16\pi}\lim_{T\to\infty}\frac{1}{T}\int_0^T dt\int d\Omega\left\{\left|\dot{h}^{TT}_{\vartheta\vartheta}\right|^2 + \left|\dot{h}^{TT}_{\vartheta\varphi}\right|^2\right\}; \tag{1.85}$$

using Parseval's theorem[3] this becomes

$$\begin{aligned}
\dot{E}^{(Q)} &= \frac{r^2}{16\pi}\sum_{j=-\infty}^{\infty}\left[\sum_{m=-2,0,2}\int d\Omega\;\omega^2_{mj}\,|H_{\vartheta\vartheta}(\omega_{mj},\vartheta,\varphi)|^2 + \sum_{m=-2,2}\int d\Omega\;\omega^2_{mj}\,|H_{\vartheta\varphi}(\omega_{mj},\vartheta,\varphi)|^2\right] \\
&= \sum_{j=-\infty}^{\infty}\sum_{m=-2,0,2}\dot{E}^{Q}_{mj},
\end{aligned} \tag{1.86}$$

where

$$\begin{aligned}
&\text{for } m=-2,2 && \dot{E}^{Q}_{mj} = \frac{r^2}{16\pi}\int d\Omega\;\left[\omega^2_{mj}\,|H_{\vartheta\vartheta}|^2 + \omega^2_{mj}\,|H_{\vartheta\varphi}|^2\right], \\
&\text{for } m=0 && \dot{E}^{Q}_{mj} = \frac{r^2}{16\pi}\int d\Omega\;\left[\omega^2_{mj}\,|H_{\vartheta\vartheta}|^2\right].
\end{aligned} \tag{1.87}$$

[3] From eq. (1.83) it follows that the amplitude in the time domain can be written as a double sum of the form:

$$h(t) = \sum_{m,j} H_{mj}e^{-i\omega_{mj}t}.$$

The double sum is equivalent to a simple sum in the proof of Parseval's theorem:

$$\begin{aligned}
&\int_0^P dt\,|h|^2 = \sum_{mm'jj'} H_{mj}H^{\star}_{m'j'}\int_0^P e^{-i(\omega_{mj}-\omega_{m'j'})t}dt = \\
&= P\sum_{mm'jj'}\delta_{mm'}\delta_{jj'}H_{mj}H^{\star}_{m'j'} = P\sum_{mj}|H_{mj}|^2
\end{aligned}$$

In terms of the integrals (1.84), the various contributions to the average power radiated appearing in formula (1.86) are given by

$$\begin{aligned}
\dot{E}^Q_{2j} &= \frac{4m_0^2}{5}(\omega_{2j})^2\left(\mathcal{I}^\alpha_{2j}+\mathcal{I}^\beta_{2j}\right)^2,\\
\dot{E}^Q_{-2j} &= \frac{4m_0^2}{5}(\omega_{-2j})^2\left(\mathcal{I}^\alpha_{-2j}-\mathcal{I}^\beta_{-2j}\right)^2,\\
\dot{E}^Q_{0j} &= \frac{6m_0^2}{5}\omega_{0j}^2\left(\mathcal{K}^\delta_j\right)^2.
\end{aligned}$$

Using Eq. (1.82) and the definitions of the various integrals, it is straightforward to show that:

$$\begin{aligned}
&\mathcal{I}^\alpha_{-2-j}=\mathcal{I}^\alpha_{2j}, \qquad \mathcal{I}^\alpha_{2-j}=\mathcal{I}^\alpha_{-2j},\\
&\mathcal{I}^\beta_{-2-j}=-\mathcal{I}^\beta_{2j}, \qquad \mathcal{I}^\beta_{2-j}=-\mathcal{I}^\beta_{-2j},\\
&\mathcal{K}^\delta_{-j}=\mathcal{K}^\delta_j.
\end{aligned}$$

Finally, from Eqs. (1.82) and (1.88) we find

$$\dot{E}^Q_{-m-j}=\dot{E}^Q_{mj}. \qquad (m=2,0,-2) \tag{1.88}$$

We will see that similar properties hold for the energy flux from a binary in which the central object is a "real" star, endowed with an extended structure: the quadrupole power spectrum has essentially the same frequency content and the same symmetry properties as the "relativistic" spectrum with $l=2$ and $m=-2,0,2$, except for the $m=1$ contribution, which is missing.

1.4.3 Meaning of the fundamental frequencies

In the previous section we have seen that the semirelativistic spectrum is a spectrum of lines at frequencies

$$\omega_{mj}=\frac{2\pi j+m\Delta\varphi}{\Delta t}\equiv j\Omega_r+m\Omega_\varphi, \tag{1.89}$$

which are linear combinations of two "fundamental frequencies", Ω_r ed Ω_φ (actually, we have only seen cases with $m=2,\ 0,\ -2$, but we are going to show later that such a formula for the spectral lines holds in general). We want to discuss briefly the meaning of these fundamental frequencies. Obviously, the frequency

$$\Omega_r=\frac{2\pi}{\Delta t} \tag{1.90}$$

corresponds to the (periodic) radial motion. Being $r(t)$ a periodic function, any function of $r(t)$ will be periodic. Every periodic function of this kind, say $a(t)$, can be expanded in a Fourier series,

$$a(t)=\sum_{k=-\infty}^{\infty}a_k e^{-ik\Omega_r t}, \tag{1.91}$$

with

$$a_k=\frac{1}{\Delta t}\int_0^{\Delta t}a(t)e^{ik\Omega_r t}dt. \tag{1.92}$$

In particular, the function $a(t) = \frac{d\varphi}{dt}$ is periodic and can be expanded in this way. Integrating the series we find

$$\varphi(t) = a_0 t + \sum_{k=-\infty}^{\infty} b_k e^{-ik\Omega_r t} \tag{1.93}$$

with

$$b_k = \frac{ia_k}{k\Omega_r} \qquad \text{for} \qquad k \neq 0, \tag{1.94}$$

while b_0 is determined by the condition

$$\varphi(0) = 0 \Longrightarrow \sum_{k=-\infty}^{\infty} b_k = 0. \tag{1.95}$$

Now, it is clear from formula (1.93) that, even if $\varphi(t)$ is not a periodic function, the function $\varphi(t) - a_0 t$ *is* periodic. This function is nothing but the angular position of the particle according to an observer rotating with constant angular velocity a_0 with respect to a static observer at infinity. This angular velocity is given by

$$a_0 = \frac{1}{\Delta t}\int_0^{\Delta t} a(t)dt = \frac{1}{\Delta t}\int_0^{\Delta t} \frac{d\varphi}{dt}dt = \frac{\Delta\varphi}{\Delta t} = \Omega_\varphi. \tag{1.96}$$

So both $r(t)$ and $\varphi(t) - \Omega_\varphi t$ are periodic functions of t with period Δt.

This means that, despite the fact that the motion is *quasi-periodic* from the point of view of a static observer at infinity, it is *exactly periodic* for an observer rotating with angular velocity Ω_φ. That's why the energy spectrum can be expanded in a Fourier series totally analogous to (1.91), but summed *over two indices* (m and j) corresponding to the existence of two (not only one) fundamental frequencies.

Chapter 2

Perturbation equations for a non-rotating star excited by a massive source

In this chapter we will give the basic equations to deal with to study the excitation of the perturbations of a non-rotating, relativistic star by a massive body orbiting the star.

In section 2.1 we will shortly recall the equations to integrate to find the equilibrium structure of the star. Then, in section 2.2 we will write down the basic equations describing the perturbations of the metric and fluid functions inside the star, and the perturbations of the metric functions in the vacuum prevailing outside. The formalism we will use to treat the interior perturbations is the one developed by Chandrasekhar and Ferrari [16], though we have cross-checked our results using also the equivalent formalism developed by Thorne and collaborators in a series of papers [85].

The formalism we use in the exterior was originally developed by Regge and Wheeler to study the stability properties of Schwarzschild black holes. Regge and Wheeler studied only the so-called axial perturbations; subsequently Zerilli extended the formalism to the polar perturbations, considering also a particle in geodesic orbit around the black hole as a possible source of excitation of the perturbations. We will often refer to this perturbation formalism, based directly on a first-order perturbation of the *metric functions*, as the *Zerilli formalism*. We will see that this formalism, after separation of the angular part of the equations through an expansion in tensor spherical harmonics, reduces our problem to a solution (with appropriate boundary conditions) of two Schrödinger-like equations with source, known as the *Regge-Wheeler equation* for the axial case and as the *Zerilli equation* for the polar case, respectively.

Here we only want to sketch the basic equations that we shall solve to compute the radiation emitted by extrasolar planetary systems. The derivation of the source terms and the solution of the Zerilli and Regge-Wheeler equations in the special case of a particle in circular orbit around the star are quite lenghty and involved; they will be deferred to Appendix C.

2.1 The equilibrium configuration

In the following we shall adopt geometric units ($G = c = 1$). We shall write the Einstein equations in the form $G_{ij} = 2T_{ij}$, and define the Riemann tensor as in [14]. The metric for a static, spherically symmetric distribution of matter can be written in the standard form:

$$ds^2 = e^{2\nu}dt^2 - e^{2\mu_2}dr^2 - r^2(d\vartheta^2 + \sin^2\vartheta d\varphi^2). \tag{2.1}$$

Inside the star, the functions ν and μ_2 can be determined by solving the Einstein equations coupled to the equations of hydrostatic equilibrium. We shall assume that the star is composed by a perfect fluid, whose energy-momentum tensor is given by

$$T^{\alpha\beta} = (p + \epsilon)u^\alpha u^\beta - pg^{\alpha\beta}, \tag{2.2}$$

where p and ϵ are respectively the pressure and the energy density, that are assumed to have an isotropical distribution, and u^α is the four-velocity of the fluid. By defining the mass contained inside a sphere of radius r as

$$m(r) = \int_0^r \varepsilon r^2 dr, \tag{2.3}$$

the relevant equations are

$$\nu_{,r} = -\frac{p_{,r}}{p+\epsilon}, \tag{2.4}$$

$$\left(1 - \frac{2m(r)}{r}\right) p_{,r} = -(\varepsilon + p)\left(pr + \frac{m(r)}{r^2}\right), \tag{2.5}$$

$$\text{and} \qquad e^{2\mu_2} = \left(1 - \frac{2m(r)}{r}\right)^{-1}. \tag{2.6}$$

When the equation of state of the fluid is specified, eqs. (2.3) and (2.5) can be solved numerically and the distribution of pressure and energy-density throughout the star can be determined. Furthermore, equation (2.4) can be integrated to give

$$\nu = -\int_0^r \frac{p_{,r}}{(\epsilon + p)} dr + \nu_0. \tag{2.7}$$

The constant ν_0 is fixed by the condition that at the boundary of the star, $r = R$, the metric reduces to the Schwarzschild metric

$$(e^{2\nu})_{r=R} = (e^{-2\mu_2})_{r=R} = 1 - 2M/R, \tag{2.8}$$

where $M = m(R)$ is the total mass.

Outside the star the metric has the standard Schwarzschild form:

$$ds^2 = \left(1 - \frac{2M}{r}\right) dt^2 - \left(1 - \frac{2M}{r}\right)^{-1} dr^2 - r^2(d\vartheta^2 + \sin^2\vartheta d\varphi^2). \tag{2.9}$$

2.2 Perturbing the equilibrium configuration

2.2.1 Polar perturbations

Let us consider first the polar, nonaxisymmetric perturbations of a spherically symmetric star, excited by a particle is in circular orbit. The gauge appropriate for the description of these perturbations can be written in the following form [33]

$$\begin{aligned} ds^2 &= e^{2\nu(r)}dt^2 - e^{2\mu_2(r)}dr^2 - r^2 d\vartheta^2 - r^2\sin^2\vartheta d\varphi^2 \\ &+ \sum_{lm}\int_{-\infty}^{+\infty} d\omega\, e^{-i\omega t}\Bigg\{ 2\left[e^{2\nu}N_{\ell m}(t,r)dt^2 - e^{2\mu_2}L_{\ell m}(t,r)dr^2\right]Y_{\ell m}(\vartheta,\varphi) \\ &- 2r^2\left[T_{\ell m}(t,r) + V_{\ell m}(t,r)\frac{\partial^2}{\partial\vartheta^2}\right]Y_{\ell m}(\vartheta,\varphi)d\vartheta^2 \\ &- 2r^2\sin^2\vartheta\left[T_{\ell m}(t,r) + V_{\ell m}(t,r)\left(\frac{1}{\sin^2\vartheta}\frac{\partial^2}{\partial\varphi^2} + \cot\vartheta\frac{\partial}{\partial\vartheta}\right)\right]Y_{\ell m}(\vartheta,\varphi)d\varphi^2 \\ &- 2r^2 V_{\ell m}(t,r)2\left[\frac{\partial^2}{\partial\varphi\partial\vartheta} - \cot\vartheta\frac{\partial}{\partial\varphi}\right]Y_{\ell m}(\vartheta,\varphi)d\vartheta d\varphi\Bigg\}, \end{aligned} \tag{2.10}$$

where $Y_{lm}(\vartheta,\varphi)$ are the scalar spherical harmonics, and the functions $N_{\ell m}(\omega,r)$, $T_{\ell m}(\omega,r)$, $V_{\ell m}(\omega,r)$, $L_{\ell m}(\omega,r)$ describe the perturbed metric. The metric functions $\nu(r)$ and $\mu_2(r)$ describe the unperturbed spacetime and are determined by numerically integrating the TOV equations for hydrostatic equilibrium for the chosed equation of state. The radial functions $[N,T,V,L]$ have to be found by solving the perturbed Einstein equations outside the star, and inside, where they couple to the hydrodynamical equations.

When a star is perturbed, each fluid element suffers an infinitesimal displacement from its equilibrium position, identified by the lagrangian displacement $\vec{\xi}$. If we write the Einstein equations, the hydrodynamical equations and the conservation of baryon number (see [17], §§4 and 11) we find that they decouple into two sets: the *polar equations*, involving the variables $[N,T,V,L]$ and the lagrangian displacement $\vec{\xi}$, and the *axial equations*, involving the off-diagonal perturbations of the metric.

We shall assume that the perturbations take place adiabatically, i.e., that the changes in the pressure and energy-density arise without dissipation.

The equations which describe the polar perturbations are the Einstein equations, the hydrodynamical equations, and the conservation of baryon number. We shall omit the explicit derivation of these equations, which can be found in the original papers. Here we only remark that the angular part of the relevant equations can be separated by performing an expansion of the equations in tensorial spherical harmonics. After the separation, we are left with a system of coupled equations involving the following variables: $N(r), L(r), T(r), V(r)$, which describe the radial part of the perturbation of the metric, and $U(r)$, $W(r)$, $\Pi(r)$, $E(r)$, which describe the radial part of the perturbation of the fluid. The resulting equations are:

$$\left[\frac{d}{dr} + \left(\frac{1}{r} - \nu_{,r}\right)\right](2T - kV) - \frac{2}{r}L = -U, \tag{2.11}$$

$$(T - V + N)_{,r} - \left(\frac{1}{r} - \nu_{,r}\right)N - \left(\frac{1}{r} + \nu_{,r}\right)L = 0, \tag{2.12}$$

$$\frac{1}{2}e^{-2\mu_2}\left[\frac{2}{r}N_{,r}+\left(\frac{1}{r}+\nu_{,r}\right)(2T-kV)_{,r}-\frac{2}{r}\left(\frac{1}{r}+2\nu_{,r}\right)L\right]+$$
$$\frac{1}{2}\left[-\frac{1}{r^2}(2nT+kN)+\omega^2e^{-2\nu}(2T-kV)\right] = \Pi, \tag{2.13}$$

$$V_{,r,r}+\left(\frac{2}{r}+\nu_{,r}-\mu_{2,r}\right)V_{,r}+\frac{e^{2\mu_2}}{r^2}(N+L)+\omega^2e^{2\mu_2-2\nu}V = 0, \tag{2.14}$$

$$W = -(T-V+L), \tag{2.15}$$

$$\Pi = -\frac{1}{2}\omega^2e^{-2\nu}W-(\epsilon+p)N, \tag{2.16}$$

$$U = \frac{[\frac{1}{2}(\omega^2e^{-2\nu}W)_{,r}+(Q+1)\nu_{,r}\frac{1}{2}(\omega^2e^{-2\nu}W)+(\epsilon_{,r}-Qp_{,r})N]}{\frac{1}{2}\left[\omega^2e^{-2\nu}+\frac{e^{-2\mu_2}\nu_{,r}}{\epsilon+p}(\epsilon_{,r}-Qp_{,r})\right]}, \tag{2.17}$$

$$E = Q\Pi+\frac{e^{-2\mu_2}}{2(\epsilon+p)}(\epsilon_{,r}-Qp_{,r})U, \tag{2.18}$$

where

$$k=\ell(\ell+1), \qquad 2n=(\ell-1)(\ell+2)=k-2, \qquad Q=\frac{(\epsilon+p)}{\gamma p}, \tag{2.19}$$

and

$$\gamma\equiv\frac{(\epsilon+p)}{p}\left(\frac{\partial p}{\partial\epsilon}\right)_s \tag{2.20}$$

is the adiabatic exponent (the derivative being taken at constant entropy s).

For *barotropic* stars, the equation of state is assumed to be of the form:

$$p=p(\epsilon), \tag{2.21}$$

so the adiabatic exponent is simply

$$\gamma=\frac{(\epsilon+p)}{p}\left(\frac{\partial p}{\partial\epsilon}\right) \tag{2.22}$$

and Q reduces to:

$$Q=\frac{\epsilon_{,r}}{p_{,r}}. \tag{2.23}$$

While neutron stars and white dwarfs are typically well described by a barotropic equation of state, such an approximation does not hold for "ordinary", Newtonian stars. In this case we can write U, according to (2.17), as:

$$U=\frac{A}{A+B}\left[W_{,r}+(Q-1)\nu_{,r}W\right]+\frac{(\epsilon_{,r}-Qp_{,r})}{A+B}N \tag{2.24}$$

where we have defined

$$A\equiv\frac{1}{2}\omega^2e^{-2\nu}, \qquad B\equiv\frac{e^{-2\mu_2}\nu_{,r}}{2(\epsilon+p)}(\epsilon_{,r}-Qp_{,r}). \tag{2.25}$$

The system (2.11)-(2.14) turns out to be linearly dependent at the origin. To circumvent this linear dependence we will replace the variable T by a new variable G, defined as:

$$\begin{aligned} G &\equiv \nu_{,r}\left[(N+X)_{,r}+\nu_{,r}(N-L)\right]+\frac{1}{r^2}(e^{2\mu_2}-1) \\ &+ \frac{1}{r^2}(e^{2\mu_2}-1)\left[(n+1)N-n(L+W)+X\right]-e^{2\mu_2}(\epsilon+p)N+\omega^2 e^{2(\mu_2-\nu)}\left[L+X+\frac{1}{2}W\right] \end{aligned} \tag{2.26}$$

where $X \equiv nV$. In this way one gets the following set of equations:

$$X_{,r,r}+\left(\frac{2}{r}+\nu_{,r}-\mu_{2,r}\right)X_{,r}+\frac{n}{r^2}e^{2\mu_2}(N+L)+\omega^2 e^{2(\mu_2-\nu)}X=0, \tag{2.27}$$

$$(r^2G)_{,r}=n\nu_{,r}(N-L)+\frac{n}{r}(e^{2\mu_2}-1)(N+L)+r(\nu_{,r}-\mu_{2,r})X_{,r}+\omega^2 e^{2(\mu_2-\nu)}rX\ , \tag{2.28}$$

$$\begin{aligned} -\nu_{,r}N_{,r} &= -G+\nu_{,r}[X_{,r}+\nu_{,r}(N-L)]+\frac{1}{r^2}(e^{2\mu_2}-1)(N-rX_{,r}-r^2G) \\ &-e^{2\mu_2}(\epsilon+p)N+\frac{1}{2}\omega^2 e^{2(\mu_2-\nu)}\left\{N+L+\frac{r^2}{n}G+\frac{1}{n}[rX_{,r}+(2n+1)X]\right\}, \end{aligned} \tag{2.29}$$

$$\begin{aligned} L_{,r}(1-D) &+ L\left[\left(\frac{2}{r}-\nu_{,r}\right)-\left(\frac{1}{r}+\nu_{,r}\right)D\right]+X_{,r}+X\left(\frac{1}{r}-\nu_{,r}\right)+DN_{,r} \\ &+ N\left(D\nu_{,r}-\frac{D}{r}-F\right)+\left(\frac{1}{r}+E\nu_{,r}\right)\left[N-L+\frac{r^2}{n}G+\frac{1}{n}\left(rX_{,r}+X\right)\right]=0\ . \end{aligned} \tag{2.30}$$

where

$$D=1-\frac{A}{2(A+B)}, \qquad E=D(Q-1)-Q, \qquad F=\frac{\epsilon_{,r}-Qp_{,r}}{2(A+B)}\ . \tag{2.31}$$

Outside the star the variables related to the fluid, Π and U, vanish and the system of equations (2.11)-(2.14) can be reduced to a single Schrödinger equation, the Zerilli equation ([90], [91]):

$$\left(\frac{d^2}{dr_*^2}+\omega^2\right)Z_{\ell m}=V\,Z_{\ell m}, \tag{2.32}$$

where the potential is given by

$$V(r)=\frac{2(r-2M)}{r^4(nr+3M)^2}[n^2(n+1)r^3+3Mn^2r^2+9M^2nr+9M^3]\ . \tag{2.33}$$

The radial variable r_* is the usual "tortoise" coordinate

$$r_*\equiv r+2M\log\left(\frac{r}{2M}-1\right). \tag{2.34}$$

We show in Appendix B that we can integrate two independent solutions of eqs. (2.27)-(2.30) for the metric perturbations, with initial conditions in $r=0$ given by the requirement that the perturbation functions be regular at the center, and obtain the general solution by a linear combination of these two solutions chosen in such a way that, at the boundary ($r=R$), the

lagrangian perturbation of the pressure is zero. A more detailed description of the integration procedure used inside the star is given in Appendix B. Once we know, from this numerical integration, the values of X, L, $X_{,r}$ and $L_{,r}$ at $r = R$, we can construct the functions $Z(R)$ and $Z_{,r_*}(R)$ through the relations

$$\begin{aligned} Z(r=R) &= \left[\frac{r}{nr+3M}\left(\frac{3M}{n}X - rL\right)\right]\Big|_{r=R} \\ Z_{,r_\star}(r=R) &= \left(1-\frac{2M}{R}\right)\left[\frac{r}{nr+3M}\left(\frac{3M}{n}X - rL\right)\right]\Big|_{r=R} \end{aligned} \tag{2.35}$$

When a particle of mass $m_0 \ll M$ orbits the star, the Zerilli equation has to be modified to include a source term $S_{\ell m}$:

$$\left(\frac{d^2}{dr_\star^2} + \omega^2 - V_\ell\right) Z_{\ell m} = S_{\ell m}. \tag{2.36}$$

This source term, in the Chandrasekhar-Ferrari gauge (see Appendix C for a derivation), is given by:

$$\begin{aligned} S_{\ell m} &= \frac{M(r-2M)[(n+3)r-3M]}{r(nr+3M)^2}\frac{8\pi}{\omega\sqrt{2}}A^{(1)}_{\ell m} + \frac{(r-2M)^2}{2(nr+3M)}\frac{8\pi}{\omega\sqrt{2}}A^{(1)}_{\ell m,r} + \\ &+ \frac{(r-2M)^2}{2(nr+3M)}8\pi A_{\ell m} + \frac{(r-2M)^2}{nr+3M}\frac{8\pi}{\sqrt{2\ell(\ell+1)}}B_{\ell m} - \\ &- \frac{16\pi(r-2M)}{\sqrt{2\ell(\ell+1)(\ell-1)(\ell+2)}}F_{\ell m} - \frac{r(r-2M)^2}{nr+3M}\frac{8\pi}{\omega\sqrt{2\ell(\ell+1)}}B^{(0)}_{\ell m,rr} - \\ &- \frac{(r-2M)(3nr^2+15Mr-4Mnr-24M^2)}{(nr+3M)^2}\frac{8\pi}{\omega\sqrt{2\ell(\ell+1)}}B^{(0)}_{\ell m,r} + \\ &+ \left\{\frac{(r-2M)(n^2r^2-3Mnr-12Mr+12M^2)}{r(nr+3M)^2} - \frac{\omega^2 r^3}{nr+3M}\right\}\frac{8\pi}{\omega\sqrt{2\ell(\ell+1)}}B^{(0)}_{\ell m}. \end{aligned} \tag{2.37}$$

The notation for the tensor spherical harmonic coefficients used here is the same as in formula (1.12), and since we are working in the frequency domain we omit, for ease of notation, a tilde (meaning "Fourier transform") over each of the coefficients.

2.2.2 Axial perturbations

The axial, perturbed line element can be written as

$$\begin{aligned} ds^2 &= e^{2\nu}dt^2 - e^{2\mu_2}dr^2 - r^2 d\vartheta^2 - r^2\sin^2\vartheta d\varphi^2 \\ &+ 2h^0_{\ell m}(t,r)\sin\vartheta Y_{\ell m,\vartheta}(\vartheta,\varphi)dtd\varphi \\ &+ 2h^1_{\ell m}(t,r)\sin\vartheta Y_{\ell m,\vartheta}(\vartheta,\varphi)drd\varphi \\ &- im2h^0_{\ell m}(t,r)\frac{1}{\sin\vartheta}Y_{\ell m}(\vartheta,\varphi)dtd\vartheta - im2h^1_{\ell m}(t,r)\frac{1}{\sin\vartheta}Y_{\ell m}(\vartheta,\varphi)drd\vartheta. \end{aligned} \tag{2.38}$$

The equations for the axial perturbation can be combined into a single wave equation by introducing a function $Z^{ax}_{lm}(\omega, r)$ related to the axial functions by the following equations

$$h^0_{lm} = -\frac{i}{\omega}\frac{d}{dr_*}\left(rZ^{ax}_{lm}\right), \qquad h^1_{lm} = -e^{-2\nu}\left(rZ^{ax}_{lm}\right), \tag{2.39}$$

where $r_* = \int_0^r e^{-\nu+\mu_2}dr$. The function $Z^{ax}_{\ell m}(\omega, r)$ satisfies a wave equation (cfr. [17], Eqs. 148-149) whose potential depends on the distribution of energy and pressure inside the star:

$$\frac{d^2Z^{ax}_{\ell m}}{dr_*^2} + \left\{\omega^2 - \frac{e^{2\nu}}{r^3}\left[\ell(\ell+1)r + r^3(\epsilon - p) - 6m(r)\right]\right\}Z^{ax}_{\ell m} = 0. \tag{2.40}$$

Outside the star, where $\epsilon = p = 0$, the axial wave equation (2.40) reduces to the Regge-Wheeler equation with source

$$\frac{d^2Z^{ax}_{\ell m}}{dr_*^2} + [\omega^2 - V^{ax}]Z^{ax}_{\ell m} = S^{ax}_{\ell m}, \tag{2.41}$$

where the Regge-Wheeler potential is

$$V^{ax} = \frac{e^{2\nu}}{r^3}\left[\ell(\ell+1)r - 6M\right]. \tag{2.42}$$

If a particle orbits the star, the equation must be modified including a source which is given by (see Appendix C for a derivation)

$$S^{ax}_{\ell m} = \frac{16\pi i}{\sqrt{2}\sqrt{\ell(\ell-1)(\ell+1)(\ell+2)}}\frac{e^{2\nu}}{r}\left[r^2\left(e^{2\nu}D_{\ell m}\right)_{,r} - \sqrt{(\ell-1)(\ell+2)}re^{2\nu}Q_{\ell m}\right]. \tag{2.43}$$

In the axial case the matching between the interior and exterior solutions is trivial, since the value of the Regge-Wheeler function at the border can be obtained through a straightforward integration from $r = 0$ of equation (2.40). The expansions required to start the integration in $r = 0$ are given in Appendix B.

Chapter 3

Gravitational wave emission by extrasolar planetary systems

In this chapter we will apply the formalism developed in the preceding chapters to compute the radiation emitted by extrasolar planetary systems (EPS's). As we said in the introduction, we shall loosely call "extrasolar planetary systems" both systems composed of a solar-type star and a planet, and systems composed of a solar-type star and a brown dwarf.

In section 3.1 we will list the parameters of some of the EPS's discovered up to now, as they were deduced from observations. Then, in section 3.2, we will compute the gravitational signal emitted by each couple star-planet due to the orbital motion, using the quadrupole formalism. After this rough estimate, in section 3.3 we will turn our attention to an interesting mechanism of gravitational-wave emission, not directly related to the orbital motion of the system: the excitation of the oscillation modes of the star by tidal interactions with the orbiting planet. Motivated by observations, which have shown that a surprisingly large fraction of the observed planets are in close, nearly circular orbits, we have considered the possibility for a planet to get sufficiently close to the central star to excite the lowest order g-modes, and possibly the fundamental one, without being disrupted by tidal forces or melted by the central star. We will show in sections 3.4 and 3.5 that for solar type stars the resonant excitation of the low-order g-modes may, in principle, be possible. When the planet is close enough to a resonance, the power lost by the system in gravitational waves can be large, and the orbit tends to shrink more rapidly due to this energy loss. In section 3.6 we will include gravitational radiation reaction effects to understand how fast the orbit evolves. In this way, we will obtain typical timescales for a planet to get off-resonance, or, equivalently, estimates on how long the amplitude of the emitted wave can go beyond some fixed observability threshold.

The main result of our analysis is that systems composed of a solar-type star and a brown dwarf in resonant conditions could, at least potentially, be detectable by the spaceborn interferometer LISA, that has been approved by NASA and should fly in a few years.

3.1 Main characteristics of the extrasolar planetary systems

Among the EPS's discovered up to now, we have selected those for which the parameters of the central star and of the planets, which we need to estimate the gravitational emission, have been determined with sufficient accuracy. These parameters are tabulated in table 3.1 and 3.2.

Table 3.1: The spectral class of the central star, its mass, M, its distance from Earth, D, the factor $\sqrt{\frac{GM}{R_s^3}}$ (rad·s^{-1}), and the ratio between the lower limit of the estimated mass of the planet, $m_0 \sin i$, and M, are tabulated for a selected set of EPS's. Strictly speaking, the bodies orbiting the stars listed below HD 114762 are classified as brown dwarfs rather than as planets.

Star	Spectral Cl.	$M_*(M_\odot)$	D (pc)	$\sqrt{\frac{GM}{R_s^3}} \cdot 10^4$	$m_0 \sin i/M_\star$
HD 75289[92]	G0 V	1.05	28.94	5.4	$3.8 \cdot 10^{-4}$
51 Peg[36]	G5 V	1.05 ± 0.09	15.36	5.1 ± 0.7	$4.2 \cdot 10^{-4}$
υ And[36]	F8 V	1.34 ± 0.12	13.47	3.7 ± 0.5	$5.3 \cdot 10^{-4}$
					$1.5 \cdot 10^{-3}$
					$3.3 \cdot 10^{-3}$
55 Cnc[36]	G8 V	0.95 ± 0.10	12.53	6.6 ± 1.0	$8.8 \cdot 10^{-4}$
ρ CrB[36]	G2 V	0.89 ± 0.05	17.43	3.8 ± 0.5	$1.1 \cdot 10^{-3}$
HD 210277[54]	G0 V	0.92	21.29	5.0	$1.3 \cdot 10^{-3}$
16 Cyg B[36]	G5 V	0.96 ± 0.05	21.62	5.0 ± 0.6	$2.0 \cdot 10^{-3}$
Gl 876[76]	M4 V	0.3	4.70	13	$6.7 \cdot 10^{-3}$
47 Uma[36]	G0 V	1.01 ± 0.05	14.08	4.5 ± 0.5	$2.2 \cdot 10^{-3}$
14 Her[54]	K0 V	0.8	18.15	8.0	$3.9 \cdot 10^{-3}$
Gl 86[54]	K1 V	0.79	10.91	8.0	$4.4 \cdot 10^{-3}$
τ Boo[36]	F7 V	1.37 ± 0.09	15.60	4.7 ± 0.6	$3.3 \cdot 10^{-3}$
HD 168443[54]	G5 V	0.94	37.88	7.2	$5.1 \cdot 10^{-3}$
70 Vir[36]	G5 V	1.01 ± 0.05	18.11	2.5 ± 0.2	$6.9 \cdot 10^{-3}$
HD 114762[36]	F9 V	0.75 ± 0.15	40.57	4.0 ± 1.0	$1.3 \cdot 10^{-2}$
HD 110833[56]	K3 V	0.75	17	8.2	$2.2 \cdot 10^{-2}$
HD 112758[56]	K0 V	0.8	16.5	8.0	$4.2 \cdot 10^{-2}$
HD 29587[56]	G2 V	1.0	45	6.1	$3.8 \cdot 10^{-2}$
HD 283750[76]	K2 V	0.75	16.5	8.4	$6.4 \cdot 10^{-2}$
HD 89707[30]	G1 V	1.2	25	6.1	$5.0 \cdot 10^{-2}$
HD 217580[56]	K4 V	0.7	18	9.1	$8.2 \cdot 10^{-2}$

Here and in the following, data will be given with the corresponding errors, when available in the literature. In the first column of table 3.1 we list the selected EPS's with the corresponding bibliography, and in column 2 the spectral class of the central stars. Most of them belong to a class similar to that of the Sun, which is a G2 V star. In column 3, 4 and 5 we tabulate, respectively, the mass of the central star, M, its distance from Earth, D, - taken from the *Extrasolar Planets Catalog* [76]- and the quantity $\sqrt{\frac{GM}{R_s^3}}$, which will be needed in the following. In most cases the presence of planets has been discovered by using accelerometric techniques, that is to say, by measuring the variations of the radial velocity of the star caused by its gravitational interaction with the planet. These techniques do not allow to determine the mass of the planet, m_0, but only the product $m_0 \sin i$, where i is the angle between the line of sight and the normal

to the orbital plane. In column 6 we list the values $m_0 \sin i$ for each planet, normalized to the mass of the central star. From the data in table 3.1 we see that the closest system is at 4.70 pc, the farthest at 45 pc, whereas the mass of the central star ranges within $[0.3, 1.37]\ M_\odot$.

Table 3.2: Orbital parameters of the planets orbiting around the stars listed in table 3.1 (1 AU = $1.495978706 \cdot 10^{13}$ cm).

Star	P	a (AU)	e
HD 75289	$3.5103 \pm 0.023\ d$	0.046	0.054 ± 0.026
51 Peg	$4.2293 \pm 0.0011\ d$	0.0520 ± 0.0015	0.012 ± 0.01
υ And	$4.6170 \pm 0.0003\ d$	0.598 ± 0.018	0.109 ± 0.04
	$241.2 \pm 1.1\ d$	0.83	0.18 ± 0.11
	$1266.6 \pm 30\ d$	2.50	0.41 ± 0.11
55 Cnc	$14.648 \pm 0.0009\ d$	0.1152 ± 0.0038	0.051 ± 0.13
ρ CrB	$39.645 \pm 0.088\ d$	0.2192 ± 0.0042	0.15 ± 0.03
HD 210277	$437 \pm 25\ d$	1.097	0.45 ± 0.08
16 Cyg B	$804 \pm 11.7\ d$	1.66 ± 0.05	0.634 ± 0.082
Gl 876	$60.85 \pm 0.15\ d$	0.21 ± 0.01	0.27 ± 0.03
47 Uma	$3.0\ y$	2.08 ± 0.06	0.03 ± 0.06
14 Her	$1619 \pm 70\ d$	2.5	0.3537 ± 0.088
Gl 86	$15.83\ d$	0.11	0.05
τ Boo	$3.3128 \pm 0.0002\ d$	0.0413 ± 0.001	0.018 ± 0.016
HD 168443	$57.9\ d$	0.277	0.54
70 Vir	$116.6 \pm 0.01\ d$	0.47 ± 0.01	0.4 ± 0.01
HD 114762	$85.03 \pm 0.08; d$	0.34 ± 0.04	0.35 ± 0.05
HD 110833	$270.04\ d$	0.8	0.69
HD 112758	$103.22\ d$	0.35	0.16
HD 29587	$3.17\ y$	2.5	0
HD 283750	$1.79\ d$	0.04	0.02
HD 89707	$298.48\ d$	0.91	0.93
HD 217580	$456.44\ d$	1	0.52

In table 3.2 we tabulate the orbital parameters of the planets orbiting around the stars listed in table 3.1, i.e. the orbital period P, the semimajor axis a, and the eccentricity e. From the data in column 2 we see that in some cases the period is very short, that is, the planet gets very close to the central star: for instance, the period can be as short as 1.79 days for the planet orbiting around HD 283750. It is important to note that short-period systems, which are the most interesting from the point of view of gravitational wave detection, are typically in circular or almost circular orbits.

3.2 Gravitational wave emission according to the Newtonian quadrupole formula

The Newtonian quadrupole formalism has been applied to compute, according to formula (1.48), the characteristic wave amplitude h_c impinging on Earth, emitted by the set of EPS's considered in the previous paragraph and, for comparison, by the binary system PSR 1913+16

Table 3.3: The maximum characteristic amplitude of the waves emitted by the selected set of EPS's and by the binary system PSR 1913+16, due to their orbital motion.

Star	$\nu_k\ (Hz)$	$h_{c\ max}$	$\nu_{max}\ (Hz)$
HD 75289	$3.3 \cdot 10^{-6}$	$2.1 \cdot 10^{-25}$	$6.6 \cdot 10^{-6}$
51 Peg	$2.8 \cdot 10^{-6}$	$4.0 \cdot 10^{-25}$	$5.5 \cdot 10^{-6}$
υ And	$2.5 \cdot 10^{-6}$	$7.9 \cdot 10^{-26}$	$5.0 \cdot 10^{-6}$
55 Cnc	$7.9 \cdot 10^{-7}$	$3.8 \cdot 10^{-25}$	$1.6 \cdot 10^{-6}$
ρ CrB	$2.9 \cdot 10^{-7}$	$1.5 \cdot 10^{-25}$	$5.8 \cdot 10^{-7}$
HD 210277	$2.6 \cdot 10^{-8}$	$1.9 \cdot 10^{-26}$	$7.9 \cdot 10^{-8}$
16 Cyg B	$1.4 \cdot 10^{-8}$	$1.6 \cdot 10^{-26}$	$5.8 \cdot 10^{-8}$
Gl 876	$1.9 \cdot 10^{-7}$	$3.5 \cdot 10^{-25}$	$3.8 \cdot 10^{-7}$
47 Uma	$1.1 \cdot 10^{-8}$	$5.3 \cdot 10^{-26}$	$2.1 \cdot 10^{-8}$
14 Her	$7.1 \cdot 10^{-9}$	$2.7 \cdot 10^{-26}$	$1.4 \cdot 10^{-8}$
Gl 86	$7.3 \cdot 10^{-7}$	$1.6 \cdot 10^{-24}$	$1.5 \cdot 10^{-6}$
τ Boo	$3.5 \cdot 10^{-6}$	$6.6 \cdot 10^{-24}$	$7.0 \cdot 10^{-6}$
HD 168443	$2.0 \cdot 10^{-7}$	$1.6 \cdot 10^{-25}$	$6.0 \cdot 10^{-7}$
70 Vir	$9.9 \cdot 10^{-8}$	$3.6 \cdot 10^{-25}$	$2.0 \cdot 10^{-7}$
HD 114762	$1.4 \cdot 10^{-7}$	$2.0 \cdot 10^{-25}$	$2.7 \cdot 10^{-7}$
HD 110833	$4.3 \cdot 10^{-8}$	$2.6 \cdot 10^{-25}$	$2.1 \cdot 10^{-7}$
HD 112758	$1.1 \cdot 10^{-7}$	$3.0 \cdot 10^{-24}$	$2.2 \cdot 10^{-7}$
HD 29587	$1.0 \cdot 10^{-8}$	$2.3 \cdot 10^{-25}$	$2.0 \cdot 10^{-8}$
HD 283750	$6.5 \cdot 10^{-6}$	$3.7 \cdot 10^{-23}$	$1.3 \cdot 10^{-5}$
HD 89707	$3.9 \cdot 10^{-8}$	$8.4 \cdot 10^{-25}$	$3.9 \cdot 10^{-8}$
HD 217580	$2.5 \cdot 10^{-8}$	$8.5 \cdot 10^{-25}$	$7.6 \cdot 10^{-8}$
PSR 1913+16	$3.6 \cdot 10^{-5}$	$1.0 \cdot 10^{-23}$	$1.4 \cdot 10^{-4}$

([42],[81],[86]). Some results are shown in figure 1, where h_c is plotted as a function of the harmonic index n. It should be reminded that PSR 1913+16 is composed of two very compact stars with masses $m_1 = 1.4411\ M_\odot$ and $m_2 = 1.3874\ M_\odot$, revolving around their center of mass in a quite eccentric orbit ($e = 0.617139$), with semimajor axis $a = 1.9490 \cdot 10^{12}$ cm, and keplerian frequency $\nu_k = 3.583 \cdot 10^{-5}$ Hz. The binary system is at a distance $D = 5$ kpc from Earth. In the upper panel of figure 1, we show two systems in which the planet moves in a nearly circular orbit around the central star, HD 283750 ($e = 0.02$) and τ Boo ($e = 0.018$). As expected, the emission is concentrated at twice the keplerian frequency, and the amplitude is comparable to the maximum wave amplitude reached by PSR 1913+16, which is shown for comparison at the bottom of the figure. However, the frequency is about ten times lower than that of the binary pulsar. In the lower panel we show the characteristic emission of two EPS's with high eccentricity, 16 Cyg B ($e = 0.634$) and HD 89707 ($e = 0.93$). In this case the gravitational emission is spread over a larger set of frequencies, all multiple of ν_k, as for PSR 1913+16.

In table 3.3 we give the keplerian frequency, the maximum characteristic amplitude on Earth, and the frequency corresponding to that maximum, for each EPS. In the last row the same data are listed for PSR 1913+16. For most systems the maximum emission frequency appears to be extremely low, in general smaller than 10^{-6} Hz. An exception is HD 283750, for which $\nu_{max} = 1.3 \cdot 10^{-5}$ Hz.

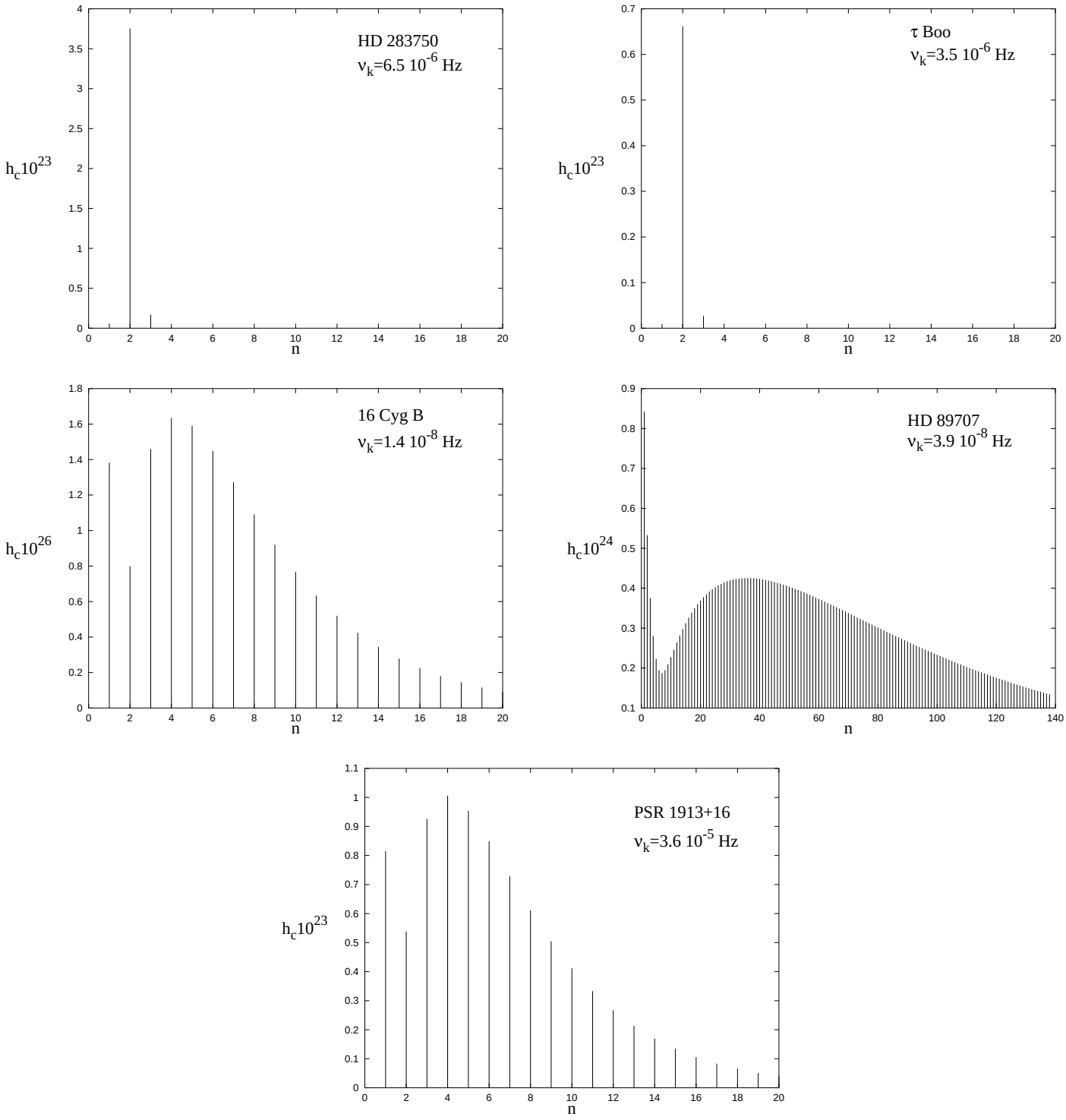

Figure 3.1: The characteristic amplitude computed from equation (1.48) is plotted versus the harmonic index n for four selected EPS's and for the binary system PSR 1913+16. For the two systems in the upper panel, HD 283750 and τ Boo, the planet moves on a nearly circular orbit, with $e = 0.02$ and $e = 0.018$, respectively. In this case the emission is concentrated at twice the keplerian frequency. The amplitude is comparable to the maximum wave amplitude emitted by the binary pulsar PSR 1913+16. In the lower part of the figure h_c is plotted for two systems with high eccentricity: 16 Cyg B ($e = 0.634$) and HD 89707 ($e = 0.93$), and for PSR 1913+16 ($e = 0.617$). The number of spectral lines (at frequencies multiple of ν_k) contributing to the signal increases with e.

3.3 Conditions for the excitation of stellar pulsations in an EPS

The numerical integration of the perturbed Einstein equations shows that a resonance occurs whenever the gravitational-wave frequency of a planet in circular orbit around a star is equal to the frequency of one of the quasi-normal modes of the star. Therefore, it is interesting to check whether the resonant excitation conditions can be fulfilled in the planetary systems listed in table 3.1. We shall first verify whether the maximum quadrupole emission frequency of the planets of our set of EPS's, ν_{max} (table 3.3, column 4) is close enough to any of the frequencies of the modes of the central star.

The oscillation frequencies of a star can be computed if we make an assumption on its internal structure, i.e. on the equation of state prevailing in the interior. We shall consider, as an example, a very simple, polytropic stellar model, with polytropic index $n = 2$. The oscillation frequencies of Newtonian polytropic stars are known to scale with the mean density of the star [24]. In table 3.4 we tabulate the dimensionless eigenfrequencies of the modes, $\nu_{mode}/(GM/R_s^3)^{1/2}$, for the chosen value of n. In order to explicitly compute the frequency of a given mode for a given star, the entries of table 3.4 have to be multiplied by the entries of table 3.1, column 5. For instance, for the star HD 89707 the frequency of the f-mode is given by $\nu = 0.28 \times 6.1 \cdot 10^{-4} = 1.7 \cdot 10^{-4}$ Hz. This number has to be compared whith $\nu_{max} = 3.9 \cdot 10^{-8}$ Hz, given in table 3.3 for the same star, which is much smaller. This means that the planet cannot excite the f-mode of the central star.

Table 3.4: The dimensionless eigenfrequencies of the modes of a polytropic stars are tabulated for the polytropic index $n = 2$.

mode	$\nu_{mode}/(GM/R_s^3)^{1/2}$	mode	$\nu_{mode}/(GM/R_s^3)^{1/2}$
p_{10}	2.58	f	0.28
p_9	2.37	g_1	0.119
p_8	2.15	g_2	0.087
p_7	1.93	g_3	0.068
p_6	1.70	g_4	0.056
p_5	1.47	g_5	0.048
p_4	1.24	g_6	0.042
p_3	1.01	g_7	0.037
p_2	0.78	g_8	0.033
p_1	0.54	g_9	0.030
		g_{10}	0.028

By repeating the same calculation for all systems and all modes, we find that it is unlikely that the stellar modes are excited in the EPS's we consider[1]. This is because the angular velocities reached by the planets are too low, and consequently the frequencies of the radiation they emit are lower than those of the f-mode or of the lowest-order g-modes of the star. Higher order g-modes could be excited, but the efficiency in producing gravitational radiation by this process would be too low.

[1]Of course, we also checked that the conditions for resonant excitation are not fulfilled for planets in our solar system.

Gravitational-wave frequencies of satellites in the solar system					
	Densities (g·cm^{-3}) and frequencies (Hz)				
	ρ	ρ/ρ_J	ν_f	ν_{sat}	$\nu_f/(2\nu_{sat})$
Moon *Earth*	5.49	4.43	$2.515 \cdot 10^{-4}$	$4.236 \cdot 10^{-7}$	297
M1 Phobos *Mars*	3.91	3.15	$2.121 \cdot 10^{-4}$	$3.629 \cdot 10^{-5}$	2.92
J14 Adrastea=J16 Metis *Jupiter*	1.24	1.00	$1.195 \cdot 10^{-4}$	$3.923 \cdot 10^{-5}$	1.52
S17 Atlas *Saturn*	0.62	0.50	$0.845 \cdot 10^{-4}$	$1.923 \cdot 10^{-5}$	2.20
U13 Cordelia *Uranus*	1.27	1.02	$1.209 \cdot 10^{-4}$	$3.455 \cdot 10^{-5}$	1.75
1989 N6 *Neptune*	1.61	1.30	$1.361 \cdot 10^{-4}$	$5.966 \cdot 10^{-6}$	11.4

Table 3.5: Average density ρ, ratio of the average density to the Jovian density, frequency of the $f-$mode, orbital frequency of the closest satellite(s) and $\nu_f/2\nu_{sat}$ for each planet in the solar system. The $f-$mode frequency ν_f is obtained by a rescaling of the corresponding frequency for Jupiter.

We also tried to understand how the gravitational-wave frequencies of *satellites* in our solar system compare with frequencies of the $f-$modes of the planets they orbit. To answer this question we used theoretical models of Jupiter available in the literature [51]. For definiteness, we chose model 1 in [51], corresponding to a non-rotating jovian model without a plasma phase transition, but this choice does not alter significantly our results. This model predicts for the $f-$mode a frequency $\nu_{f,J} = 119.5\ \mu$Hz. To give a rough estimate of the $f-$mode frequencies ν_f for the other planets in the solar system, we simply rescaled the $f-$mode of Jupiter with the various average planetary densities ρ:

$$\nu_f^2/\rho = \nu_{f,J}^2/\rho_J \qquad \Longrightarrow \qquad \nu_f = (\rho/\rho_J)^{1/2}\,\nu_{f,J} \tag{3.1}$$

The average density of the planets was calculated from the values of masses and radii in [50], while for Uranus we used the values measured by Voyager 2 and reported in [58] (p. 212).

For each planet, we compared the $f-$mode frequency obtained in this way with the gravitational wave frequency of its closest satellite (note that Jupiter has two close satellites, J14 Adrastea and J16 Metis, orbiting at a frequency which is the same within the experimental errors); the results are in table 3.5. The last column in the table is the ratio $\nu_f/2\nu_{sat}$ (which should be equal to 1 for the $f-$mode to be excited). In the best case, corresponding to the satellites of Jupiter, the ratio is 1.52: therefore, satellites in the solar system don't seem to be in resonant conditions with the $f-$mode of the planets they orbit.

3.4 Tidal disruption

We have just seen that the quasi-normal mode frequencies are higher than typical quadrupole emission frequencies in the EPS's discovered up to now. According to recent theories on the

evolution of planetary systems [36], there could exist planets moving on orbits even closer to the central star than those observed until now. These planets could happen to have quadrupole emission frequencies comparable to the quasi-normal mode frequencies, thus exciting the oscillation modes of the central star and enhancing the gravitational emission of the system.

That's why we tried to understand whether it is possible for a planet to approach a star at such a short distance that its angular velocity is high enough to excite the f-mode, or the lowest-order g-modes, without being disrupted by tidal forces. We also want to impose the additional condition that the star does not accrete matter onto the planet.

In this section we will show that these conditions are equivalent to impose that neither the planet nor the star overflow their *Roche lobe*. We would like to stress that this limit takes into account only the gravitational interaction between the planet and the star. There may exist other processes that would prevent the planet to reach the innermost orbit allowed by the Roche-lobe analysis, and we will consider one of them (namely, the effect of heating by the central star) in the following.

We shall assume, for simplicity, that the planet flies on a circular orbit with keplerian angular velocity ω_k and radius R_0, and consequently emits gravitational radiation at the frequency $\omega^{GW} = 2\omega_k$. Let us indicate the dimensionless frequency tabulated in table 3.4 multiplied by 2π as k_{mode}: for instance, $k_{g_1} = 0.750$. The keplerian frequency of the motion is given by:

$$\omega_k = \left[\frac{G\left(m_0 + M\right)}{R_0^3}\right]^{1/2} \tag{3.2}$$

The excitation condition for the g_i-mode is

$$\omega_{g_i} = 2\omega_k, \tag{3.3}$$

Since in Newtonian theory the frequencies of modes are known to scale with the mean density, we can define a constant k_{g_i} by the relation

$$\omega_{g_i} = \left[\frac{GM}{R_s^3} k_{g_i}\right]^{1/2}. \tag{3.4}$$

Formula (3.3) yields a relation between the orbital radius R_0 and the stellar radius R_s:

$$R_0 = \left(1 + \frac{m_0}{M}\right)^{1/3} \left(\frac{4}{k_{g_i}}\right)^{1/3} R_s \simeq \left(\frac{4}{k_{g_i}}\right)^{1/3} R_s. \tag{3.5}$$

Can a planet reach the orbital separation R_0 defined by formula (3.5), exciting the corresponding oscillation mode, without being broken apart by tidal forces and without accreting matter from the central star? The planet can bear tidal forces without being broken apart only if it lies within its Roche lobe. To define the Roche lobe, consider the reference frame corotating with the two masses, with origin in their center of mass. Let the $x - y$ plane coincide with the orbital plane, and let the $x-$axis coincide with the axis connecting the two masses, oriented from m_0 to M. In this reference frame, m_0 has coordinates $\mathbf{x_p} = (-a_p, 0)$, M has coordinates $\mathbf{x}_\star = (a_\star, 0)$ and $R_0 = a_p + a_\star$. Obviously:

$$a_p = \frac{M}{m_0 + M} R_0, \tag{3.6}$$

$$a_\star = \frac{m_0}{m_0 + M} R_0. \tag{3.7}$$

The Newtonian potential describing the interaction between the two masses and a test particle of mass $m \ll m_0 \leq M$ can be written, in this reference frame:

$$U(\mathbf{x}) = U(x,y) = -\frac{Gm_0}{|\mathbf{x}-\mathbf{x_p}|} - \frac{GM}{|\mathbf{x}-\mathbf{x}_\star|} - \frac{1}{2}\omega_k^2|\mathbf{x}|^2 \tag{3.8}$$

where the last term is the centrifugal potential. The test particle's energy is, of course, given by:

$$E = \frac{mv^2}{2} + mU(x,y) \tag{3.9}$$

The equipotential surfaces $U = E$, where the test particle's velocity $v = 0$, are called "Hill's surfaces", and lie between regions where the particle's motion is allowed ($v^2 > 0$, v real) and regions where it is forbidden. For large, negative values of E these surfaces have the shape of two spheroids, one centered on m_0 and the other on M. Within the spheroids the gravitational attraction of the planet (or of the star) dominates. As the energy grows, the spheroids deform, and finally they touch on the axis connecting the star and the planet. When they touch, the spheroids are called *Roche lobes*. For still larger values of the energy the spheroids join forming a single surface, and the orbits of a test particle can get close to each of the two masses. Clearly, a particle will not overcome the gravitational attraction of (say) the planet, only if it lies within its Roche lobe.

Consider the intersections of the equipotential surfaces with the $x-y$ plane. The curve corresponding to the Roche lobes is called the *first Lagrangian curve*. The equilibrium positions for the test particle are called *Lagrangian points*. It is reasonable to estimate the Roche radius R_{RL} of the planet, defined as the radius of the circle centered on m_0 and tangent to the first Lagrangian curve, as the minimum of the distances from this curve and m_0 along the $x-$ and $y-$ axes.

The condition for the excitation of the g_i-mode, for a fixed stellar model and a fixed planetary mass m_0, has to be compatible with the condition that the radius of the planet is less than the Roche radius, $R_p < R_{RL}$, and this translates into a limit on the average density:

$$\rho_p > \rho_{RL} \tag{3.10}$$

If we introduce the dimensionless quantity $\overline{R}_{RL}$, defined as:

$$R_{RL} = R_0\,\overline{R}_{RL} \tag{3.11}$$

from equation (3.5) it follows that:

$$R_{RL} = \left[\frac{4}{k_{g_i}}\left(1+\frac{m_0}{M}\right)\right]^{1/3}\overline{R}_{RL}R_s \simeq \left(\frac{4}{k_{g_i}}\right)^{1/3}\overline{R}_{RL}R_s \tag{3.12}$$

(the last equality holds if $m_0 \ll M$). Hence the planetary density ρ_p has to be greater than:

$$\rho_{RL} = m_0\left(\frac{4\pi R_{RL}^3}{3}\right)^{-1} = \frac{k_{g_i}m_0/M}{4\left(1+m_0/M\right)\overline{R}_{RL}^3}\rho_\star \simeq \frac{k_{g_i}m_0/M}{4\overline{R}_{RL}^3}\rho_\star \tag{3.13}$$

where, as before, the last equality holds if $m_0 \ll M$.

To compute numerically R_{RL} we have used the following method. Since on the orbital plane we have the following relations:

$$|\mathbf{x}-\mathbf{x_p}| = \left[(x+a_p)^2+y^2\right]^{1/2}$$
$$|\mathbf{x}-\mathbf{x}_\star| = \left[(x+a_\star)^2+y^2\right]^{1/2}$$

the potential along the $x-$axis is simply:

$$U(x,0) = -\frac{Gm_0}{|x+a_p|} - \frac{GM}{|x-a_\star|} - \frac{1}{2}\omega_k^2 x^2 \tag{3.14}$$

The function $U(x,0)$ has a maximum U_{RL} in the interval $(-a_p, a_\star)$, corresponding to the first Lagrangian point L_1. The value of the function at the maximum is also the value of the potential on the surface enclosing the Roche lobe. We find a second intersection between this surface and the $x-$axis (moving towards negative values of x) where $U(x,0)$ attains the value U_{RL}.

Analogously, moving along the parallel to the $y-$axis through m_0, we will cross the Roche lobe surface where the function

$$U(-a_p, y) = -\frac{Gm_0}{|y|} - \frac{GM}{(R_0^2+y^2)} - \frac{1}{2}\omega_k^2(a_p^2+y^2). \tag{3.15}$$

is equal to U_{RL}. The smaller value of the intersections obtained in this way is the value of the Roche radius. Once the Roche radius is known, we can compute the ratio between the "critical" Roche density and the stellar density, ρ_{RL}/ρ_*, for a fixed value of $m_0/M_\star$.

Table 3.6: Ratios of the critical density of the planet ρ_{RL} to the central star density ρ_* for different values of the mass ratio, m_0/M, and different oscillation modes of a polytropic star with $n = 2$ (see text).

	m_0/M					
	10^{-6}	10^{-5}	10^{-4}	10^{-3}	10^{-2}	10^{-1}
f	7.89	7.95	8.04	-	-	-
g_1	1.43	1.44	1.45	1.49	1.58	1.83
g_2	0.75	0.76	0.77	0.79	0.83	0.96
g_3	0.47	0.47	0.47	0.49	0.52	0.60
g_4	0.32	0.32	0.32	0.33	0.35	0.41
g_5	0.23	0.23	0.23	0.24	0.26	0.30
g_6	0.17	0.18	0.18	0.18	0.19	0.22
g_7	0.14	0.14	0.14	0.14	0.15	0.18
g_8	0.11	0.11	0.11	0.12	0.12	0.14
g_9	0.09	0.09	0.09	0.10	0.10	0.12
g_{10}	0.08	0.08	0.08	0.08	0.09	0.10

The results are shown in table 3.6, which has to be read as follows. Suppose that the ratio between the mass of a planet and that of the central star is $m_0/M = 10^{-3}$. The frequency of the quadrupole radiation emitted by the planet will coincide with that of the first g-mode of the star, and the planet will not be disrupted, only if its density is higher that $1.49\ \rho_\star$. We have also checked whether the star overflows its Roche lobe and accretes matter onto the planet, and excluded from table 3.6 the corresponding cases.

It should be reminded that the ratio between the mean density of the planets of the solar system and that of the Sun is 3.9 for Mercury and the Earth, 3.7 for Venus, 2.8 for Mars, 0.9 for Jupiter, etc. A comparison of these values with the data of table 3.6 suggests that, in principle, there can exist EPS's in which the low-order g-modes could be excited by a resonant process. For instance, a planet like the Earth could approach a polytropic star ($n = 2$) with the mass of the sun at a distance close enough to excite the g_1-mode without being disrupted by the tidal interaction, whereas a planet like Jupiter could only be at a distance good to excite the second g-mode.

By the Roche-lobe analysis we can also deduce another interesting information. Suppose that a planetary system made of a star with the mass of the Sun and a planet in circular orbit is located at a fiducial distance $D = 10$ pc. We do not make any assumption on the internal structure of the star, but assign the values of the mass and of the mean density of the planet. In particular, we consider five orbiting bodies: three of them have masses and densities equal to those of Mercury, the Earth, and Jupiter. The fourth has a mass equal to 13 times the mass of Jupiter (the deuterium burning limit; see, e.g., [75]) and the same density as Jupiter; the fourth is a brown dwarf of 40 jovian masses. We want to answer the following questions:

- what is the minimum radius of the orbit?
- what is the corresponding quadrupole emission frequency $\nu^{GW} = 2\nu_k$?
- what is the corresponding characteristic amplitude on Earth?

The answer is in table 3.7, where the required data are given for the four planets and the brown dwarf. Note that the minimum radius of the orbit, in the brown dwarf case, is determined by the condition of mass transfer *from* the central star: being the brown dwarf quite dense ([12]) mass accretion from the central star occurs before tidal disruption of the brown dwarf.

Table 3.7: We tabulate the minimum radius of the circular orbit, R_0^{min}, the quadrupole emission frequency, ν^{GW}, and the characteristic amplitude of the corresponding wave emitted by four planets orbiting around a star with mass $M_\odot$ and radius $R_\odot$. We assume that the planets have mass and density equal to those of Mercury, Earth and Jupiter. The last planet has 13 times the mass of Jupiter and the same density. The case of a brown dwarf of 40 jovian masses is also included. These data are obtained by imposing that the planets and the central stars lie inside their Roche lobe, and that the system is located at $D = 10$ pc from Earth.

Type of planet	R_0^{min} (cm)	$\nu^{GW} = 2\nu_k$	h_c
Mercury	$9.6 \cdot 10^{10}$	$1.2 \cdot 10^{-4}$	$1.8 \cdot 10^{-27}$
Earth	$9.6 \cdot 10^{10}$	$1.2 \cdot 10^{-4}$	$3.2 \cdot 10^{-26}$
Jupiter	$1.6 \cdot 10^{11}$	$5.9 \cdot 10^{-5}$	$6.2 \cdot 10^{-24}$
13×Jupiter	$1.6 \cdot 10^{11}$	$5.7 \cdot 10^{-5}$	$7.9 \cdot 10^{-23}$
Brown Dwarf	$1.0 \cdot 10^{11}$	$1.1 \cdot 10^{-4}$	$3.8 \cdot 10^{-22}$

From table 3.7 we see that some planets could emit quadrupole radiation at a frequency in the bandwidth of space interferometers, and with an amplitude which could be even ten times bigger than that emitted by the binary pulsar PSR 1913+16. In addition, if the quadrupole radiation resonates with a mode of the star, the amount of emitted energy could be even larger.

Before turning to quantitative estimates, based on the direct integration of the Einstein equations, of the enhancement in gravitational wave emission due to resonant effects, we want to discuss how effects of heating of the planet by the central star change the picture we have just discussed.

3.5 Temperature effects

Besides the tidal interaction with the central star, other, non-gravitational effects can affect the stability of a planet orbiting close to a solar-like star. The most important of these destabilizing effects is probably the possibility of a melting of the orbiting planet, due to heating by the central star. In this section we will carry out an analysis of these temperature effects valid for gaseous, Jupiter-like planets, based on the corresponding analysis in [41]. The limits posed by tidal and melting effects can be expressed as forbidden regions in an Hertzsprung-Russell (luminosity vs. temperature) diagram for the planet. Since the planet's temperature is related to its distance from the central star, for each given distance we can compare the destabilizing effects due to temperature to those due to tidal interactions. We will show that temperature effects are typically negligible, at least for a gaseous planet, with respect to the limits posed by the Roche-lobe condition.

Take a star of fixed mass and radius, M and R_s, and a planet on an orbit of radius R_0. The planetary mass and radius, m_0 and R_p, are also fixed. We shall suppose, for concreteness, that the planet has radius and mass corresponding to those of Jupiter, and is in a resonant condition with the $g_{10}-$mode. Knowing the stellar mass, we can compute the stellar luminosity from the known value $L_\odot = 3.827 \cdot 10^{33}$ erg/s using the mass-luminosity relationship for main-sequence stars:

$$L_\star \propto M^{3.5}. \tag{3.16}$$

The star's effective temperature, $T_\star$, can then be computed from:

$$L_\star = 4\pi R_s^2 \sigma T_\star^4, \tag{3.17}$$

where $\sigma = ac/4$, $a = 7.57 \cdot 10^{-15}$ erg cm^{-3} K^{-4} and c is the speed of light. Knowing $T_\star$ and $L_\star$, the planet's temperature T_p and luminosity L_p (at the orbital radius R_0) can be estimated from:

$$T_p = T_\star \left(\frac{R_s}{2R_0}\right)^{1/2} [f(1-A)]^{1/4}, \tag{3.18}$$

$$L_p = L_\star (1-A) \left(\frac{R_p}{2R_0}\right)^2, \tag{3.19}$$

assuming, for example, the albedo A to be the same as Jupiter's ($A = A_{Jup} = 0.35$). The factor f is 1 if the heat of the primary can be assumed to be evenly distributed over the planet, and 2 if only one side reradiates the absorbed heat. For a gas giant such as Jupiter, it can be taken equal to 1 [41].

From these formulas we see that there is a one-to-one relationship between the planet's orbital radius, R_0, and temperature, T_p. At each given R_0 (or, which is the same, at each given

T_p) we can compute the Roche-lobe radius R_{RL} using the methods described before, and the corresponding critical luminosity L_{RL}:

$$L_{RL} = L_\star(1-A)\left(\frac{R_{RL}}{2R_0}\right)^2 \tag{3.20}$$

Note that the luminosity, depending only on the ratio $R_{RL}/R_0 = \bar{R}_{RL}$, does *not* depend on the orbital radius: the critical line for tidal disruption in a temperature/luminosity (Hertzsprung-Russell) diagram is *horizontal*.

We shall now deal with the effects of stellar heating on the stability of the planetary atmosphere. At a given temperature, the gas in the stellar atmosphere can escape if the mean square velocity of the particles (hydrogen atoms) is greater than the escape velocity. This *classical Jeans escape flux* (see, e.g., [13]) can be shown to be proportional to the factor $e^{-\lambda}(\lambda+1)$, where

$$\lambda = \frac{Gm_H m_0}{kT_p R_p} \tag{3.21}$$

(m_H is the mass of an hydrogen atom). The Jeans escape mechanism becomes important (according to [41]) when $\lambda = \lambda_{crit} = 30$. Using formula (3.19), this means that the planetary atmosphere evaporates significantly when the luminosity is greater than a critical value, L_T, given by:

$$L_T = \left(\frac{Gm_H m_0}{2kT_p R_0 \lambda_{crit}}\right)^2 (1-A)L_\star. \tag{3.22}$$

Formulas (3.20) and (3.22) correspond to the anticipated instability limits in a Hertzsprung-Russell diagram for the planet due, respectively, to tidal effects and to the evaporation of the planetary atmosphere. We have explicitly computed the corresponding curves for a Jovian-like planet around the $n = 3$ polytropic stellar model considered before, choosing the central density in such a way that $M = M_\odot$ and $R_s = R_\odot$.

In figure 3.2 we plot the orbital radius, in AU, versus $\log(L_p/L_\odot)$. The plot clearly shows that tidal interactions are always more effective than evaporation in destabilizing a gaseous planet like Jupiter. For example, a jovian planet orbiting at a radius $R_0 = 1.08 \cdot 10^{-2}$ AU$=$ $1.61 \cdot 10^6$ km (corresponding to the mode g_{10}) would have a temperature $T_p = 2409$ K, and a luminosity such that $\log(L/L_\odot) = -3.494$. This value of the luminosity has to be compared with a critical "tidal" luminosity $\log(L_{RL}/L_\odot) = -3.486$ and with the even higher value $\log(L_T/L_\odot) = -2.547$.

From the previous discussion we can expect that temperature effects would be even less effective in the case of rocky planets such as the Earth, since the temperatures needed to melt a rock would almost surely be higher than those required for the evaporation of the atmosphere of a gaseous planet.

The discussion of melting effects for brown dwarfs is much more complicated. For simplicity, we assume that a brown dwarf orbits at a radius corresponding to the mode g_4, and that it has the same values of f and A as Jupiter. Then we get, for the temperature of a brown dwarf due to heating by the central star, a value $T_p = 3026$ K, which is much higher than the equilibrium temperature $T_e = 436$ K predicted by models of isolated, evolved, 40 jovian-masses brown dwarfs [12]. This means that dealing with the evaporation of the brown dwarf requires an understanding of the details of its atmosphere. These details are quite uncertain. Brown dwarfs

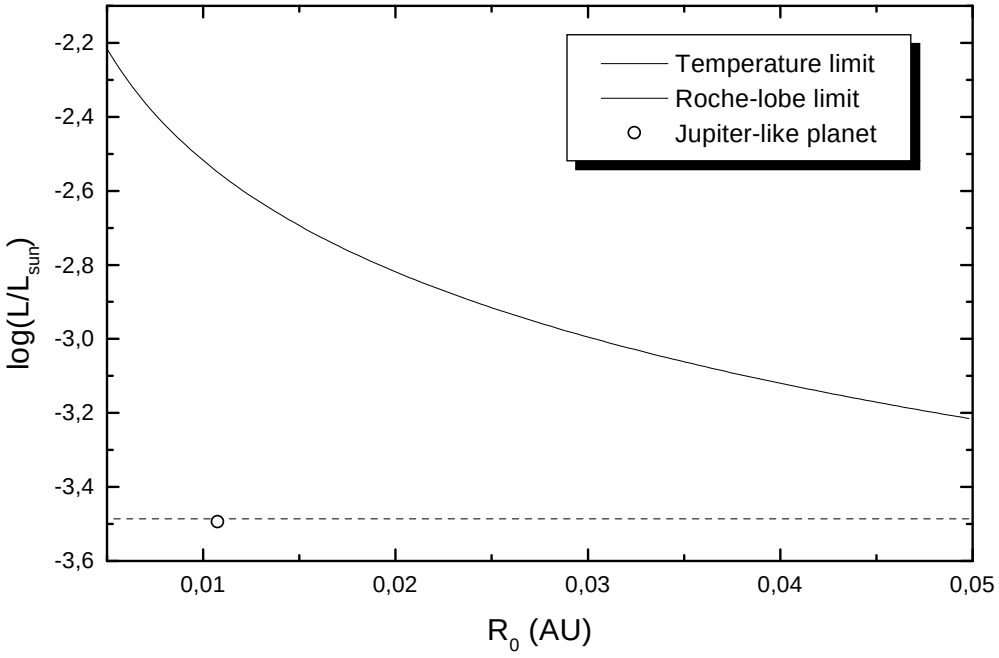

Figure 3.2: Hertzsprung-Russell diagram for a gaseous planet orbiting a solar-type star. The dot corresponds to a planet like Jupiter in a circular orbit corresponding to the mode g_{10}. The dashed line limits the region excluded by tidal disruption, the solid one limits the region excluded by melting effects.

have high surface gravities and low effective temperatures, so their atmosphere is composed mostly of molecules and condensed grains [12]. We expect the high surface gravity to increase the escape velocity, thus decreasing the effects of Jeans evaporation, but a detailed calculation would definitely be required.

3.6 Resonant emission amplitudes and timescales

Having checked that, at least in principle, the excitation conditions could be met in real EPS's, we have turned to the integration of the Einstein equations.

For this purpose we have chosen the same stellar model considered in [32]. It is a simple polytropic model, i.e., the equation of state has the form

$$p = p_0 \Theta^{n+1}, \qquad \epsilon = \epsilon_0 \Theta^n, \tag{3.23}$$

but it is quite well suited to reproduce the properties of a solar-type star. The model is non-barotropic (as it should be, since the temperature in a normal star is not constant), and we have fixed the adiabatic coefficient to be $\gamma = 5/3$. We have chosen a ratio between central density and pressure (in geometric units!) $\alpha_0 = \epsilon_0/p_0 = 5.53 \cdot 10^5$, close to the corresponding value for the sun, and a polytropic index $n = 3$. We have also fixed the central density to be 76 g·cm^{-3}. With this choice, our polytropic stellar model has a mass $M = M_\odot$ and a radius $R = R_\odot$.

Table 3.8: Ratios of the critical density of the planet ρ_{RL} to the central star density ρ_* for different oscillation modes of a polytropic star with $n = 3$ and for mass ratios: $\mu_{Earth} = M_{Earth}/M_\odot = 3.0 \cdot 10^{-6}$, $\mu_{Jup} = M_{Jup}/M_\odot = 9.6 \cdot 10^{-4}$ $\mu_{BD} = M_{BD}/M_\odot = 3.8 \cdot 10^{-2}$. In boldface, the models whose excitation is allowed by the Roche-lobe analysis. See table 3.6 for comparison.

	f	g_1	g_2	g_3	g_4	g_5	g_6	g_7	g_8	g_9	g_{10}
μ_{Earth}	20.8	12.5	7.21	4.64	**3.24**	**2.38**	**1.83**	**1.45**	**1.17**	**0.97**	**0.82**
μ_{BD}	-	-	-	-	**3.68**	**2.71**	**2.08**	**1.65**	**1.34**	**1.11**	**0.93**
μ_{Jup}	21.7	13.0	7.49	4.82	3.37	2.48	1.90	1.51	1.22	1.01	**0.85**

We have carried out the Roche-lobe analysis for three orbiting bodies: a planet with the same mass and radius as the Earth, a planet with the same mass and radius as Jupiter, and a brown dwarf with mass $M_{BD} = 40 M_J$. The corresponding critical ratios for each oscillation mode are shown in table 3.8; we have evidentiated in boldface the modes for which the excitation is not excluded by the Roche-lobe analysis. An Earth-like planet (having $\rho_{Earth}/\rho_\odot = 3.9$) could excite modes of order greater than 3. The same is true for a brown dwarf: an evolved brown dwarf of 40 jovian masses, according to the models in [12], would have a radius $R = 5.9 \cdot 10^9$ cm, and a value of $\rho/\rho_\odot = 64$, but it would accrete matter from the central star before exciting the mode g_3. A Jupiter-like planet ($\rho_J/\rho_\odot = 0.9$), on the other hand, could only excite modes of order greater than 9, without being disrupted by tidal interactions.

Table 3.9: Frequencies of gravitational-wave emission (in μHz) for different oscillation modes of a solar-mass polytropic star with $n = 3$, and corresponding quadrupole amplitudes at $D = 10$ pc for a planet like the Earth, a planet like Jupiter and a brown dwarf of 40 jovian masses. Only the modes not excluded by the Roche-lobe analysis are shown.

	ν_{GW}	$h_{Q,\oplus}$	$h_{Q,BD}$	$h_{Q,Jup}$
g_4	112.5	$3.0 \cdot 10^{-26}$	$3.9 \cdot 10^{-22}$	-
g_5	96.6	$2.7 \cdot 10^{-26}$	$3.5 \cdot 10^{-22}$	-
g_6	84.7	$2.5 \cdot 10^{-26}$	$3.2 \cdot 10^{-22}$	-
g_7	75.4	$2.3 \cdot 10^{-26}$	$3.0 \cdot 10^{-22}$	-
g_8	67.9	$2.2 \cdot 10^{-26}$	$2.8 \cdot 10^{-22}$	-
g_9	61.8	$2.0 \cdot 10^{-26}$	$2.6 \cdot 10^{-22}$	-
g_{10}	56.7	$1.9 \cdot 10^{-26}$	$2.4 \cdot 10^{-22}$	$6.1 \cdot 10^{-24}$

For each oscillation mode allowed by the Roche-lobe analysis we give, in table 3.9, the gravitational wave frequencies and the corresponding quadrupole amplitudes at a fiducial distance $D = 10$ pc.

As anticipated, the integration of the Einstein equations shows that resonances occur at frequencies corresponding to the quasi-normal modes. These resonances are typically sharper and narrower than those found by Kojima for compact stars: indeed, the resolution in ω (or R_0) required to compute the resonance curves is so high that numerical instabilities occur before we can determine the exact height of the peak!

On the other hand, the planet will never be exactly at the resonant radius R_{res}. Suppose it is orbiting at a radius $R_0 = R_{res} + \Delta R$. A typical behaviour of the ratio h_R/h_Q as a function of ΔR is shown in figure 3.3. The figure shows that, for example, in the case of the g_4-mode one can reach values of h_R/h_Q greater than 10 for ΔR of the order of a few kilometers, 100 for ΔR of the order of hundreds of meters, and 1000 for ΔR of the order of some meter.

The almost-perfect power law in h_R/h_Q as a function of ΔR is expected. We are basically dealing with a system that can be modelled as a damped oscillator (corresponding to the star; the damping is due to the emission of gravitational waves) with a forcing term (the gravitational waves emitted by the planet in its orbit). A power-law behaviour is typical of forced oscillators close to a resonance [45]. If we fit the computed behaviors with a linear function, of the form:

$$(\log h_R/h_Q) = a_{g_n} + b_{g_n}(\log \Delta R) \tag{3.24}$$

we get:

$$b_{g_4} = -0.97, \qquad b_{g_7} = -0.95, \qquad b_{g_{10}} = -0.95,$$
$$a_{g_4} = 1.38, \qquad a_{g_7} = 0.19, \qquad a_{g_{10}} = -0.83.$$

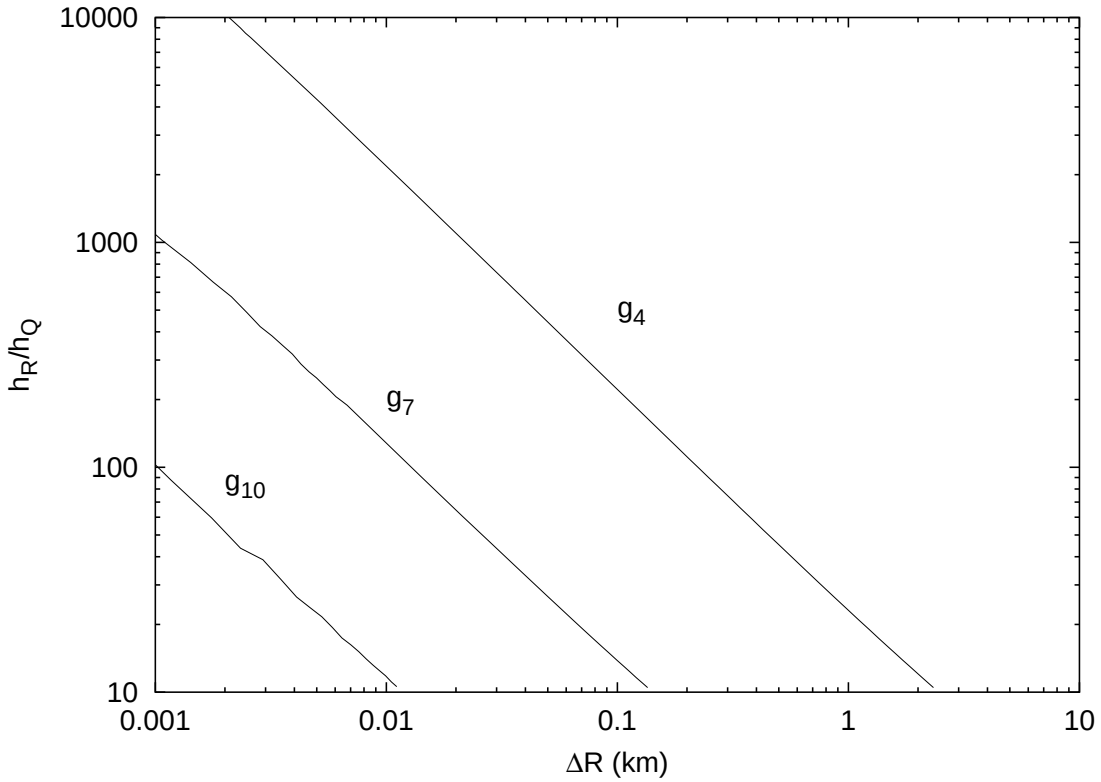

Figure 3.3: The power-law behaviour of h_R/h_Q as a function of ΔR (in km) close to the resonance corresponding to a g_4-, g_7- and $g_{10}-$mode, for a star of mass $M = M_\odot$.

Since the resonance is so sharp, we can expect a system close enough to the resonance to loose a lot of energy in gravitational waves, until the emission is stopped by some viscous mechanism and the planet goes off resonance. How long can a planet emit with a ratio h_R/h_Q greater than some fixed amount? To answer this question we need to take into account the

evolution of the orbit, that so far we have ignored; in other words, we must take into account radiation reaction effects.

This can be done as follows. In any binary system, as the system emits energy in gravitational waves, the loss of energy causes the orbit to shrink. This means that a planet in an EPS will not hover around in a circular orbit forever, but it will eventually spiral down the central star, and the inspiral will be faster and faster as we get closer and closer to a resonance corresponding to a quasi-normal mode of the star, since there the gravitational emission is stronger.

How much time will the planet spend in a region corresponding to a value of h_R/h_Q greater than some fixed limit, before reaching the peak corresponding to the quasi-normal mode? The corresponding time-scale can be seen as an upper limit on the time the system can spend emitting waves of amplitude greater than that fixed amount.

Let us trun to the computation of this time-scale, taking into account effects of gravitational radiation reaction on the evolution of the planetary orbit. Consider the geodesic equations for a mass orbiting a non-rotating star. They can be written in the usual form:

$$\frac{dt}{d\tau} = E\left(1 - \frac{2M}{R_0}\right)^{-1}, \qquad \frac{d\varphi}{d\tau} = \frac{L_z}{R_0^2}, \qquad \left(\frac{dr}{d\tau}\right)^2 + V(L_z, r) = E^2, \tag{3.25}$$

where E is the planet's energy per unit mass, and L_z is the particle's angular momentum per unit mass. The effective potential for radial motion is given by:

$$V(L_z, r) = (1 - 2M/r)(1 + L_z^2/r^2). \tag{3.26}$$

For a circular orbit $\frac{\partial V(L_z,r)}{\partial r} = 0$, and this implies:

$$L_z^2 = \frac{MR_0}{1 - 3M/R_0}. \tag{3.27}$$

Furthermore, since $E^2 = V(L_z(R_0), R_0)$, the energy per unit mass for a particle in circular orbit is given by:

$$E = \frac{1 - 2M/R_0}{\sqrt{1 - 3M/R_0}}. \tag{3.28}$$

The evolution of the orbit can be determined using conservation of energy. In the *adiabatic approximation* we assume that the time-scale over which the orbital radius evolves is much longer than the orbital period:

$$\tau \gg P = \frac{2\pi}{\omega_k}. \tag{3.29}$$

Under this assumption, the (circular) orbit shrinks due to the energy emitted in gravitational waves, according to the law:

$$m_0 \left\langle \frac{dE}{dt} \right\rangle + \left\langle \frac{dE}{dt} \right\rangle_{GW} = 0, \tag{3.30}$$

or

$$m_0 \dot{E} + \dot{E}_{GW} = 0. \tag{3.31}$$

Here and in the following, by an overdot, or by the symbols $\langle .. \rangle$, we shall mean an average over many orbital periods. The idea is that, since the orbit evolves slowly with respect to the orbital

period, the perturbing object will go through a series of "quasi-geodesic" states; in each of these states, the usual formalism can be used to find the energy emitted in gravitational waves, and hence the evolution of the orbit.

The energy emitted in gravitational waves, $\dot{E}_{GW}$, can be determined as described in section C.3. Now, the radius of the orbit evolves according to:

$$\dot{R}_0 = \frac{dR_0}{dE}\dot{E}. \tag{3.32}$$

Using (3.28) and (3.31) this equation can be written in the form:

$$\dot{R}_0 = -\frac{2R_0^2}{m_0 M}\frac{(1-3M/R_0)^{3/2}}{(1-6M/R_0)}\dot{E}_{GW}. \tag{3.33}$$

Introducing $\mu \equiv m_0/M$ we can define $\dot{\mathcal{E}}(R_0)$ as:

$$\dot{\mathcal{E}}(R_0) \equiv \mu^{-2}\dot{E}_{GW}, \tag{3.34}$$

and write the evolution equation for the orbital radius as

$$\dot{R}_0 = -\mu\frac{2R_0^2}{M^2}\frac{(1-3M/R_0)^{3/2}}{(1-6M/R_0)}\dot{\mathcal{E}}(R_0). \tag{3.35}$$

Separating variables and integrating we get the time required for the planetary orbit to shrink from a radius $R_0^{(2)}$ to a radius $R_0^{(1)}$ due to radiation-reaction effects:

$$\Delta T(R_0^{(2)} > R_0^{(1)} \to R_0^{(1)}) = -\frac{M^2}{2\mu}\int_{R_0^{(2)}}^{R_0^{(1)}} \frac{(1-6M/R_0)}{(1-3M/R_0)^{3/2}R_0^2}\frac{dR_0}{\dot{\mathcal{E}}(R_0)}. \tag{3.36}$$

We consider only the $\ell = 2$ emission. Then, defining $\bar{Z}_{22}^{out} = \tilde{Z}_{22}^{out}/m_0$ and using equation (C.121) for the power radiated in $\ell = 2$, we have:

$$\dot{\mathcal{E}}(R_0) = \frac{3(\omega M)^2\left|\bar{Z}_{22}^{out}\right|^2}{\pi}. \tag{3.37}$$

Going back to physical units, equation (3.36) can be written as:

$$\Delta T(R_0^{(2)} > R_0^{(1)} \to R_0^{(1)}) = -G\frac{M^2}{2\mu}\int_{R_0^{(2)}}^{R_0^{(1)}} \frac{(1-6GM/c^2R_0)}{(1-3GM/c^2R_0)^{3/2}R_0^2}\frac{dR_0}{\dot{\mathcal{E}}(R_0)}. \tag{3.38}$$

This formula allows us to compute the timescale required for a planet to go from a fixed value of h_R/h_Q (say, 10) to the resonant radius. These timescales are given in table 3.10.

From the data in table 3.10 and the quadrupole amplitudes in table 3.9 we see that, for example, a brown dwarf exciting the mode g_4 could reach amplitudes $\sim 2\cdot 10^{-20}$ for ~ 3 years, and $\sim 4\cdot 10^{-21}$ for ~ 400 years; on the other hand, a planet like Jupiter resonant with the mode g_{10} could reach amplitudes $\sim 3\cdot 10^{-22}$ for ~ 2 years, and $\sim 6\cdot 10^{-23}$ for ~ 300 years.

Things would not be significantly different if we considered more realistic models of solar-type stars, such as those discussed in [19]. More complex models of the sun are different in many respects from the ones we computed using our simple polytropic model, and they normally yield slightly higher oscillation frequencies, as we can see from table 3.11. Considering the effects of contamination from interstellar material on the heavy element abundance in the sun [18], the oscillation times grow a little, getting even closer to the values computed in our

Table 3.10: In column 2 we give the frequency, ν_{GW}, of the wave emitted when a planet moves around the host star on an orbit resonant with a g-mode allowed by the Roche lobe analysis (see text). Because of resonant effects, the amplitude of the wave is amplified by a factor greater than A (column 3) when the companion spans a radial region of thickness ΔR (column 4), which is the same for all planets. In the last three columns we give the time interval ΔT needed for the three companions to span the region ΔR and reach the resonance, because of radiation reaction effects.

Mode	ν_{GW} (μHz)	A	ΔR(m)	ΔT_E(yrs)	ΔT_{BD}(yrs)	ΔT_J(yrs)
g_4	112.5	10	1700	$5.4 \cdot 10^6$	$4.3 \cdot 10^2$	-
		50	312	$3.8 \cdot 10^4$	3.0	-
g_5	96.6	10	616	$2.7 \cdot 10^6$	$2.1 \cdot 10^2$	-
		50	113	$1.9 \cdot 10^4$	1.5	-
g_6	84.7	10	240	$1.4 \cdot 10^6$	$1.1 \cdot 10^2$	-
		50	44	$9.6 \cdot 10^3$	$7.5 \cdot 10^{-1}$	-
g_7	75.4	10	98	$7.0 \cdot 10^5$	55	-
		50	18	$5.0 \cdot 10^3$	$3.9 \cdot 10^{-1}$	-
g_8	67.9	10	42	$3.8 \cdot 10^5$	30	-
		50	8	$2.5 \cdot 10^3$	$1.9 \cdot 10^{-1}$	-
g_9	61.8	10	18	$1.9 \cdot 10^5$	15	-
		50	3	$1.5 \cdot 10^3$	$1.2 \cdot 10^{-1}$	-
g_{10}	56.7	10	8	$1.0 \cdot 10^5$	7.8	$3.1 \cdot 10^2$
		50	1	$6.7 \cdot 10^2$	$5.3 \cdot 10^{-2}$	2.1

Table 3.11: Frequencies (in μHz) for different oscillation modes of a solar-mass polytropic star with $n = 3$, and for a more realistic solar model. Data for the "realistic" solar model were kindly provided by J. Christensen-Dalsgaard [20].

	g_1	g_2	g_3	g_4	g_5	g_6	g_7	g_8	g_9	g_{10}
Polytrope ($n = 3$)	221.4	167.9	134.8	112.5	96.6	84.7	75.4	67.9	61.8	56.7
"Realistic" model	296.6	256.6	222.5	194.6	171.0	151.9	136.2	123.3	112.5	103.3

polytropic model. In any event, our frequencies are at least qualitatively correct to give order-of-magnitude estimates for the effects of resonant gravitational-wave emission we are considering in our study. We feel that our considerations on the gravitational-wave amplitudes and on the excitation timescales would not be substantially modified if we considered more realistic solar models.

3.7 Conclusions

The main results obtained regarding extrasolar planetary systems can be summarized as follows:

- One of the observed EPS's, HD283750, emits waves with a maximum characteristic amplitude $h_c \sim 4 \cdot 10^{-23}$ and a corresponding frequency $\nu \sim 1.3 \cdot 10^{-5}$ Hz. These values are quite interesting, especially when compared to the maximum amplitude $h_c \sim 10^{-23}$ and frequency $\nu \sim 1.4 \cdot 10^{-4}$ Hz of the Hulse-Taylor binary pulsar (PSR 1913+16).

- The Roche-lobe analysis has shown that EPS's at a fiducial distance $D = 10$ pc can emit, in their orbital motion, waves of amplitude as large as $h_c^{max} \sim 10^{-22}$ and frequency as high as $\nu^{max} \sim 10^{-4}$ Hz; furthermore, the excitation conditions could be satisfied for some of the g-modes in solar-type stars.

- The integration of the Einstein equations shows that, for low-order $g-$modes, one can reach values of h_R/h_Q greater than:

  10 for radial fine tunings ΔR of the order of a few kilometers,

  100 for ΔR of the order of hundreds of meters,

  1000 for ΔR of the order of some meter.

  Close to a resonance, the amplitude for low-order modes for an $n = 3$ polytrope is well fitted by the law:

  $$(\log h_R/h_Q) = a_{g_n} + b_{g_n}(\log \Delta R),$$

  where $b_{g_n} \simeq -0.95$, and a_{g_n} depends on the order of the mode.

- The radiation reaction analysis shows that, for the stellar model we have chosen, a brown dwarf exciting the mode g_4 could reach amplitudes $\sim 2 \cdot 10^{-20}$ for ~ 3 years, and $\sim 4 \cdot 10^{-21}$ for ~ 400 years; on the other hand, a planet like Jupiter resonant with the mode g_{10} could reach amplitudes $\sim 3 \cdot 10^{-22}$ for ~ 2 years, and $\sim 6 \cdot 10^{-23}$ for ~ 300 years.

Figure 3.4 shows the sensitivity curve for LISA (i.e., the amplitude required at each frequency to observe a signal with a signal-to-noise ratio greater than 5) along with some of the most interesting results obtained by our analysis. Though significantly larger in amplitude than the signal emitted by the binary pulsar, the waves emitted by the observed system HD283750 are not detectable with the current LISA design. The same is true for a "resonant" system composed by a solar-type star and a jupiter-like planet, but a brown dwarf in resonant conditions could potentially be detectable.

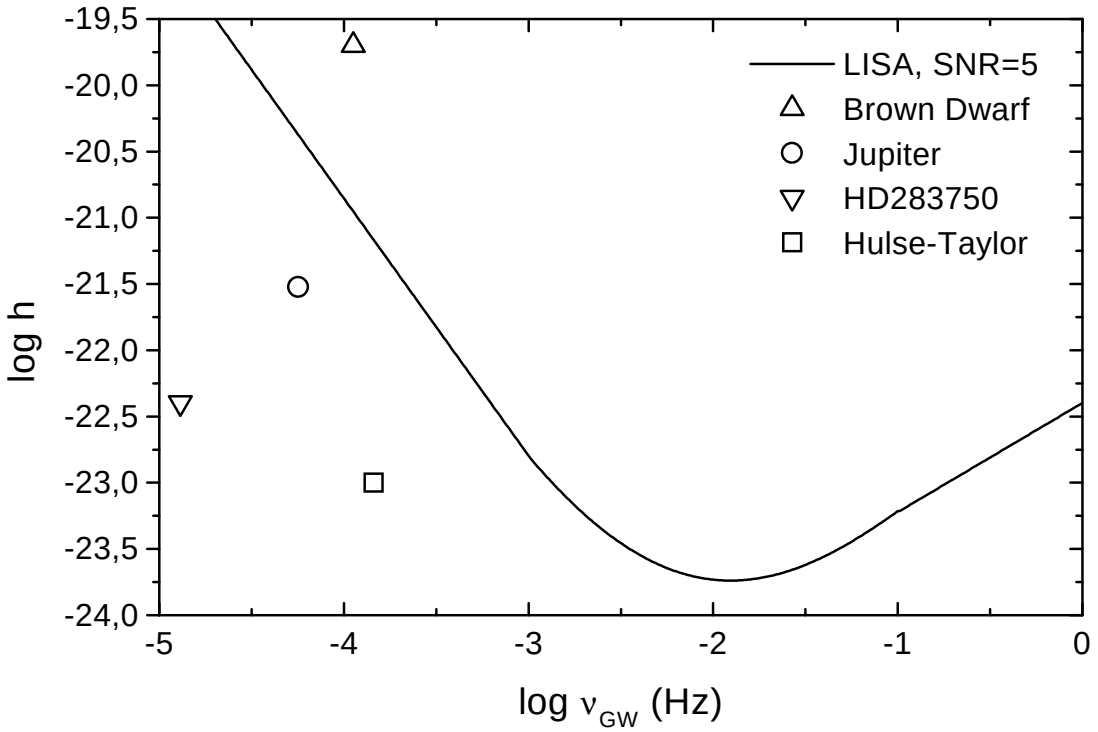

Figure 3.4: The solid curve is LISA's sensitivity curve, representing the amplitude required to observe a signal with signal-to-noise ratio greater than 5. The different dots represent a brown dwarf in resonant conditions with amplification 50, a jupiter-like planet in resonant conditions with the same amplification factor, and two *observed* binaries: HD283750 (an extrasolar planetary system) and PSR 1913+16 (the Hulse-Taylor binary pulsar).

Chapter 4

Gravitational wave emission by compact binaries

At variance with the preceding chapter, in this chapter we shall consider binaries which radiate gravitational waves with large intensity and at frequencies accessible to ground-based interferometers. Such system must not only be massive, they must also orbit each other at very small separations (a few hundred kilometers or less). These massive objects are expected to be the end products of stellar evolution: neutron stars and black holes. Since a large fraction of all stars are in close binary systems, the dead remnants of stellar evolution may contain a significant number of binary systems whose components are neutron stars or black holes, and are close enough together to be driven into coalescence by gravitational radiation reaction in a time smaller than the age of the universe. The binary pulsar 1913+16 is an example of such a system, and will coalesce $\sim 3.5 \times 10^8$ years from now.

Gravitational radiation reaction, at least when the binary members are widely separated, tends to circularize and shrink the orbit. So, even if the system is born initially with a large eccentricity, when the waves enter the frequency band of earth-based interferometers the two bodies in the binary spiral together emitting periodic gravitational waves at a single frequency (equal to twice the orbital frequency) that sweeps upward ("chirps") toward a maximum. This maximum is around 1 kHz for neutron star binaries, and around $10M_{BH}/M_\odot$ for black hole binaries when the larger black hole has mass M_{BH}. During the first part of the frequency sweep the waveform can be fairly accurately computed from the quadrupole formalism, but as the objects get closer Post-Newtonian orbital effects and effects due to the extended structure of the bodies become more and more significant. In the final, merging phase, the full equations of general relativity and detailed hydrodynamical models are definitely needed for a prediction of the gravitational wave signal we may observe.

When dealing with extrasolar planetary systems we considered only the polar, $\ell = 2$ (quadrupolar) contribution to the emitted radiation, since this contribution be shown to be dominant in the total power output, especially in Newtonian regimes. We also restricted our attention, in the preliminary exploration of excitation phenomena that we carried out there, to bodies in circular orbit around the star. Here we want to carry out a more general analysis: we shall include all multipoles, taking into account also the axial part of the radiation (since these contributions, as we will see, may become important in strong-field regimes), and study effects due to the orbital eccentricity, to carry out a more general analysis of the excitation conditions.

As we show in Appendix C, the computation of the source term and the solution of the equations in the "standard" Zerilli approach is quite cumbersome, and polar and axial perturbations

have to be dealt with separately. Instead of dealing directly with perturbations of the metric functions, it turns out to be much easier and more elegant to consider the perturbations of the Weyl scalars in the Newman-Penrose null tetrad formalism. This approach also leads, after a separation of the angular part (which now is accomplished in terms of spin-weighted spherical harmonics) to a radial equation, known as the *Bardeen-Press-Teukolsky* (BPT) equation [4, 83]. The solutions to the BPT equation carry information both on the polar and on the axial parts of the perturbation, and the source term is much simpler to deal with than in the Zerilli approach. So we have used the BPT formalism to consider the general case of particles in closed, eccentric orbit around the star, and only used the Zerilli formalism as a check of the correctness of our results in the circular limit $e \to 0$ (which is physically very important, since compact binaries, as we said before, will move on circular orbits by the time the waves they emit enter the bandwidth of interferometers).

Figure 4.1 shows that, indeed, binary neutron stars are a promising source for the interferometers now under construction. There we plot the sensitivity curves of GEO600, VIRGO and LIGO, modelled using fits given in section 7.4 of [39], along with predicted estimates for the amplitudes of signals coming from neutron star mergers at distances from earth of 20 Mpc and 100 Mpc. It can be shown [25] that the crucial ingredient to extract the inspiral signal from the noise with a matched-filtering technique is a good theoretical estimate of the *phase* of the wave in the region were the interferometers are more sensitive, i.e. at gravitational wave frequencies $\lesssim 1$ kHz.

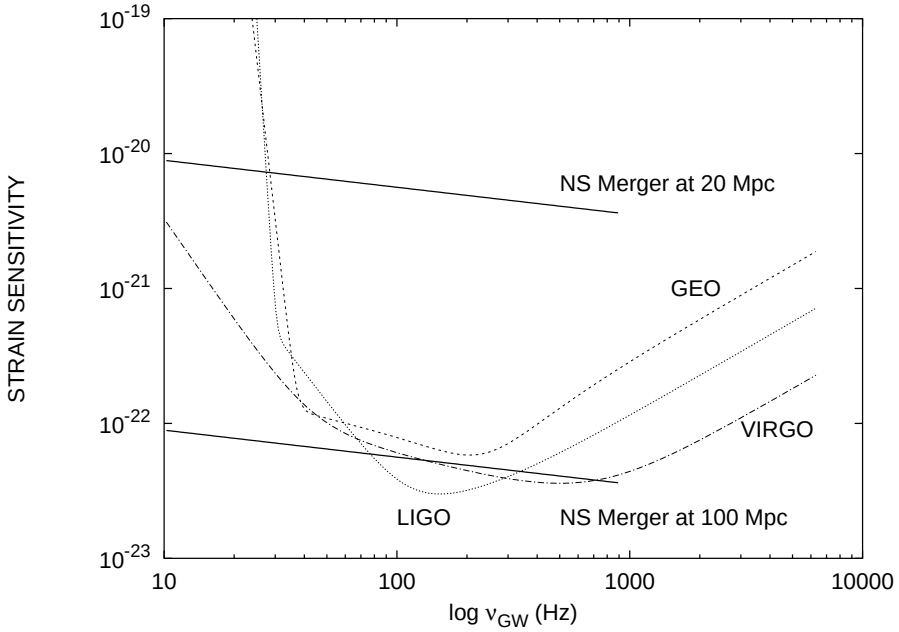

Figure 4.1: The sensitivity curves for the ground-based interferometers GEO 600, VIRGO and LIGO are compared to the strength of signals coming from neutron star binaries at a distance of 20 Mpc and 100 Mpc. The noise power spectral densities of the detectors are modelled using fits given in section 7.4 of the review by Grischuk *et al.* [39].

Our main interest has been to understand to what extent effects due to the extended structure of stars can affect the theoretical modeling of this signal, and consequently the detection of the waves. Of course, our perturbative formalism allows us to take into account the structure of only one of the bodies. Nonetheless, we hope the information we gain in this way can be used to

infer some information on a real binary coalescence, especially considering that a stable, long-lasting simulation of such a coalescence (despite the many efforts done to evolve numerically the full, non-linear Einstein equations [61]) is still probably a long way to come.

The plan of this chapter is as follows. In section 4.1 we describe the Bardeen-Press-Teukolsky perturbative approach, leaving some technical details to Appendix D. In section 4.2 we apply the formalism to particles in closed, eccentric orbits around a star, and compare results with those obtained through the semirelativistic formalism developed in section 1.4. We show that the stellar structure introduces qualitatively and quantitatively new effects, among which are the appearance of an axial component in the radiation and, consequently, a beating between the polar and axial components; a significant reduction in the total power radiated in $\ell = 2$; a great enhancement in the wave amplitude if the stellar quasi-normal modes are excited. The possibility to excite the quasi-normal modes in an astrophysical binary coalescence is considered, both for neutron-star and black-hole binaries, in section 4.3. There we show that the excitation of black hole quasi-normal modes can only occur in a collapse; for neutron stars, the f-mode excitation is highly implausible unless the star is rotating. The g-modes, on the other hand, could be excited in a frequency band relevant for earth-based interferometers, and we will explore this issue in the future. In section 4.4 we consider the orbital evolution of binary systems in our perturbative approach, for general (not necessarily circular) orbits. In section 4.5 we compare the emission features of a system composed by a star and a test mass with those of a system composed by a black hole and a test mass, and discuss how effects due to the equation of state affect the emitted power. In section 4.6 we analyze our perturbative results in the light of those obtained in the literature using Post-Newtonian approximations, either in the test mass or in the comparable mass limit. We compute differences in the number of cycles between different stellar models and black holes, and discuss the reductions in signal-to-noise ratio due to a non-optimal modeling of the signal. Finally, in section 4.7 we give an argument in favour of the perturbative approximation, showing that fluid and metric perturbations remain small up to very little orbital separations, or, in other words, that the perturbative approach seems to hold surprisingly good up to very late stages of the coalescence.

4.1 The Bardeen-Press-Teukolsky (BPT) approach

To describe the perturbations of the Schwarzschild spacetime prevailing outside the star we can use the BPT equation [4, 83]

$$\left\{\Delta^2\frac{d}{dr}\left[\frac{1}{\Delta}\frac{d}{dr}\right]+\left[\frac{(r^4\omega^2+4i(r-M)r^2\omega)}{\Delta}-8i\omega r-2n\right]\right\}\Psi_{\ell m}(\omega,r)=-T_{\ell m}(\omega,r), \tag{4.1}$$

where $\Delta = r^2 - 2Mr$. The BPT function, $\Psi_{\ell m}$, is related to the perturbation of the Weyl scalar $\delta\Psi_4$ by

$$\Psi_{\ell m}(\omega,r)=\frac{1}{2\pi}\int d\Omega\; dt\; e^{i\omega t}\;{}_{-2}S^{*}_{\ell m}(\vartheta,\varphi)\left[r^4\;\delta\Psi_4(t,r,\vartheta,\varphi)\right], \tag{4.2}$$

and ${}_{-2}S_{\ell m}(\vartheta,\varphi)$ is the spin-weighted spherical harmonic of spin-weight $s=-2$. Spin-weighted spherical harmonics are defined and expressed in terms of ordinary spherical harmonics in Appendix G.

The advantage of using the BPT equation is that $\delta\Psi_4$ is invariant under gauge transformations and infinitesimal tetrad rotations, and that the squares of its real and imaginary parts are

proportional to the energy flux of the outgoing radiation at infinity in the two polarizations. In addition, the source term $T_{\ell m}(\omega, r)$, which will be discussed in detail in the next section, has a much simpler form than the source of the Sasaki-Nakamura equation, which was used to study the gravitational emission in the case of open orbits in [33].

At the surface of the star, and in general whenever $T_{\ell m}(\omega, r) = 0$, the relation between $\Psi_{\ell m}$, the Zerilli function $Z_{\ell m}$ (which for clarity we shall here denote by $Z^{pol}_{\ell m}$) and the Regge-Wheeler function $Z^{ax}_{\ell m}$ is

$$\begin{aligned} \Psi_{\ell m} &= \frac{r^3\sqrt{n\,(n+1)}}{4\omega}\left[V^{ax} Z^{ax}_{\ell m} + (W^{ax} + 2i\omega)\,\Lambda_+ Z^{ax}_{\ell m}\right] \\ &- \frac{r^3\sqrt{n\,(n+1)}}{4}\left[V^{pol} Z^{pol}_{\ell m} + \left(W^{pol} + 2i\omega\right)\Lambda_+ Z^{pol}_{\ell m}\right], \end{aligned} \tag{4.3}$$

where $\Lambda_+ = \frac{d}{dr_*} + i\omega = \frac{\Delta}{r^2}\frac{d}{dr} + i\omega$, and

$$\begin{aligned} V^{ax} &= \frac{2\Delta}{r^5}\left[(n+1)r - 3M\right] \\ W^{ax} &= \frac{2}{r^2}(r - 3M) \\ V^{pol} &= \frac{2\Delta}{r^5(nr+3M)^2}\left[n^2(n+1)r^3 + 3Mn^2r^2 + 9M^2nr + 9M^3\right] \\ W^{pol} &= 2\frac{nr^2 - 3Mnr - 3M^2}{r^2(nr+3M)}. \end{aligned}$$

According to (4.3) we can write $\Psi_{\ell m}$ as a sum of an axial and a polar part, i.e.

$$\Psi_{\ell m} = \Psi^{ax}_{\ell m} + \Psi^{pol}_{\ell m}, \tag{4.4}$$

where

$$\begin{aligned} \Psi^{ax}_{\ell m} &= \frac{r^3\sqrt{n\,(n+1)}}{4\omega}\left[V^{ax} Z^{ax}_{\ell m} + (W^{ax} + 2i\omega)\,\Lambda_+ Z^{ax}_{\ell m}\right] \\ \Psi^{pol}_{\ell m} &= -\frac{r^3\sqrt{n\,(n+1)}}{4}\left[V^{pol} Z^{pol}_{\ell m} + \left(W^{pol} + 2i\omega\right)\Lambda_+ Z^{pol}_{\ell m}\right]. \end{aligned} \tag{4.5}$$

However, in the following we will show that depending on the value of the sum of the harmonic indices $(\ell + m)$, only the polar or the axial part of $\Psi_{\ell m}$ have to be selected.

The inhomogeneous BPT equation (4.1) can be integrated by constructing a Green function which ensures that $\delta\Psi_4$ matches regularly with the interior solution at the boundary of the star, and behaves as a pure outgoing wave at infinity. This problem has been solved by Detweiler in the case of black holes [29]; here we shortly describe the simple generalization of the method to the case of stars. First we discuss some symmetry properties of the functions involved in the problem we want to solve. Under complex conjugation, spherical harmonics behave as $Y^*_{\ell m}(\vartheta, \varphi) = (-1)^m Y_{\ell -m}(\vartheta, \varphi)$; consequently, the perturbed metric functions in (2.10) and the functions $Z^{pol}_{\ell m}$ and $Z^{ax}_{\ell m}$ satisfy the following property:

$$F^*_{\ell m}(r, \omega) = (-1)^m F_{\ell -m}(r, -\omega).$$

From eqs. (4.5) it follows that

$$\begin{aligned} \left(\Psi^{ax}_{\ell m}(\omega, r)\right)^* &= (-1)^{m+1}\,\Psi^{ax}_{\ell -m}(-\omega, r) \\ \left(\Psi^{pol}_{\ell m}(\omega, r)\right)^* &= (-1)^m\,\Psi^{pol}_{\ell m}(-\omega, r). \end{aligned} \tag{4.6}$$

By inspection of the source term, we find that $\Psi_{\ell m}$ must satisfy an additional relation

$$\Psi^*_{\ell m}(r,\omega) = (-1)^\ell \Psi_{\ell -m}(r,-\omega). \tag{4.7}$$

In order for (4.6) and (4.7) to be consistent, and looking at eqs. (4.4) we see that the following selection rule must hold

- if $(\ell+m)$ is even, $\Psi_{\ell m} = \Psi^{pol}_{\ell m}$,
- if $(\ell+m)$ is odd, $\Psi_{\ell m} = \Psi^{ax}_{\ell m}$.

Thus, depending on the value of the harmonic indices ℓ and m, $\Psi_{\ell m}$ is either polar or axial. As explained in Appendix B, integrating the equations of stellar perturbations, (2.27)–(2.30) and (2.40), in the interior of the star, we can construct the functions $Z^{ax}_{\ell m}(\omega, R_s)$ and $Z^{pol}_{\ell m}(\omega, R_s)$ and their first derivatives at $r = R_s$; from them we compute $\Psi^{ax}_{\ell m}(\omega, R_s)$ and $\Psi^{pol}_{\ell m}(\omega, R_s)$, as given in eqs. (4.5), and their first derivatives, which are needed to integrate the BPT equation outside the star. However, it should be noted that the regularity condition imposed at $r = 0$ allows to determine $Z^{ax}_{\ell m}$ and $Z^{pol}_{\ell m}$ only up to an unknown amplitude, $\chi_{\ell m}(\omega)$, to be determined by the matching conditions at the boundary of the star. In what follows, we shall indicate as $\bar\Psi^{ax}_{\ell m}(\omega, R_s)$ and $\bar\Psi^{pol}_{\ell m}(\omega, R_s)$ the values of the axial and polar part of the wavefunction $\Psi_{\ell m}$ as computed by numerical integration of the interior equations. The problem we want to solve therefore is

$$\begin{aligned}
&\mathbb{L}_{BPT}\Psi_{\ell m}(\omega, r) = -T_{\ell m}(\omega, r) \\
&\Psi_{\ell m}(r\to\infty) = r^3 e^{\mathrm{i}\omega r_*} A_{\ell m}(\omega) \\
&\Psi_{\ell m}(\omega, R_s) = \chi_{\ell m}(\omega)\bar\Psi_{\ell m}(\omega, R_s) \\
&\Psi'_{\ell m}(\omega, R_s) = \chi_{\ell m}(\omega)\bar\Psi'_{\ell m}(\omega, R_s),
\end{aligned} \tag{4.8}$$

where $\mathbb{L}_{BPT}$ is the differential operator on the left hand side of the BPT equation. If $(\ell+m)$ is even, $\bar\Psi_{\ell m}(\omega, R_s) = \bar\Psi^{pol}_{\ell m}(\omega, R_s)$, whereas if $(\ell+m)$ is odd $\bar\Psi_{\ell m}(\omega, R_s) = \bar\Psi^{ax}_{\ell m}(\omega, R_s)$. $A_{\ell m}(\omega)$ is the unknown wave amplitude to be determined. The general solution of eqs. (4.8) is

$$\Psi_{\ell m}(\omega, r) = -\frac{1}{W_{\ell m}}\left[\Psi^0_{\ell m}\int_{R_s}^{r}\frac{dr'}{\Delta^2}\,\Psi^1_{\ell m}\,T_{\ell m} + \Psi^1_{\ell m}\int_{r}^{\infty}\frac{dr'}{\Delta^2}\,\Psi^0_{\ell m}\,T_{\ell m}\right], \tag{4.9}$$

where $\Psi^0_{\ell m}$ and $\Psi^1_{\ell m}$ are two independent solutions of the homogeneous BPT equation defined as

$$\begin{cases} \mathbb{L}_{BPT}\Psi^0_{\ell m}(\omega, r) = 0 \\ \Psi^0_{\ell m}(\omega, r\to\infty) = r^3 e^{\mathrm{i}\omega r_*} \end{cases}, \qquad \begin{cases} \mathbb{L}_{BPT}\Psi^1_{\ell m}(\omega, r) = 0 \\ \Psi^1_{\ell m}(\omega, R_s) = \bar\Psi_{\ell m}(\omega, R_s) \\ \Psi^1_{\ell m}{}'(\omega, R_s) = \bar\Psi'_{\ell m}(\omega, R_s) \end{cases}, \tag{4.10}$$

and $W_{\ell m}(\omega)$ is the Wronskian

$$W_{\ell m}(\omega) = \frac{1}{\Delta}\left[\Psi^1_{\ell m}\Psi^0_{\ell m\,,r} - \Psi^0_{\ell m}\Psi^1_{\ell m\,,r}\right]. \tag{4.11}$$

From eq. (4.9) it is easy to see that the amplitude of the wave at infinity is

$$A_{\ell m}(\omega) = -\frac{1}{W_{\ell m}(\omega)}\int_{R_s}^{\infty}\frac{dr'}{\Delta^2}\,\Psi^1_{\ell m}(\omega, r')\,T_{\ell m}(\omega, r'). \tag{4.12}$$

The detailed computation of the amplitude (4.12), both for circular and eccentric orbits, is given in Appendix D, where, in particular, we show that (in the general case of eccentric orbits) it can be written as

$$A_{\ell m}(\omega) = -\frac{1}{W_{\ell m}(\omega)}\,\frac{2\pi}{\Delta t}\sum_{j=-\infty}^{+\infty}\delta\left(\omega-\omega_{mj}\right)\int_{R_s}^{\infty}\frac{dr'}{\Delta^2}\,\Psi^{1}_{\ell m}(\omega,r')\,T_{0\;\ell m}(\omega,r'). \tag{4.13}$$

We shall now compute the "relativistic" time-averaged energy-flux

$$\dot{E}^R \equiv \left\langle\frac{dE}{dt}\right\rangle = \lim_{T\to\infty}\frac{E}{T} = \lim_{T\to\infty}\frac{1}{T}\sum_{\ell m}\int d\omega\left(\frac{dE}{d\omega}\right)_{\ell m}, \tag{4.14}$$

where the energy spectrum, $\frac{dE}{d\omega}$, can be expressed in terms of the wave amplitude at infinity $A_{\ell m}(\omega)$ as

$$\left(\frac{dE}{d\omega}\right)_{\ell m} = \frac{1}{2\omega^2}|A_{\ell m}(\omega)|^2. \tag{4.15}$$

Since the wave amplitude can be written, according to eq. (4.13), as

$$A_{\ell m}(\omega) = \sum_{j=-\infty}^{\infty}\hat{A}_{\ell m}(\omega)\delta(\omega-\omega_{mj}) \tag{4.16}$$

we have

$$\begin{aligned}\dot{E}^R &= \lim_{T\to\infty}\frac{1}{T}\sum_{\ell m}\sum_{j=-\infty}^{+\infty}\int d\omega\;{}''\delta(\omega-\omega_{mj})^{2}{}''\,\frac{1}{2\omega^2}|\hat{A}_{\ell m}(\omega)|^2 \\ &= \sum_{\ell m}\sum_{j=-\infty}^{+\infty}\frac{1}{4\pi\omega_{mj}^2}\,|\hat{A}_{\ell m}(\omega_{mj})|^2 \equiv \sum_{\ell m}\sum_{j=-\infty}^{+\infty}\dot{E}^R_{\ell mj},\end{aligned} \tag{4.17}$$

where ${}''\delta^{2}{}''$ is the regularized squared δ-function, such that

$$\lim_{T\to\infty}\frac{2\pi}{T}{}''\delta(\omega-\omega_{mj})^{2}{}'' = \delta(\omega-\omega_{mj}), \tag{4.18}$$

and we have defined the time-averaged power spectrum

$$\dot{E}^R_{\ell mj} \equiv \frac{1}{4\pi\omega_{mj}^2}|\hat{A}_{\ell m}(\omega_{mj})|^2. \tag{4.19}$$

In conclusion, the gravitational emission is characterized by a series of spectral lines at frequencies ω_{mj}.

From the symmetry properties (1.82)

$$\omega_{-m-j} = -\omega_{mj} \tag{4.20}$$

and

$$\hat{A}^*_{\ell m}(\omega_{mj}) = (-1)^{\ell}\,\hat{A}_{\ell-m}(\omega_{-j-m}), \qquad j>0 \tag{4.21}$$

it follows that

$$\dot{E}^R_{\ell-m-j} = \dot{E}^R_{\ell mj}. \tag{4.22}$$

Thus, once we know the power spectrum $\dot{E}^R_{\ell mj}$ as a function of the frequencies ω_{mj}, for an assigned value of ℓ and for positive m, the spectrum for negative m is obtained through Eq. (4.22).

As the energy lost in gravitational waves,

$$\dot{E}^R = \sum_{\ell m}\sum_{j=-\infty}^{+\infty}\dot{E}^R_{\ell mj} \equiv \sum_{\ell m}\sum_{j=-\infty}^{+\infty}\frac{1}{4\pi\omega_{mj}^2}\,|\hat{A}_{\ell m}(\omega_{mj})|^2, \tag{4.23}$$

so the angular momentum lost in gravitational waves can be written as a sum of terms in the following way:

$$\dot{L}^R_z = \sum_{\ell m}\sum_{j=-\infty}^{+\infty}\dot{L}^R_{z,\ell mj} \equiv \sum_{\ell m}\sum_{j=-\infty}^{+\infty}\frac{m}{4\pi\omega_{mj}}\,|\hat{A}_{\ell m}(\omega_{mj})|^2. \tag{4.24}$$

Since $\delta\Psi_4(t,r,\vartheta,\varphi)$ and the gravitational wave amplitude in the radiation gauge are related by

$$\delta\Psi_4(t,r,\vartheta,\varphi) = -\frac{1}{2}\left[\ddot{h}^{TT}_+(t,r,\vartheta,\varphi) + \mathrm{i}\ddot{h}^{TT}_\times(t,r,\vartheta,\varphi)\right] \tag{4.25}$$

using Eq. (4.2) we find

$$\left[rh^{TT}_{+\,\ell m}(t,r,\vartheta,\varphi)\right]_{r\to\infty} = {}_{-2}S_{\ell m}(\vartheta,0)\ \mathrm{Re}\, e^{im\varphi}\sum_{j=-\infty}^{\infty}\frac{2}{\omega_{mj}^2}\,\hat{A}_{\ell m}(\omega_{mj})e^{-i\omega_{mj}(t-r_*)} \tag{4.26}$$

$$\left[rh^{TT}_{\times\,\ell m}(t,r,\vartheta,\varphi)\right]_{r\to\infty} = {}_{-2}S_{\ell m}(\vartheta,0)\,\mathrm{Im}\, e^{im\varphi}\sum_{j=-\infty}^{\infty}\frac{2}{\omega_{mj}^2}\,\hat{A}_{\ell m}(\omega_{mj})e^{-i\omega_{mj}(t-r_*)}$$

where we have separated the $\varphi-$dependence of the spin weighted spherical harmonics, writing ${}_{-2}S_{\ell m}(\vartheta,\varphi) = {}_{-2}S_{\ell m}(\vartheta,0)\,e^{im\varphi}$.

4.2 Comparison between the perturbative and semirelativistic approaches

Using the theoretical framework described in the previous section, we have numerically integrated the equations of stellar perturbations for a set of bound orbits identified by selected values of the orbital parameters (E, L_z), or, equivalently, (e, r_P). The stellar model we have chosen for the calculations described in this section is a polytrope with $n = 1$, $\alpha_0 = 4.48974$ and $R_s/M = 4.739$. In computing the energy flux, we have seen that the energy is emitted at a discrete, infinite set of frequencies ω_{mj}, with $-\infty < j < +\infty$, defined in eq. (1.81). The output of our perturbative calculations are the amplitudes of the spectral lines $\dot{E}^R_{\ell mj}$ (4.19) and the corresponding waveforms (4.26).

The energy computed by the semirelativistic approach is also emitted at the same discrete frequencies ω_{mj}; however, whereas the quadrupole emission is resticted to $\ell = 2$, $m = (-2, 0, 2)$ for $h^{TT}_{\vartheta\vartheta}$ and $m = (-2, 2)$ for $h^{TT}_{\vartheta\varphi}$, for the relativistic calculations $\ell \geq 2$ and $-\ell < m < \ell$ for both polarizations. So we can only compare the two approaches restricting our relativistic calculation to $\ell = 2$ and comparing the quadrupole spectral lines $\dot{E}^Q_{mj}$ with the $\ell = 2$ relativistic lines $\dot{E}^R_{2mj}$. In figure 4.2 we show, as an example, the energy output for

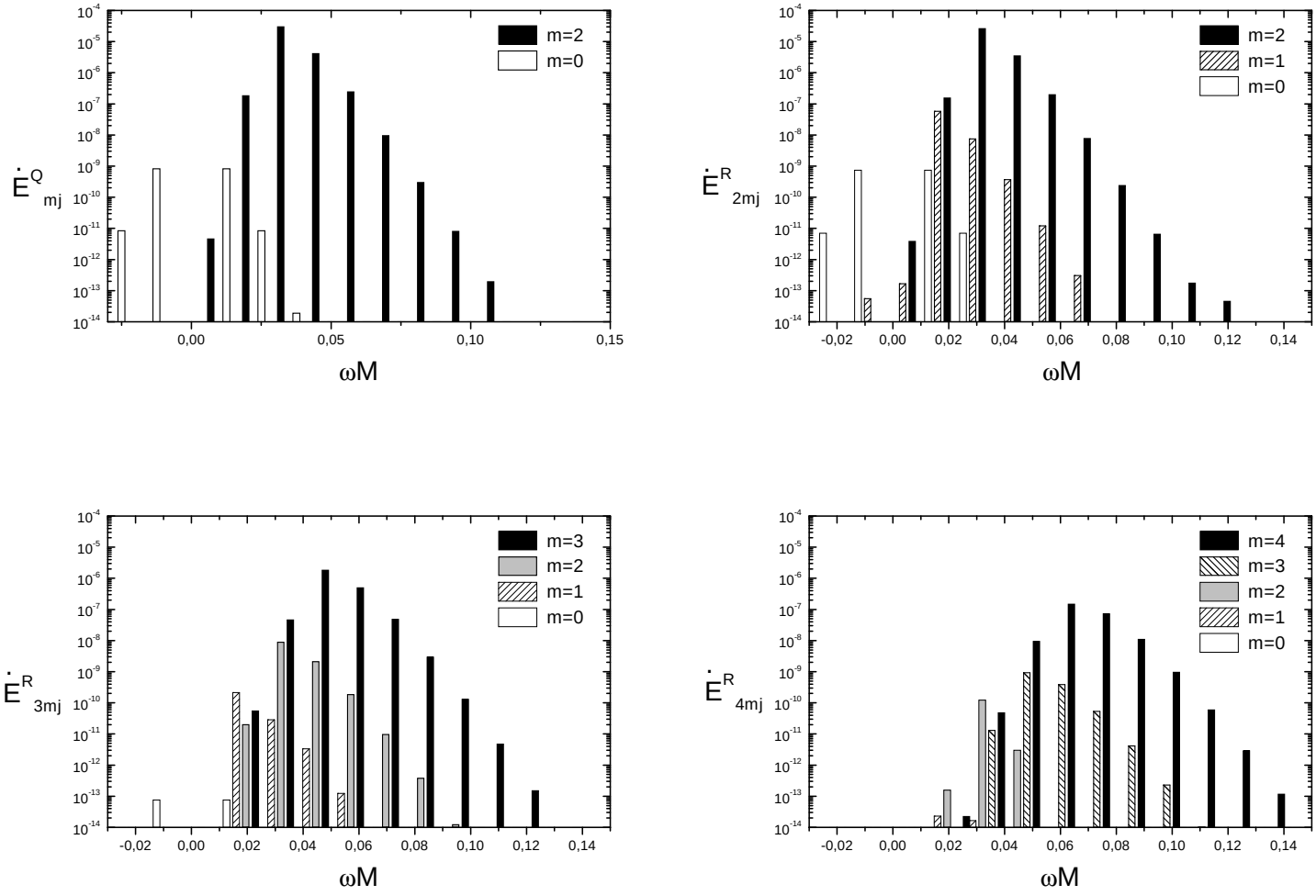

Figure 4.2: The gravitational emission associated to an eccentric orbit with $e = 0.1$ and $r_P = 3R_s$, is illustrated by plotting the amplitude of the spectral lines versus the dimensionless frequency $M\omega_{mj}$. The radiation computed by the hybrid quadrupole approach $\dot{E}^Q_{mj}$ (upper panel, left) has to be compared with that computed by the relativistic approach, $\dot{E}^R_{\ell mj}$, for $\ell = 2$ (upper panel, right). In the lower panel we plot the relativistic $\ell = 3$ and $\ell = 4$ contributions.

an orbit with periastron $r_P = 3R_s$ and eccentricity $e = 0.1$ computed by the quadrupole approach, and the relativistic results for $\ell = 2,\ 3$ and 4, for the same orbit. The spectral lines are plotted for the discrete values of the dimensionless frequency $M\omega_{mj}$, and for assigned values of positive m. We do not plot the lines corresponding to negative values of m because they can be obtained through a reflection across the zero frequency axis of the positive ones, by virtue of the symmetry property (4.22). A comparison of the quadrupole emission (upper panel, left) with the $\ell = 2$ relativistic emission (upper panel, right), shows that for $m = 0$ and $m = 2$ the two spectra are qualitatively similar. As expected, the three plots which refer to the perturbative results show that most of the energy is emitted in the $\ell = 2$ multipole, and that for each ℓ, the $\ell = m$ component is always larger than the others.

It is known that for particles in circular orbit around black holes the total power emitted in each multipole

$$\dot{E}^R_\ell = \sum_{j=-\infty}^{\infty} \sum_{m=-2}^{2} \dot{E}^R_{\ell mj} \tag{4.27}$$

scales with the multipole order as $\dot{E}^R_\ell \sim p^{2-\ell}$, where p is the orbital semi-latus rectum [66]. This power-law scaling was found analytically. Subsequently, Cutler *et al.* [27] numerically integrated the BPT equation for a Schwarzschild black hole with a point particle moving on bound orbits. They showed that the same result holds, at least in order of magnitude, also for particles in eccentric orbits. We find that a similar power law exists also for stars, both for circular and eccentric orbits, as indicated in figure 4.3 where, as an example, we plot the ratio $\dot{E}^R_\ell/\dot{E}^R_2$ as a function of ℓ, for an orbit with $e = 0.1$ and $p = 15.64$ ($r_P = 3\ R_s$).

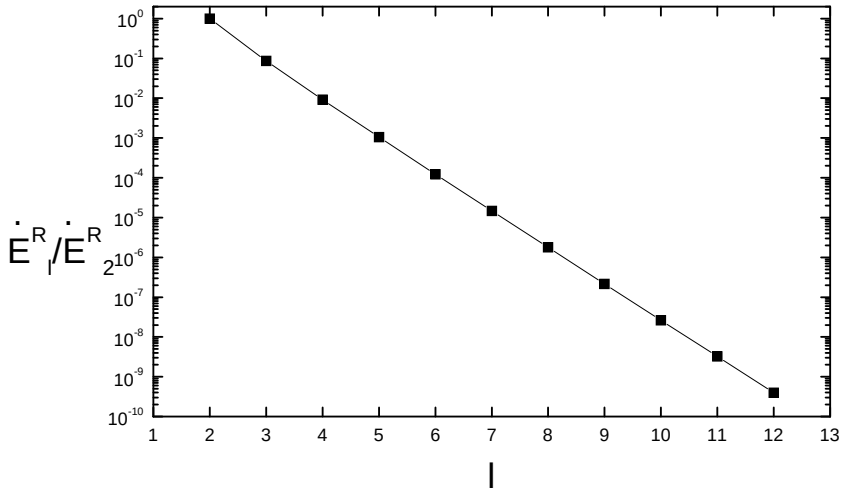

Figure 4.3: The ratio of the total power emitted in the ℓ-th multipole, $\dot{E}^R_\ell$, to the total power emitted in $\ell = 2$, $\dot{E}^R_2$, is plotted as a function of ℓ, for an orbit with $e = 0.1$ and $p = 15.64$ ($r_P = 3\ R_s$). It clearly shows a power law behaviour $\dot{E}^R_\ell \sim p^{\ell-2}$.

In table 4.1 we tabulate the ratio $\dot{E}^R_\ell/\dot{E}^R_2$ for different values of ℓ and for two circular orbits with $R_0 = 3\ R_s$ and $R_0 = 10\ R_s$, respectively. In figure 4.4 we show how the energy output

Table 4.1: Ratio of the power in the ℓ-th multipole, $\dot{E}^R_\ell$, to the power in $\ell = 2$ multipole for two circular orbits of radius $R_0 = 3R_s$ and $R_0 = 10R_s$, respectively.

	$\dot{E}^R_\ell / \dot{E}^R_2$	
ℓ	$3R_s$	$10R_s$
3	$8.6 \cdot 10^{-2}$	$2.7 \cdot 10^{-2}$
4	$9.2 \cdot 10^{-3}$	$9.2 \cdot 10^{-4}$
5	$1.0 \cdot 10^{-3}$	$3.3 \cdot 10^{-5}$
6	$1.2 \cdot 10^{-4}$	$1.2 \cdot 10^{-6}$

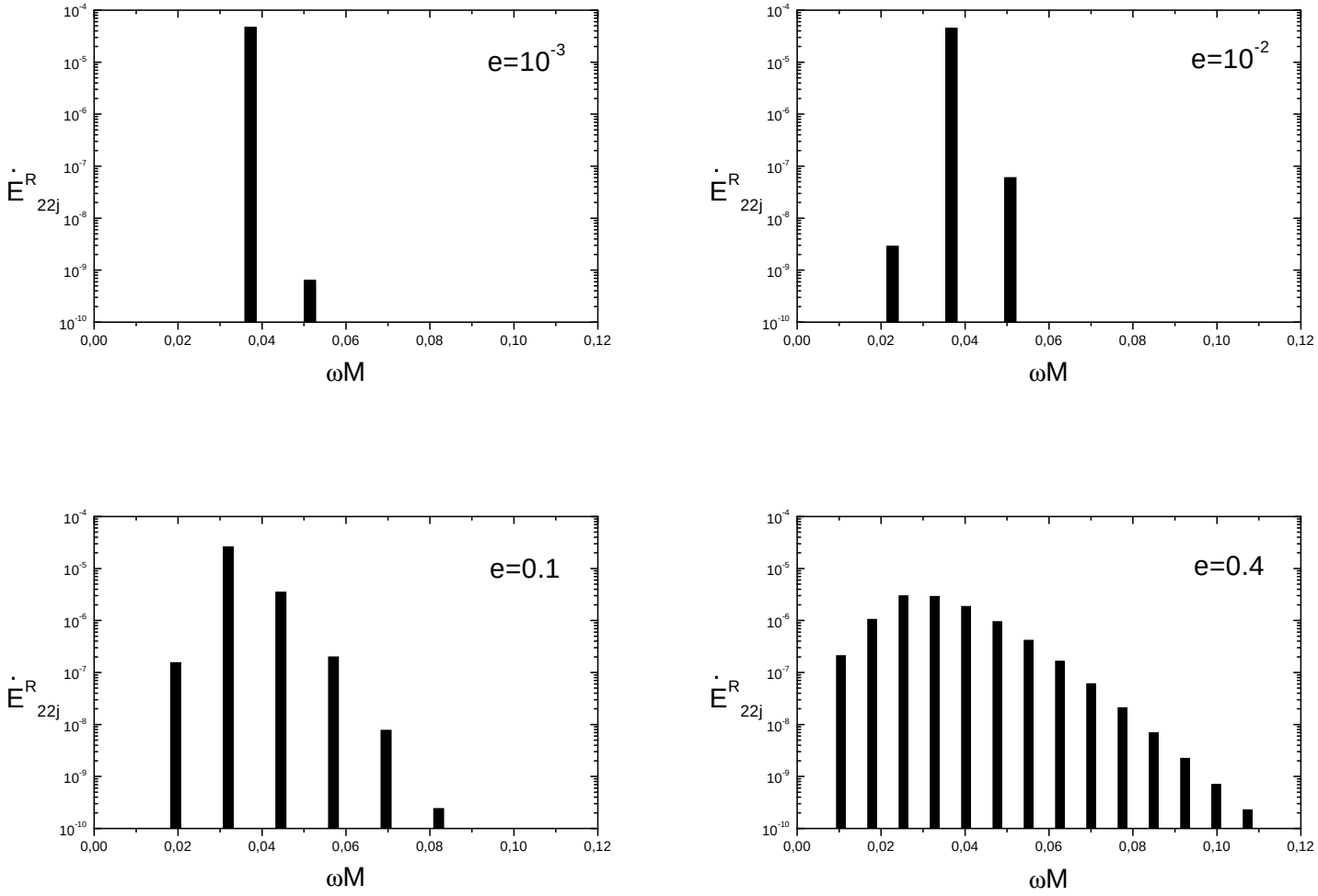

Figure 4.4: In this figure we show how the spectral content of the gravitational emission changes as a function of the eccentricity, plotting the spectral lines $\dot{E}^R_{\ell mj}$ as a function of the dimensionless frequency $M\omega_{mj}$, for $\ell = m = 2$ and for the same value of the periastron $r_P = 3\ R_s$. As the eccentricity increases, the location of the highest line shifts slightly towards a lower frequency, and higher order harmonics become more relevant.

obtained by the relativistic approach varies as a function of the eccentricity of the orbit; we consider four cases, $e = 10^{-3},\ 10^{-2},\ 0.1,\ 0.4$. All orbits have the same periastron ($r_P = 3R_s$), and the plots are given for $\ell = m = 2$, since this is the dominant contribution to the emitted radiation.

In the zero eccentricity limit, the whole power is concentrated in the harmonic with $j = 0$, corresponding to a frequency $\omega_{circ} = 2\frac{\Delta\varphi}{\Delta t} = 2\omega_k$, where ω_k is the keplerian orbital frequency; as the eccentricity increases, the frequency of the highest line slightly decreases, and higher order harmonics become significant.

We have compared the total power computed by the quadrupole formalism

$$\dot{E}^Q = \sum_{j=-\infty}^{\infty} \sum_{m=-2,0,2} \dot{E}^Q_{mj} \tag{4.28}$$

with that emitted in the $\ell = 2$ multipole, $\dot{E}^R_2$, defined in eq. (4.27) and computed by the perturbative approach, for different values of the eccentricity and of the periastron. We find that, in general, $\dot{E}^R_2$ is sistematically smaller than $\dot{E}^Q$. The amount of emitted radiation affects the orbital evolution of the system and the shape of the gravitational signal, in particular during the latest phases of coalescence, where the orbit is already circularized. To understand the relevance of this effect, which may be important for the detection of these signals by the ground based interferometers VIRGO and LIGO, we have computed the relative difference

$$\frac{\dot{E}^R_2 - \dot{E}^Q}{\dot{E}^Q} \tag{4.29}$$

for circular orbits, as a function of the orbital radius, R_0. The results are shown in figure 4.5. For large values of the radius the relative difference tends, as expected, to zero; at a distance of 10 stellar radii it is about 7 %, and it becomes greater than 14 % when the two stars are 3 R_s apart.

In order to check the correctness of our results, we have repeated the calculation by a different approach, integrating the inhomogeneous Zerilli and the Regge-Wheeler equations for the same orbits. The results agree to the round-off error.

The situation changes if the point mass moves on an orbit "resonant" with a mode of the star, which means the following. For the model of star we are considering, the lowest frequency mode is the fundamental one, whose frequency is $\omega_f M = 0.12034$. To excite this mode the mass should move on an orbit such that the frequency of one of the spectral lines of the quadrupole emission, ω_{mj}, with $m = -2, 0, 2$, is very close to, or coincides with ω_f. We find that, as the quadrupole spectral line frequency ω_{mj} approaches ω_f for some value of m and j, the amplitude of the emitted radiation, computed in the perturbative approach, increases. This suggests that the excitation mechanism could be seen as a resonant scattering of the gravitational wave emitted by the system in the orbital motion (the quadrupole wave) on the potential barrier generated by the perturbed star. Indeed, the discrete nature of the power spectrum emitted in the quasi periodic motion of the point mass suggests an analogy with an atomic laser: in this picture, the atomic energy levels correspond to the quasi-normal mode frequencies, and the quadrupole radiation frequencies to the energy of the electromagnetic radiation exciting them.

In order to excite the fundamental mode of our star, the two bodies must be very close, and therefore it is reasonable to assume that the orbit is circular and that ω_{mj} reduces to ω_{circ} defined above.

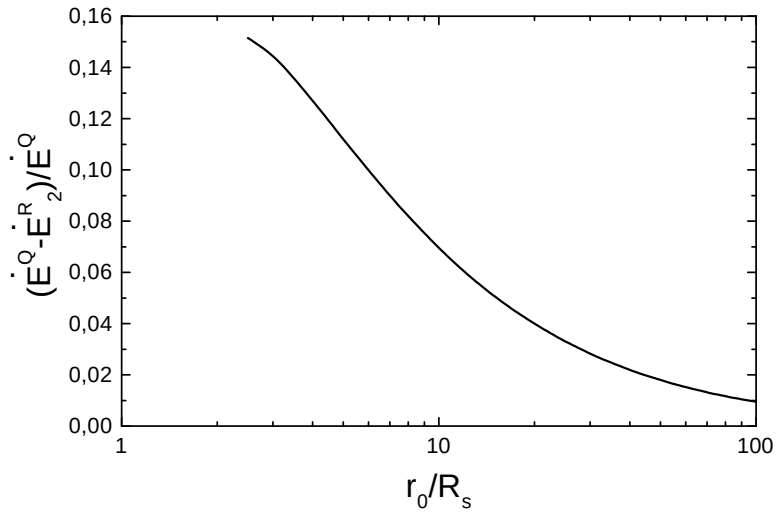

Figure 4.5: The relative difference between the total power $\dot{E}^Q$ computed by the hybrid quadrupole approximation, and the total power emitted in the $\ell = 2$ multipole, $\dot{E}_2^{(R)}$, computed by the relativistic approach, is plotted for circular orbits as a function of the radius R_0 (given in units of the stellar radius). When the point mass moves on an orbit far from the star the two approaches give the same result; the quadrupole emission becomes significantly larger than $\dot{E}_2^{(R)}$ for $R_0 < 10\, R_S$.

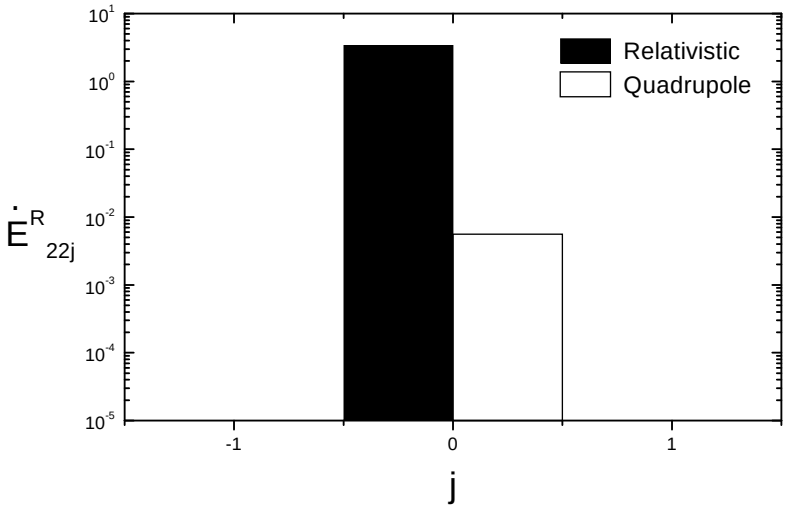

Figure 4.6: The spectral line emitted by the system when the point mass moves on a close circular orbit is compared to the same quantity computed by the hybrid quadrupole formalism. The relativistic line (in black) is much larger than the quadrupole one (in white), because the frequency of the quadrupole line coincides with that of the fundamental mode of the star, ω_f, and a mechanism of resonant excitation occurs (see text).

To show how efficient this resonant mechanism could be, in figure 4.6 we plot the energy output $\dot{E}^R_{22j}$, and the corresponding quadrupole energy $\dot{E}^Q_{2j}$ for a point mass moving on an orbit such that $\omega_{circ} = \omega_f$ ($R_0 = 1.37417\ R_s$).

From this figure we see that the situation changes dramatically with respect to the non-resonant case: the energy emitted in the relativistic calculation is about 600 times larger than that computed by the quadrupole approximation. Whether the fundamental mode could be excited during the coalescence of neutron star binary systems is, however, questionable, and we will discuss the issue in more depth in the following section.

It should be mentioned that the f-mode excitation by a particle in circular orbit around a star was studied also by Kojima [45]. In his paper he only considered circular orbits and polar perturbations with $\ell = 2,\ m = \pm 2$. We find the same qualitative behaviour, although with minor differences of the order of 10% in the wave amplitude. We are confident in the correctness of our results since, as mentioned above, we got them using two completely different formalisms, one based on the Regge-Wheeler, the other on the Newman-Penrose approach.

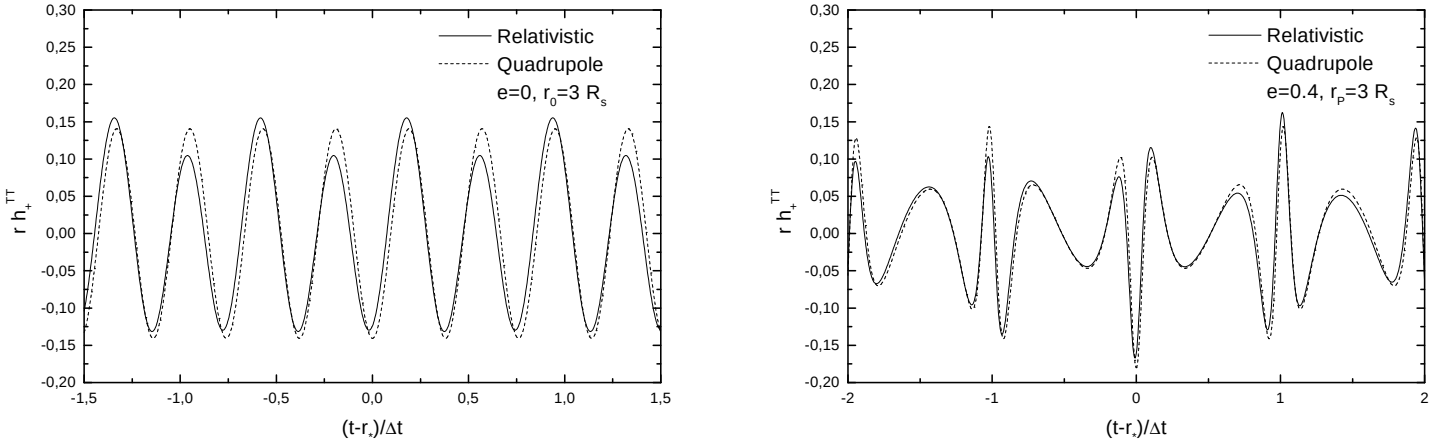

Figure 4.7: The left panel shows the h^{TT}_+ component of the gravitational wave emitted when the point mass moves on a circular orbit with $R_0 = 3\ R_s$, versus the retarded time in units of the orbital period. Since we assume that the observer is on the equatorial plane, the $h^{TT}_\times$ component vanishes. In order to compare the relativistic waveform (continuous line) with the waveform computed by the hybrid quadrupole approach (dashed line), only the $\ell = 2$ component of the relativistic signal is shown. The difference between the two signals is basically due to the $m = 1$ contribution of the axial perturbations to the relativistic waveform (see text). In the right panel we show the h^{TT}_+ component of the gravitational wave emitted when the point mass moves on an eccentric orbit with $e = 0.4$ and $r_P = 3R_s$. The structure of the waveform is much more complicated, but the beating of the frequencies induced by the $m = 1$ axial contribution is still present.

In the left panel of figure 4.7, we show the $+$ polarization of the waveform (the $\times$ polarization is zero because we assume the observer is on the equatorial plane) for a circular orbit with radius $R_0 = 3R_s$, and for $\ell = 2$. The gravitational waveform obtained in the quadrupole approximation is also shown (dashed lines) for comparison. There are two remarkable effects. The first is that the $m = 1$ axial contribution to the relativistic waveform, which is usually ignored, is not negligible. Indeed it induces a beating of the axial and polar frequencies, clearly

seen in the figure. The second effect is that the average of the amplitudes of the positive (or of the negative) peaks in the relativistic waveform, is smaller than that of the quadrupole waveform. This is related to the fact that the $\ell = 2$ relativistic energy output is systematically smaller than that of the quadrupole as we get close to the star (see figure 4.5).

A case with large eccentricity ($e = 0.4$) is shown in the right panel of the same figure. The structure of the waveforms is now much more complicated. However, both effects seen in the circular case are still present. The beating of the axial and polar frequencies produces similar changes in the maxima of the wave amplitude, i.e about 10 % in both cases. We have found that the relative contribution between the axial and polar emission $\dot{E}_\ell^{R\ ax}/\dot{E}_\ell^{R\ pol}$ is quite independent of eccentricity and decreases approximately as $\approx 1/p$, or, which is the same, as $\approx v^2$ (this behaviour was indeed found analitycally by Poisson in [66] for a particle orbiting a black hole). Thus, the beating becomes negligible at large distances, but it might be significant in the late stages of the inspiralling.

4.3 Excitation of quasi-normal modes in a compact binary coalescence

In the last section we have seen that, if an appropriate resonance condition between orbital frequencies and quasi-normal mode frequencies is satisfied, the stellar quasi-normal modes can be excited. Now we want to understand whether the quasi-normal modes of compact objects (stars or black holes) can be excited in an astrophysically plausible compact binary coalescence. We will conclude that it seems very unlikely to excite the quasi-normal modes of a black hole or the fundamental mode of a neutron star, unless the star is rotating. The possibility to excite the g-modes of a neutron star is an open and interesting question, which deserves to be studied more in detail, especially to assess its detectability or to understand possible dephasing effects that the excitation could have on the waveform of the coalescing binary.

First of all, we want to answer the following question: can we excite the quasi-normal modes of a black hole in a binary coalescence? Consider a test mass orbiting the black hole in circular orbit; the following considerations would not be substantially altered if we considered particles in more general, eccentric orbits. Recall that the frequency of black hole quasi-normal modes scales with the inverse of the black hole mass M_{BH}; since most of the radiation is emitted in the $\ell = m$ component, the resonance condition for the n-th quasi-normal mode overtone belonging to the ℓ-th multipole is:

$$M_{BH}\omega_n^\ell = mM_{BH}\omega_k = mp^{-3/2}, \tag{4.30}$$

with $\ell = m$. Let us concentrate on $\ell = 2$. The quasi-normal modes of Schwarzschild black holes have been computed accurately up to very high overtones using a continued fraction technique [60], and it turns out that the $\ell = 2$ overtone with lower frequency (if one excludes the so-called algebraically special mode, which is degenerate at zero frequency) is the one with $n = 10$, for which $M_{BH}\omega_{10}^2 = 0.06326$. Applying the excitation condition to this overtone, the corresponding value of p turns out to be 3.97. It is well known that only *unstable* orbits are possible for $p < 6$: this means that the possibility of exciting black-hole quasi-normal modes with a particle in a *stable*, closed orbit is minimal, unless one goes to very high multipole orders - in which case, of course, we cannot expect the total power to increase significantly because of the excitation. Of course, this does not rule out the excitation of black hole quasi-normal modes

in a stellar collapse, and such an excitation is indeed present both in numerical and perturbative simulations of collapse.

Let us now turn our attention to stars. The stellar g-modes can probably be excited by a resonant mechanism in some binary systems, but the relevance of this type of excitation on the detectability of gravitational waves is still to be understood, and we plan to study this problem in the future. Here we concentrate instead on the fundamental mode of oscillation (f-mode). The conditions that must be satisfied in order to excite the stellar f-mode, besides the excitation condition (4.30), are essentially two: the one imposed by an eventual general-relativistic orbital instability (i.e., the existence of an Innermost Stable Circular Orbit or ISCO) and the condition that the stars must be at least detached (or possibly quite far away, so that perturbation theory holds with a good enough accuracy).

The existence of an ISCO due to an orbital instability has been questioned by recent numerical computations by Uryu *et al.* [87], who computed sequences of binary neutron stars in quasi-equilibrium, parametrized by the distance among the stars, in full GR, and found only an hydrodynamic (not an orbital) instability which showed up through the appearance of a cusp in the sequence of quasi-equilibrium configuration. Anyway, if an ISCO exists, as Post-Newtonian computations seem to indicate, then, in order for the modes to be excited, the frequency of the f-mode must be smaller than the gravitational wave emission frequency at the ISCO. Let us concentrate on two identical neutron stars, both of mass M_{star}. Post-Newtonian predictions differ quite sensibly on the location of the ISCO, depending on the approach used to expand the Einstein equations. For example, Kidder, Will and Wiseman [43] and Damour, Iyer and Sathyaprakash [28] predict respectively that the gravitational wave frequency at the ISCO is given, in terms of the mass of each star, by:

$$\nu_{ISCO}^{DIS} = 2859.7 M_\odot / M_{star}, \qquad \nu_{ISCO}^{KWW} = 1894.0 M_\odot / M_{star}. \tag{4.31}$$

Of course these relations only involve the masses of the objects, since Post-Newtonian calculations do not take into account any structural effect nor any dependence of the ISCO on the stellar equation of state.

To understand whether it is possible or not to excite the f-mode in a binary neutron star coalescence we will focus on three different models for the EOS, chosen among the set studied in [7] (see [8] for more details). They are:

- Pandharipande, model A. The star is described in terms of pure neutron matter, the dynamics of which is dictated by a nonrelativistic hamiltonian containing a semiphenomenological interaction potential [62].

- Wiringa, Fiks and Fabrocini, model WFF. Neutron star matter is treated as a mixture of neutrons, protons, electrons and muons in β-equilibrium. The nuclear hamiltonian includes two- and three-body potentials. With respect to models A and B, the ground state energy of neutron star matter is computed using a more sophisticated and accurate many-body technique [88].

- Pandaripande & Smith, model L. Neutrons are assumed to interact through exchange of $\omega-$, $\rho-$ and $\sigma-$mesons. While the exchange of heavy particles (ω and ρ) is described in terms of nonrelativistic potentials, the effect of the $\sigma-$meson is taken into account using relativistic field theory and the mean-field approximation [63]. The physical assumptions underlying this *hybrid* approach are somewhat different from those of the previous models.

Models A and L, though quite old, have been chosen as quite extreme representatives of nuclear physics motivated EOS's, while model WFF is a good candidate as a modern, "realistic" model for the EOS. Anyway, here we are just interested in an explorative survey of the possibility to excite the f-mode in a binary coalescence, and we will not touch upon the issue of the reliability of the different EOS's.

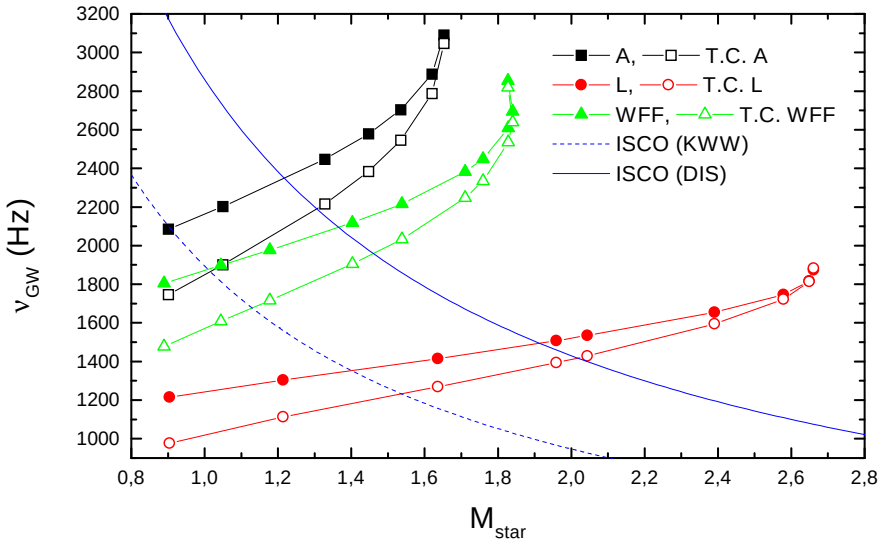

Figure 4.8: The hyperbolas are the limits imposed by the orbital ISCO, according to the predictions by Kidder, Will and Wiseman (KWW) and by Damour, Iyer and Sathyaprakash (DIS), as functions of the mass of each of the two stars (in solar mass units). The lines with filled symbols correspond to the f-mode computed for a non-rotating star, the ones with empty symbols correspond to the frequency limit imposed by the touch condition (which of course, being dependent on the stellar radius, depends also on the EOS). Even when the ISCO condition does not prevent the excitation of the f-mode, the severe constraint imposed by the touch condition does.

In figure 4.8, lines with filled symbols show the frequency of the f-mode, that we have computed for different stellar models described by the three different EOS's, as a function of the mass of each of the two stars (remember that the two stars are supposed to be equal in mass and radius to each other). In the figure, hyperbolas correspond to the frequency limits imposed by the ISCO. The curves with filled symbols show that, for each equation of state, at least in a certain mass range, the f-mode frequency can be lower than the limit imposed by the ISCO. In other words, depending on the stellar model, the ISCO limit does not always prevent the excitation of the f-modes.

But, unluckily, this is not the final word. We must take into account not only the frequency limit imposed by the ISCO, but also the condition that the stars must be detached if the mode has to be excited during a coalescence. We will simply impose the f-mode frequency to be smaller than the "contact" frequency corresponding to a separation $2R_{star}$, where R_{star} is the

radius of each star, i.e.:

$$\nu_f < \nu_{touch} = \frac{1}{2\pi}\left\{2\sqrt{\frac{G\cdot 2M_{star}}{(2R_{star})^3}}\right\} \tag{4.32}$$

In figure 4.8, the lines with empty symbols correspond to the contact frequency, which is smaller than the f-mode frequency for all the EOS's we have considered, except for the highest-mass model represented by EOS L (which, however, seems not to be viable because of the ISCO condition!). So in all cases shown (and we recall that EOS A and L are quite extreme models among the ones considered in the literature) the stars touch *before* the excitation condition of the f-mode is satisfied.

Observations [68] seem to indicate the possible existence of more compact stars (for example, stars with mass $M_{star} \sim 1.4M_\odot$ and radius $R_{star} \sim 7$ km), and this would reduce the limits imposed by the touch condition. On the other hand, when the radius decreases the frequency of the mode increases according to the semiempirical law given by Andersson and Kokkotas [2]:

$$\nu_f = \left(0.78 + 1.635\sqrt{\frac{\tilde{M}}{\tilde{R}^3}}\right) \text{ kHz}, \tag{4.33}$$

where

$$\tilde{M} = \frac{M_{star}}{1.4M_\odot}, \qquad \tilde{R} = \frac{R_{star}}{10\text{ km}}.$$

We have performed a numerical test, computing the f-mode for a wide range of polytropic models (varying both α_0 and n). In all cases we considered, the touch condition prevents the excitation of the f-mode of a non-rotating star in the coalescence phase.

An alternative idea to excite the f-mode could be that of considering a binary composed by a neutron star *and a black hole*. In this case the critical radius is the so-called *tidal radius* R_{tidal}, given by [10]:

$$R_{tidal} \sim 2.4R\left(\frac{M_{BH}+M_{star}}{M_{star}}\right)^{1/3}, \tag{4.34}$$

where M_{BH} is the black hole mass. Clearly, the quantity in round parentheses is of order unity (in fact, it is always greater than one!), so this limit is *always* more stringent than the touch condition. The essential reason is that tidal effects due to the black hole are always stronger, being the object more compact, than tidal effects due to a neutron star.

Despite these negative conclusions, we should not forget that in all our considerations we have not taken into account stellar rotation, which allows the excitation of the f-mode at larger orbital distances [48]. We shall soon extend our work to rotating stars to understand, among other things, if the excitation of the f-mode can play any role in a realistic astrophysical scenario.

4.4 Orbital evolution

The evolution under radiation reaction of bound orbits (not necessarily circular orbits) in the spacetime surrounding a Schwarzschild black hole or a non-rotating neutron star is best described using the parameters (p, e) that we introduced in section 1.4.1, as suggested in [27].

Bound orbits are represented by those points in the (p, e) plane which satisfy the inequalities $0 \leq e \leq 1$, $p \geq 6 + 2e$. Following [27], we will call the boundary $p = 6 + 2e$ the *separatrix*. Indeed, a study of the effective potential in terms of p and e shows that this line corresponds to unstable circular orbits, and whenever $p < 6 + 2e$ the orbit is a plunging one.

In the absence of radiation reaction, p and e are constants of the motion, since they are in a one-to-one relation with the orbital energy and angular momentum, as can be seen from equations (1.68). If we include radiation reaction using the adiabatic approximation, p and e evolve slowly over a time scale which is long compared to the orbital period, and the evolution of a given orbit traces a trajectory in the (p, e) plane. The evolution of p and e can be deduced from equations (1.68); using the chain rule for derivatives on the energy and angular momentum conservation equations,

$$m_0 \dot{E} + \dot{E}_{GW} = 0 \tag{4.35}$$
$$m_0 \dot{L}_z + \dot{L}_{z,GW} = 0, \tag{4.36}$$

we get:

$$-\dot{E}_{GW} = \left(\frac{\partial E}{\partial p}\right) m_0 \dot{p} + \left(\frac{\partial E}{\partial e}\right) m_0 \dot{e} \tag{4.37}$$
$$-\dot{L}_{z,GW} = \left(\frac{\partial L_z}{\partial p}\right) m_0 \dot{p} + \left(\frac{\partial L_z}{\partial e}\right) m_0 \dot{e} \tag{4.38}$$

Inverting the previous relations we can find $\dot{p}$ and $\dot{e}$ in terms of the energy and angular momentum lost in gravitational waves:

$$m_0 \dot{p} = \frac{2(p-3-e^2)^{1/2}}{(p-6-2e)(p-6+2e)} \times \left[p^{3/2}(p-2-2e)^{1/2}(p-2+2e)^{1/2}\dot{E}_{GW} - (p-4)^2 \dot{L}_{z,GW}/M\right] \tag{4.39}$$

$$m_0 \dot{e} = \frac{(p-3-e^2)^{1/2}}{ep(p-6-2e)(p-6+2e)} \times \left\{-p^{3/2}(p-2-2e)^{1/2}(p-2+2e)^{1/2}\dot{E}_{GW} + \right. \\ \left. + (1-e^2)\left[(p-2)(p-6)+4e^2\right]\dot{L}_{z,GW}/M\right\} \tag{4.40}$$

Notice that the equations are singular at the separatrix, $p = 6 + 2e$. The energy and angular momentum losses can be evaluated using the BPT formalism through formulas (4.23) and (4.24). So the crucial ingredients in the computation of the orbital evolution are the energy and angular momentum lost at any given couple of orbital parameters (e, p). In section 4.2 we have seen that, at a given semi-latus rectum p (or at a given orbital velocity $v = p^{-1/2}$), the power computed by the semirelativistic approach is sensibly different from the power in $\ell = 2$ computed by the full perturbative approach, and this difference is also evident in the waveforms we have shown in figure 4.7. In general, we expect the deviations from the quadrupole and semirelativistic quadrupole computations to grow (and the orbital evolution to change) as the orbital separation p decreases. The main question we want to answer in this chapter is basically: how significant are these deviations when we take into account the structure of the central object? For example, what kind of difference can we expect if the central object is a neutron star instead of a black hole, or when we take into account different models for the neutron star matter EOS?

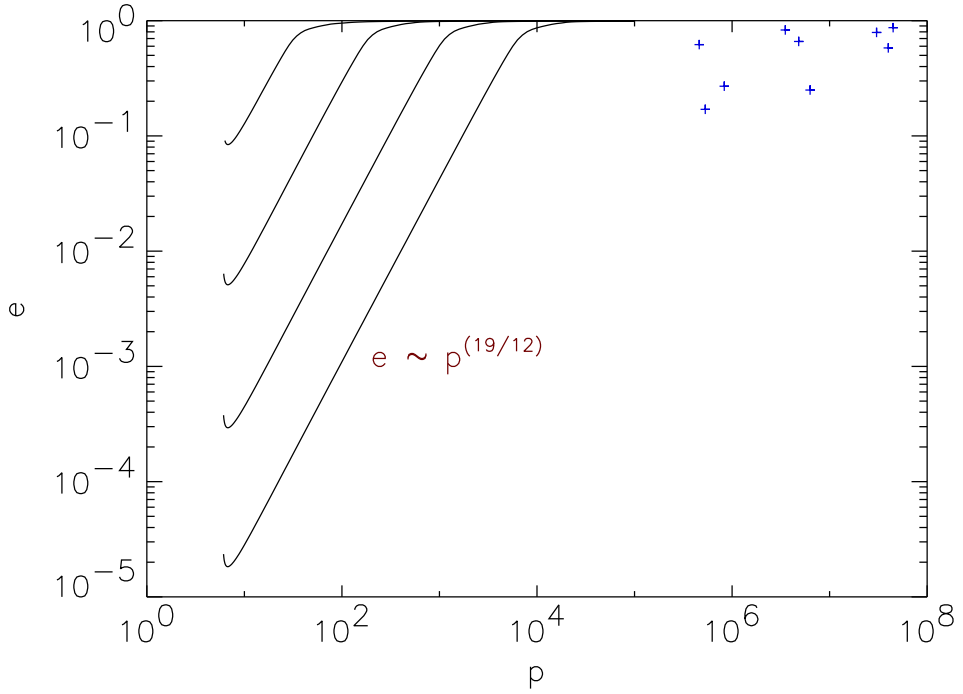

Figure 4.9: Evolution of the eccentricity as a function of orbital separation for different initial values of p, and initial eccentricity $e \sim 1$. Unless the system is formed with very large eccentricity at small ($p \lesssim 10^3$) orbital separations, when $p \sim 10^2$ and the signal enters the interferometers' bandwidth the orbit will be, in practice, perfectly circular. At large orbital separations the eccentricity scales as $p^{19/12}$, as predicted by the newtonian quadrupole formula [65].

A first answer is that, since structure-induced deviations at large distances are small, one of the key predictions of the quadrupole formula, i.e., that radiation reaction tends to circularize the orbits, remains true. If we take as initial data for our evolution the measured parameters for binary pulsars given in [53], for example, it is clear from figure 4.9 that, unless a binary system is formed with large eccentricity at very small orbital separations ($p \lesssim 10^3$), the eccentricity will always be practically zero by the time the waves enter the VIRGO/LIGO bandwidth, which corresponds to orbital separations $p \sim 10^2$. The blue dots in the figure correspond to observational data on the orbital separation and eccentricity of binary pulsars taken from [53]. From the evolutionary tracks shown in the plot we deduce that all observed binary pulsars will have essentially zero eccentricity by the time they get close enough to be detectable by ground-based interferometers. Since the evolution at large distances is accurately described by the quadrupole approximation, this prediction is not altered when we include structural effects in the evolution.

Still, the structure of the central object could make a difference on the number of cycles the binary spends in the interferometer bandwidth. Such a difference could reduce drastically the signal-to-noise ratio in a measurement of the waves emitted by the system with respect to the signal-to-noise ratio that would be achieved when matched-filtering the signal with an exact model for the waveform. We will investigate this issue in the following sections.

4.5 Comparison between neutron stars and black holes

In this section we will show what kind of difference we can expect in the power output from a binary system composed by a black hole and a test mass and a binary system composed by a neutron star and a test mass. In particular, we will study how such a difference depends on the model we choose for the EOS describing the neutron star structure.

As a first step, we have checked our numerical codes by specializing them to the black hole case, and comparing with existing results in the literature. In particular, we have repeated some of the calculations performed by Poisson *et al.* in a series of papers (see, in particular, [66], [3], [27], [67]) in which they dealt with a problem essentially analogous to ours, computing (both analytically and numerically) the radiation emitted by a system composed by a *Schwarzschild black hole* and a test mass. Our black hole code has proven to be able to reproduce extremely well their results. Then we compared the results obtained for the black hole with those we get when we consider the neutron star-test mass case. The aim of this computation was essentially to investigate what kind of difference (if any) is present in the orbital evolution of a system composed by a black hole and a test mass, or by a star and a test mass.

As a "normalized" measure of the difference in the power emitted (and, as a consequence, in the orbital evolution) we will use the ratio $P(v)$ between the power $\dot{E}$ predicted by our relativistic calculation (either for the black hole or for a neutron star model) and that predicted by the Newtonian quadrupole formula in the test mass case (1.51), $\dot{E}_N$:

$$P(v) \equiv \dot{E}/\dot{E}_N. \tag{4.41}$$

In the point-mass limit the function $P(v)$ is effectively "universal", in the following sense. For a Schwarzschild black hole this function only depends on the orbital velocity (or orbital separation), and not on the mass of the particle, nor on the mass of the black hole (both $\dot{E}$ and $\dot{E}_N$ scale in the same way with M and m_0). Indeed, for a particle orbiting a Schwarzschild black hole one can expand the BPT equation in powers of v/c and solve it order by order; Tanaka *et al.* (see [79] for a complete description of their method, and [78] for a shorter discussion of the results) were able to obtain in this way an analytic Taylor-series expansion of $P(v)$ (with logarithmic corrections), up to order v^{11}. We will give numerically the coefficients of this expansion in formula (4.55). For stars this "universality" is valid only *for each given equilibrium stellar model*: so, once we specify the EOS and a given value of the central density (of course, for each given EOS we have a one-parameter family of stable neutron stars), the function $P(v)$ can be thought of as a "form factor" for the response of the star and/or the black hole, which describes how the effects due to the non-pointlike nature of the extended object modify the naive quadrupole-formula prediction. Looking at the shape of the function $P(v)$ for different equations of state we can not only see the difference between the black hole case and different stellar models; we can also try to understand, at least qualitatively, what may happen to the gravitational wave emission by the "real" binary system when we choose different models for the high density equation of state.

Before spending some words on the accuracy of our codes we want to stress again that, in the test mass limit, $P(v)$ can be computed within any required level of accuracy. Consider for example a test mass orbiting a Schwarzschild black hole; in this case we know analytically from [66], and numerically from [27], that the relative contribution of each multipole to the total power output scales as $p^{2-\ell}$. This prediction is clearly verified by our numerical codes, as can be seen in figure 4.10, where we plot the relative contributions to $P(v)$ originating from multipoles with $\ell = 2,\ 3,\ 4$ as a function of $v = p^{-1/2}$.

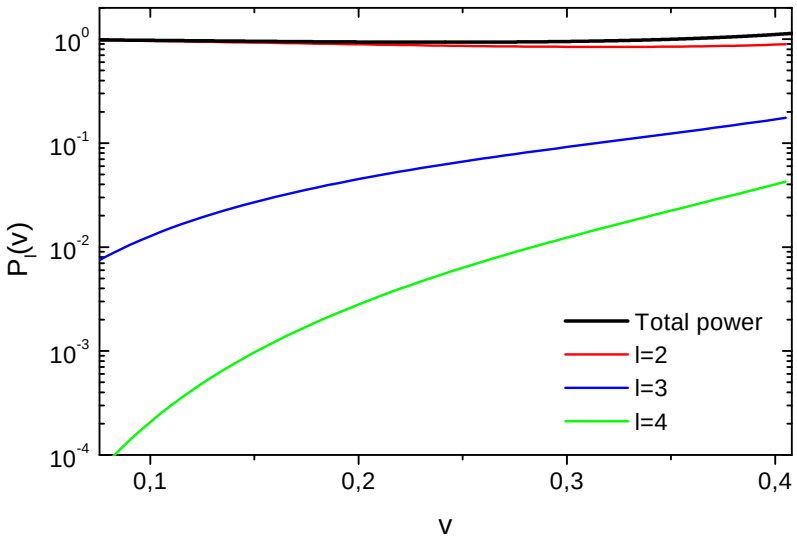

Figure 4.10: Contributions to the total power emitted by a black hole and a test particle for different values of ℓ.

This means that, for any given v, we can compute the power output at any given level of accuracy by summing enough multipoles in the formula for the total power emitted by the system. Since we have checked that the same power-law behaviour holds also for stars (see figure 4.3), we can use a similar criterion to compute $P(v)$ "exactly" for any given stellar model.

We have checked that our black hole code can reproduce with great accuracy the numbers in paper [26], were the case of circular orbits was studied numerically in detail. In particular, using a suitably high number of points (typically ~ 100) in our Gauss-Legendre integration routines (see Appendix B.5), we can reproduce all the numbers given in their table I (where multipoles from $\ell = 2$ to $\ell = 5$ are summed to get the total power for many values of p) and in tables II, III and IV (where they give the contributions $\dot{E}_{\ell m}$, for different values of m and ℓ, at $p = 10$, 150 and 1000, respectively) with an accuracy of (at least) less than one part in 10^6. To measure the error involved in the truncation of the sum over multipoles,

$$\sum_{\ell=2}^{\ell_{max}} \dot{E}_\ell,$$

we can evaluate the relative contribution of $\dot{E}_{\ell_{max}}$ to the total power emitted. In our calculations we have chosen to sum multipoles up to $\ell = 7$; that's because at the ISCO ($p = 6$), for a Schwarzschild black hole, we find that

$$\dot{E}_7 \left[\sum_{\ell=2}^{7} \dot{E}_\ell\right]^{-1} = 1.82 \cdot 10^{-5},$$

while at $p = 174.6$ (corresponding to a frequency of 10 Hz, when the emitted signal enters the LIGO/VIRGO sensitivity band and most of the cycles spent by the binary in the band is

accumulated) the same quantity is equal to $1.35 \cdot 10^{-12}$. The first number is a measure of the largest error we can expect in our calculations, but the second is much more indicative of the order of magnitude of the error involved in the computation of the number of cycles and signal-to-noise ratio, since most of the cycles are spent by the test mass in a region far away from the central object (at frequencies less than about 300-400 Hz).

The crucial question is now: how does the power emitted, and hence the orbital evolution, depend on the presence of a black hole or a star in the binary? And if the central object is a star, what is the role played by the high-density equation of state?

Table 4.2: We give here the parameters for the polytropic models we consider in our analysis: polytropic index, ratio $\alpha_0 = \epsilon_0/p_0$ of central energy density to central pressure, mass and radius. In all the models, the central energy density is chosen in such a way that the stellar mass is equal to $1.4 M_\odot$ (the "canonical" neutron star mass value).

Model number	n	α_0	M ($M_\odot$)	R_s (km)
1	1	4.48974	1.4	9.8
2	1	9.669	1.4	15
3	1.5	8.205	1.4	15
4	1.5	2.146	1.4	9

To answer these questions we picked three different, simplified models for our star. They are polytropic models whose parameters we give in table 4.2. Comparing models 2 and 3 we can see qualitatively the effect of varying the *stiffness* (i.e., the polytropic index) of the equation of state for a fixed mean stellar density (or for a fixed compactness M/R_s, which is the same); likewise, comparing models 1 and 2 we can see what happens when the compactness varies for a fixed polytropic index. We have chosen to include model 4 because it is extremely compact, so we expect it to yield results very close to those obtained with the black hole code.

In the following, since we are interested in effects that take place in the last phases of coalescence, when the orbit is already circularized, we will always limit our discussion to test masses in *circular orbits*.

First of all, let us see what happens to the emission from a given stellar model when we take into account contributions coming from multipoles with $\ell > 2$. Let us focus, for concreteness, on model 2. The contribution of each multipole to the total power is shown as a function of the particle's orbital velocity in figure 4.11. In the plot, the upper limit on v is chosen imposing the condition that the orbital radius $R_0 = pM$ be greater than the stellar radius.

The contribution from $\ell = 2$ (red curve) clearly shows a peak at the velocity corresponding to the usual f-mode resonance condition, $\omega_f^{\ell=2} = 2\omega_k$. However, the curve for $\ell = 3$ is peaked at a *different* value of the orbital velocity, corresponding to the excitation condition $\omega_f^{\ell=3} = 3\omega_k$. Similarly, we find peaks for each ℓ at velocities corresponding to

$$\omega_f^\ell = \ell\omega_k, \tag{4.42}$$

which means that the leading ($\ell = m$) gravitational wave contribution from each ℓ must be resonant with the f-mode frequency *for the given multipole* in order for the mode to be excited. Since the mode frequencies grow less rapidly than integers with the multipole order, the excitation condition for $\ell = 3$ (for example) corresponds to lower velocities and lower orbital frequencies: even if we cannot observe the excitation of the quadrupole f-mode, we may be

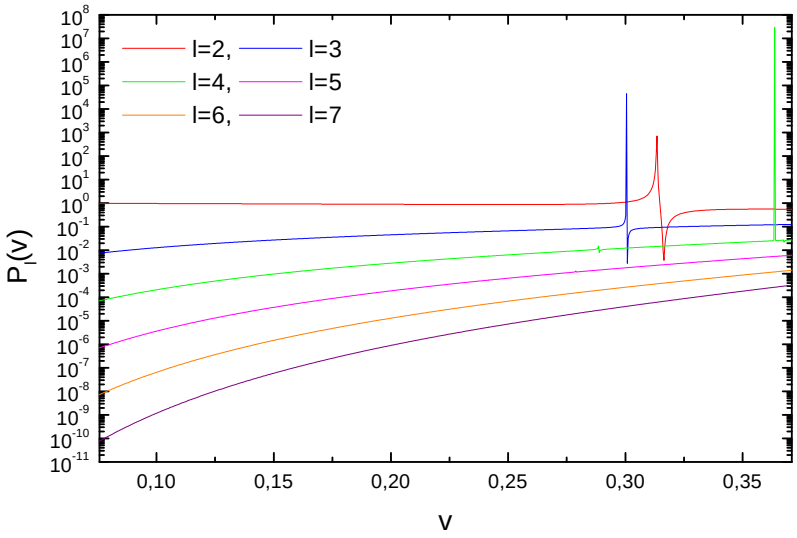

Figure 4.11: Contributions to the total power for different values of ℓ. The model shown here is model 2 ($n = 1$, $R_s = 15$ km). As usual, the power in each multipole is normalized to $\dot{E}_N$.

able, in principle, to observe an *octupole* excitation! When ℓ id large enough, we even start seeing the excitation of the first p-mode (see the green peak at the right of the figure, corresponding to the curve for $\ell = 4$).

As the multipole order increases, the peaks become higher and narrower; a high resolution in v is required to "catch" the peaks when $\ell > 4$ (indeed, in place of the peak, we observe just a kink corresponding to the f-mode excitation in the curve for $\ell = 4$, and the resolution we used to produce the plot was unable to resolve peaks for $\ell > 4$).

The total power spectrum for our model 2 is compared to the other models in figure 4.12. We recall here that all models, for ease of comparison, were chosen to have the same mass.

Models 1 and 3 show two peaks each, correponding respectively to the excitation of the $\ell = 2$ and $\ell = 3$ f-modes. The higher, narrower peak corresponds to $\ell = 2$, while the peak for the quadrupole mode is larger and about 100 times smaller. In model 2, besides the two peaks corresponding to the excitation of the f mode in $\ell = 2$ and $\ell = 3$, a third peak, corresponding to the excitation of the first p-mode in $\ell = 4$, is visible. Model 4, as expected, is almost indistinguishable from the black hole, and only the $\ell = 3$ f-mode excitation can be seen in this plot. Notice that all maxima are accompanied by corresponding minima, although not always we have used a numerical grid in v fine enough to resolve the minima for narrower peaks. Comparing models 2 and 3 one can see that, for a given compactness M/R_s, the peaks for model 2, which is stiffer, are higher and at lower frequency than those for model 3 (which is softer). At a fixed polytropic index, the peaks are higher and at lower frequency for model 2 than for model 1, which is more compact.

The behaviour in frequency is quite obvious, since mode frequencies typically scale with the mean density of the star, as is well known from Newtonian pulsation theory, because of the virial theorem. Not so obvious is the fact that the star seems to "respond more" to the excitation when the equation of state is stiffer (smaller n) at a given value for the compactness M/R_s, or

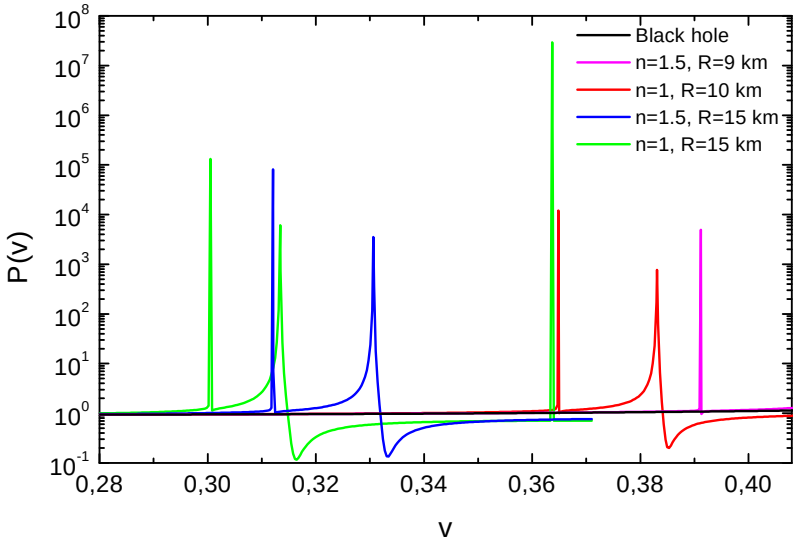

Figure 4.12: Total power output for models 1 (red), 2 (green), 3 (blue) and 4 (purple). The peaks shown are due to the excitation of the stellar quasi-normal modes (see text for a discussion). In models 2 and 3, the curves are truncated at a value of v corresponding to an orbital radius equal to the stellar radius. The black curve corresponds to the black hole case.

(which is the same) when the stellar radius is larger for a given value of the mass.

Table 4.3: In this table we give, for each peak shown in figure 4.12 and each stellar model: the type and multipole order of the excited mode, the velocity of the test mass at the peak, the corresponding keplerian frequency and the mode frequency in Hz, the orbital radius of the test mass in resonant conditions in km and the same quantity in units of the stellar radius.

Model	Mode	ℓ	v	ν_k (Hz)	ν_f (Hz)	R_0 (km)	R_0/R_s
1	f	3	0.365	1119	3358	15.5	1.59
1	f	2	0.383	1296	2593	14.1	1.44
2	f	3	0.300	626	1879	22.9	1.53
2	f	2	0.313	711	1422	21.0	1.40
2	p	4	0.364	1110	4440	15.6	1.04
3	f	3	0.312	702	2105	21.2	1.41
3	f	2	0.331	835	1671	18.9	1.26
4	f	3	0.391	1379	4138	13.5	1.50

In table 4.3 we give, for each peak shown in figure 4.12 and for each of the four stellar models: the excited stellar mode, the value of ℓ for which the excitation takes place, the peak velocities, the corresponding keplerian frequencies calculated from

$$\nu_k = \frac{2.9979 \cdot 10^5 \, v^3}{2\pi M_{km}},$$

where M_{km} is the stellar mass in kilometers (recall that $1M_\odot = 1.4768$ km!), the mode frequencies (related to the keplerian frequencies by $\nu_{mode} = \ell\nu_k$), and finally the orbital radius

$$R_0 = pM_{km} = M_{km}/v^2,$$

in kilometers and in units of the stellar radius.

We will come back to a qualitative analysis of the resonances, based on a very simple model, in the next section. But first we want to answer the following question: when do the different stellar models begin to deviate significantly (if they do) from a black hole, in terms of the predicted power output?

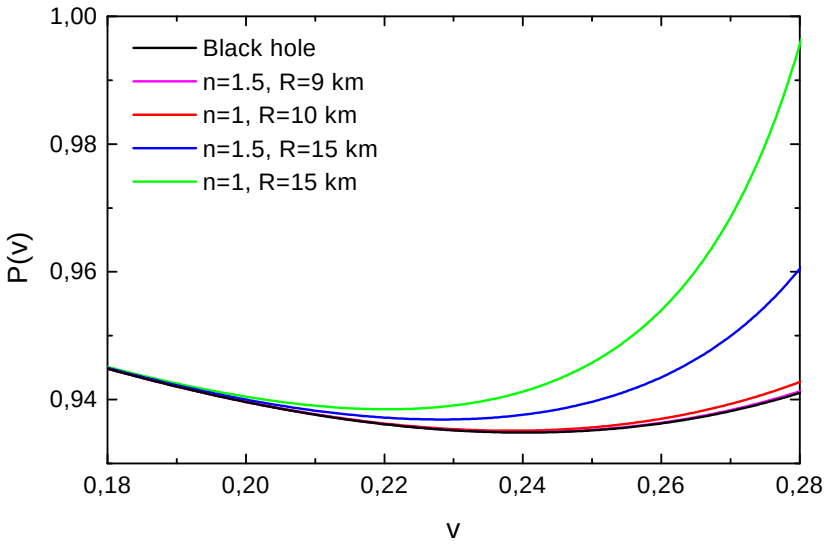

Figure 4.13: We show $P(v)$ for the black hole model and our four stellar models in the low-velocity region. Significant deviations clearly begin to show up, at least for stiffer models, at velocities $v \sim c/4$. Models 1 and 4 are much more similar to the black hole case up to much higher orbital velocities.

The answer is in figure 4.13, which clearly shows that effects due to the stellar structure typically begin to play a role when the orbital velocity is $v \simeq 0.25$. Not only, as shown by the analysis of the peaks given above, stiffer models tend to "respond more" and earlier to the excitation; from figure 4.13 we see also that they tend to deviate earlier from the power output predicted by the black hole case.

The meaning of this result in terms of orbital frequencies and detectability of the waves crucially depends on the way in which we interpret the result. In the *point mass limit*, a velocity $v = c/4$ corresponds to a keplerian frequency $\nu_k = 360.6$ Hz, a gravitational wave frequency $\nu_{GW} = 721.2$ Hz and an orbital radius of 33 km. At this orbital separation, strongly nonlinear effects will probably take over, and we cannot trust our linear theory any more. But suppose we want to extrapolate our results to *equal masses*. The standard procedure used in the literature for this purpose [27, 78] is to substitute in all formulas the particle mass m_0 by the reduced mass of the system μ, and the stellar mass M by the total mass of the binary M_t:

$$m_0 \to \mu, \qquad M \to M_t. \tag{4.43}$$

If we adopt this procedure and express the total mass of the system in kilometers, a quarter of the speed of light corresponds to a gravitational wave frequency $\nu_{GW} = 2\nu_k$ and to an orbital separation r given by

$$\nu_{GW} = \frac{2.9979 \cdot 10^5 \; v^3}{\pi M_t}, \qquad r = M_t/v^2.$$

For a "typical" neutron star binary of total mass 2.8 $M_\odot$ these formulas yield $\nu_{GW} = 360.6$ Hz, and $r = 66$ km.

Now, the maximum sensitivity window for Earth-based interferometers corresponds to frequencies of the order of a few hundred Hz. Thus, if we assume the naive extrapolation procedure just described to hold, we can expect changes due to the structure to presumably play such an important role in changing the waveform of an observed signal, that the very detection of the signal could be at risk. This would not be true if we stick to the test mass limit, since at frequencies of about 700 Hz the sensitivity of interferometers is already too low for the signal-to-noise ratio to be sensibly altered by a change in the theoretical waveform.

4.5.1 A toy model for resonances

Following [45], let us model the star by a harmonic oscillator with frequency σ_0 and inverse damping time a, i.e.,

$$A_s(t) = Ce^{-(a + i\sigma_0)t}\,, \tag{4.44}$$

which satisfies the differential equation

$$\ddot{x} + 2a\dot{x} + (\sigma_0^2 + a^2)x = 0\,. \tag{4.45}$$

Now, the effect of a particle orbiting the star in a circular orbit at radius R_0 (corresponding to a frequency σ) can be seen as a driving force acting on the oscillator, that we can write as

$$f = b\sigma^2 e^{-i\sigma t}. \tag{4.46}$$

If we now consider the above differential equation with the additional force

$$\ddot{x} + 2a\dot{x} + (\sigma_0^2 + a^2)x = b\sigma^2 e^{-i\sigma t}\,. \tag{4.47}$$

and try solutions of the form

$$A(t) = A(\sigma)e^{-i\sigma t}\,, \tag{4.48}$$

we find that

$$A(\sigma) = \frac{-b\sigma^2}{\sigma^2 - \sigma_0^2 - a^2 + 2ia\sigma}. \tag{4.49}$$

If the solution is normalized to some constant value of the amplitude (e.g. the quadrupole), the modulus squared of the total amplitude of the normalized solution is

$$|\tilde{A}|^2 = |1 + A(\sigma)|^2 = \frac{[(1-b)\sigma^2 - \sigma_0^2 - a^2]^2 + [2a\sigma]^2}{[\sigma^2 - \sigma_0^2 - a^2]^2 + [2a\sigma]^2}. \tag{4.50}$$

This quantity is the analogous, in our harmonic oscillator model, of the total power radiated in GW, normalized to the power without resonances; in other words, the function $|\tilde{A}|^2$ should model quite well the curve $P(v)$ in regions close to a resonance.

Some interesting properties of this function are:

- In the limit $a \ll \sigma$, it has a maximum in $\sigma = \sigma_0$ and a minimum in $\sigma = \sigma_0/\sqrt{1-b}$;
- The height of the maximum is $\dfrac{b\sigma_0}{2a}$, and the value of the function at the minimum is $\dfrac{2a\sqrt{1-b}}{b\sigma_0}$;
- This model predicts that, before the resonance, the energy output is 1, while after the resonance the energy output is $(1-b)$.

From our calculations, we can obtain the frequency of the maximum and the minimum (and therefore b), as well as the height at the peak (which gives a). Thus all the parameters of the model are easily obtained and we can compare with the actual results.

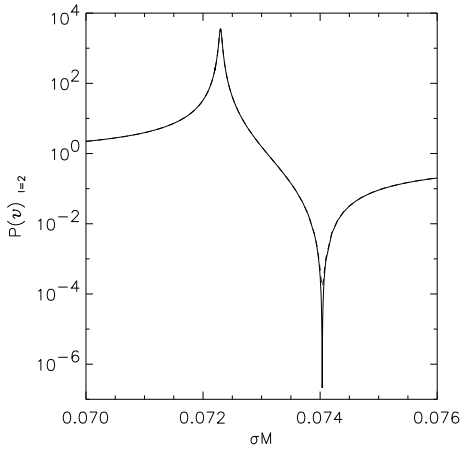

Figure 4.14: The solid line is the numerical prediction for the ($l = 2, m = \pm 2$) contribution to the total power emitted in GW, normalized to the quadrupole power, as a function of σM, for our model 3 ($n = 1.5$, $R_s = 15$ km). The dashed line is the toy model prediction.

In figure 4.14 we show the ($l = 2, m = \pm 2$) contribution to the total power emitted in GW normalized to the quadrupole power, as a function of σM, for our model 3 ($n = 1.5$, $R_s = 15$ km). For clarity, we only show a zoom of the region near the resonance. The solid line is the numerical solution and the dashed line is the simple analytical formula (4.50). The lines are practically indistinguishable (relative differences are of order 10^{-3}), except very close to the minimum, when the "exact" numerical solution is less accurate due to numerical problems, and the comparison cannot be made confidently. It is remarkable that the simple analytical model works surprisingly well in all the range, not only capturing the parabolic behavior in the region $|\sigma - \sigma_0|^2 \ll 1$ [45]. but also capturing the global behavior of the function with high accuracy.

The excellent agreement between the numerical result and the model motivates us to follow up our discussion and ask the following question: can the effect of the resonance be extracted from the global signal?

The answer is shown in figure 4.15, where we plot the numerical result as a function of v (solid lines) and the result of *extracting* the effect of the resonance with dashed lines. In order to obtain the resonance-free curve, we simply divided the total function by the model given in (4.50). This leaves out results unaffected at lower frequencies (small v), and removes the extra contribution to the power given by the resonance.

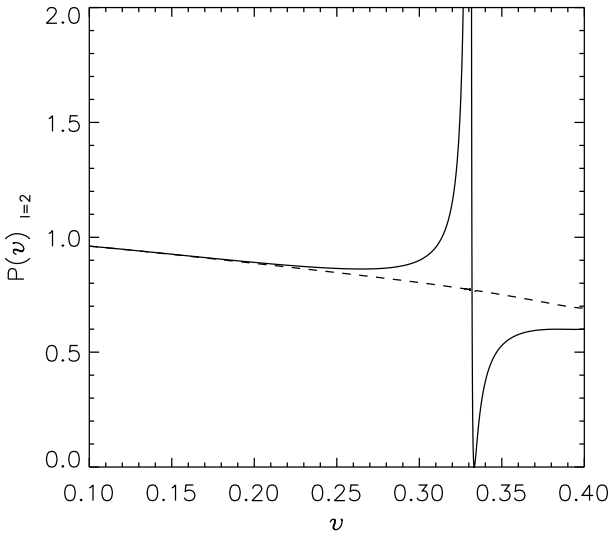

Figure 4.15: The solid curve is the same as in figure 4.14, the dashed curve shows the result obtained dividing the solid curve by the toy model prediction ("cleaning up the resonance").

We found that the same procedure can be applied satisfactorily to the rest of stellar models and higher order harmonics. Of course, an interesting question to answer is the following: is the curve which is left out when we extract resonances "universal"? From a preliminary investigation the curve which is left after the subtraction process does not seem to be "universal". Loosely speaking, this means that the extended structure of the star plays a role in the binary's evolution even when quasi-normal mode resonances are not taken into account. We plan to investigate this issue in more detail in the future.

4.6 Comparison with the Post-Newtonian formalism

As a compact binary spirals together, driven by gravitational radiation reaction, its inspiral waveform sweeps upward in frequency ("chirps"). The planned ground-based interferometers will observe the last several thousand cycles of inspiral, from a frequency ~ 10 Hz to a frequency ~ 1 kHz, depending on their sensitivity window (see figure 4.1). Generally, theoretical calculations of the waveform are done using the Post-Newtonian approximation to general relativity. Post-Newtonian modulations to the amplitude of the wave are believed to be far less important than modulations in the wave frequency (and hence in the wave's phase) [25], because the crucial ingredient for detection is an accurate phasing of the theoretical waveform with the actual waveform, which is needed to extract the signal from the detector's noise (and, eventually, to infer the source's parameters) using a matched-filtering technique. This is the reason why usually people working on Post-Newtonian theory limit to the so-called *restricted Post-Newtonian approximation*, in which the wave phase is computed at Newtonian order and only PN corrections to the phase are included.

In this section we want to understand if (and how fast) such a Post-Newtonian expansion converges to the results we get by our perturbative approach, from three different points of view. We want to understand

- how a Post-Newtonian expansion alters the total power emitted by the system at each

given v,

- how it affects the number of cycles spent by the binary in the detector's bandwidth, and
- how much the signal-to-noise ratio is reduced because of the truncation of the expansion with respect to an "exact" calculation.

Before answering these questions, we need to make a brief digression on Post-Newtonian theory. The Post-Newtonian expansion is based upon an assumption of slow motion, i.e., it is an expansion in terms of the orbital velocity of the binary. If we limit consideration to the test mass case, the orbital velocity v, orbital radius R_0, keplerian frequency ν_k and gravitational wave frequency ν_{GW} are related by

$$v = \sqrt{M/R_0} = (2\pi M \nu_k)^{1/3} = \left(\frac{2\pi M \nu_{GW}}{m}\right)^{1/3}, \tag{4.51}$$

where M is the stellar mass. In the last line we have used the resonance condition $\nu_{GW} = m\nu_k$, where typically the resonant component is the one with $m = \ell$, and the most important contribution comes from $\ell = 2$.

As we said before, the detection of the waves and the extraction of the source's parameters is possible only if theoretical templates are able to predict with a very good accuracy the phase evolution of the signal. The phase evolution, in turn, depends on the evolution of the frequency of the waves, which is determined by the equation

$$\frac{d\nu_{GW}}{dt} = \dot{E}\left(\frac{dE}{d\nu_{GW}}\right)^{-1}. \tag{4.52}$$

Analogously to what we did in formula (4.41), defining a function $P(v)$ as the ratio of the "exact" power output to the power output predicted by the Newtonian quadrupole formula, let us define a function $Q(v)$ as

$$Q(v) \equiv \left(\frac{dE}{d\nu_{GW}}\right) \cdot \left(\frac{dE}{d\nu_{GW}}\right)_N^{-1} = \frac{(1-6v^2)}{(1-3v^2)^{3/2}}. \tag{4.53}$$

where it is easy to show that, in the Newtonian limit,

$$\left(\frac{dE}{d\nu_{GW}}\right)_N = -\frac{\pi m_0 M}{3v}. \tag{4.54}$$

Of course, the analytic expression for $P(v)$ is not known, but as discussed in section 4.5 we can compute it within any desired numerical accuracy using our perturbation codes, both in the case of stars and of black holes. We have already mentioned that a PN expansion of the BPT equation [78, 79] yields a Taylor-series expansion (with logarithmic corrections) for this function:

$$\begin{aligned} P(v) &= 1 - 3.7113v^2 + 12.566v^3 - 4.9285v^4 - 38.293v^5 + (115.73 - 16.305\ln v)v^6 + \\ &- 101.51v^7 + +(-117.50 - 52.743\ln v)v^8 + (719.13 - 204.89\ln v)v^9 + \\ &+ (-1216.9 + 116.64\ln v)v^{10} + (958.93 + 473.62\ln v)v^{11} + \ldots \end{aligned} \tag{4.55}$$

Analogously, we can expand the function $Q(v)$ as

$$Q(v) = 1 - \frac{3}{2}v^2 - \frac{81}{8}v^4 - \frac{675}{16}v^6 - \frac{19845}{128}v^8 - \frac{137781}{256}v^{10} + \ldots \tag{4.56}$$

We shall indicate the previous series, truncated at the n-th order, as $Q_n(v)$. One of the essential features of the function $\left(\frac{dE}{d\nu_{GW}}\right)$ is that it should vanish at $v = v_{ISCO} = 1/\sqrt{6}$. That's why we will find useful to write down another (partial) Taylor expansion for $Q(v)$, in which this feature is retained by expanding only the denumerator of $Q(v)$:

$$Q(v) = \left(1 - 6v^2\right)\left(1 + \frac{9}{2}v^2 + \frac{135}{8}v^4 + \frac{945}{16}v^6 + \frac{25515}{128}v^8 - \frac{168399}{256}v^{10} + \dots\right) \quad (4.57)$$

We shall call the n-th order approximation to this function $Q_n^{(p)}(v)$, to remember that it's only a partial expansion, in the sense just explained.

Since the calculation of $P(v)$ in the test mass limit is exact within any required numerical accuracy, one can use this calculation to check the convergence of the Post-Newtonian expansion for test masses orbiting a Schwarzschild black hole (where, as we have just seen, an analytic formulas is available up to order v^{11}). This convergency check has been done by Poisson in [67]. The series turns out to be quite poorly convergent, especially if one uses a normal Taylor expansion instead of more refined techniques, such as Padé approximants, developed just for the purpose of getting a faster and more monotonic convergence rate [28].

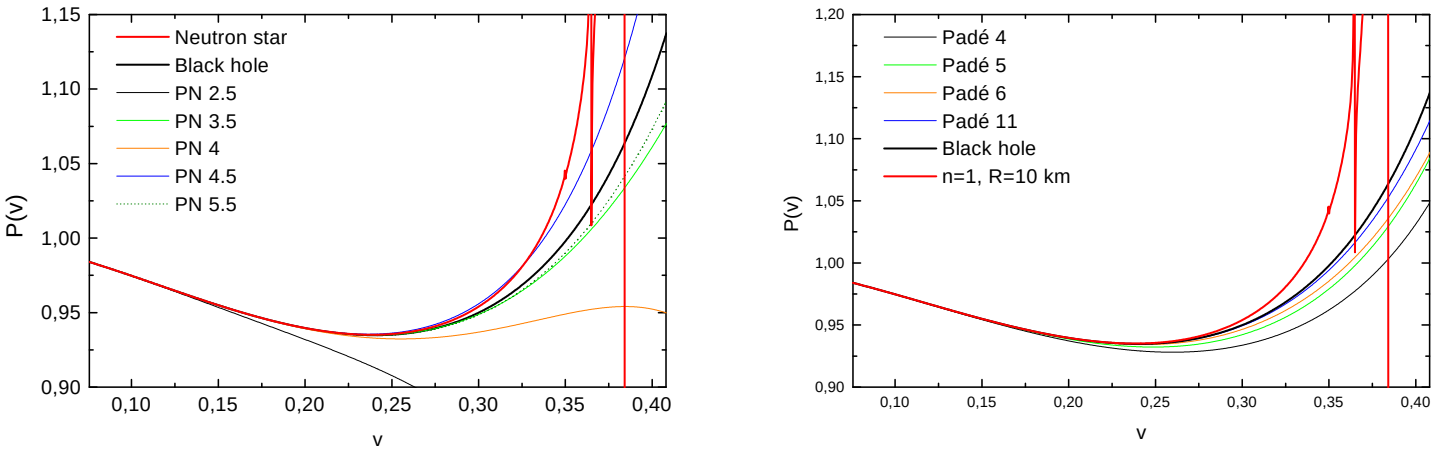

Figure 4.16: We show the power emitted in gravitational waves (normalized to the quadrupole emission) for a Schwarzschild black hole, and for our model 1, as functions of the orbital velocity v. Both curves were obtained summing multipoles from $\ell = 2$ to $\ell = 7$. For comparison, we also show the point-like Post-Newtonian approximation at several orders: on the left we use a standard Taylor series expansion, on the right we show curves obtained by applying the Padé procedure described in Appendix F at different orders in v. The v-range is chosen so that the orbital frequency (extrapolated to equal masses) sweeps from 10 Hz, where the signal first enters the LIGO-VIRGO sensitivity window, to the ISCO ($p = 6$). The standard Post-Newtonian expansion, though slowly and erratically, seems to converge to the Schwarzschild result; the Padé approximants show a much more monotonic behaviour. Even though we show here one of the more compact stellar models we have taken into account, and hence, in a sense, one which is "quite close to a black hole", the effect of the stellar structure on the power emitted is quite clear. The spikes in the neutron star curve correspond to the resonances visible in figure 4.12.

One can get an idea of how badly the Taylor series converges from the left panel in figure 4.16. The Post-Newtonian results shown there refer to the computation in [78], which yields

formula (4.55). By "PN k" we mean, adopting the standard terminology, the result obtained truncating the Post-Newtonian expansion at order v^n, with $n = 2k$. Though slowly and with quite an erratic behaviour, the curves seem to converge to the exact black hole result. Notice especially the bad behaviour of the curves labelled "PN 2.5" (order v^5) and "PN 4" (order v^8). The convergence gets much better if we use the Padé technique described in Appendix F, as one can see at a glance from the right panel in figure 4.16..

Clearly, being developed especially for the "black hole+test mass" case, the PN expansion *does not* converge to the power output of the "star+test mass" system, even though we show in both figures one of the most compact stellar models we have taken into account, which, as one could expect on the basis of physical intuition, is not too different from the black hole case. Perhaps the procedure described in [79] can be extended to build "ad hoc" Post-Newtonian expansions which hold for specific stellar models, or perhaps we can find a "universal" behaviour subtracting peaks from the background on the basis of the toy model described in the previous section. Anyway, our results show that, for sure, no "universal" test mass PN expansions exist. One must either build PN expansions holding *for a given stellar model* (though it would be interesting to understand how well a "regular" Taylor series expansion can approximate the function $P(v)$ close to the peaks), or use a semiempirical approach as described in section 4.5.1 to infer a "universal" behaviour from the different models, superimposing "by hand" the model-dependent resonant behaviours at the peaks.

4.6.1 The equal-mass case

In the last section, to avoid confusion, we always referred to Post-Newtonian calculations performed for *test masses* orbiting a Schwarzschild black hole. It will be useful for the following considerations to give here the known results on Post-Newtonian expansions when the binary members have comparable masses. In this case, both the relativistic energy and the flux function are not known analytically (the general relativistic two body problem is still unsolved, even for point masses!). The only unambiguously known terms of the PN-expansion for the energy read

$$E(v) = -\frac{\eta v^2}{2}\left[1 - \left(\frac{9+\eta}{12}\right)v^2 - \left(\frac{81 - 57\eta + \eta^2}{24}\right)v^4\right] \tag{4.58}$$

while for the flux function the calculations performed up to now yield (see [39] and references therein, but notice that there is a misprint in the flux function, formula (A45) !)

$$\begin{aligned}\dot{E}(v) &= \frac{32\eta^2 v^{10}}{5}\left[1 - \left(\frac{1247}{336} + \frac{35\eta}{12}\right)v^2 + 4\pi v^3 + \right. \\ &+ \left.\left(-\frac{44711}{9072} + \frac{9271\eta}{504} + \frac{65\eta^2}{18}\right)v^4 - \left(\frac{8191}{672} + \frac{535\eta}{24}\right)\pi v^5\right],\end{aligned} \tag{4.59}$$

where

$$\eta \equiv \frac{m_0 M}{(m_0 + M)^2} \tag{4.60}$$

is the so-called symmetric mass ratio, ranging from 0 (point-mass case) to $1/4$ (equal-mass case). Essentially, finite-mass effects appear, in this approach, as η-dependent corrections to the Taylor-series expansion coefficients of the flux function.

4.6.2 Difference in the number of cycles

We have just seen that significant differences between a star and a black hole show up, in the test mass case, for orbital velocities $v \sim c/4$. What kind of difference does this make on the number of cycles the binary spends in the bandwidth of an interferometer? To answer this question, here we shall compute this number for the four stellar models we have considered, for a black hole, and we shall compare these numbers with those obtained from the analytic formula (4.41) truncated at different orders, both using a standard Taylor expansion and a Padé expansion.

The number of cycles spent by the binary in a given velocity interval $(v_i,\ v_f)$ - or in a given orbital frequency interval $(\omega_{k,i},\ \omega_{k,f})$, which is the same - can easily be computed from

$$N = \int_{\omega_{k,f}}^{\omega_{k,i}} 2\omega_k(t)dt = \int_{v_f}^{v_i} \frac{\omega_k}{\pi}\frac{dE/dv}{\dot{E}_{lost}}dv, \tag{4.61}$$

where $\omega_k = \sqrt{M/R_0^3} = v^3/M$ is, as usual, the keplerian frequency. From the Newtonian quadrupole formula (1.51), the energy $\dot{E}_{lost}$ lost in gravitational waves can be written in terms of the orbital velocity as

$$\dot{E}_{lost} = -\frac{32}{5}\frac{m_0^2 v^{10}}{M^2}. \tag{4.62}$$

From $v = \sqrt{M/R_0}$ and the relativistic formula for the energy of a particle in circular orbit we get

$$\frac{dE}{dv} = m_0\frac{d}{dv}\frac{1-2v^2}{(1-3v^2)^{1/2}} = -m_0 v\frac{1-6v^2}{(1-3v^2)^{3/2}}. \tag{4.63}$$

In the Newtonian limit, since the total (kinetic+potential) energy of the binary is, by virtue of the virial theorem,

$$E_N = -\frac{m_0 M}{2R_0} = -\frac{1}{2}m_0 v^2, \tag{4.64}$$

the analogous expression is

$$\left(\frac{dE}{dv}\right)_N = -m_0 v, \tag{4.65}$$

so that

$$\frac{dE/dv}{(dE/dv)_N} = Q(v) = \frac{1-6v^2}{(1-3v^2)^{3/2}}, \tag{4.66}$$

where $Q(v)$ is the function defined in equation (4.53) above. So the number of cycles for some "exact" $P(v)$ (either in the black hole or in the neutron star case) can be written as

$$N = \int_{v_f}^{v_i} \frac{\omega_k}{\pi}\frac{(dE/dv)_N}{\dot{E}_N}\frac{Q(v)}{P(v)}dv = \frac{M}{m_0}\int_{v_f}^{v_i} \frac{5}{32\pi v^6}\frac{Q(v)}{P(v)}dv, \tag{4.67}$$

while the number of cycles in the n-th Post-Newtonian approximation is given by

$$N^{(n)} = \int_{v_f}^{v_i} \frac{\omega_k}{\pi}\frac{(dE/dv)_N}{\dot{E}_N}\frac{Q_n(v)}{P_n(v)}dv = \frac{M}{m_0}\int_{v_f}^{v_i} \frac{5}{32\pi v^6}\frac{Q_n(v)}{P_n(v)}dv. \tag{4.68}$$

We shall assume that the binary enters the sensitivity window of the interferometer when the gravitational-wave frequency is 10 Hz, and truncate the signal at a radius of $6M$, corresponding to the last stable circular orbit. Then we get:

$$\frac{m_0}{M}N = \int_{v_f}^{v_i} \frac{5}{32\pi v^6}\frac{Q(v)}{P(v)}dv. \tag{4.69}$$

We can further assume, following [78] and [67] (though this assumption is quite unjustified !) that the number of cycles in the comparable-mass case can be obtained from formula (4.67) for an "exact" calculation, or from formula (4.68) for a Post-Newtonian expansion, by the naive extrapolation (4.43). Remember that a reason to adopt this extrapolation procedure, as explained in chapter 1, comes from the fact that by this procedure we can recover the correct, equal masses Newtonian quadrupole formula (1.50) from the corresponding formula for test masses (1.51).

The numbers obtained from formula (4.69), and extrapolating to equal masses according to the "naive" procedure, are given in table 4.4. The difference between various models, when we extrapolate to equal masses, is at most of a couple of cycles. This number may look small, but even this small difference may induce a relevant dephasing of the wave and reduce drastically the signal-to-noise ratio.

Table 4.4: In this table we give the number of cycles to go from an orbital frequency corresponding to 10 Hz to the ISCO. In the first column we give the model the calculation refers to, in the second the number obtained from formula (4.67), in the third the corresponding extrapolation to equal masses (which amount to a multiplication by a factor 4 of column 2).

Model	$(m_0/M)N$	N (equal masses)
1	4037.397	16149.59
2	4037.282	16149.13
3	4037.902	16151.61
4	4037.417	16149.67
Black hole	4037.399	16149.60

In table 4.5, for comparison with the paper by Tanaka *et al.* [78], we give the difference,

$$\Delta N^{(n)} = N^{(n)} - N^{(11)}_{exact}, \tag{4.70}$$

between the number of cycles swept by the binary in the frequency range from 10 Hz to the ISCO, computed according to formula (4.68), and the number of cycles computed assuming, as in the paper by Tanaka, Tagoshi and Sasaki [78], that the Post-Newtonian formula at order v^{11} yields the correct energy output, i. e.

$$N^{(11)}_{TTS} = \int_{v_f}^{v_i} \frac{\omega_k}{\pi}\frac{(dE/dv)_N}{\dot{E}_N}\frac{Q(v)}{P_{11}(v)}dv = \frac{M}{m_0}\int_{v_f}^{v_i} \frac{5}{32\pi v^6}\frac{Q(v)}{P_{11}(v)}dv. \tag{4.71}$$

We also give the "real" number of cycles $N^{(pert)}$ swept by the binary in this same frequency range according to our perturbative calculation, assuming of course that the central object is a Schwarzschild black hole and summing multipoles up to $\ell = 7$.

Finally, in table 4.6, we assume as exact the v^{11}-accurate Post-Newtonian result by Tanaka, Tagoshi and Sasaki, compute the number of cycles extrapolating this result to equal masses and compare to the same number computed at the n-th *comparable masses* Post-Newtonian

order (using either a standard Taylor expansion or a Padé approximant, as specified in the first column). The results are drastically different at all calculated, equal mass Post-Newtonian orders, both when we use the standard Taylor expansion or the Padé procedure. This result shows that either a higher-order equal-mass Post-Newtonian expansion or a more reliable test-mass-to-equal-mass extrapolation procedure is needed.

Table 4.5: For five different binary systems, composed by stars or black holes of masses given in the first row, we give, extrapolating to equal masses our test-particle results, the difference between the number of cycles computed at the n-th Post-Newtonian order and the number of cycles, $N^{(11)}_{TTS}$, computed assuming that the v^{11} energy output is exact (see text). In the last two rows we give the total number of cycles for each binary, computed both assuming that the v^{11} energy output is exact, and using a relativistic perturbative calculation that takes into account all multipoles up to $\ell = 7$. When we disagree with the results given in [78], we put their results in parentheses.

n	$(1.4M_\odot, 1.4M_\odot)$	$(10M_\odot, 10M_\odot)$	$(1.4M_\odot, 10M_\odot)$	$(1.4M_\odot, 40M_\odot)$	$(1.4M_\odot, 70M_\odot)$
0	-118	12	9.0 (9.6)	100	140
2	239	67	225 (223)	312	352 (353)
3	10	6.3	17	40	57 (56)
4	-1.3	1.2	1.5 (1.6)	13	25 (24)
5	11	8.8	23 (22)	56	79 (78)
6	-0.17	-0.019 (-0.018)	-0.19	0.75	3.4 (2.7)
7	1.1	1.1	2.5	7.9	14 (13)
8	0.94	0.91	2.1	6.7	11
9	0.11	0.12	0.27 (0.25)	0.93	2.4 (1.7)
10	0.20	0.20	0.46	1.5	3.3 (2.6)
11	0.17	0.17	0.39	1.3	2.9 (2.2)
$N^{(11)}_{TTS}$	16149.75	589.51	3567.53	1250.36	758.45
$N^{(pert)}$	16149.60	589.45	3567.40	1249.95	757.77

Table 4.6: This table must be read just like table 4.5, except that here Post-Newtonian results refer to the n-th *comparable masses* Post-Newtonian order (using either a standard Taylor expansion or a Padé approximant, as specified in the first column).

n	$(1.4M_\odot, 1.4M_\odot)$	$(10M_\odot, 10M_\odot)$	$(1.4M_\odot, 10M_\odot)$	$(1.4M_\odot, 40M_\odot)$	$(1.4M_\odot, 70M_\odot)$
0	-118	123	9	100	140
2	363	89	225	323	360
3	126	22	17	46	60
4	103	12	1.5	17	26
5	123	24	23	63	82
Padé 4	113	16	30	13	10.5

4.6.3 Reduction in signal-to-noise ratio

In order to know what Post-Newtonian order is needed to do an accurate estimation of the parameters of a binary using data from ground-based inteferometers, the number of cycles in the band is nothing more than a good indicator. In fact, it has been suggested [25] that whether the error in the number of cycles is less than unity or not is a useful guideline to examine the accuracy of Post-Newtonian formulas as templates. Anyway, a much more significant and meaningful measure of the accuracy of a Post-Newtonian signal is given by the reduction in the signal-to-noise ratio produced by the use of a given approximant with respect to the signal-to-noise ratio achieved using the "true" signal. Let us define this quantity more precisely.

Our perturbative calculation, in a sense which has been explained many times before, yields the "true" signal emitted by the binary in the test mass limit. We are now interested in computing the reduction in the signal-to-noise ratio due to the fact that we use a Post-Newtonian template $h_n(t)$ instead of the "exact", relativistic template $h(t)$. This reduction in signal-to-noise ratio can be calculated to be

$$\mathcal{R}_n \equiv \frac{S/N|_{actual}}{S/N|_{max}} = \frac{|(h|h_n)|}{\sqrt{(h|h)\,(h_n|h_n)}}, \tag{4.72}$$

where the inner product between two templates is defined as

$$(g|h) = 2\int_0^\infty \frac{\tilde{g}^*(\nu)\tilde{h}(\nu) + \tilde{g}(\nu)\tilde{h}^*(\nu)}{S(\nu)} d\nu. \tag{4.73}$$

Here $S(\nu)$ is the spectral density of the detector noise; in modeling the spectral density we follow Poisson [67], who uses the function (appropriate for the advanced LIGO-type detectors)

$$S(\nu) = \frac{S_0}{5}\left[(\nu_0/\nu)^4 + 2 + (\nu/\nu_0)^2\right] \tag{4.74}$$

for $\nu > 10$ Hz; for $\nu < 10$ Hz we take, as Poisson does, $S(\nu) = 0$ (seismic noise kills the sensitivity of the detector at such low frequencies). The frequency at which $S(\nu)$ is minimum, ν_0, can be set equal to 70 Hz.

We use the so-called restricted Post-Newtonian approximation, in which the amplitude is described accurately to Newtonian order, while the phase is described "exactly" in the case of $\tilde{h}(\nu)$ and up to the n-th Post-Newtonian order in the case of $\tilde{h}_n(\nu)$. Then we get

$$\tilde{h}(\nu) = \mathcal{A}\nu^{-7/6}e^{i\psi(\nu)} \tag{4.75}$$

$$\tilde{h}_n(\nu) = \mathcal{A}\nu^{-7/6}e^{i\psi_n(\nu)} \tag{4.76}$$

where $\mathcal{A}$ is a constant, and the wave frequency evolves according to the formula

$$\frac{d\nu}{dt} = \frac{96 m_0 v^{11}}{5\pi M^3}\frac{P(v)}{Q(v)}. \tag{4.77}$$

Integrating we get

$$t(v)/M = t_i/M + \frac{5M}{32 m_0}\int_{v_i}^{v} \frac{Q(v')}{v'^9 P(v')} dv' \tag{4.78}$$

for time as a function of velocity, and

$$\Phi(v) = \Phi_i + \frac{5M}{16 m_0}\int_{v_i}^{v} \frac{Q(v')}{v'^6 P(v')} dv' \tag{4.79}$$

for the phase of the wave, $\Phi = \int 2\pi\nu dt$.

To get the frequency-domain phase functions ψ and ψ_n appearing in formulas (4.75) and (4.76) we use the stationary phase approximation [84]. Let us concentrate on ψ (ψ_n is dealt with analogously). The stationary phase approximation yields

$$\psi(\nu) = 2\pi\nu t(v) - \Phi(v) - \pi/4, \tag{4.80}$$

so that

$$\psi(\nu) = 2(t_i/M)v^3 - \Phi_i - \pi/4 + \frac{5M}{16m_0}\int_{v_i}^{v} \frac{(v^3 - v'^3)}{v'^9}\frac{Q(v')}{P(v')}dv'. \tag{4.81}$$

The signal is cut at the frequency corresponding to the ISCO,

$$\pi M\nu_{ISCO} = (M/r_{ISCO})^{3/2} = 6^{-3/2}, \tag{4.82}$$

and the phase is adjusted to maximize the integral using the following procedure.

The numerical value of $\mathcal{R}_n$ depends on the values of the constants t_i and Φ_i appearing in formula (4.81), and on the values of the constants t_{ni} and Φ_{ni} appearing in the analogous formula for $\psi_n(\nu)$. To maximize $\mathcal{R}_n$, we set $t_i = t_{ni}$ and choose $\Phi_i - \Phi_{ni}$ in such a way that $\Delta\psi$ vanishes at the value of ν for which the function $x^{-7/3}(x^{-4} + 2 + 2x^2)^{-1}$ is maximum. This occurs when $x = x_{max} \simeq 0.6654$, corresponding to $\nu_{max} \simeq 46.58$ Hz and $v_{max} \simeq 0.08966(M/M_\odot)^{1/3}$.

With these choices, we get for the difference in the phase functions

$$\Delta\psi = \psi - \psi_n = \frac{5M}{16m_0}\int_{v_{max}}^{v} \frac{(v^3 - v'^3)}{v'^9}\left[\frac{Q(v')}{P(v')} - \frac{Q_n(v')}{P_n(v')}\right]dv'. \tag{4.83}$$

Finally, a straightforward calculation, using the definition of the reduction in signal-to-noise ratio, shows that

$$\mathcal{R}_n = I^{-1}\int_{1/7}^{x_{ISCO}} \frac{x^{-7/3}\cos\Delta\psi}{x^{-4} + 2 + 2x^2}dx, \tag{4.84}$$

where $x \equiv \nu/\nu_0$ and (of course) $x_{ISCO} \equiv \nu_{ISCO}/\nu_0$. The normalization constant,

$$I = \int_{1/7}^{x_{ISCO}} \frac{x^{-7/3}}{x^{-4} + 2 + 2x^2}dx, \tag{4.85}$$

ensures that $\mathcal{R}_n = 1$ when $\psi(\nu) = \psi_n(\nu)$. In the previous calculation, which only applies (strictly speaking) to the test mass case, the ratio m_0/M appears in $\Delta\psi$, formula (4.83). Following again Poisson [67], we will let this ratio become large according to the prescription (4.43), without modifying (as we should) the expressions for $P(v)$ and $Q(v)$. We are basically assuming that the qualitative behaviour of these functions is not strongly affected by "turning on" the parameter η introduced in formula (4.60). These equal mass corrections can be seen as corrections to the Post-Newtonian coefficients of the flux function, but unluckily these corrections have been computed only up to order v^5 - see formula (4.59). The hope is that our conclusions, despite this inherent inconsistency, will be at least qualitatively correct in the comparable mass limit.

In table 4.7 we use the method just described to compare the Post-Newtonian computations performed by Tanaka, Tagoshi and Sasaki [79] with the "exact" Schwarzschild black hole result, obtained, as usual, summing multipoles up to $\ell = 7$. For comparison with table I in the errata of Poisson's paper we show results obtained using, in formula (4.83):

1) the exact function $Q(v)$ (4.53),

2) the Taylor expansion $Q_n(v)$ (4.56),

3) the partial Taylor expansion $Q_n^{(p)}(v)$ (4.57),

but we extend his analysis to include, besides the standard Taylor expansion of $P(v)$, the one obtained using Padé approximants as described in Appendix F. We omit Padé approximants at order 7 and 10 because, as shown in Appendix F, diagonal and subdiagonal Padé approximants at these orders have poles in the region of integration, and one should use different Padé approximants (e.g., superdiagonal ones) to avoid this inconvenient.

Poisson's original reason for using the three functions was to explore the effect of knowing the exact location of the ISCO - which is correctly taken into account in cases 1 and 3, but not in case 2 - on the reduction in signal-to-noise ratio. It turned out that his original conclusion (that the ISCO knowledge is important in increasing the SNR) was biased by a numerical error in his codes. No significant, systematic increase in the SNR is given by using the partial expansion instead of the full Taylor expansion of $Q(v)$. We notice also that our results do not agree perfectly with those given by Poisson in Table I of his errata, but we have performed various code checks and our signal-to-noise reduction $\mathcal{R}_n$ converges much better than Poisson's to unity as the order of the Post-Newtonian approximation increases.

In reading table 4.7 one must keep in mind that unavailability of a copy of the true signal means that the effective strength of the signal reduces from h to $\mathcal{R}_n h$, hence the span of the detector reduces by the factor $\mathcal{R}_n$. The number of events a detector can detect being proportional to the cube of the distance, such a reduction in the overlap between the true and approximated signals means a drop in the number of detectable events by a factor $\mathcal{R}_n^3$: for example, a loss of 10 % (20 %) in the signal-to-noise ratio means a 27 % (50 %) loss in the number of events. If we demand that we should be able to detect about 90 % (99 %) of the signals that we would detect had we known the true general relativistic signal, then we should have an overlap not less than 0.965 (0.997).

As in [67], for reasons explained above, our results are obtained by extrapolating to comparable masses according to the prescription (4.43). Our results explicitly refer to three binary systems, that can be seen as a "canonical" $(1.4M_\odot, 1.4M_\odot)$ neutron star binary, a $(1.4M_\odot, 10M_\odot)$ neutron star-black hole binary and a $(10M_\odot, 10M_\odot)$ black hole binary. Let us focus on the $(1.4M_\odot, 1.4M_\odot)$ neutron star binary. What happens if we use the "true neutron star's form factor" $P(v)$ (for some given equilibrium model) instead of the "black hole's form factor"? The answer is given in tables 4.8 and 4.9, which are analogous to model A in table 4.7, but are obtained using the function $P(v)$ coming out of the numerical integration of two neutron star models: model 1 and model 2, respectively. In both cases, we have summed multipoles up to $\ell = 7$ and the results are extremely similar to those obtained for the $(1.4M_\odot, 1.4M_\odot)$ binary in table 4.7.

Basically, our results confirm the ones obtained by Poisson in the errata: if we trust the extrapolation procedure (4.43) and we require that we should be able to detect at least 90 % (99 %) of the signals, then we should push the Post-Newtonian expansion up to an order between 6 and 7. Since comparable mass Post-Newtonian templates are known only up to order 5, the key issue seems to be: is it better to extrapolate perturbative, test mass results with the naive procedure (4.43) or to use the available, comparable mass PN templates? Or maybe, can we find some better way of extrapolating "test-mass-in-a-fixed-background" results to comparable masses?

We will give some arguments in favour of the second option (that of extrapolating perturbative results to the equal-mass case) in the next section.

4.7 How good is the perturbative approximation?

When we perturb a star from its equilibrium configuration, the natural scale for the perturbations is the ratio between the mass of the perturbing object and the stellar mass. A natural question to ask is: for a given mass ratio, how small are the perturbations when the orbiting mass is close? Or, in other words, when do we expect the perturbative approximation to break down?

We can obtain an answer to this question by inspecting the behaviour of the perturbation functions inside the star. Of course we expect the largest motions to be those involving the quadrupole perturbations, so we have looked at the radial behaviour of perturbation functions with $\ell = 2$. Furthermore, since fluid motions are involved only in the polar case, we have fixed our attention on the polar perturbed equations.

Our procedure to understand how large perturbations are with respect to the "background", equilibrium configuration is the following. First of all, we integrate the perturbation equations using regularity conditions at the center of the star. This yields the radial behaviour of all the metric and fluid perturbations. Anyway, this procedure, since we are considering *linear* perturbations on a fixed background, does not fix the overall scale of the perturbations. To fix this scale we must solve the "full" problem, i.e., we must find the amplitude at infinity of the solution to the equations with source and rescale all perturbation functions using this (complex) amplitude at infinity. Since the largest component comes from $m = \ell$, we have rescaled all perturbations with these angular indices using the modulus of the amplitude at infinity Z_{22}.

It turns out that the perturbative approximation is surprisingly good even when the test mass is very close. We have chosen, for illustrative purposes, a circular orbit with orbital radius equal to 3 stellar radii. The chosen stellar model corresponds to model 1 in table 4.2.

In figure 4.17 we show the behaviour of the fluid perturbations in this case. We plot the radial component of the lagrangian displacement normalized to the radius of the star $\xi_r(r)/R$, the lagrangian perturbation of the pressure normalized to the equilibrium pressure distribution $\Delta p(r)/p(r)$, and the lagrangian perturbation of the energy density normalized to the equilibrium energy density $\Delta\epsilon(r)/\epsilon(r)$. Similarly, in figure 4.18, we plot the behaviour of the perturbed metric functions $\nu(r)$ and $\mu_2(r)$ with respect to their equilibrium values. Looking at the expression for the perturbed metric (2.10), we clearly have to compare the values of $2N(r)$ and $2L(r)$ to unity.

Even at this small orbital separation the perturbations are extremely small, and of course things get much better when the orbital separation is larger (unless we are close to a resonance, in which case, of course, the perturbative approximation, strictly speaking, always breaks down).

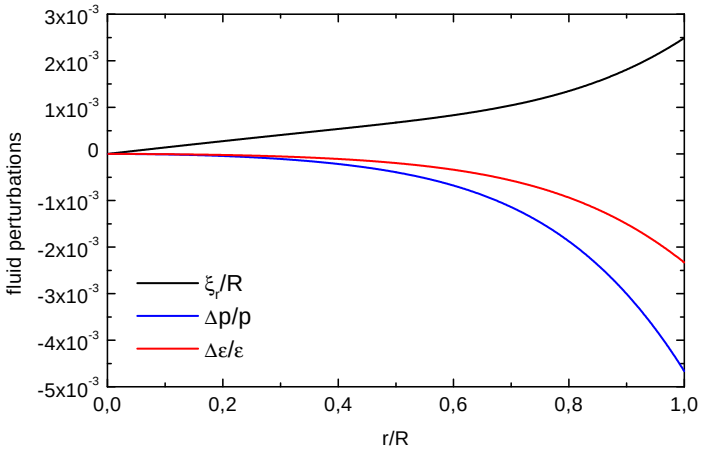

Figure 4.17: Fluid perturbations at 3 stellar radii for model 1. The black curve is the radial component of the lagrangian displacement normalized to the radius of the star, $\xi_r(r)/R$; the blue curve is the lagrangian perturbation of the pressure normalized to the equilibrium pressure distribution, $\Delta p(r)/p(r)$; the red curve is the lagrangian perturbation of the energy density normalized to the equilibrium energy density, $\Delta\epsilon(r)/\epsilon(r)$.

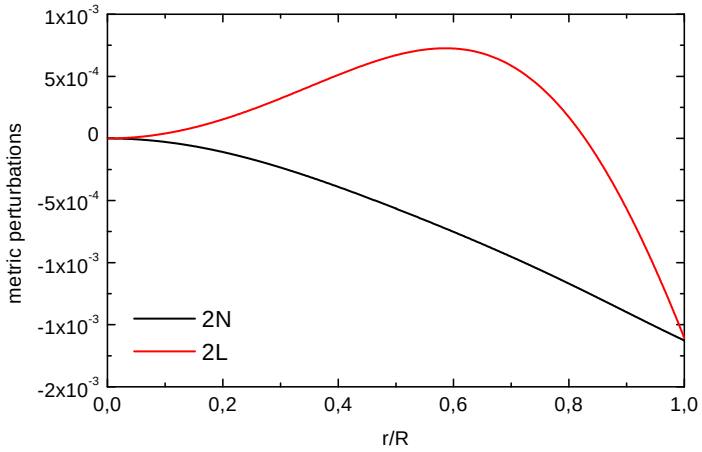

Figure 4.18: Metric perturbations at 3 stellar radii for model 1. The values of $2N(r)$ and $2L(r)$, compared to unity, are a measure of the deviations of the perturbed metric functions $\nu(r)$ and $\mu_2(r)$ with respect to their equilibrium values.

Table 4.7: Reduction in signal-to-noise ratio with respect to the "exact" *black hole* solution incurred when matched filtering with approximate, Post-Newtonian templates. For each binary system, the first column lists the order n of the approximation. The second column lists $\mathcal{R}_n$ as calculated using the exact expression for $Q(v)$; the third column lists $\mathcal{R}_n$ as calculated using the fully expanded expression for $Q(v)$; the fourth column lists $\mathcal{R}_n$ as calculated using the partially expanded expression for $Q(v)$. The fourth, fifth and sixth columns list the same quantities using the Padé expansion, instead of the standard Taylor expansion. Notice that the numbers referring to the 7th and 10th Padé approximants have been omitted, since the corresponding approximants have poles in the region of integration (see Appendix F).

	Taylor			**Padé**		
n	$Q_n(v)$	$Q(v)$	$Q_n^{(p)}(v)$	$Q_n(v)$	$Q(v)$	$Q_n^{(p)}(v)$
			System A ($1.4M_\odot$+$1.4M_\odot$)			
4	0.56562	0.49075	0.42246	0.58521	0.71790	0.98961
5	0.47184	0.53911	0.68222	0.72930	0.92023	0.84162
6	0.95073	0.93475	0.91760	0.98999	0.99950	0.99261
7	0.99685	0.99759	0.98357	-	-	-
8	0.99339	0.99436	0.99533	0.99805	0.99878	0.99942
9	0.99972	0.99917	0.99854	0.99776	0.99852	0.99921
10	0.99994	0.99996	0.99944	-	-	-
11	0.99995	0.99996	0.99941	0.99996	0.99996	0.99934
			System B ($1.4M_\odot$+$10M_\odot$)			
4	0.84743	0.39512	0.29148	0.34738	0.54002	0.75159
5	0.24153	0.29245	0.40179	0.41132	0.78112	0.52539
6	0.77563	0.67621	0.60282	0.82966	0.97109	0.90766
7	0.87789	0.99572	0.85055	-	-	-
8	0.85477	0.87635	0.89609	0.93370	0.96352	0.99157
9	0.99467	0.95948	0.93712	0.93123	0.96086	0.98957
10	0.98973	0.99606	0.97564	-	-	-
11	0.99252	0.99710	0.97212	0.99596	0.99966	0.96707
			System C ($10M_\odot$+$10M_\odot$)			
4	0.82329	0.69157	0.49080	0.50448	0.78664	0.82476
5	0.35149	0.44226	0.58679	0.55793	0.93404	0.71820
6	0.96166	0.80826	0.74129	0.86408	0.99181	0.96101
7	0.88729	0.99976	0.93043	-	-	-
8	0.88149	0.91576	.942566	0.95498	0.98998	0.99932
9	0.99961	0.98096	.958935	0.95378	0.98926	0.99912
10	0.99329	0.99806	0.99232	-	-	-
11	0.99537	0.99911	0.98977	0.99734	0.99983	0.98632

Table 4.8: Reduction in signal to noise ratio incurred when comparing with a neutron star described by model 1.

	Taylor			**Padé**		
n	$Q_n(v)$	$Q(v)$	$Q_n^{(p)}(v)$	$Q_n(v)$	$Q(v)$	$Q_n^{(p)}(v)$
			($1.4M_\odot$+$1.4M_\odot$)			
4	0.56658	0.49158	0.42317	0.58381	0.71548	0.98856
5	0.47132	0.53804	0.67991	0.72683	0.91793	0.84397
6	0.95267	0.93672	0.91960	0.98879	0.99901	0.99385
7	0.99605	0.99856	0.98508	-	-	-
8	0.99232	0.99333	0.99432	0.99729	0.99809	0.99881
9	0.99998	0.99970	0.99919	0.99695	0.99778	0.99854
10	0.99976	0.99982	0.99988	-	-	-
11	0.99978	0.99984	0.99986	0.99983	0.99988	0.99982

Table 4.9: Reduction in signal to noise ratio incurred when comparing with a neutron star described by model 2.

	Taylor			**Padé**		
n	$Q_n(v)$	$Q(v)$	$Q_n^{(p)}(v)$	$Q_n(v)$	$Q(v)$	$Q_n^{(p)}(v)$
			($1.4M_\odot$+$1.4M_\odot$)			
4	0.57051	0.49416	0.42497	0.57970	0.70850	0.97642
5	0.46915	0.53476	0.67408	0.72017	0.90484	0.85403
6	0.96803	0.95095	0.93237	0.97581	0.98871	0.99807
7	0.98464	0.99516	0.99798	-	-	-
8	0.97981	0.98087	0.98196	0.98585	0.98687	0.98792
9	0.99194	0.99282	0.99370	0.98531	0.98635	0.98740
10	0.99057	0.99066	0.99241	-	-	-
11	0.99060	0.99068	0.99244	0.99071	0.99079	0.99255

Conclusions

In this thesis we have applied the perturbative formalism to study the gravitational wave emission form extrasolar planetary systems and from compact binary systems.

The main results obtained on **extrasolar planetary systems** can be summarized as follows:

1) From quadrupole estimates on the emission of *observed* extrasolar planetary systems we found that one of them, HD283750, emits waves with a maximum amplitude $h_c \sim 4 \cdot 10^{-23}$ and a corresponding frequency $\nu \sim 1.3 \cdot 10^{-5}$ Hz. Although the emission frequencies are too small for the signal to be detectable by LISA, these values are quite interesting, especially when compared to the maximum amplitude $h_c \sim 10^{-23}$ and frequency $\nu \sim 1.4 \cdot 10^{-4}$ Hz of a *compact* binary such as the Hulse-Taylor binary pulsar (PSR 1913+16).

2) A Roche-lobe analysis, carried out to understand how close a planet can get to the star without being destroyed by tidal forces, has shown that EPS's at a fiducial distance $D = 10$ pc can emit, in their orbital motion, waves of amplitude as large as $h_c^{max} \sim 10^{-22}$ and frequency as high as $\nu^{max} \sim 10^{-4}$ Hz. Furthermore, a planet could, at least in principle, be close enough to tidally excite g-modes in solar-type stars.

3) The integration of the Einstein equations has shown that, for low-order $g-$modes, one can reach values of h_R/h_Q greater than:

   – 10 for distances between the resonant radius and the orbital radius, ΔR, of the order of a few kilometers,

   – 100 for ΔR of the order of hundreds of meters,

   – 1000 for ΔR of the order of some meter.

   Close to a resonance, the amplitude for low-order modes for an $n = 3$ polytrope is well fitted by the law:

   $$(\log h_R/h_Q) = a_{g_n} + b_{g_n}(\log \Delta R),$$

   where $b_{g_n} \simeq -0.95$, and a_{g_n} depends on the order of the mode.

4) A radiation reaction analysis in the adiabatic approximation has shown that, for the stellar model we have chosen, a brown dwarf exciting the mode g_4 could reach amplitudes $\sim 2 \cdot 10^{-20}$ for ~ 3 years, and $\sim 4 \cdot 10^{-21}$ for ~ 400 years; on the other hand, a Jupiter-like planet resonant with the mode g_{10} could reach amplitudes $\sim 3 \cdot 10^{-22}$ for ~ 2 years, and $\sim 6 \cdot 10^{-23}$ for ~ 300 years.

5) Though significantly larger in amplitude than the signal emitted by the binary pulsar, the waves emitted by the strongest emitting observed system, HD283750, are not detectable with the current LISA design. The same is true for a "resonant" system composed by a solar-type star and a jupiter-like planet, but a brown dwarf in resonant conditions *could* potentially be detectable.

The main results obtained regarding **compact binaries in the perturbative approach** can be summarized as follows:

1) We have compared results obtained from the perturbative (Bardeen-Press-Teukolsky) formalism for bound, eccentric orbits around a star with what we called the semirelativistic quadrupole formalism, for the purpose of understanding the role played by effects due to the stellar structure on the emitted waves. We found that the stellar structure produces qualitatively and quantitatively new effects with respect to the semirelativistic quadrupole formalism, among which:

   – the appearance of an axial component in the radiation and, consequently, a beating between the polar and axial components (this beating is also ignored in the so-called restricted Post-Newtonian approximation, which is commonly used to build signal templates);
   – a significant reduction in the total power radiated in $\ell = 2$;
   – a great enhancement in the wave amplitude if the stellar quasi-normal modes are excited.

2) The possibility to excite the quasi-normal modes in an astrophysical binary coalescence has been considered, both for neutron-star and black-hole binaries, showing that:

   – the excitation of black hole quasi-normal modes can only occur in a collapse;
   – for neutron stars, the f-mode excitation is highly implausible unless the star is rotating. The g-modes, on the other hand, could be excited in a frequency band relevant for earth-based interferometers, and we will explore this issue in the future.

3) We have considered the orbital evolution of binary systems in our perturbative approach, and we expect the stellar structure not to alter one of the basic predictions of the Newtonian quadrupole formula, i.e., that a system in the LIGO-VIRGO band, even if born with large eccentricity, will move, because of radiation reaction, on a *circular* orbit.

4) Concentrating on circular orbits, we have compared the emission features of a system composed by a star and a test mass with those of a system composed by a black hole and a test mass. We have found that the total power output predicted in the case of a star excited by a test mass differs sensibly from the power output for a test mass orbiting a black hole:

   – the stellar power output shows peaks due to the excitation of the stellar modes in the various multipoles. The excitation condition is

   $$\omega^{\ell}_{mode} = \ell\omega_k,$$

   where ω_k is the keplerian orbital frequency of the test mass and ω^{ℓ}_{mode} is the frequency of the mode in the given multipole.

- sensible differences with the black hole case, induced by the extended structure of the star and/or the excitation of the stellar modes, begin to show up when the orbital velocity of the test mass is about one fourth of the speed of light.
- A simple, forced oscillator toy model allows us to subtract the effects of a resonance from the "background". In the future, we plan to use this simple model to give reasonable estimates of the emission amplitudes and timescales, e.g., of high-order g-modes, which are cumbersome (if not impossible) to compute numerically.

5) We have compared our perturbative results with those obtained in the literature using Post-Newtonian approximations, either in the test mass or in the comparable mass limit. We have computed differences in the number of cycles between different stellar models and black holes, and discussed the reductions in signal-to-noise ratio due to a non-optimal modeling of the signal. We found that:

   - The variation in the number of cycles due to structural effects depends, of course, on the equation of state, but is at most (for neutron star binaries in the bandwidth of earth-based interferometers) of the order of about 3 cycles.
   - On the basis of test-mass results, one expects that an equal-mass Post-Newtonian approximation accurate at least to order v^6 or v^7 is required, both for stellar and black hole binaries, for the signal not to loose phase and the matched filtering technique to work in a detection scenario.

6) We tried to understand when the perturbative approach breaks down by inspecting the relative variations of fluid and metric perturbations with respect to their equilibrium values. We found that these relative variations are very small even at orbital radii $R_0 \sim 3R_s$, where R_s is the stellar radius.

Appendix A

The explicit expressions of the tensor harmonics

In this appendix we list the explicit expressions of the polar and axial tensor spherical harmonics. They are:

$$\mathbf{a}^{(0)}_{\ell m} = \begin{pmatrix} (t) & (\varphi) & (r) & (\vartheta) \\ Y_{\ell m}(\varphi,\vartheta) & 0 & 0 & 0 \\ 0 & 0 & 0 & 0 \\ 0 & 0 & 0 & 0 \\ 0 & 0 & 0 & 0 \end{pmatrix} \tag{A.1}$$

$$\mathbf{a}^{(1)}_{\ell m} = \frac{i}{\sqrt{2}} \begin{pmatrix} (t) & (\varphi) & (r) & (\vartheta) \\ 0 & 0 & Y_{\ell m}(\varphi,\vartheta) & 0 \\ 0 & 0 & 0 & 0 \\ Y_{\ell m}(\varphi,\vartheta) & 0 & 0 & 0 \\ 0 & 0 & 0 & 0 \end{pmatrix} \tag{A.2}$$

$$\mathbf{a}_{\ell m} = \begin{pmatrix} (t) & (\varphi) & (r) & (\vartheta) \\ 0 & 0 & 0 & 0 \\ 0 & 0 & 0 & 0 \\ 0 & 0 & Y_{\ell m}(\varphi,\vartheta) & 0 \\ 0 & 0 & 0 & 0 \end{pmatrix} \tag{A.3}$$

$$\mathbf{b}^{(0)}_{\ell m} = \imath n(\ell) r \begin{pmatrix} (t) & (\varphi) & (r) & (\vartheta) \\ 0 & \frac{\partial Y_{\ell m}}{\partial \varphi} & 0 & \frac{\partial Y_{\ell m}}{\partial \vartheta} \\ \frac{\partial Y_{\ell m}}{\partial \varphi} & 0 & 0 & 0 \\ 0 & 0 & 0 & 0 \\ \frac{\partial Y_{\ell m}}{\partial \vartheta} & 0 & 0 & 0 \end{pmatrix} \tag{A.4}$$

$$\mathbf{b}_{\ell m} = n(\ell) r \begin{pmatrix} (t) & (\varphi) & (r) & (\vartheta) \\ 0 & 0 & 0 & 0 \\ 0 & 0 & \frac{\partial Y_{\ell m}}{\partial \varphi} & 0 \\ 0 & \frac{\partial Y_{\ell m}}{\partial \varphi} & 0 & \frac{\partial Y_{\ell m}}{\partial \vartheta} \\ 0 & 0 & \frac{\partial Y_{\ell m}}{\partial \vartheta} & 0 \end{pmatrix} \tag{A.5}$$

$$\mathbf{c}^{(0)}_{\ell m} = n(\ell) r \begin{pmatrix} (t) & (\varphi) & (r) & (\vartheta) \\ 0 & -\sin\vartheta \frac{\partial Y_{\ell m}}{\partial \vartheta} & 0 & \frac{1}{\sin\vartheta}\frac{\partial Y_{\ell m}}{\partial \varphi} \\ -\sin\vartheta \frac{\partial Y_{\ell m}}{\partial \vartheta} & 0 & 0 & 0 \\ 0 & 0 & 0 & 0 \\ \frac{1}{\sin\vartheta}\frac{\partial Y_{\ell m}}{\partial \varphi} & 0 & 0 & 0 \end{pmatrix} \tag{A.6}$$

$$\mathbf{c}_{\ell m} = \imath n(\ell) r \begin{pmatrix} (t) & (\varphi) & (r) & (\vartheta) \\ 0 & 0 & 0 & 0 \\ 0 & 0 & -\sin\vartheta \frac{\partial Y_{\ell m}}{\partial \vartheta} & 0 \\ 0 & -\sin\vartheta \frac{\partial Y_{\ell m}}{\partial \vartheta} & 0 & \frac{1}{\sin\vartheta}\frac{\partial Y_{\ell m}}{\partial \varphi} \\ 0 & 0 & \frac{1}{\sin\vartheta}\frac{\partial Y_{\ell m}}{\partial \varphi} & 0 \end{pmatrix} \tag{A.7}$$

$$\mathbf{d}_{\ell m} = \imath m(\ell) r^2 \begin{pmatrix} (t) & (\varphi) & (r) & (\vartheta) \\ 0 & 0 & 0 & 0 \\ 0 & -\sin\vartheta X_{\ell m} & 0 & -\sin\vartheta W_{\ell m} \\ 0 & 0 & 0 & 0 \\ 0 & -\sin\vartheta W_{\ell m} & 0 & \frac{1}{\sin\vartheta} X_{\ell m} \end{pmatrix} \tag{A.8}$$

$$\mathbf{f}_{\ell m} = m(\ell) r^2 \begin{pmatrix} (t) & (\varphi) & (r) & (\vartheta) \\ 0 & 0 & 0 & 0 \\ 0 & -\sin^2\vartheta W_{\ell m} & 0 & X_{\ell m} \\ 0 & 0 & 0 & 0 \\ 0 & X_{\ell m} & 0 & W_{\ell m} \end{pmatrix} \tag{A.9}$$

$$\mathbf{g}_{\ell m} = \frac{r^2}{\sqrt{2}} \begin{pmatrix} (t) & (\varphi) & (r) & (\vartheta) \\ 0 & 0 & 0 & 0 \\ 0 & \sin^2\vartheta Y_{\ell m} & 0 & 0 \\ 0 & 0 & 0 & 0 \\ 0 & 0 & 0 & Y_{\ell m} \end{pmatrix} \tag{A.10}$$

where

$$n(\ell) = \frac{1}{\sqrt{2\ell(\ell+1)}}, \tag{A.11}$$

$$m(\ell) = \frac{1}{\sqrt{2\ell(\ell+1)(\ell-1)(\ell+2)}} \tag{A.12}$$

and

$$X_{\ell m}(\vartheta,\varphi) = 2\frac{\partial}{\partial\varphi}\left[\frac{\partial}{\partial\vartheta} - \cot\vartheta\right] Y_{\ell m}(\vartheta,\varphi), \tag{A.13}$$

$$W_{\ell m}(\vartheta,\varphi) = \left[\frac{\partial^2}{\partial\vartheta^2} - \cot\vartheta\frac{\partial}{\partial\vartheta} - \frac{1}{\sin^2\vartheta}\frac{\partial^2}{\partial^2\varphi}\right] Y_{\ell m}(\vartheta,\varphi). \tag{A.14}$$

A.1 Note on the normalization of the harmonics

Note that all tensor harmonics are normalized to 1, except $(\mathbf{a}^{(1)}_{\ell m}, \mathbf{b}^{(0)}_{\ell m}, \mathbf{c}^{(0)}_{\ell m})$, as shown below. For this reason the coefficients $A^{(1)}_{\ell m}, B^{(0)}_{\ell m}, Q^{(0)}_{\ell m}$ will be defined with a minus sign.

$$
\begin{aligned}
(\mathbf{a}^{(1)}_{\ell m}, \mathbf{a}^{(1)}_{\ell m}) &= \int a^{(1)*}_{\ell m\mu\nu} a^{(1)}_{\ell m\lambda\rho} \eta^{\mu\lambda}\eta^{\nu\rho} d\Omega \\
&= 2\int \eta^{tt}\eta^{rr}\frac{(-i)i}{2} Y^{\star}_{\ell m} Y_{\ell m} d\Omega = -\int Y^{\star}_{\ell m} Y_{\ell m} d\Omega = -1
\end{aligned}
$$

$$
\begin{aligned}
(\mathbf{b}^{(0)}_{\ell m}, \mathbf{b}^{(0)}_{\ell m}) &= \int b^{(0)*}_{\ell m\mu\nu} b^{(0)}_{\ell m\lambda\rho} \eta^{\mu\lambda}\eta^{\nu\rho} d\Omega \\
&= 2\int \frac{(-ir)ir}{2\ell(\ell+1)} \left\{ \eta^{tt}\eta^{\varphi\varphi} Y^{\star}_{\ell m,\varphi} Y_{\ell m,\varphi} + \eta^{tt}\eta^{\vartheta\vartheta} Y^{\star}_{\ell m,\vartheta} Y_{\ell m,\vartheta} \right\} d\Omega \\
&= -\frac{1}{\ell(\ell+1)} \int \left\{ \frac{Y^{\star}_{\ell m,\varphi} Y_{\ell m,\varphi}}{\sin^2\vartheta} + Y^{\star}_{\ell m,\vartheta} Y_{\ell m,\vartheta} \right\} \sin\vartheta d\vartheta d\varphi \\
&= -\frac{1}{\ell(\ell+1)} \int Y^{\star}_{\ell m} \left\{ -Y_{\ell m,\vartheta\vartheta} - \cot\vartheta Y_{\ell m,\vartheta} + \frac{m^2 Y_{\ell m}}{\sin^2\vartheta} \right\} d\Omega \\
&= -\frac{1}{\ell(\ell+1)} \int Y^{\star}_{\ell m} \left\{ \ell(\ell+1) Y_{\ell m} \right\} d\Omega = -1
\end{aligned}
$$

$$
\begin{aligned}
(\mathbf{c}^{(0)}_{\ell m}, \mathbf{c}^{(0)}_{\ell m}) &= \int c^{(0)*}_{\ell m\mu\nu} c^{(0)}_{\ell m\lambda\rho} \eta^{\mu\lambda}\eta^{\nu\rho} d\Omega \\
&= 2\int \frac{r^2}{2\ell(\ell+1)} \left\{ \eta^{tt}\eta^{\varphi\varphi} \sin^2\vartheta Y^{\star}_{\ell m,\vartheta} Y_{\ell m,\vartheta} + \eta^{tt}\eta^{\vartheta\vartheta} \frac{Y^{\star}_{\ell m,\varphi} Y_{\ell m,\varphi}}{\sin^2\vartheta} \right\} d\Omega \\
&= -\frac{1}{\ell(\ell+1)} \int \left\{ \frac{Y^{\star}_{\ell m,\varphi} Y_{\ell m,\varphi}}{\sin^2\vartheta} + Y^{\star}_{\ell m,\vartheta} Y_{\ell m,\vartheta} \right\} \sin\vartheta d\vartheta d\varphi \\
&= -\frac{1}{\ell(\ell+1)} \int Y^{\star}_{\ell m} \left\{ -Y_{\ell m,\vartheta\vartheta} - \cot\vartheta Y_{\ell m,\vartheta} + \frac{m^2 Y_{\ell m}}{\sin^2\vartheta} \right\} d\Omega \\
&= -\frac{1}{\ell(\ell+1)} \int Y^{\star}_{\ell m} \left\{ \ell(\ell+1) Y_{\ell m} \right\} d\Omega = -1
\end{aligned}
$$

Appendix B

Asymptotic conditions for the perturbation equations and integration method

In this Appendix we give the asymptotic conditions we need for the numerical integrations of the homogeneous perturbation equations. To solve the polar and axial perturbation problems with the Green function technique for **stellar** perturbations, we need (as explained in Appendix C for the Zerilli approach, and in section 4.1 for the BPT approach):

- Regular (i.e., non-singular) expansions of the *polar* perturbation functions at the center of the star ($r = 0$), and a matching prescription to obtain the vacuum (Zerilli) solution at the border of the star ($r = R$) from the perturbation functions obtained integrating numerically outwards. These expansions and the matching prescriptions are explained in section B.1.

- A regular (i.e., non-singular) expansions of the *axial* perturbation function at the center of the star ($r = 0$). Since we know that in this case the perturbation equations can be expressed as a single wave equation, formula (2.40), which automatically reduces to the vacuum (Regge-Wheeler) equation outside, the matching prescription at the border is trivial. The required expansion at the center is given in section B.2.

- An asymptotic expansion of both the Zerilli and Regge-Wheeler functions, satisfying purely *outgoing* wave conditions at infinity. These expansions are given in section B.3.

For **black hole** perturbations we follow exactly the same procedure as in the stellar case, replacing the matching conditions at the border of the star with an asymptotic expansion of both the Zerilli and Regge-Wheeler functions, satisfying purely *ingoing* wave conditions at the black hole horizon. This expansion is given in section B.4.

Finally, in section B.5, we briefly describe the Gauss-Legendre integration method we used to perform the integrals appearing in the source terms.

B.1 Polar perturbations inside the star

Here we outline the procedure to obtain the values of the Zerilli function and its first derivative at the border of the star from a numerical integration of the polar system of perturbation equations for the interior, (2.27)-(2.30) .

We shall assume that, near the origin, the functions have the asymptotic expansion

$$(X, G, N, L) = (X_0, G_0, N_0, L_0)r^x + (X_2, G_2, N_2, L_2)r^{x+2} + \dots \ , \tag{B.1}$$

where both the exponent x and the coefficients of the expansion have to be determined by inserting equation (B.1) into equations (2.27)-(2.30), and by setting to zero the coefficients of different powers of r. From the lower order terms we obtain a homogeneous algebraic system of four equations for the four coefficients (X_0, G_0, N_0, L_0)

$$\begin{aligned}
&x(x+1)X_0 + n(L_0 + N_0) = 0 \\
&[(a-b)x + \omega_0^2]X_0 - (x+2)G_0 + n(a+b)N_0 - n(a-b)L_0 = 0 \\
&\left[(a-b)x + \frac{\omega_0^2}{2n}(x+2n+1)\right] X_0 - G_0 + a(x-1)N_0 + \frac{1}{2}\omega_0^2 N_0 + \frac{1}{2}\omega_0^2 L_0 = 0 \\
&2\left[x\left(\frac{n+1}{n}\right) + 2\right] X_0 + (x+1)(N_0 + L_0) = 0,
\end{aligned} \tag{B.2}$$

where a and b are the coefficients of the expansion of the metric functions

$$e^{2\mu_2} \sim 1 + br^2 = 1 + \left(\frac{2}{3}\epsilon_0\right) r^2, \qquad e^{2\nu} \sim 1 + ar^2 = 1 + \left(p_0 + \frac{1}{3}\epsilon_0\right) r^2. \tag{B.3}$$

The system (B.2) admits a non-trivial solution only if the determinant is zero. This condition provides an indicial equation for the determination of x

$$na(x+1)(x-\ell)^2(x+\ell+1)^2 = 0 \ . \tag{B.4}$$

We see that there are only two coincident values of x which correspond to regular solutions, i.e. $x = l$. That means that, although our original system is of order five, only two independent solutions are acceptable. A possible choice for the two independent solutions is

$$\begin{aligned}
1) \qquad & L_0 = 0, \qquad N_0 = 1, \qquad X_0 = -\frac{n}{\ell(\ell+1)}N_0, \\
& G_0 = +\frac{1}{2}(\ell-1)\left\{a + b - \frac{1}{\ell(\ell+1)}[(a-b)\ell + \omega_0^2]\right\} N_0 \ ,
\end{aligned} \tag{B.5}$$

$$\begin{aligned}
2) \qquad & N_0 = 0 \qquad L_0 = 1, \qquad X_0 = -\frac{n}{\ell(\ell+1)}L_0, \\
& G_0 = -\frac{1}{2}(\ell-1)\left\{a - b + \frac{1}{\ell(\ell+1)}[(a-b)\ell + \omega_0^2]\right\} L_0 \ .
\end{aligned} \tag{B.6}$$

The coefficients (X_2, G_2, N_2, L_2) in the expansion (B.1) can be found by equating to zero the coefficients of the next power of x into the expanded equations.

A numerical integration of equations (2.27)-(2.30), with the initial conditions (B.5)-(B.6), yields two independent solutions.

Are these two independent solutions sufficient to satisfy the boundary conditions required by the problem?

As in the Newtonian case, we need to impose that the lagrangian perturbation of the pressure Δp vanishes at the surface $r = R$, but in addition we need to impose that the interior solution joins continuously with the solution in the exterior of the star. In order to satisfy the continuity condition at $r = R$, eqs. (2.11)-(2.14), which are equivalent to eqs. (2.27)-(2.30), must reduce

to those appropriate to the vacuum. So we just need to take a linear combination of the two independent solutions in such a way that the remaining condition $\Delta p = 0$ (or equivalently $U = 0$) is fulfilled. Notice that the metric perturbations are continuous at the surface of the star, but their derivatives may not be. For example, the equation for $W_{,r}$ for polytropic equations of state reads

$$W_{,r} + \nu_{,r}(Q-1)W = U, \tag{B.7}$$

and we know from the equations that W and U tend to zero at $r = R$. However, Q diverges there, and in general the product QW tends to a finite value at the stellar radius. Since $W_{,r}$ is zero outside the star, we find that for polytropic equations of state with $n \leq 1$ $W_{,r}$ is discontinuous. Since by inspection of the equations it can be shown that $(W + L)_{,r}$ is continuous at the surface, the condition to be imposed is

$$[L_{,r}]_{outside} = [W_{,r} + L_{,r}]_{inside}\,. \tag{B.8}$$

So the two degrees of freedom given by equation (B.5) and (B.6) are precisely what we do need to match the interior and the exterior solution, and to satisfy the condition $\Delta p = 0$.

B.2 Axial perturbations inside the star

For the purpose of numerical integration, it is useful to rewrite the axial wave equation (2.40), which is expressed in terms of a "modified tortoise coordinate"

$$r_* = \int_0^r e^{-\nu+\mu_2} dr, \tag{B.9}$$

in terms of the usual Schwarzschild coordinate r. Introducing a variable $X \equiv rZ$, equation (2.40) can be shown to be equivalent to the second order equation

$$X_{,r,r} - \frac{e^{2\mu_2}}{r}\left\{2 + r^2\left[\epsilon - p - \frac{6M(r)}{r^3}\right]\right\}X_{,r} - e^{2\mu_2}\frac{\mu^2}{r^2}X + \sigma^2 e^{2(\mu_2-\nu)}X = 0. \tag{B.10}$$

If we further define $\Sigma \equiv \sigma e^{-\nu_0}$, where ν_0 is the value of the metric function ν at the center, it can be easily verified that the non-singular expansion of the solution to this second-order differential equation, close to $r = 0$, is:

$$X = r^{\ell+2} + F_0 r^{\ell+4}, \tag{B.11}$$

where:

$$F_0 = \frac{1}{2(2\ell+3)}\left\{(\ell+2)\left[\frac{2\ell-1}{3}\epsilon_0 - P_0\right] - \Sigma^2\right\}. \tag{B.12}$$

B.3 Asymptotic expansions at infinity of the Zerilli and Regge-Wheeler functions

The asymptotic expansions of the Zerilli function satisfying a purely-outgoing wave condition at radial infinity ($r \to \infty$) is:

$$Z^{pol}(r \to \infty) \sim e^{i\omega r_*}\left[1 + \frac{a}{r} + \frac{b}{r^2}\right] \tag{B.13}$$

where

$$a = \frac{i(n+1)}{\omega}, \qquad b = -\frac{(n^3 + n^2 + 3in\omega M + 6i\omega M)}{2n\omega^2},$$

while for the Regge-Wheeler function we have

$$Z^{ax}(r \to \infty) \sim e^{i\omega r_*}\left[1 + \frac{a}{r} + \frac{b}{r^2}\right] \tag{B.14}$$

where

$$a = \frac{i(n+1)}{\omega}, \qquad b = -\frac{(n^2 + n + 3i\omega M)}{2\omega^2}.$$

B.4 Asymptotic expansions at the horizon of the Zerilli and Regge-Wheeler functions

The asymptotic expansions of the Zerilli function satisfying a purely ingoing wave condition close to the horizon of a Schwarzschild black hole ($r \to 2M$) is:

$$Z^{pol}(r \to 2M) \sim e^{-i\omega r_*}\left[1 + a(r-2M) + b(r-2M)^2\right] \tag{B.15}$$

where

$$\begin{aligned}
a &= \frac{i(4n^2+4n+3)}{2M(8n\omega M + 12\omega M + 2in + 3i)}, \\
b &= -(4n^4 + 8n^3 + 13n^2 + 3n + 16i\omega M n^3 + 28i\omega M n^2 + 48i\omega M n + 27i\omega M) \\
&\times \left[4M^2(32\omega^2M^2n^2 + 24i\omega M n^2 + 96\omega^2M^2n + 72i\omega M n + \right. \\
&+ \left. 54i\omega M + 72\omega^2M^2 - 4n^2 - 12n - 9)\right]^{-1}.
\end{aligned}$$

For the Regge-Wheeler function the corresponding expansion is

$$Z^{ax}(r \to 2M) \sim e^{-i\omega r_*}\left[1 + a(r-2M) + b(r-2M)^2\right] \tag{B.16}$$

with

$$a = \frac{i(2n-1)}{2M(i + 4\omega M)}, \qquad b = -\frac{n^2 - n + 1 + 4in\omega M - 5i\omega M}{4M^2(8\omega^2M^2 + 6i\omega M - 1)}.$$

B.5 Gauss-Legendre method for the integrations

The key idea behind Gaussian quadratures [70] is to approximate the integral of a function by a sum of its functional values (at *suitably chosen*, not necessarily equally spaced abscissas), multiplied by weighting coefficients chosen to increase the order of the integration formula. The method is particularly good for polynomials, and, in particular, given the weight function $W(x)$, we can find a set of weights w_j and of abscissas x_j such that the approximation

$$\int_a^b W(x)f(x)dx \simeq \sum_{j=1}^{N} w_j f(x_j) \tag{B.17}$$

is exact if $f(x)$ is a polynomial. Given a weight function $W(x)$, one can define a scalar product of two functions f and g over the weight function W as:

$$\langle f|g\rangle \equiv \int_a^b W(x)f(x)g(x)dx, \tag{B.18}$$

and define in the usual way the notions of orthonormality and orthogonality of functions. Then one can find a set of orthogonal polynomials $p_j(x)$ that includes exactly one polynomial of order j for each j, and all of which are mutually orthogonal. The fundamental theorem of Gaussian quadratures states that the abscissas of the $N-$point Gaussian quadrature formula with weighting function $W(x)$ in the interval (a, b) are precisely the roots of $p_N(x)$ for the same integral and weighting function. So, given a weighting function, one can:

- Generate the orthogonal polynomials,
- Find their roots, which are the ascissas x_j
- Compute the associated weights, e.g. by the formula

$$w_j = \frac{\langle p_{N-1}|p_{N-1}\rangle}{p_{N-1}(x_j)p'_N(x_j)} \tag{B.19}$$

A simple and useful case of "classical" orthogonal polynomials is given by the Gauss-Legendre polynomials, associated to a constant weight function:

$$W(x) = 1, \quad -1 < x < 1$$

and obtainable from the recursion relations

$$(j+1)P_{j+1} = (2j+1)xP_j - jP_{j-1}. \tag{B.20}$$

The weights are given, in this case, by

$$w_j = \frac{2}{(1-x_j^2)\left[P'_N(x_j)\right]^2}. \tag{B.21}$$

A routine that scales the range of integration from (a, b) to $(-1, 1)$, and provides ascissas x_j and weights w_j for the integration formula (B.17) is provided in [70]. This is the routine we use in the program, but since we need to change the range of integration many times, we scale "by

hand" the abscissas and the weights from the "standard" ones to the ones we need, denoted by a bar, using the relations:

$$\bar{x}_j = \frac{b-a}{2} x_j + \frac{b+a}{2}, \qquad \bar{w}_j = \frac{b-a}{2} w_j. \tag{B.22}$$

We usually use $N = 20$ points for the integrations, but if high-order harmonics ($j \gtrsim 10$) contribute significantly to the sum we sometimes need to increase this value (up to $N \sim 100$) to achieve better accuracy.

Appendix C

Solution of the equations in the Zerilli approach

C.1 The polar case

C.1.1 Derivation of the polar source term in the general case

The polar part of the perturbed metric, in Chandrasekhar-Ferrari gauge, is written as

$$h^{pol}_{\ell m} = \begin{pmatrix} 2e^{2\nu}NY_{\ell m} & 0 & 0 & 0 \\ 0 & -2e^{2\psi}H_{11} & 0 & -r^2VX_{\ell m} \\ 0 & 0 & -2e^{2\mu_2}LY_{\ell m} & 0 \\ 0 & -r^2VX_{\ell m} & 0 & -2e^{2\mu_3}H_{33} \end{pmatrix} , \tag{C.1}$$

where

$$H_{11} = \left[TY_{\ell m} + V\left(\frac{1}{\sin^2\vartheta}\frac{\partial^2}{\partial\varphi^2} + \cot\vartheta\frac{\partial}{\partial\vartheta} \right) Y_{\ell m} \right] ,$$

$$H_{33} = \left[TY_{\ell m} + V\frac{\partial^2}{\partial\vartheta^2}\, Y_{\ell m} \right] ,$$

and furthermore

$$e^{2\psi} = r^2\sin^2\vartheta , \qquad e^{2\mu_3} = r^2 .$$

The line element can be expressed as

$$\begin{aligned} ds^2 &= e^{2\nu}[1+2NY_{\ell m}e^{-i\omega t}]dt^2 - e^{2\mu_2}[1+2LY_{\ell m}e^{-i\omega t}]dr^2 \\ &- r^2\{1+2[TY_{\ell m}+VY_{\ell m,\vartheta\vartheta}e^{-i\omega t}\}d\vartheta^2 \\ &- r^2\sin^2\vartheta\{1+2[TY_{\ell m}+V(Y_{\ell m,\vartheta}\cot\vartheta - \frac{m^2}{\sin^2\vartheta}Y_{\ell m})]e^{-i\omega t}\}d\varphi^2 \\ &- 4imr^2V[Y_{\ell m,\vartheta} - \cot\vartheta Y_{\ell m}]e^{-i\omega t}d\vartheta d\varphi \end{aligned} \tag{C.2}$$

Denoting by (0 1 2 3) the variables ($t\ r\ \vartheta\ \varphi$) and using **Maple** we get the perturbed Einstein equations. The components we are interested in are:

$$\delta R_{03} = -i\omega Y_{\ell m,\vartheta}\left\{V - T - L\right\}$$
$$[43]_{MTB} \tag{C.3}$$
$$\delta R_{02} = i\omega Y_{\ell m}\left\{\left(\frac{d}{dr} + \frac{1}{r} - \nu_{,r}\right)\left[2T - \ell(\ell+1)V\right] - \frac{2}{r}L\right\}$$
$$[44]_{MTB} \tag{C.4}$$
$$\delta R_{23} = -Y_{\ell m,\vartheta}\left\{(T - V + N)_{,r} - \left(\frac{1}{r} - \nu_{,r}\right)N - \left(\frac{1}{r} + \nu_{,r}\right)L\right\}$$
$$[45]_{MTB} \tag{C.5}$$
$$\delta G_{22} = Y_{\ell m}\left\{\frac{2}{r}N_{,r} + \left(\frac{1}{r} + \nu_{,r}\right)\left[2T - \ell(\ell+1)V\right]_{,r} - \ell(\ell+1)\frac{e^{-2\nu}}{r^2}N\right.$$
$$\left. - \quad \frac{2ne^{-2\nu}}{r^2}T + \omega^2 e^{-4\nu}[2T - \ell(\ell+1)V] - \frac{2}{r}\left(\frac{1}{r} + 2\nu_{,r}\right)L\right\}$$
$$[49]_{MTB} \tag{C.6}$$
$$\delta R_{11} = -\frac{\sin 2\vartheta}{2}Y_{\ell m,\vartheta}\left\{r^2 e^{2\nu}\left[V_{,rr} + 2\left(\frac{1}{r} + \nu_{,r}\right)V_{,r} + \frac{e^{-2\nu}}{r^2}(N+L) + \omega^2 e^{-4\nu}V\right]\right\}$$
$$+ \quad \{\ldots\}\,Y_{\ell m} + \{\ldots\}\,Y_{\ell m}\sin^2\vartheta$$
$$[51]_{MTB} \tag{C.7}$$

where we have indicated in square parentheses the relevant equations in MTB.

The components of the stress–energy tensor that we need can be obtained by inspection of the polar spherical harmonics:

$$T_{02} = T_{tr} = \frac{i}{\sqrt{2}}A^{(1)}_{\ell m}Y_{\ell m} \tag{C.8}$$

$$T_{22} = T_{rr} = A_{\ell m}Y_{\ell m} \tag{C.9}$$

$$T_{03} = T_{t\vartheta} = \frac{ir}{\sqrt{2\ell(\ell+1)}}B^{(0)}_{\ell m}Y_{\ell m,\vartheta} \tag{C.10}$$

$$T_{23} = T_{r\vartheta} = \frac{r}{\sqrt{2\ell(\ell+1)}}B_{\ell m}Y_{\ell m,\vartheta} \tag{C.11}$$

$$T_{11} = T_{\varphi\varphi} = \frac{r^2}{\sqrt{2}}\left(G_{\ell m}\sin^2\vartheta Y_{\ell m} - \frac{F_{\ell m}}{\sqrt{\ell(\ell+1)(\ell-1)(\ell+2)}}W_{\ell m}\right) \tag{C.12}$$

$$T_{33} = T_{\vartheta\vartheta} = \frac{r^2}{\sqrt{2}}\left(G_{\ell m}Y_{\ell m} + \frac{F_{\ell m}}{\sqrt{\ell(\ell+1)(\ell-1)(\ell+2)}}W_{\ell m}\right) \tag{C.13}$$

The perturbed Einstein equations are:

$$\delta G_{\mu\nu} = 8\pi \left(T_{\mu\nu} - \frac{1}{2} g_{\mu\nu} T \right) \Longleftrightarrow \delta G_{\mu\nu} = 8\pi T_{\mu\nu} \tag{C.14}$$

so that (remember that the unperturbed metric is diagonal!):

$$\delta R_{02} = 8\pi T_{02} \tag{C.15}$$
$$\delta R_{03} = 8\pi T_{03} \tag{C.16}$$
$$\delta R_{23} = 8\pi T_{23} \tag{C.17}$$
$$\delta G_{22} = 8\pi T_{22} \tag{C.18}$$

On the other hand:

$$\begin{aligned} \delta R_{11} &= 8\pi \left(T_{11} - \frac{1}{2} g_{11} T \right) = \\ &= 8\pi \left[T_{11} - \frac{1}{2} g_{11} \left(g^{00} T_{00} + g^{11} T_{11} + g^{22} T_{22} + g^{33} T_{33} \right) \right] = \\ &= 4\pi \left[T_{11} - \sin^2 \vartheta T_{33} \right] \end{aligned} \tag{C.19}$$

Now, we can use Legendre's equation to eliminate the second derivative with respect to ϑ in the definition of $W_{\ell m}$ and write

$$W_{\ell m} = -2 \cot \vartheta Y_{\ell m, \vartheta} + \left[\frac{2m^2}{\sin^2 \vartheta} - \ell(\ell+1) \right] Y_{\ell m} \tag{C.20}$$

This means that both T_{11} and T_{33} can be written as

$$T_{11} = \bar{T}_{11} + \{\ldots\} Y_{\ell m}, \qquad T_{33} = \bar{T}_{33} + \{\ldots\} Y_{\ell m} \tag{C.21}$$

where we have denoted by a bar the $Y_{\ell m, \vartheta}-$dependent part, and $\bar{T}_{11} = -\sin^2 \vartheta \bar{T}_{33}$.

Hence we have

$$\delta R_{11} = 8\pi \sin 2\vartheta Y_{\ell m, \vartheta} \frac{r^2 F_{\ell m}}{\sqrt{2\ell(\ell+1)(\ell-1)(\ell+2)}} + \ldots Y_{\ell m} \tag{C.22}$$

and the equations we have to manipulate are:

$$\left(\frac{d}{dr} + \frac{1}{r} - \nu_{,r} \right) [2T - \ell(\ell+1)V] - \frac{2}{r} L = S_{A_1} \equiv \frac{8\pi A^{(1)}_{\ell m}}{\omega \sqrt{2}} \tag{C.23}$$

$$T + L - V = S_{B_0} \equiv \frac{8\pi r B^{(0)}_{\ell m}}{\omega \sqrt{2\ell(\ell+1)}} \tag{C.24}$$

$$\begin{aligned} &(T - V + N)_{,r} - \left(\frac{1}{r} - \nu_{,r} \right) N - \left(\frac{1}{r} + \nu_{,r} \right) L = \\ &= S_B \equiv -\frac{8\pi r B_{\ell m}}{\sqrt{2\ell(\ell+1)}} \end{aligned} \tag{C.25}$$

$$\begin{aligned} &\frac{2}{r} N_{,r} + \left(\frac{1}{r} + \nu_{,r} \right) [2T - \ell(\ell+1)V]_{,r} - \ell(\ell+1) \frac{e^{-2\nu}}{r^2} N \\ &- \frac{2n e^{-2\nu}}{r^2} T + \omega^2 e^{-4\nu} [2T - \ell(\ell+1)V] - \frac{2}{r} \left(\frac{1}{r} + 2\nu_{,r} \right) L = S_A \equiv 8\pi A_{\ell m} \end{aligned} \tag{C.26}$$

$$V_{,rr} + 2\left(\frac{1}{r} + \nu_{,r}\right) V_{,r} + \frac{e^{-2\nu}}{r^2}(N + L) + \omega^2 e^{-4\nu} V = \tag{C.27}$$

$$= \quad S_F \equiv -\frac{16\pi r F_{\ell m}}{(r-2M)\sqrt{2\ell(\ell+1)(\ell-1)(\ell+2)}}$$

Now we manipulate the equations, following the procedure described in [14], to get the Zerilli equation *with source*. First of all, we define

$$X \equiv nV$$

and obtain T from (C.23):

$$T = S_{B_0} - L + V. \tag{C.28}$$

This implies also that

$$2T - \ell(\ell+1)V = 2(S_{B_0} - L - X). \tag{C.29}$$

Substituting in (C.23) we get

$$(X + L)_{,r} = -\left(\frac{2}{r} - \nu_{,r}\right)(L + X) + \frac{X}{r} - \frac{1}{2}S_{A_1} + S_{B_0,r} + \left(\frac{1}{r} - \nu_{,r}\right) S_{B_0} \tag{C.30}$$

which, substituted in (C.27), gives

$$N_{,r} = aN + bL + cX + d \tag{C.31}$$

where

$$a = \frac{n+1}{r-2M} \tag{C.32}$$

$$b = -\frac{1}{r} - \frac{n}{r-2M} + \frac{M}{r(r-2M)} + \frac{M^2}{r(r-2M)^2} + \frac{\omega^2 r^3}{(r-2M)^2} \tag{C.33}$$

$$c = -\frac{1}{r} + \frac{1}{r-2M} + \frac{M^2}{r(r-2M)^2} + \frac{\omega^2 r^3}{(r-2M)^2} \tag{C.34}$$

$$d = \frac{r}{2}S_A - (1 + r\nu_{,r})\frac{1}{2}S_{A_1} \tag{C.35}$$

$$+ \quad \left[\left(\frac{1}{r} - \nu_{,r}\right)(1 + r\nu_{,r}) + \frac{ne^{-2\nu}}{r} - r\omega^2 e^{-4\nu}\right] S_{B_0}$$

Now, eq. (C.26) implies

$$(N - L)_{,r} = \left(\frac{1}{r} - \nu_{,r}\right) N + \left(\frac{1}{r} + \nu_{,r}\right) L + S_B - S_{B_0,r} \tag{C.36}$$

and hence

$$X_{,r} \quad = \quad (X + L)_{,r} + (N - L)_{,r} - N_{,r} = -\frac{nr + 3M}{r(r-2M)}N \tag{C.37}$$

$$- \quad \left[\frac{M^2 + \omega^2 r^4}{r(r-2M)^2} - \frac{n}{r-2M} - \frac{M}{r(r-2M)}\right](X + L) - \frac{n+1}{r-2M}X$$

$$+ \quad \left\{-\frac{r}{2}S_A + \frac{M}{2(r-2M)}S_{A_1} + S_B - \left[r\nu_{,r}\left(\frac{1}{r} - \nu_{,r}\right) + \frac{ne^{-2\nu}}{r} - r\omega^2 e^{-4\nu}\right] S_{B_0}\right\}$$

At this point we can define the Zerilli function

$$Z \equiv rV - \frac{r^2}{nr+3M}(X+L) \tag{C.38}$$

and compute the second derivative of Z with respect to r_*. We use eq. (C.27) to eliminate $V_{,rr}$ and equations eq. (C.30) and eq. (C.37); after a rather lengthy calculation, defining the Zerilli potential

$$V^{(+)} = \frac{2(r-2M)}{r^4(nr+3M)^2}\left[n^2(n+1)r^3 + 3Mn^2r^2 + 9M^2nr + 9M^3\right], \tag{C.39}$$

we obtain

$$\begin{aligned} Z_{,r_*r_*} &= \left[\omega^2 - V^{(+)}\right]\left[\frac{r^2}{nr+3M}(X+L) - rV\right] + S = \\ &= \left[V^{(+)} - \omega^2\right] Z + S \end{aligned} \tag{C.40}$$

where the source is

$$\begin{aligned} S &= \frac{M(r-2M)[(n+3)r-3M]}{r(nr+3M)^2}S_{A_1} + \frac{(r-2M)^2}{2(nr+3M)}S_{A_1,r} + \\ &+ \frac{(r-2M)^2}{2(nr+3M)}S_A - \frac{(r-2M)^2}{nr+3M}S_{B_0,rr} - \frac{(nr^2+9Mr-12M^2)(r-2M)}{r(nr+3M)^2}S_{B_0,r} + \\ &+ \frac{r-2M}{r}\left[\frac{(n+1)(nr-3M)}{(nr+3M)^2} - \frac{\omega^2r^3}{(r-2M)(nr+3M)}\right]S_{B_0} - \\ &- \frac{(r-2M)^2}{r(nr+3M)}S_B + \frac{(r-2M)^2}{r}S_F \end{aligned} \tag{C.41}$$

Putting back the definitions of the source terms and the (ℓ, m) dependence we finally have:

$$\begin{aligned} S_{\ell m} &= \frac{M(r-2M)[(n+3)r-3M]}{r(nr+3M)^2}\frac{8\pi}{\omega\sqrt{2}}A^{(1)}_{\ell m} + \frac{(r-2M)^2}{2(nr+3M)}\frac{8\pi}{\omega\sqrt{2}}A^{(1)}_{\ell m,r} + \\ &+ \frac{(r-2M)^2}{2(nr+3M)}8\pi A_{\ell m} + \frac{(r-2M)^2}{nr+3M}\frac{8\pi}{\sqrt{2\ell(\ell+1)}}B_{\ell m} - \\ &- \frac{16\pi(r-2M)}{\sqrt{2\ell(\ell+1)(\ell-1)(\ell+2)}}F_{\ell m} - \frac{r(r-2M)^2}{nr+3M}\frac{8\pi}{\omega\sqrt{2\ell(\ell+1)}}B^{(0)}_{\ell m,rr} - \\ &- \frac{(r-2M)(3nr^2+15Mr-4Mnr-24M^2)}{(nr+3M)^2}\frac{8\pi}{\omega\sqrt{2\ell(\ell+1)}}B^{(0)}_{\ell m,r} + \\ &+ \left\{\frac{(r-2M)(n^2r^2-3Mnr-12Mr+12M^2)}{r(nr+3M)^2} - \frac{\omega^2r^3}{nr+3M}\right\}\frac{8\pi}{\omega\sqrt{2\ell(\ell+1)}}B^{(0)}_{\ell m} \end{aligned} \tag{C.42}$$

C.1.2 Specialization of the polar source term to the circular case

Let us list the tensor harmonic components of the stress energy tensor of a particle moving in a general orbit around the star. If we write the polar part of the expansion in the form:

$$\begin{aligned} \mathbf{T}^{pol} &= \sum_{\ell m}\Big[A^{(0)}_{\ell m}\mathbf{a}^{(0)}_{\ell m} + A^{(1)}_{\ell m}\mathbf{a}^{(1)}_{\ell m} + A_{\ell m}\mathbf{a}_{\ell m} + \\ &\quad + B^{(0)}_{\ell m}\mathbf{b}^{(0)}_{\ell m} + B_{\ell m}\mathbf{b}_{\ell m} + G_{\ell m}\mathbf{g}_{\ell m} + F_{\ell m}\mathbf{f}_{\ell m}\Big], \end{aligned} \tag{C.43}$$

the components of the stress-energy tensor,

$$T^{\mu\nu} = \frac{m_0}{\sqrt{-g}} \frac{dT}{d\tau} \frac{dz^\mu}{dt} \frac{dz^\nu}{dt} \delta(r - R(t)) \delta^{(2)}(\Omega - \Omega(t)), \tag{C.44}$$

have the following expressions:

$$A_{\ell m} = \frac{m_0}{r^2} \frac{dT}{d\tau} e^{-4\nu} \left(\frac{dR}{dt} \right)^2 \delta(r - R(t)) Y^*_{\ell m} \Big|_{(\Theta(t),\Phi(t))} \tag{C.45}$$

$$A^{(1)}_{\ell m} = \mathrm{i} \frac{\sqrt{2} m_0}{r^2} \frac{dT}{d\tau} \frac{dR}{dt} \delta(r - R(t)) Y^*_{\ell m} \Big|_{(\Theta(t),\Phi(t))} \tag{C.46}$$

$$B_{\ell m} = 2n(\ell) m_0 \frac{dT}{d\tau} \frac{1}{r - 2M} \frac{dR}{dt} \delta(r - R(t)) \frac{dY^*_{\ell m}}{dt} \Big|_{(\Theta(t),\Phi(t))} \tag{C.47}$$

$$B^{(0)}_{\ell m} = \mathrm{i} 2n(\ell) m_0 \frac{dT}{d\tau} \frac{1 - \frac{2M}{r}}{r} \delta(r - R(t)) \frac{dY^*_{\ell m}}{dt} \Big|_{(\Theta(t),\Phi(t))} \tag{C.48}$$

$$\begin{aligned} F_{\ell m} &= 2m(\ell) m_0 \frac{dT}{d\tau} \delta(r - R(t)) \left\{ \frac{d\Theta}{dt} \frac{d\Phi}{dt} X^*_{\ell m} \Big|_{(\Theta(t),\Phi(t))} \right. \\ &+ \left. \frac{1}{2} \left[\left(\frac{d\Theta}{dt} \right)^2 - \sin^2 \vartheta \left(\frac{d\Phi}{dt} \right)^2 \right] W^*_{\ell m} \Big|_{(\Theta(t),\Phi(t))} \right\} \end{aligned} \tag{C.49}$$

Notice that, in computing $A^{(1)}_{\ell m}$ and $B^{(0)}_{\ell m}$, we have taken into account the minus sign due to the different normalization of the harmonics.

We will only use the Zerilli formalism as a check for the more general calculation of the waves emitted by particles in closed orbits, which will be performed using the BPT approach. So, in the following, we explicitly compute the coefficients appearing in formula (C.42) only in the simple case of circular orbits ($r = R_0 =$const). In this case the geodesic equations (1.58) become:

$$\frac{d\varphi}{d\tau} = \frac{L_z}{r^2} = \frac{L_z}{R_0^2}, \qquad \frac{dt}{d\tau} = E \left(1 - \frac{2M}{R_0} \right)^{-1}, \qquad \frac{dr}{d\tau} = 0. \tag{C.50}$$

and the particle's energy and angular momentum are given by:

$$E = \left(1 - \frac{2M}{R_0} \right) \left(1 - \frac{3M}{R_0} \right)^{-1/2} \tag{C.51}$$

$$L_z = \sqrt{\frac{M R_0}{1 - 3M/R_0}}. \tag{C.52}$$

Hence the only non-zero functions appearing in the source (2.37) are $B^{(0)}_{\ell m}$ and $F_{\ell m}$. Without loss of generality, we consider orbits on the equatorial plane ($\Theta(t) = \pi/2$, $\frac{d\Theta}{dt} = 0$) and compute the Fourier transform of the stress-energy tensor coefficients[1].

For an equatorial orbit, since $\varphi = m\omega_k t$, where $\omega_k = \sqrt{M/R_0^3}$ is the keplerian frequency, we can write

$$Y^*_{\ell m}\,\big|_{(\pi/2,\Phi(t))} = \Theta_{\ell m}(\pi/2)e^{-im\omega_k t}, \tag{C.53}$$

so we have:

$$\frac{dY^*_{\ell m}}{dt}\,\big|_{(\pi/2,\Phi(t))} = -im\omega_k Y^*_{\ell m}\,\big|_{(\pi/2,\Phi(t))}\ . \tag{C.54}$$

Now, eq. (C.48) yields:

$$\begin{aligned} B^{(0)}_{\ell m} &= i\sqrt{\frac{2}{\ell(\ell+1)}}m_0\frac{dT}{d\tau}\frac{1-\frac{2M}{r}}{r}\delta(r-R(t))\frac{dY^*_{\ell m}}{dt}\,\big|_{(\pi/2,\Phi(t))} \qquad \text{(C.55)}\\ &= i\sqrt{\frac{2}{\ell(\ell+1)}}\frac{m_0}{\sqrt{1-3M/R_0}}\frac{1-\frac{2M}{r}}{r}\delta(r-R_0)(-im\omega_k)Y^*_{\ell m}\,\big|_{(\pi/2,\Phi(t))} = \\ &= \sqrt{\frac{2}{\ell(\ell+1)}}\frac{mm_0\omega_k}{\sqrt{1-3M/R_0}}\frac{1-\frac{2M}{r}}{r}\delta(r-R_0)\Theta_{\ell m}(\pi/2)e^{-im\omega_k t}. \end{aligned}$$

Using the relation

$$\int_{-\infty}^{+\infty} e^{i(\omega-m\omega_k)t}dt = 2\pi\delta(\omega-m\omega_k), \tag{C.56}$$

we find:

$$B^{(0)}_{\ell m}(\omega) = \sqrt{\frac{2}{\ell(\ell+1)}}\frac{mm_0\omega_k}{\sqrt{1-\frac{3M}{R_0}}}\frac{1-2M/r}{r}\Theta_{\ell m}(\pi/2)\delta(r-R_0)\delta(\omega-m\omega_k), \tag{C.57}$$

where $\omega_k = \sqrt{M/R_0^3}$.

For $F_{\ell m}$ we proceed in the same way. We just need to note that the angular dependence, since $\frac{d\Theta}{dt} = 0$ and $\Theta(t) = \pi/2$ (we are on the equatorial plane!) can be written in this way:

$$\begin{aligned} &- \left\{\frac{\sin^2\vartheta}{2}\left(\frac{d\Phi}{dt}\right)^2\left[\frac{\partial^2}{\partial\vartheta^2} - \cot\vartheta\frac{\partial}{\partial\vartheta} - \frac{1}{\sin^2\vartheta}\frac{\partial^2}{\partial\varphi^2}\right]Y^*_{\ell m}\right\}\big|_{(\pi/2,\Phi(t))} = \\ &= -\left\{\frac{1}{2}\left(\frac{d\Phi}{dt}\right)^2\left[Y^*_{\ell m,\vartheta\vartheta} - Y^*_{\ell m,\varphi\varphi}\right]\right\}\big|_{(\pi/2,\Phi(t))}\ , \end{aligned} \tag{C.58}$$

where we have used the definition of $W_{\ell m}$. Since the Legendre equation implies:

$$\left[Y^*_{\ell m,\vartheta\vartheta} + Y^*_{\ell m,\varphi\varphi}\right]\big|_{(\pi/2,\Phi(t))} = -\ell(\ell+1)Y^*_{\ell m}\,\big|_{(\pi/2,\Phi(t))} \tag{C.59}$$

[1] As usual, the Fourier transforms are defined as

$$B^{(0)}_{\ell m}(\omega) = \frac{1}{2\pi}\int_{-\infty}^{+\infty} B^{(0)}_{\ell m}(t)\,e^{i\omega t}dt, \qquad F_{\ell m}(\omega) = \frac{1}{2\pi}\int_{-\infty}^{+\infty} F_{\ell m}(t)\,e^{i\omega t}dt.$$

we obtain:

$$\left[Y^*_{\ell m,\vartheta\vartheta} - Y^*_{\ell m,\varphi\varphi}\right]\Big|_{(\pi/2,\Phi(t))} = \left[2m^2 - \ell(\ell+1)\right] Y^*_{\ell m}\Big|_{(\pi/2,\Phi(t))} . \tag{C.60}$$

Now we can proceed as before. Substituting the geodesic equations in (C.49) yields

$$F_{\ell m} = \frac{m_0\left[\ell(\ell+1) - 2m^2\right]}{\sqrt{2(\ell-1)\ell(\ell+1)(\ell+2)}} \frac{M/R_0^3}{\sqrt{1-3M/R_0}} \delta(r-R_0) Y^*_{\ell m}\Big|_{(\pi/2,\Phi(t))} . \tag{C.61}$$

Thus, the Fourier transform of $F_{\ell m}$ is:

$$F_{\ell m}(\omega) = \frac{m_0\left[\ell(\ell+1) - 2m^2\right]}{\sqrt{2(\ell-1)\ell(\ell+1)(\ell+2)}} \frac{M/R_0^3}{\sqrt{1-\frac{3M}{R_0}}} \Theta_{\ell m}(\pi/2)\delta(r-R_0)\delta(\omega - m\omega_k) \tag{C.62}$$

Notice that the function $\Theta_{\ell m}$, as defined in Appendix G, is related to the spherical harmonics by:

$$Y_{\ell m}(\vartheta,\varphi) = \Theta_{\ell m}(\vartheta) e^{im\varphi} \tag{C.63}$$

while the associated Legendre function $\tilde{P}_{\ell m}$ is related to the spherical harmonics by:

$$Y_{\ell m}(\vartheta,\varphi) = (-1)^m \sqrt{\frac{(2\ell+1)(\ell-m)!}{4\pi(\ell+m)!}} \tilde{P}_{\ell m}(\cos\vartheta) e^{im\varphi} \tag{C.64}$$

Since in our calculations on extrasolar planetary systems we consider only the excitation of polar modes by a particle in circular orbit, and the energy output in $\ell = 2$, $m = 0$ can be ignored, for symmetry reasons we can consider only terms with $\ell = m = 2$. Since:

$$\tilde{P}_{22}(\cos\vartheta) = 3(1 - \cos^2\vartheta) \tag{C.65}$$

the only angular function that we need to compute is:

$$\Theta_{22}(\pi/2) = \sqrt{\frac{5}{4\pi\cdot 4!}} \cdot 3 = \sqrt{\frac{15}{32\pi}} \tag{C.66}$$

C.1.3 Solution for circular orbits in the polar case

Let us now turn to the task of solving the Zerilli equation with source (2.36). Since we are interested in the emission of gravitational waves, we want a solution to the equation satisfying both a *matching condition* at the border of the star and a *purely-outgoing wave condition* at infinity.

This general solution can be obtained by the Green's functions method. The values of the Zerilli function and its first derivative at the surface of the star ($r = R$) can be obtained from formula (2.35) integrating the system of equations (2.27)-(2.30) from the center to the surface of the star. The asymptotic expansions used to start the integration at the center of the star, and a discussion on the method used to superimpose two linearly independent solutions to obtain a physical solution satisfying the condition that the lagrangian pressure vanishes at $r = R$, can be found in Appendix B. Let $Z^{(1)}_{\ell m}$ be a solution satisfying the "matching" conditions (2.35), and let $Z^{(2)}_{\ell m}$ be a solution satisfying the purely-outgoing wave condition at radial infinity,

$$Z^{(2)}_{\ell m}(r\to\infty) \sim e^{i\omega r_\star}. \tag{C.67}$$

$Z^{(1)}_{\ell m}$ will be, asymptotically, a superposition of purely ingoing and purely outgoing waves:

$$Z^{(1)}_{\ell m} \sim A^{out}_{\ell m} e^{i\omega r_\star} + A^{in}_{\ell m} e^{-i\omega r_\star} \tag{C.68}$$

The general solution can be written in terms of $Z^{(1)}_{\ell m}$ and $Z^{(2)}_{\ell m}$ as:

$$Z_{\ell m} = \frac{1}{W_{\ell m}} \left\{ Z^{(2)}_{\ell m} \int_R^r Z^{(1)}_{\ell m} S dr_\star - Z^{(1)}_{\ell m} \int_\infty^r Z^{(2)}_{\ell m} S dr_\star \right\} \tag{C.69}$$

where $W_{\ell m}$ is the wronskian, defined as

$$W_{\ell m} \equiv \left(Z^{(1)}_{\ell m} Z^{(2)}_{\ell m, r_\star} - Z^{(2)}_{\ell m} Z^{(1)}_{\ell m, r_\star} \right) = 2i\omega A^{in}_{\ell m}. \tag{C.70}$$

(The last equality can be obtained evaluating W, which of course is a constant, in the limit $r \to \infty$). From the general form of the solution we can find the amplitude of the Zerilli function at infinity: that is, if we write the asymptotic form of the general solution as

$$Z_{\ell m}(r \to \infty) \sim Z^{out}_{\ell m} e^{i\omega r_\star}, \tag{C.71}$$

then

$$Z^{out}_{\ell m} = \frac{1}{2i\omega A^{in}_{\ell m}} \int_R^\infty Z^{(1)}_{\ell m} S_{\ell m} dr_\star \tag{C.72}$$

Inserting formulas (C.57) and (C.62) in equation (2.37) we can write the source for a particle in circular orbit as:

$$S_{\ell m} = A_{\ell m}(r)\delta(r - R_0) + B_{\ell m}(r)\delta'(r - R_0) + C_{\ell m}(r)\delta''(r - R_0) \tag{C.73}$$

Taking into account the fact that $dr = (1 - 2M/r)dr_\star$ and using formula (C.73), we can write the integral appearing in formula (C.72) in this form:

$$\begin{aligned}
Z_{int} &= \int_R^\infty Z^{(1)}_{\ell m} S dr_\star = \qquad (C.74)\\
&= \int_R^\infty Z^{(1)}_{\ell m} \frac{[A_{\ell m}(r)\delta(r - R_0) + B_{\ell m}(r)\delta'(r - R_0) + C_{\ell m}(r)\delta''(r - R_0)]}{1 - 2M/r} dr \equiv \\
&\equiv \int_R^\infty Z^{(1)}_{\ell m} \left[A^\star_{\ell m}(r)\delta(r - R_0) + B^\star_{\ell m}(r)\delta'(r - R_0) + C^\star_{\ell m}(r)\delta''(r - R_0)\right] dr = \\
&= [Z^{(1)}_{\ell m} A^\star_{\ell m} - (Z^{(1)}_{\ell m} B^\star_{\ell m})' + (Z^{(1)}_{\ell m} C^\star_{\ell m})''] = \\
&= Z^{(1)}_{\ell m}(R_0)[A^\star_{\ell m}(R_0) - B^{\star\,\prime}_{\ell m}(R_0) + C^{\star\,\prime\prime}_{\ell m}(R_0)] \\
&+ Z^{(1)\,\prime}_{\ell m}(R_0)[-B^\star_{\ell m}(R_0) + 2C^{\star\,\prime}_{\ell m}(R_0)] + Z^{(1)\,\prime\prime}_{\ell m}(R_0) C^\star_{\ell m}(R_0)
\end{aligned}$$

Here we have defined $A^\star_{\ell m}$, $B^\star_{\ell m}$ and $C^\star_{\ell m}$ as the corresponding functions without a star, divided by $(1 - 2M/r)$; the last equality follows from the well known properties of the δ-function:

$$\int f(x)\delta'(x)dx = -f'(x)$$

$$\int f(x)\delta''(x)dx = f''(x)$$

At this point, the outgoing wave amplitude at infinity, $Z^{out}_{\ell m}$, is expressed in terms of known functions. We have computed the functions $A^\star_{\ell m}(r)$, $B^\star_{\ell m}(r)$, $B'_\star(r)$ and their derivatives with

the help of a *Maple* code, **ABC** (see Appendix H), and then simplified the result by hand. The result is:

$$Z_{int} = 4\pi\Theta_{\ell m}(\pi/2)\left[Z^{(1)}_{\ell m}(R_0)C_0(R_0) + Z^{(1)}_{\ell m}{}'(R_0)C_1(R_0) + Z^{(1)}_{\ell m}{}''(R_0)C_2(R_0)\right] \quad \text{(C.75)}$$

where

$$C_0(r) = A^\star(r) - \frac{8M[(r-4M)(\ell+2)(\ell^3-1) - 6M(\ell^2+\ell+1)]}{\ell(\ell+1)(2nr+6M)^3\sqrt{1-3M/r}} \quad \text{(C.76)}$$

$$C_1(r) = \frac{4r(1-2M/r)}{\ell(\ell+1)(2nr+6M)\sqrt{1-3M/r}} \quad \text{(C.77)}$$

$$C_2(r) = \frac{-4r^2(1-2M/r)^2}{\ell(\ell+1)(2nr+6M)\sqrt{1-3M/r}} \quad \text{(C.78)}$$

and

$$\begin{aligned} A^\star(r) &= -\frac{2}{r^2\left[r(\ell^2+\ell-2)+6M\right]^2\ell(\ell+1)(\ell-1)(\ell+2)\sqrt{1-3M/r}} \times \\ &\times \left[9M\ell^5r^2 - 3\ell^5r^3 + \ell^4r^3 - 4\ell r^3 - 72m^2M^3 + 36M^3\ell^2 + 36\ell M^3\right. \\ &+ 7r^3\ell^3 - 16Mr^2 - M\ell^4r^2 + 16\ell Mr^2 + 16rM^2 - r^3\ell^6 + 6Mr^2\ell^2 + \\ &+ 32M^2\ell^3r - 12m^2M^2r\ell - 12m^2M^2r\ell^2 - 40\ell rM^2 + \\ &+ \left. 24rm^2M^2 + 16rM^2\ell^4 - 24rM^2\ell^2 - 17Mr^2\ell^3 + 3Mr^2\ell^6\right] \end{aligned} \quad \text{(C.79)}$$

Notice that the integral (C.75) contains a factor $\Theta_{\ell m}(\pi/2)$, and so it is zero (when $\ell = 2$) for $m = \pm 1$. This is a special case of a selection rule that can be shown to hold in general (see section 4.1 for a proof): only when $(\ell + m)$ is even there is a contribution to the polar radiation emitted by the system.

Now that we have the expression for the integral, the only missing piece to get the wave amplitude at infinity (C.72) is the wronskian. Being constant, the wronskian can be evaluated from the numerical solutions $Z^{(1)}_{\ell m}$, $Z^{(2)}_{\ell m}$ and their derivatives at any value[2] of the radial variable r, using the definition (C.70).

[2]For example, one possibility is to evaluate the wronskian at a large value of r. Writing the real part of the asymptotic (pure wave) solution to the Zerilli equation in terms of trigonometric functions,

$$Z^{(1)}_{\ell m} \sim \alpha\cos(\omega r_\star) + \beta\sin(\omega r_\star),$$

then $\left|A^{in}_{\ell m}\right| = (\alpha^2+\beta^2)^{1/2}/2$, and

$$|W_{\ell m}| = \omega(\alpha^2+\beta^2)^{1/2}.$$

Here α and β are functions of ω (and also functions of (ℓ, m), although we have not explicitly indicated this dependence) to be determined by matching the integrated solution with the asymptotic behaviour of $Z_{\ell m}$ for large r, which is given in Appendix B.3, formula (B.13). The real part of the expansion is given by:

$$\begin{aligned} Z_{\ell m} &\to \left\{\alpha - \frac{n+1}{\omega}\frac{\beta}{r} - \frac{1}{2\omega^2}\left[n(n+1)\alpha - 3M\omega\left(1+\frac{2}{n}\right)\beta\right]\frac{1}{r^2} + \ldots\right\}\cos\omega r_\star \\ &- \left\{\beta + \frac{n+1}{\omega}\frac{\alpha}{r} - \frac{1}{2\omega^2}\left[n(n+1)\beta + 3M\omega\left(1+\frac{2}{n}\right)\alpha\right]\frac{1}{r^2} + \ldots\right\}\sin\omega r_\star. \end{aligned} \quad \text{(C.80)}$$

We note incidentally that the asymptotic behaviour (C.80) is slightly different from the one given in the literature (e.g. in [16], [52]), because the term of order r^{-2} contains a factor $3M\omega\left(1+\frac{2}{n}\right)$ instead of $\frac{3}{2}M\omega\left(1+\frac{2}{n}\right)$. We have checked this result by explicit substitution of a generic expansion in powers of r^{-1} in the Zerilli equation, and also checking that it can be obtained from the recursion relations given in [15].

C.2 The axial case

C.2.1 Derivation of the source term in the axial case

The axial part of the perturbed metric can be written as

$$\mathbf{h}^{ax}_{\ell m} = \begin{pmatrix} (t) & (\varphi) & (r) & (\vartheta) \\ 0 & h_0 \sin\vartheta \frac{\partial Y_{\ell m}}{\partial \vartheta} & 0 & -h_0 \frac{1}{\sin\vartheta}\frac{\partial Y_{\ell m}}{\partial \varphi} \\ h_0 \sin\vartheta \frac{\partial Y_{\ell m}}{\partial \vartheta} & 0 & h_1 \sin\vartheta \frac{\partial Y_{\ell m}}{\partial \vartheta} & 0 \\ 0 & h_1 \sin\vartheta \frac{\partial Y_{\ell m}}{\partial \vartheta} & 0 & -h_1 \frac{1}{\sin\vartheta}\frac{\partial Y_{\ell m}}{\partial \varphi} \\ -h_0 \frac{1}{\sin\vartheta}\frac{\partial Y_{\ell m}}{\partial \varphi} & 0 & -h_1 \frac{1}{\sin\vartheta}\frac{\partial Y_{\ell m}}{\partial \varphi} & 0 \end{pmatrix}. \tag{C.82}$$

The relevant Einstein equations we obtain from this metric are

$$\delta G_{r\varphi} = -\frac{1}{2}e^{-2\nu}\left\{\ddot{h_1} - \dot{h_0}' + \frac{2}{r}\dot{h_0} + \frac{2n}{r^2}e^{2\nu}h_1\right\}\sin\vartheta Y_{\ell m,\vartheta}, \tag{C.83}$$

$$\delta G_{\vartheta\varphi} = -\frac{1}{2}\left\{\left(1-\frac{2M}{r}\right)h_1' + \frac{2M}{r^2}h_1 - \left(1-\frac{2M}{r}\right)^{-1}\dot{h_0}\right\}\sin\vartheta \cdot W_{\ell m}(\vartheta,\varphi) \tag{C.84}$$

The axial part of the stress-energy tensor (C.44) can be expanded as

$$\mathbf{T}^{ax} = \sum_{\ell m}(Q_{\ell m}{}^{(0)}\mathbf{c}^{(0)}_{\ell m} + Q_{\ell m}\mathbf{c}_{\ell m} + D_{\ell m}\mathbf{d}_{\ell m}). \tag{C.85}$$

We only need to compute two components of the perturbed stress-energy tensor:

$$T_{r\varphi} = -\frac{ir}{\sqrt{2\ell(\ell+1)}}Q_{\ell m}\ \sin\vartheta\ Y_{\ell m,\vartheta}, \tag{C.86}$$

$$T_{\varphi\vartheta} = -\frac{ir^2}{\sqrt{2\ell(\ell+1)(\ell-1)(\ell+2)}}D_{\ell m}\ \sin\vartheta\ W_{\ell m}. \tag{C.87}$$

The expansion in tensor spherical harmonics allows us to throw out the angular dependence in the two perturbed Einstein equations with source:

$$\delta G_{r\varphi} = 8\pi T_{r\varphi}$$

$$-\frac{1}{2}e^{-2\nu}\left\{\ddot{h_1} - \dot{h_0}' + \frac{2}{r}\dot{h_0} + \frac{2n}{r^2}e^{2\nu}h_1\right\} = -\frac{8\pi ir}{\sqrt{2\ell(\ell+1)}}Q_{\ell m},$$

$$\delta G_{\vartheta\varphi} = 8\pi T_{\vartheta\varphi}$$

$$-\frac{1}{2}\left\{\left(1-\frac{2M}{r}\right)h_1' + \frac{2M}{r^2}h_1 - \left(1-\frac{2M}{r}\right)^{-1}\dot{h_0}\right\} = -\frac{8\pi ir^2}{\sqrt{2\ell(\ell+1)(\ell-1)(\ell+2)}}D_{\ell m}.$$

Integrating the equations we can find α and β by the asymptotic matching of equation (C.80) with the numerical solution. Once α and β are known, we can evaluate the absolute value of the amplitude of the solution at radial infinity:

$$|Z^{out}_{\ell m}| = \frac{|Z_{int}|}{|W_{\ell m}|} = \frac{|Z_{int}|}{\omega(\alpha^2+\beta^2)^{1/2}} \tag{C.81}$$

We can write these equations as

$$\ddot{h_1} - \dot{h_0}' + \frac{2}{r}\dot{h_0} + \frac{2ne^{2\nu}}{r^2}h_1 = A, \tag{C.88}$$

$$e^{2\nu}h_1' + \frac{2M}{r^2}h_1 - e^{-2\nu}\dot{h_0} = B, \tag{C.89}$$

where

$$A = \frac{16\pi i}{\sqrt{2\ell(\ell+1)}}re^{2\nu}Q_{\ell m}, \tag{C.90}$$

$$B = \frac{16\pi i}{\sqrt{2\ell(\ell+1)(\ell-1)(\ell+2)}}r^2 D_{\ell m}. \tag{C.91}$$

From eq. (2.12) we get

$$\dot{h_0} = e^{4\nu}h_1' + \frac{2Me^{2\nu}}{r^2}h_1 - e^{2\nu}B \tag{C.92}$$

and

$$\dot{h_0}' = e^{4\nu}h_1'' + \frac{6Me^{2\nu}}{r^2}h_1' + \left(\frac{2Me^{2\nu}}{r^2}\right)_{,r} h_1 - \left(e^{2\nu}B\right)_{,r}; \tag{C.93}$$

by replacing eq. (C.92) and (C.93) in eq. (C.88), and defining the Regge-Wheeler function

$$h_1 = re^{-2\nu}Z^{ax}, \tag{C.94}$$

after some straightforward algebraic manipulation we find

$$\begin{aligned}&\ddot{Z}^{ax} - \frac{d^2Z^{ax}}{dr_*^2} - \frac{e^{2\nu}}{r^3}\left[-2(n+1)r + 6M\right]Z^{ax} \\ &= \frac{2^{2\nu}}{r}\left[A + \frac{2}{r}e^{2\nu}B - \left(Be^{2\nu}\right)_{,r}\right].\end{aligned} \tag{C.95}$$

Substituting the definitions of A and B and taking the Fourier transform on both sides finally yields

$$\frac{d^2Z^{ax}_{\ell m}}{dr_*^2} + [\omega^2 - V^{ax}]Z^{ax}_{\ell m} = S^{ax}_{\ell m}, \tag{C.96}$$

where the potential

$$V^{ax} = \frac{e^{2\nu}}{r^3}\left[\ell(\ell+1)r - 6M\right] \tag{C.97}$$

and

$$S^{ax}_{\ell m} = \frac{16\pi i}{\sqrt{2}\sqrt{\ell(\ell-1)(\ell+1)(\ell+2)}}\frac{e^{2\nu}}{r}\left[r^2\left(e^{2\nu}D_{\ell m}\right)_{,r} - \sqrt{(\ell-1)(\ell+2)}re^{2\nu}Q_{\ell m}\right]. \tag{C.98}$$

C.2.2 Specialization of the axial source term to the circular case

The coefficients appearing in formulas (C.87) and (C.87) are given in the general case by

$$\begin{aligned} Q_{\ell m} &= \frac{i2n(\ell)}{r} m_0 e^{-2\nu} \frac{dR}{d\tau} \delta(r - R(t)) \left\{ \frac{d\Phi}{dt} \sin\Theta(t) \, \frac{\partial {Y_{\ell m}}^*}{\partial \vartheta} \Big|_{(\Theta(t),\Phi(t))} \right. \\ &\quad \left. - \frac{1}{\sin\Theta(t)} \frac{\partial {Y_{\ell m}}^*}{\partial \varphi} \Big|_{(\Theta(t),\Phi(t))} \right\}, \end{aligned}$$

$$\begin{aligned} D_{\ell m} &= im(\ell) m_0 \frac{dT}{d\tau} \delta(r - R(t)) \, \delta^{(2)}(\Omega - \Omega(t)) \, \times \\ &\times \left\{ \frac{X^*_{\ell m}}{\sin\vartheta} \left[\sin^2\vartheta \left(\frac{d\Phi}{dt} \right)^2 - \left(\frac{d\Theta}{dt} \right)^2 \right] + 2W^*_{\ell m} \sin\vartheta \left(\frac{d\Theta}{dt} \right) \left(\frac{d\Phi}{dt} \right) \right\}. \end{aligned}$$

The only non-zero source term for a particle in a circular, equatorial orbit is

$$\begin{aligned} D_{\ell m} &= \frac{2m_0 m}{\sqrt{2\ell(\ell+1)(\ell-1)(\ell+2)}} \frac{dT}{d\tau} \delta(r - R(t)) \left(\frac{d\Phi}{dt} \right)^2 Y^*_{\ell m} \Big|_{(\pi/2,\Phi(t))} = \qquad \text{(C.99)} \\ &= \frac{2m_0 m}{\sqrt{2\ell(\ell+1)(\ell-1)(\ell+2)}} \frac{MR_0}{\sqrt{1 - \frac{3M}{R_0}}(1 - \frac{2M}{R_0})} \frac{r - 2M}{r^5} \delta(r - R_0) Y^*_{\ell m} \Big|_{(\pi/2,\Phi(t))} \end{aligned}$$

Proceeding as we did for the polar terms, we find that its Fourier transform is given by

$$\begin{aligned} D_{\ell m}(\omega) &= \frac{2m_0 m}{\sqrt{2\ell(\ell+1)(\ell-1)(\ell+2)}} \frac{MR_0}{\sqrt{1 - \frac{3M}{R_0}}(1 - \frac{2M}{R_0})} \frac{r - 2M}{r^5} \times \qquad \text{(C.100)} \\ &\times \delta(r - R_0) \delta(\omega - m\omega_k) \Theta_{\ell m,\vartheta}(\pi/2). \end{aligned}$$

If we only consider terms with $\ell = 2$,

$$Y_{21}(\vartheta, \varphi) = \Theta_{21}(\vartheta) e^{i\varphi} = -\sqrt{\frac{15}{8\pi}} \frac{1}{2} \sin(2\vartheta) e^{i\varphi}, \qquad \text{(C.101)}$$

so that

$$\Theta_{21,\vartheta}(\vartheta) = -\sqrt{\frac{15}{8\pi}} \cos(2\vartheta) \qquad \text{(C.102)}$$

and

$$\Theta_{21,\vartheta}(\pi/2) = \sqrt{\frac{15}{8\pi}}. \qquad \text{(C.103)}$$

C.2.3 Solution of the equations in the axial case

The solution of the axial equation can be found following exactly the same procedure as in the polar case. For circular orbits we plug in the source (C.98) the expression for the Fourier transform of the only nonzero coefficient (C.100), and then solve the equation by the Green's function technique. This procedure yields the following expression for the integral appearing in the wave amplitude at infinity:

$$Z^{ax}_{int} = \frac{4\pi\Theta_{\ell m,\vartheta}(\pi/2)}{\omega}\left[Z^{(1),ax}_{\ell m}(R_0)C_0(R_0) + Z^{(1),ax\ \prime}_{\ell m}(R_0)C_1(R_0)\right] \tag{C.104}$$

where

$$C_0(r) = \frac{4mM(r-2M)}{r^4\ell(\ell+1)(\ell-1)(\ell+2)\sqrt{1-3M/r}} \tag{C.105}$$

$$C_1(r) = rC_0(r) \tag{C.106}$$

Now, instead of a factor $\Theta_{\ell m}(\pi/2)$, the integral (C.104) contains $\Theta_{\ell m,\vartheta}(\pi/2)$, so it is zero (when $\ell = 2$) for $m = 0, \pm 2$. This is again a special case of the selection rule that holds in general (see section 4.1): only when $(\ell + m)$ is odd there is a contribution to the axial radiation emitted by the system.

C.3 Power and amplitude of the waves

In this section we shall compute the power and amplitude of the waves emitted by a binary system according to our perturbative formalism, and show how to compare results with the predictions of the quadrupole formalism. We have computed the gravitational-wave amplitude for circular orbits using the quadrupole approximation in chapter 1. Using geometrized units, our result (1.53) can be rewritten as:

$$h_Q \equiv \sqrt{\frac{2}{3}}\sqrt{\langle\tilde{h}^{(n)}_{\vartheta\vartheta}\rangle^2 + \langle\tilde{h}^{(n)}_{\vartheta\varphi}\rangle^2} = \tag{C.107}$$

$$= \sqrt{\frac{2}{3}}\sqrt{\frac{1}{4\pi}\int d\Omega\left[|h_+(2\omega_k)|^2 + |h_\times(2\omega_k)|^2\right]} = \frac{8}{\sqrt{15}}\frac{m_0}{r}(\omega_k R_0)^2$$

In Appendix E we show that the amplitude of the metric perturbations at radial infinity is related to the outgoing wave amplitudes of the Zerilli and Regge-Wheeler functions by

$$\hat{h}_{\ell m\ \mu\nu} = -\frac{e^{i\omega r_*}}{r}\sqrt{2\ell(\ell+1)(\ell-1)(\ell+2)}\left\{\frac{Z^{ax,out}(\omega)}{\omega}\hat{d}_{\ell m\ \mu\nu} + Z^{out}(\omega)\,\hat{f}_{\ell m\ \mu\nu}\right\}. \tag{C.108}$$

It turns out that most of the radiation is emitted in the polar part of the wave, so that we can limit ourselves to consider the polar part of the amplitude,

$$h_+(\omega) + ih_\times(\omega) = -\sum_{\ell m}\sqrt{(\ell-1)\ell(\ell+1)(\ell+2)}\frac{e^{i\omega r_\star}}{r}Z^{out}_{\ell m}\ {}_2Y_{\ell m} = \tag{C.109}$$

$$= -\sum_{\ell m} 2\sqrt{n(n+1)}\frac{e^{i\omega r_\star}}{r}Z^{out}_{\ell m}\ {}_2Y_{\ell m},$$

where ${}_2Y_{\ell m}$ is the $s = 2$ spin-weighted spherical harmonic (see Appendix G). Remembering the orthonormality relation for the spin-weighted spherical harmonics, it follows that

$$\frac{1}{4\pi}\int d\Omega \left[|h_+|^2 + |h_\times|^2\right] = \frac{\left[2\sqrt{n(n+1)}\delta(\omega - m\omega_k)\right]^2}{4\pi r^2}\sum_{\ell m}\left|\tilde{Z}^{out}_{\ell m}\right|^2. \tag{C.110}$$

If we consider only the $\ell = 2$ part of the metric perturbation, we can define the "relativistic" amplitude of gravitational waves at radial infinity, computed in the perturbative approach, as:

$$\begin{aligned} h_R\delta(\omega - m\omega_k) &\equiv \sqrt{\frac{2}{3}}\sqrt{\frac{1}{4\pi}\int d\Omega \left[|h_+|^2 + |h_\times|^2\right]} \\ &= \frac{2\sqrt{n(n+1)}m_0\left|\bar{Z}^{out}_{22}(2\omega_k)\right|}{\sqrt{3\pi}r}\delta(\omega - m\omega_k). \end{aligned} \tag{C.111}$$

Here we have defined $\left|\bar{Z}^{out}_{22}\right| \equiv \left|\tilde{Z}^{out}_{22}\right|/m_0$ and, in summing over m, we have used the symmetry property $\left|\bar{Z}^{out}_{22}\right| = \left|\bar{Z}^{out}_{2,-2}\right|$. We have also ignored the (small) $\ell = 2$, $m = 0$ component of the radiation.

To compare the perturbative approach with the quadrupole approximation we will compute the ratio

$$\frac{h_R}{h_Q} = \frac{\sqrt{5n(n+1)}}{\sqrt{\pi}}\frac{\left|\bar{Z}^{out}_{22}(\omega)\right|}{(\omega R_0)^2}, \tag{C.112}$$

where $\omega = 2\omega_k$ is the gravitational-wave frequency. In this ratio, h_Q takes into account only the orbital motion, while h_R is due both to the orbital motion and to the gravitational emission of the star.

A consistency check: of course, we would have obtained the same ratio (C.112) if we compared, instead of the characteristic amplitudes, the moduli of the factors appearing in front of the spin-weighted spherical harmonics in formulas (1.56) and (C.109).

From the gravitational-wave amplitude (C.109) we can also compute the energy radiated per unit frequency and unit solid angle. According to formula (1.39) we have:

$$\begin{aligned} \left(\frac{dE}{d\Omega d\omega}\right) &= \frac{\omega^2 r^2}{8}\left\{|h_+(\omega, r, \vartheta, \varphi)|^2 + |h_\times(\omega, r, \vartheta, \varphi)|^2\right\} = \\ &= \frac{\omega^2 n(n+1)}{2}\sum_{\ell m \ell' m'} Z^{out}_{\ell m}(\omega) Z^{out\,\star}_{\ell' m'}(\omega)\,{}_2Y_{\ell m}\,{}_2Y^\star_{\ell' m'} \end{aligned} \tag{C.113}$$

Integrating over the solid angle, and using the normalization relation for spin-weighted spherical harmonics

$$\int d\Omega\,{}_2Y_{\ell m}\,{}_2Y^\star_{\ell' m'} = 1, \tag{C.114}$$

we get:

$$\frac{dE}{d\omega} = \sum_{\ell m}\frac{\omega^2 n(n+1)}{2}\left|Z^{out}_{\ell m}(\omega)\right|^2 = \sum_{\ell m}\frac{\omega^2(\ell-1)\ell(\ell+1)(\ell+2)}{8}\left|Z^{out}_{\ell m}(\omega)\right|^2. \tag{C.115}$$

From equations (C.57), (C.62) and (C.72), we deduce that

$$Z^{out}_{\ell m} = \delta(\omega - m\omega_k)\tilde{Z}^{out}_{\ell m} \tag{C.116}$$

where $\tilde{Z}^{out}_{\ell m}$ is just a complex number. Hence:

$$\frac{dE}{d\omega} = \sum_{\ell m} \frac{\omega^2(\ell-1)\ell(\ell+1)(\ell+2)}{8}\delta^2(\omega - m\omega_k)\left|\tilde{Z}^{out}_{\ell m}(\omega)\right|^2. \tag{C.117}$$

The squared delta is not troublesome to deal with. In practice, we always compute an average over many periods of the energy emission rate:

$$\begin{aligned} \dot{E}_{GW} &= \lim_{T\to\infty}\frac{E}{T} = \lim_{T\to\infty}\frac{1}{T}\int d\omega \frac{dE}{d\omega} = \\ &= \int d\omega \sum_{\ell m} \frac{\omega^2(\ell-1)\ell(\ell+1)(\ell+2)}{8}\frac{1}{2\pi}\left|\tilde{Z}^{out}_{\ell m}(\omega)\right|^2 \times \\ &\times \lim_{T\to\infty}\frac{2\pi}{T}\delta^2(\omega - m\omega_k). \end{aligned} \tag{C.118}$$

But the limit appearing in the last equation is just (see, e.g., [80])

$$\lim_{T\to\infty}\frac{2\pi}{T}\delta^2(\omega - m\omega_k) = \delta(\omega - m\omega_k) \tag{C.119}$$

and we get, for this average emission rate:

$$\dot{E}_{GW} = \sum_{\ell m} \frac{(\ell-1)\ell(\ell+1)(\ell+2)}{16\pi}(m\omega_k)^2\left|\tilde{Z}^{out}_{\ell m}(\omega)\right|^2. \tag{C.120}$$

If we limit to circular orbits and restrict the computation to $\ell = 2$, since (ignoring the small contribution from $m = 0$) only terms with $m = \pm 2$ contribute, and $\left|\tilde{Z}^{out}_{22}\right| = \left|\tilde{Z}^{out}_{2,-2}\right|$, equation (C.120) reduces to:

$$\dot{E}^{\ell=2}_{GW} = \frac{12\omega_k^2}{\pi}\left|\tilde{Z}^{out}_{22}\right|^2 = \frac{3\omega^2_{GW}}{\pi}\left|\tilde{Z}^{out}_{22}\right|^2, \tag{C.121}$$

where $\omega_{GW} = 2\omega_k$ is the gravitational wave emission frequency.

Appendix D

The source term in the BPT approach

In this Appendix we discuss the procedure to find the wave amplitude $A_{\ell m}(\omega)$, that we know to be given by eq. (4.12):

$$A_{\ell m}(\omega) = -\frac{1}{W_{\ell m}(\omega)} \int_{R_s}^{\infty} \frac{dr'}{\Delta^2} \, \Psi^{\,1}_{\ell m}(\omega, r') \, T_{\ell m}(\omega, r'). \tag{D.1}$$

We shall assume that the pointlike mass m_0 which excites the perturbations of the star follows a geodesic of the unperturbed spacetime on the equatorial plane, with energy E and angular momentum L_z. We wrote down the geodesic equations (1.58) when we described the semi-relativistic quadrupole approach, and there we showed that closed orbits are periodic in the radial coordinate, and quasi-periodic in the φ-coordinate, i.e.

$$\begin{aligned} r(t + \Delta t) &= r(t) \\ \varphi(t + \Delta t) &= \varphi(t) + \Delta\varphi. \end{aligned} \tag{D.2}$$

The source term of the BPT equation (4.1) is

$$\begin{aligned} T_{\ell m}(\omega, r) &= -2\sqrt{n(n+1)} r^4 T_{(n)(n)\ell m}(\omega, r) - 2\sqrt{n}\Delta\Lambda_+ \frac{r^5}{\Delta} T_{(n)(\bar{m})\ell m}(\omega, r) \\ &- \frac{\Delta}{2r}\Lambda_+ \frac{r^6}{\Delta}\Lambda_+ r T_{(\bar{m})(\bar{m})\ell m}(\omega, r)\,, \end{aligned} \tag{D.3}$$

and can be found as follows. The stress-energy tensor of the orbiting mass

$$T^{\mu\nu} = \sum_{k=-\infty}^{\infty} \frac{4\pi m_0}{r^2|\gamma|} \frac{dz^\mu}{d\tau} \frac{dz^\nu}{d\tau} \, \delta\Big(t - t_k(r)\Big) \delta^{(2)}\Big(\Omega - \Omega_k(r)\Big), \tag{D.4}$$

where $t_k(r),\ \Omega_k(r)$ are the time and angular position of the mass on the $k-$th semi-orbit, is projected onto the Newman-Penrose tetrad[1], $(l, n, m, \bar{m})$, to find its tetrad components $T_{(p)(q)} = T^{\mu\nu} e_{(p)\mu} e_{(q)\nu}$.

[1] Explicitly, the tetrad legs are given by

$$\begin{aligned} l_\mu &= (1, -\frac{r^2}{\Delta}, 0, 0), \\ n_\mu &= \frac{1}{2}(\frac{\Delta}{r^2}, 1, 0, 0), \\ m_\mu &= \frac{1}{\sqrt{2}}(0, 0, -r, -ir\sin\vartheta), \\ \bar{m}_\mu &= \frac{1}{\sqrt{2}}(0, 0, -r, ir\sin\vartheta). \end{aligned}$$

This yields

$$T_{(p)(q)} = \sum_{\epsilon=\pm 1} \sum_{k=-\infty}^{+\infty} \frac{4\pi m_0}{r^2\gamma} \left(\frac{dz^\mu}{d\tau} e_{(p)\mu}\right) \left(\frac{dz^\nu}{d\tau} e_{(q)\nu}\right) \cdot \delta(t - t_k^\epsilon(r)) \delta^{(2)}(\Omega - \Omega_k^\epsilon(r)), \quad \text{(D.5)}$$

where the only expressions in parentheses we need to compute are

$$\begin{aligned} \frac{dz^\mu}{d\tau} n_\mu &= \frac{\Delta}{2r^2}\left(\frac{dt}{d\tau} + \frac{r^2}{\Delta}\frac{dr}{d\tau}\right) = \frac{\Delta\gamma\sigma}{2r^2}\left(\frac{dt}{dr} + \frac{r^2}{\Delta}\frac{dr}{d\tau}\right) = \frac{\Delta\gamma\sigma}{2r^2}\left(\frac{dt}{dr} + \frac{dr_*}{dr}\right) \\ \frac{dz^\mu}{d\tau} \bar{m}_\mu &= -\frac{r}{\sqrt{2}}\left(\frac{d\vartheta}{d\tau} - \mathrm{i}\sin\vartheta \frac{d\varphi}{d\tau}\right) . \end{aligned} \quad \text{(D.6)}$$

The tetrad components of the stress-energy tensor are subsequently decomposed using the spin-weighted spherical harmonics ${}_sS_{\ell m}(\theta,\phi)$, and Fourier expanded, as follows

$$T_{(p)(q)\ell m}(\omega, r) = \frac{1}{2\pi}\int dt d\Omega e^{i\omega t}\, {}_sS^*_{\ell m}(\Omega)\, T_{(p)(q)}(t, r, \Omega), \quad \text{(D.7)}$$

where $s = -2, -1, 0$ for $T_{(\bar{m})(\bar{m})}, T_{(n)(\bar{m})}, T_{(n)(n)}$ respectively.

As a result of this procedure, we will show that:

- In the circular case,

$$T_{\ell m}(\omega, r) = \delta(\omega - m\omega_k) T_{0\ \ell m}(\omega, r) . \quad \text{(D.8)}$$

  where ω_k is the keplerian frequency for the circular motion;

- In the eccentric case,

$$T_{\ell m}(\omega, r) = \frac{2\pi}{\Delta t} \sum_{j=-\infty}^{+\infty} \delta(\omega - \omega_{mj})\, T_{0\ \ell m}(\omega, r). \quad \text{(D.9)}$$

  where the frequencies

$$\omega_{mj} = \frac{2\pi j + m\Delta\varphi}{\Delta t} \equiv j\Omega_r + m\Omega_\varphi, \quad \text{(D.10)}$$

  were already defined[2] in eq. (1.81).

Consider for example the eccentric case (analogous considerations hold for the circular case). Using eq. (D.9), the wave amplitude (D.1) can be written as

$$A_{\ell m}(\omega) = -\frac{1}{W_{\ell m}(\omega)} \frac{2\pi}{\Delta t} \sum_{j=-\infty}^{+\infty} \delta(\omega - \omega_{mj}) \int_{R_s}^{\infty} \frac{dr'}{\Delta^2}\, \Psi^1_{\ell m}(\omega, r')\, T_{0\ \ell m}(\omega, r'), \quad \text{(D.11)}$$

where

$$T_{0\ \ell m}(r,\omega) = -2\sqrt{n(n+1)} r^4 T_{0(n)(n)} - 2\sqrt{n}\Delta\Lambda_+ \frac{r^5}{\Delta} T_{0(n)(\bar{m})} - \frac{\Delta}{2r}\Lambda_+ \frac{r^6}{\Delta}\Lambda_+ r T_{0(\bar{m})(\bar{m})} . \quad \text{(D.12)}$$

[2] As we have already shown, Ω_r and Ω_φ are the two characteristic frequencies of the problem. The frequency $\Omega_r = \frac{2\pi}{\Delta t}$ is associated to the periodicity of the radial motion, whereas $\Omega_\varphi = \frac{\Delta\varphi}{\Delta t}$ is the angular velocity of an inertial observer with respect to which the φ-motion of the orbiting mass appears to be periodic.

So, in order to calculate the amplitude at infinity (D.11), we have to perform integrations of the form

$$\int_{R_s}^{\infty} \frac{dr'}{\Delta^2}\, \Psi^{\,1}_{\ell m}(\omega, r')\; T_{0\;\ell m}(\omega, r') \tag{D.13}$$

for some (fixed) frequencies ω which are known once we have integrated the geodesic equations and obtained Ω_r and Ω_φ. Now we shall enter into the details of the computation of these integrals, both for circular and for eccentric orbits.

D.1 The circular case

D.1.1 Computation of the source

Here we want to compute the source (D.3) in the case of a circular orbit of radius R_0 on the equatorial plane ($\vartheta = \pi/2$). We define

$$\dot{f} \equiv \frac{df}{d\tau} \quad (f \text{ generic function of } \tau), \qquad \bar{\gamma} \equiv \dot{t} = \frac{E}{1 - \frac{2M}{R_0}}, \qquad \omega_k \equiv \frac{d\varphi}{dt} = \frac{\dot{\varphi}}{\bar{\gamma}}\,. \tag{D.14}$$

The stress–energy tensor is

$$\begin{aligned} T^{\mu\nu} &= 4\pi m_0 \int d\tau\; \dot{z}^\mu \dot{z}^\nu\; \delta^{(4)}(\underline{x} - \underline{z}(\tau)) = \\ &= 4\pi m_0 \int d\tau\; \dot{z}^\mu \dot{z}^\nu\; \frac{1}{r^2}\delta(r - R_0)\delta(\Omega - \Omega(\tau))\delta(t - t(\tau)) = \\ &= \frac{4\pi m_0}{\bar{\gamma} r^2}\; \dot{z}^\mu \dot{z}^\nu\; \delta(r - R_0)\delta(\Omega - \Omega(\tau))\Big|_{\tau=\tau(t)}\,. \end{aligned} \tag{D.15}$$

Formulas (D.6), in this case, reduce to

$$\begin{aligned} \dot{z}^\mu n_\mu &= \frac{\Delta}{2r^2}\bar{\gamma}, \\ \dot{z}^\mu \bar{m}_\mu &= \frac{\mathrm{i}r}{\sqrt{2}}\omega_K \bar{\gamma}, \end{aligned} \tag{D.16}$$

so, setting $m_0 = 1$, we find

$$\begin{aligned} T_{(n)(n)}(t, r, \Omega) &= \frac{\pi\Delta^2\bar{\gamma}}{r^6}\delta(r - R_0)\delta(\Omega - \Omega(\tau)) \\ T_{(n)(\bar{m})}(t, r, \Omega) &= \frac{\mathrm{i}\sqrt{2}\pi\Delta\bar{\gamma}\omega_K}{r^3}\delta(r - R_0)\delta(\Omega - \Omega(\tau)) \\ T_{(\bar{m})(\bar{m})}(t, r, \Omega) &= -2\pi\bar{\gamma}\omega_K^2\delta(r - R_0)\delta(\Omega - \Omega(\tau))\,. \end{aligned} \tag{D.17}$$

The corresponding Fourier transforms (D.7), reminding that

$${}_sS^*_{\ell m}(\vartheta, \varphi) = {}_s\; S^*_{\ell m}\left(\frac{\pi}{2}, 0\right) e^{\mathrm{i}m\varphi}$$

and

$$\frac{1}{2\pi}\int dt\; e^{\mathrm{i}(\omega - m\omega_k)t} = \delta(\omega - m\omega_k),$$

are given by

$$\begin{aligned} T_{(n)(n)\ell m}(\omega,r) &= \frac{\pi\Delta^2\bar{\gamma}}{r^6}\,{}_oS^*_{\ell m}(\pi/2,0)\delta(r-R_0)\delta(\omega-m\omega_K), \\ T_{(n)(\bar{m})\ell m}(\omega,r) &= \frac{\mathrm{i}\sqrt{2}\pi\Delta\bar{\gamma}\omega_K}{r^3}\,{}_{-1}S^*_{\ell m}(\pi/2,0)\delta(r-R_0)\delta(\omega-m\omega_K), \\ T_{(\bar{m})(\bar{m})\ell m}(\omega,r) &= -2\pi\bar{\gamma}\omega_K^2\,{}_{-2}S^*_{\ell m}(\pi/2,0)\delta(r-R_0)\delta(\omega-m\omega_K)\,. \end{aligned} \tag{D.18}$$

Therefore we can write the source of the BPT equation (D.3) as

$$T_{\ell m}(\omega,r)=\delta(\omega-m\omega_K)\left[{}_0S^*_{\ell m}\,{}_0U_{\ell m}+{}_{-1}S^*_{\ell m}\,{}_{-1}U_{\ell m}+{}_{-2}S^*_{\ell m}\,{}_{-2}U_{\ell m}\right], \tag{D.19}$$

where the functions ${}_sU_{\ell m}$ will contain terms of the following form

$$\begin{aligned} \int g(r)\partial_r\left[f(r)\delta(r-R_0)\right] &= \int\partial_r\left[g(r)f(r)\delta(r-R_0)\right]-\int\partial_r g(r)f(r)\delta(r-R_0)= \\ &= -g'(R_0)f(R_0) \end{aligned}$$

(the boundary integral obviously vanishes). This is equivalent to say that

$$\partial_r\left[f(r)\delta(r-R_0)\right]=f(R_0)\partial_r\delta(r-R_0); \tag{D.20}$$

indeed,

$$\begin{aligned} \int g(r)\partial_r\left[f(r)\delta(r-R_0)\right] &= \int g(r)f(R_0)\partial_r\delta(r-R_0)= \\ &= -\int\partial_r\left[g(r)f(R_0)\right]\delta(r-R_0)=-g'(R_0)f(R_0). \end{aligned} \tag{D.21}$$

In order to evaluate the wave amplitude, we need to perform the integral given in eq. (D.13), and we are going to use the property (D.20) in writing the expressions of ${}_{-\mathbf{s}}\mathbf{U}_{\ell\mathbf{m}}$. We also define $\Delta_0\equiv\Delta(R_0)$, and replace ω by $m\omega_K$. Thus we get:

$$\begin{aligned} {}_0U_{\ell m} &= \left(-2\pi\sqrt{n(n+1)}\frac{\bar{\gamma}\Delta_0^2}{R_0^2}\right)\delta(r-R_0) \\ {}_{-1}U_{\ell m} &= -2\sqrt{n}\,\Delta\left(\frac{\Delta}{r^2}\frac{\partial}{\partial r}+\mathrm{i}m\omega_K\right)\frac{R_0^5}{\Delta_0}\left(\frac{\mathrm{i}\pi\sqrt{2}\Delta_0\bar{\gamma}\omega_K}{R_0^3}\delta(r-R_0)\right)= \\ &= -2\pi\mathrm{i}\,\sqrt{2n}\,\bar{\gamma}\,\omega_K\,R_0^2\left(\frac{\Delta^2}{r^2}\frac{\partial}{\partial r}+\mathrm{i}m\omega_K\Delta_0\right)\delta(r-R_0)= \\ &= \delta(r-R_0)\left(2\pi\,\sqrt{2n}\,m\,\bar{\gamma}\,\omega_K^2\,\Delta_0\,R_0^2\right)-\delta'(r-R_0)\frac{\Delta^2}{r^2}\left(2\pi\mathrm{i}\,\sqrt{2n}\,\bar{\gamma}\,\omega_K\,R_0^2\right) \\ {}_{-2}U_{\ell m} &= -\frac{\Delta}{2r}\left(\frac{\Delta}{r^2}\frac{\partial}{\partial r}+\mathrm{i}m\omega_K\right)\frac{r^6}{\Delta}\left(\frac{\Delta}{r^2}\frac{\partial}{\partial r}+\mathrm{i}m\omega_K\right)r\left(-2\pi\,\bar{\gamma}\,\omega_k^2\,\delta(r-R_0)\right)= \\ &= \pi\bar{\gamma}\,\omega_K^2\,R_0\left(\frac{\Delta^2}{r^3}\frac{\partial}{\partial r}+\mathrm{i}m\omega_K\frac{\Delta}{r}\right)\left(r^4\frac{\partial}{\partial r}+\mathrm{i}m\omega_K\frac{r^6}{\Delta}\right)\delta(r-R_0) \\ &= \delta(r-R_0)\left[\mathrm{i}\pi\,m\,\omega_K^3\,\bar{\gamma}\,\frac{\Delta_0^2}{R_0^2}\,\left(\frac{r^6}{\Delta}\right)'_o-\pi\,m^2\,\omega_K^4\,\bar{\gamma}\,R_0^6\right]+ \\ &\quad+\delta'(r-R_0)\left[\Delta r^3\left(2\pi\mathrm{i}\;m\omega_K^3\,\bar{\gamma}\,R_0\right)+\Delta^2\left(4\pi\,\omega_K^2\,\bar{\gamma}\,R_0\right)\right]+ \\ &\quad+\delta''(r-R_0)\left[\Delta^2 r\,\left(\pi\,\omega_K^2\,\bar{\gamma}\,R_0\right)\right] \end{aligned}$$

where we have factored out the terms depending on r.

D.1.2 Evaluation of the integrals

The results obtained in the previous section immediately imply that

$$\frac{\tilde{T}}{\Delta^2} = \delta(\omega - m\omega_K)\left[\delta(r-R_0)A_{\ell m} + \delta'(r-R_0)B_{\ell m} + \delta''(r-R_0)C_{\ell m}\right], \tag{D.22}$$

with

$$\begin{aligned} A_{\ell m} &= {}_0S^*_{\ell m}\left[-2\pi\sqrt{n(n+1)}\,\frac{\bar\gamma}{R_0^2}\right] + {}_{-1}S^*_{\ell m}\left[2\pi\,\sqrt{2n}\,m\,\bar\gamma\,\omega_K^2\,\frac{R_0^2}{\Delta_0}\right] + \\ &\quad + {}_{-2}S^*_{\ell m}\left[\mathrm{i}\pi\,m\,\omega_K^3\,\bar\gamma\,\frac{1}{R_0^2}\left(\frac{r^6}{\Delta}\right)'_o - \pi\,m^2\,\omega_K^4\,\bar\gamma\,\frac{R_0^6}{\Delta^2}\right] \qquad \text{(D.23)} \\ B_{\ell m} &= {}_{-1}S^*_{\ell m}\left[-\frac{1}{r^2}\,\left(2\pi\mathrm{i}\,\sqrt{2n}\,\bar\gamma\omega_K\,R_0^2\,\right)\right] + \\ &\quad {}_{-2}S^*_{\ell m}\left[\frac{r^3}{\Delta}\,\left(2\pi\mathrm{i}\,m\,\omega_K^3\,\bar\gamma\,R_0\,\right) + \left(4\pi\,\omega_K^2\,\bar\gamma\,R_0\,\right)\right] \qquad \text{(D.24)} \\ C_{\ell m} &= {}_{-2}S^*_{\ell m}\left[r\,\left(\pi\,\omega_K^2\,\bar\gamma\,R_0\right)\right]. \qquad \text{(D.25)} \end{aligned}$$

The integral (D.13), ignoring the common factor $\delta(\omega - m\omega_K)$ (that we have already taken into account) is then

$$\begin{aligned} &\int_{R_s}^{\infty} dr\,\left[\delta(r-R_0)A_{\ell m} + \delta'(r-R_0)B_{\ell m} + \delta''(r-R_0)C_{\ell m}\right]\,\Psi^1_{\ell m} = \\ &= A_{\ell m}(R_0)\Psi^1_{\ell m}(R_0) - (B_{\ell m}\Psi^1_{\ell m})'_{r=R_0} + (C_{\ell m}\Psi^1_{\ell m})''_{r=R_0} = \\ &= \left[\Psi^1_{\ell m}\,(A_{\ell m} - B'_{\ell m} + C''_{\ell m}) + \Psi^{1'}_{\ell m}\,(-B_{\ell m} + 2C'_{\ell m}) + \Psi^{1''}_{\ell m}\,(C_{\ell m})\right]_{r=R_0}. \end{aligned} \tag{D.26}$$

Now, using

$$\left(\frac{r^6}{\Delta}\right)' = \frac{2r^6}{\Delta^2}(2r-5M), \qquad \left(\frac{r^3}{\Delta}\right)' = \frac{r^3}{\Delta^2}(r-4M), \qquad (2r-5M) - (r-4M) = r - M\,,$$

we obtain:

$$\begin{aligned} A_{\ell m} - B'_{\ell m} + C''_{\ell m} &= {}_0S^*_{\ell m}\left[-2\pi\sqrt{n(n+1)}\,\frac{\bar\gamma}{R_0^2}\right] + \qquad \text{(D.27)} \\ &\quad + {}_{-1}S^*_{\ell m}\left[2\pi\,\sqrt{2n}\,m\,\bar\gamma\,\omega_K^2\,\frac{R_0^2}{\Delta_0} - 4\pi\mathrm{i}\,\sqrt{2n}\,\bar\gamma\,\omega_K\,\frac{1}{R_0}\right] + \\ &\quad + {}_{-2}S^*_{\ell m}\left[2\mathrm{i}\pi\,m\,\omega_K^3\,\bar\gamma\,\frac{R_0^4}{\Delta_0^2}\,(R_0 - M) - \pi\,m^2\,\omega_K^4\,\bar\gamma\,\frac{R_0^6}{\Delta_0^2}\right] \\ -B_{\ell m} + 2C'_{\ell m} &= {}_{-1}S^*_{\ell m}\left[2\pi\mathrm{i}\,\sqrt{2n}\,\bar\gamma\,\omega_K\right] + \qquad \text{(D.28)} \\ &\quad + {}_{-2}S^*_{\ell m}\left[-2\pi\mathrm{i}m\omega_K^3\bar\gamma\frac{R_0^4}{\Delta_0} - 2\pi\omega_K^2\bar\gamma R_0\right] \\ C_{\ell m} &= {}_{-2}S^*_{\ell m}\left[\pi\omega_K^2\bar\gamma R_0^2\right]. \qquad \text{(D.29)} \end{aligned}$$

From formulas (D.26), (D.27), (D.28), (D.29) we can evaluate the integral (D.13) which, divided by the wronskian, gives the wave amplitude and then the energy spectrum.

D.2 The eccentric case

D.2.1 Computation of the source

Let us consider the case of an eccentric orbit. For later use, we remind that:

$$\frac{dt}{d\tau} = \frac{r^2 E}{\Delta}, \qquad \frac{dr}{d\tau} = \sigma\gamma, \qquad \frac{d\varphi}{d\tau} = \frac{L_z}{r^2},$$

$$\frac{dr_*}{dr} = \frac{r^2}{\Delta}, \qquad \frac{dt}{dr} = \frac{r^2}{\Delta}\frac{E\sigma}{\gamma}, \qquad \frac{dr_*}{dr} + \frac{dt}{dr} = \frac{r^2}{\Delta}\left(1 + \frac{E\sigma}{\gamma}\right), \qquad \Lambda_\pm = \frac{\Delta}{r^2}\left(\partial_r \pm \mathrm{i}\omega\frac{r^2}{\Delta}\right),$$

where $\gamma \equiv \left|\frac{dr}{d\tau}\right|$, $\sigma \equiv \mathrm{sign}(\frac{dr}{d\tau})$.

The stress–energy tensor is

$$T^{\mu\nu} = 4\pi m_0 \int d\tau \frac{dz^\mu}{d\tau}\frac{dz^\nu}{d\tau}\delta^{(4)}(\underline{x} - \underline{z}(\tau)). \tag{D.30}$$

We have

$$\delta(\bar{r} - r(\tau)) = \sum_i \frac{1}{\left|\frac{dr}{d\tau}\right|_{\tau_i(\bar{r})}}\delta(\tau - \tau_i(\bar{r}))\,, \tag{D.31}$$

where the $\tau_i(\bar{r})$ are solutions of the equation

$$r(\tau) = \bar{r}\,. \tag{D.32}$$

There is a solution if the mass falls onto the star, two if it is scattered from the star. We consider the case of a mass orbiting around the star, so there are two solution for each orbit. The source $S(r)$ is the sum of the $S^\epsilon_k(r)$ corresponding to the various branches of the trajectory. Here $k = -\infty, \ldots, +\infty$ denotes the k-th orbit, and $\epsilon = \pm 1$ denotes the branch: $+1$ when the mass is going from the periastron r_P to the apoastron r_A, -1 when it is going from r_A to r_P. So,

$$T^{\mu\nu} = \sum_{\epsilon=\pm1}\sum_{k=-\infty}^{+\infty} \frac{4\pi m_0}{r^2\gamma}\frac{dz^\mu}{d\tau}\frac{dz^\nu}{d\tau}\delta(t - t^\epsilon_k(r))\delta^{(2)}(\Omega - \Omega^\epsilon_k(r))\,. \tag{D.33}$$

If we put

$$T_{(p)(q)} = \sum_{\epsilon=\pm1}\sum_{k=-\infty}^{+\infty} T^\epsilon_{k(p)(q)}\,, \tag{D.34}$$

then

$$\begin{aligned}
T^\epsilon_{k(n)(n)} &= \frac{4\pi m_0\Delta^2\gamma}{4r^6}\left(\frac{dt}{dr} + \frac{dr_*}{dr}\right)^2 \delta(t - t^\epsilon_k(r))\delta^{(2)}(\Omega - \Omega^\epsilon_k(r)) \\
T^\epsilon_{k(n)(\bar{m})} &= -\frac{4\pi m_0\Delta\sigma}{2\sqrt{2}r^3}\left(\frac{dt}{dr} + \frac{dr_*}{dr}\right)\left(\frac{d\vartheta}{d\tau} - \mathrm{i}\sin\vartheta\frac{d\varphi}{d\tau}\right)\delta(t - t^\epsilon_k(r))\delta^{(2)}(\Omega - \Omega^\epsilon_k(r)) \\
T^\epsilon_{k(\bar{m})(\bar{m})} &= \frac{4\pi m_0}{2\gamma}\left(\frac{d\vartheta}{d\tau} - \mathrm{i}\sin\vartheta\frac{d\varphi}{d\tau}\right)^2 \delta(t - t^\epsilon_k(r))\delta^{(2)}(\Omega - \Omega^\epsilon_k(r))\,.
\end{aligned} \tag{D.35}$$

We remind that, on the equatorial plane, ${}_sS^*_{\ell m}(\Omega(r)) =_s S_{\ell m}(\pi/2,0)e^{-\mathrm{i}m\varphi}$. This implies that the Fourier transforms (D.7), if we put $m_0 = 1$, are given by

$$\begin{aligned}
T^{\epsilon}_{k(n)(n)}(\omega,r) &= \frac{\Delta^2\gamma}{2r^6}\left(\frac{dt}{dr}+\frac{dr_*}{dr}\right)^2_{t^{\epsilon}_k(r)} {}_0S^*(\Omega^{\epsilon}_k(r))e^{\mathrm{i}\omega t^{\epsilon}_k} = \\
&= \frac{\gamma}{2r^2}\left(1+\frac{2E\sigma}{\gamma}+\frac{E^2}{\gamma^2}\right){}_0S^*_{\ell m}(\pi/2,0)e^{\mathrm{i}(\omega t^{\epsilon}_k - m\varphi^{\epsilon}_k)} \\
T^{\epsilon}_{k(n)(\bar{m})}(\omega,r) &= -\frac{\Delta\sigma}{\sqrt{2}r^3}\left(\frac{dt}{dr}+\frac{dr_*}{dr}\right)_{t^{\epsilon}_k(r)}\left(\frac{d\vartheta}{d\tau}-\mathrm{i}\sin\vartheta\frac{d\varphi}{d\tau}\right)_{\Omega^{\epsilon}_k(r)} {}_{-1}S^*_{\ell m}(\Omega^{\epsilon}_k(r))e^{\mathrm{i}(\omega t^{\epsilon}_k - m\varphi^{\epsilon}_k)} \\
&= \frac{\mathrm{i}}{\sqrt{2}}L_z\frac{1}{r^3}\left(\sigma+\frac{E}{\gamma}\right){}_{-1}S^*_{\ell m}(\pi/2,0)e^{\mathrm{i}(\omega t^{\epsilon}_k - m\varphi^{\epsilon}_k)} \\
T^{\epsilon}_{k(\bar{m})(\bar{m})}(\omega,r) &= \frac{1}{\gamma}\left(\frac{d\vartheta}{d\tau}-\mathrm{i}\sin\vartheta\frac{d\varphi}{d\tau}\right)^2_{\Omega^{\epsilon}_k(r)} {}_{-2}S^*(\Omega^{\epsilon}_k(r))e^{\mathrm{i}\omega t^{\epsilon}_k} = \\
&= -L_z^2\frac{1}{\gamma r^4}{}_{-2}S^*_{\ell m}(\pi/2,0)e^{\mathrm{i}(\omega t^{\epsilon}_k - m\varphi^{\epsilon}_k)}
\end{aligned}$$

We already found, dealing with the semirelativistic quadrupole computation, that, if the solution of the geodesic equations for $t \in \left[0, \frac{\Delta t}{2}\right]$ is (1.75), the solution for $t \in \left[-\frac{\Delta t}{2}, 0\right]$ is (1.76), and the generic branch of the trajectory is (1.77). If we sum on the two branches $\epsilon = \pm 1$, we get

$$\begin{aligned}
T_{k(n)(n)}(\omega,r) &= e^{\mathrm{i}k[\omega\Delta t - m\Delta\varphi]}{}_0S^*_{\ell m}(\pi/2,0)\left[\left(\frac{1}{r^2}\left(\gamma+\frac{E^2}{\gamma}\right)\cos(\omega T - m\Phi)\right)+\right. \\
&\quad \left.+\mathrm{i}\left(\frac{2E}{r^2}\sin(\omega T - m\Phi)\right)\right] \qquad \text{(D.36)} \\
T_{k(n)(\bar{m})}(\omega,r) &= e^{\mathrm{i}k[\omega\Delta t - m\Delta\varphi]}{}_{-1}S^*_{\ell m}(\pi/2,0)\frac{\sqrt{2}L_z}{r^3}\left[-\sin(\omega T - m\Phi)+\right. \\
&\quad \left.+\mathrm{i}\left(\frac{E}{\gamma}\cos(\omega T - m\Phi)\right)\right] \qquad \text{(D.37)} \\
T_{k(\bar{m})(\bar{m})}(\omega,r) &= e^{\mathrm{i}k[\omega\Delta t - m\Delta\varphi]}{}_{-2}S^*_{\ell m}(\pi/2,0)\left[-2L_z^2\frac{1}{\gamma r^4}\cos(\omega T - m\Phi)\right]. \qquad \text{(D.38)}
\end{aligned}$$

So, $T^{lm}(\omega,r)$ can be written in the form

$$T_{(p)(q)\ell m}(\omega,r) = \left(\sum_{k=-\infty}^{+\infty} e^{ik[\omega\Delta t - m\Delta\varphi]}\right) T_{0(p)(q)\ell m}(\omega,r)\,. \qquad \text{(D.39)}$$

where the k–dependence is only in the exponential. In general, the following relation holds:

$$\sum_{k=-\infty}^{+\infty} e^{\mathrm{i}kX} = 2\pi\sum_{j=-\infty}^{+\infty}\delta(X-2\pi j)\,. \qquad \text{(D.40)}$$

If we define $X(\omega) \equiv \omega\Delta t - m\Delta\varphi$, the solutions of $X(\omega) = 2\pi j$ are

$$\omega_{mj} = \frac{2\pi j + m\Delta\varphi}{\Delta t}\,, \qquad \text{(D.41)}$$

so

$$\sum_{k=-\infty}^{+\infty} e^{\mathrm{i}kX(\omega)} = 2\pi \sum_{j=-\infty}^{+\infty} \delta\left(X\left(\omega\right) - 2\pi j\right) =$$

$$= \sum_{j=-\infty}^{+\infty} \frac{2\pi}{\left|\frac{dX}{d\omega}\right|_{\omega_{mj}}} \delta\left(\omega - \omega_{mj}\right) = \sum_{j=-\infty}^{+\infty} \frac{2\pi}{\Delta t} \delta\left(\omega - \omega_{mj}\right)$$

and eq. (D.39) can be written as

$$T_{(p)(q)\ell m}\left(\omega, r\right) = \frac{2\pi}{\Delta t} \sum_{j=-\infty}^{+\infty} \delta\left(\omega - \omega_{mj}\right) T_{0(p)(q)\ell m}\left(\omega, r\right). \tag{D.42}$$

Of course, this implies eq. (D.9), i.e.

$$T_{\ell m}(\omega, r) = \frac{2\pi}{\Delta t} \sum_{j=-\infty}^{+\infty} \delta\left(\omega - \omega_{mj}\right) T_{0\ \ell m}(\omega, r). \tag{D.43}$$

D.2.2 Evaluation of the integrals

Let us compute the integral

$$\frac{2\pi}{\Delta t} \int_{R_s}^{\infty} \frac{dr'}{\Delta^2}\, \Psi^1_{\ell m}(\omega, r')\ T_{0\ \ell m}(\omega, r'), \tag{D.44}$$

where $T_{0\ \ell m}(\omega, r)$ is, from formula (D.3):

$$\begin{aligned} T_{0\ \ell m}(\omega, r) &= -2\sqrt{n(n+1)} r^4 T_{0(n)(n)\ell m}(\omega, r) \\ &- 2\sqrt{n}\Delta\Lambda_+ \frac{r^5}{\Delta} T_{0(n)(\bar{m})\ell m}(\omega, r) - \frac{\Delta}{2r}\Lambda_+ \frac{r^6}{\Delta}\Lambda_+ r T_{0(\bar{m})(\bar{m})\ell m}(\omega, r)\,. \end{aligned} \tag{D.45}$$

From the expression of $T_{0\ \ell m}(r, \omega)$ we see that the last two terms contain the differential operator Λ_+ applied to a function of r; when we evaluate the integral (D.44) these terms can be integrated by parts defining the operators $\hat{\Lambda}_\pm = \frac{r^2}{\Delta}\Lambda_\pm$, where $\Lambda_\pm = \frac{d}{dr_*} \pm i\omega$, and using the property

$$\int_{R_s}^{\infty} dr f(r)\hat{\Lambda}_+ g(r) = -\int_{R_s}^{\infty} dr g(r)\hat{\Lambda}_- f(r) \tag{D.46}$$

which holds if, as always in our case, $f(r)$ or $g(r)$ vanishes at the extrema of the integration.

We split the integral in three pieces labeled by their spin weight,

$$\int_{R_s}^{\infty} \frac{dr'}{\Delta^2}\, \Psi^1_{\ell m}(\omega, r')\ T_{0\ \ell m}(\omega, r') = \int_{R_s}^{\infty} dr (I_0 + I_{-1} + I_{-2})\,, \tag{D.47}$$

and we have, omitting the harmonic indices (ℓ, m):

$$\begin{aligned} I_0 &= -2\sqrt{n(n+1)}\frac{r^4}{\Delta^2}\tilde{T}_{0(n)(n)}\Psi^1 = \\ &= -2\sqrt{n(n+1)}\,{}_0S^*_{\ell m}(\pi/2, 0)\frac{r^2}{\gamma\Delta^2}(\gamma^2 + E^2)\Psi^1 \cos(\omega T - m\Phi) + \end{aligned}$$

$$
\begin{aligned}
& -4\mathrm{i}\sqrt{n(n+1)}\,{}_0S^*_{\ell m}(\pi/2,0)\frac{r^2}{\Delta^2}E\Psi^1\sin(\omega T-m\Phi)\\
I_{-1} &= -2\sqrt{n}\frac{\Psi^1}{\Delta}\Lambda_+\frac{r^5}{\Delta}\tilde{T}_{0(n)(\bar{m})}=-2\sqrt{n}\frac{\Psi^1}{r^2}\hat{\Lambda}_+\frac{r^5}{\Delta}\tilde{T}_{0(n)(\bar{m})}=\\
&= 2\sqrt{n}\frac{r^5}{\Delta}\tilde{T}_{0(n)(\bar{m})}\left(\partial_r-i\omega\frac{r^2}{\Delta}\right)\frac{\Psi^1}{r^2}=\\
&= 2\sqrt{n}\frac{r^5}{\Delta}\tilde{T}_{0(n)(\bar{m})}\left[\frac{1}{r^2}\Psi^{1'}-\left(\frac{2}{r^3}+\frac{i\omega}{\Delta}\right)\Psi^1\right]=\\
&= -2\sqrt{2n}\,{}_{-1}S^*L_z\left[\frac{1}{\Delta}\Psi^{1'}-\left(\frac{2}{r\Delta}+\frac{i\omega r^2}{\Delta^2}\right)\Psi^1\right]\left[\sin(\omega T-m\Phi)-i\frac{E}{\gamma}\cos(\omega T-m\Phi)\right]\\
I_{-2} &= -\frac{\Psi^1}{2r\Delta}\Lambda_+\frac{r^6}{\Delta}\Lambda_+r\tilde{T}_{0(\bar{m})(\bar{m})}=-\frac{\Psi^1}{2r^3}\hat{\Lambda}_+r^4\hat{\Lambda}_+r\tilde{T}_{0(\bar{m})(\bar{m})}=\\
&= \left(\hat{\Lambda}_-\frac{\Psi^1}{2r^3}\right)r^4\hat{\Lambda}_+r\tilde{T}_{0(\bar{m})(\bar{m})}=-\frac{r}{2}\tilde{T}_{0(\bar{m})(\bar{m})}\hat{\Lambda}_-r^4\hat{\Lambda}_-\frac{\Psi^1}{r^3}=\\
&= -\frac{r}{2}\tilde{T}_{0(\bar{m})(\bar{m})}\hat{\Lambda}_-r^4\left(\partial_r-i\omega\frac{r^2}{\Delta}\right)\frac{\Psi^1}{r^3}=\\
&= -\frac{r}{2}\tilde{T}_{0(\bar{m})(\bar{m})}\hat{\Lambda}_-r\left(\Psi^{1'}-\frac{3\Psi^1}{r}-i\omega\frac{r^2}{\Delta}\Psi^1\right)=\\
&= -\frac{r}{2}\tilde{T}_{0(\bar{m})(\bar{m})}\left(\partial_r-i\omega\frac{r^2}{\Delta}\right)\left(r\Psi^{1'}-3\Psi^1-i\omega\frac{r^3}{\Delta}\Psi^1\right)
\end{aligned}
$$

Now, since

$$
\partial_r\left(r\Psi^{1'}-3\Psi^1-i\omega\frac{r^3}{\Delta}\Psi^1\right)=r\Psi^{1''}-2\Psi^{1'}-i\omega\frac{r^3}{\Delta}\Psi^{1'}-i\omega\frac{r^3}{\Delta^2}(r-4M)\Psi^1
$$

we get:

$$
I_{-2} = -\frac{1}{2}\tilde{T}_{0(\bar{m})(\bar{m})}\left(r^2\Psi^{1''}-2\left(r+i\omega\frac{r^4}{\Delta}\right)\Psi^{1'}+2i\omega\frac{r^4}{\Delta^2}(r-M)\Psi^1-\frac{\omega^2r^6}{\Delta^2}\Psi^1\right)
$$

Actually, to remove the $1/\gamma$ divergent terms we integrate in $d\chi$ the quantities

$$
\tilde{I}_s\equiv I_s\gamma\left(\frac{d\tau}{d\chi}\right)\,, \tag{D.48}
$$

whose expressions are:

$$
\begin{aligned}
\tilde{I}_0 &= -2\sqrt{n(n+1)}\frac{r^2}{\Delta^2}\,{}_0S^*_{\ell m}\Psi^1\\
&\times\ \left[(\gamma^2+E^2)\cos(\omega T-m\Phi)+2i\gamma E\sin(\omega T-m\Phi)\right]\left(\frac{d\tau}{d\chi}\right),\\
\tilde{I}_{-1} &= -2\sqrt{2n}\,{}_{-1}S^*_{\ell m}L_z\left[\frac{1}{\Delta}\Psi^{1'}-\left(\frac{2}{r\Delta}+\frac{i\omega r^2}{\Delta^2}\right)\Psi^1\right]\\
&\times\ \left[\gamma\sin(\omega T-m\Phi)-iE\cos(\omega T-m\Phi)\right]\left(\frac{d\tau}{d\chi}\right), \qquad \text{(D.49)}\\
\tilde{I}_{-2} &= {}_{-2}S^*_{\ell m}L_z^2\cos(\omega T-m\Phi)\\
&\times\ \left[\frac{\Psi^{1''}}{r^2}-\frac{2\Psi^{1'}}{\Delta r}\left(\frac{\Delta}{r^2}+i\omega r\right)+\frac{\Psi^1}{\Delta^2}\left[2i\omega(r-M)-\omega^2r^2\right]\right]\left(\frac{d\tau}{d\chi}\right).
\end{aligned}
$$

D.3 Computation of the derivatives of the BPT function

In order to evaluate explicitly formulas (D.26) and (D.49) we must be able to compute the function $\Psi^{1}_{\ell m}$ and its derivatives. Since we integrate numerically, depending on the selection rule given in section 4.1, either the Zerilli or the Regge-Wheeler homogeneous equations, in order to know $\Psi^{1}_{\ell m}$ and its derivatives we must differentiate formulas (4.5), giving the relation between the perturbation functions in the two approaches.

Now we turn to this computation. We shall define an auxiliary function X to simplify the algebra,

$$X \equiv \Psi^1/r^3. \tag{D.50}$$

From formulas (4.5) we see then that, except for a constant factor whose expression depends on the selection rule, we have, both in the polar and in the axial case, a relation of the form

$$X = VZ + (W + 2\mathrm{i}\omega)\left(\frac{\Delta}{r^2}Z_{,r} + \mathrm{i}\omega Z\right). \tag{D.51}$$

Using the fact that (in both cases)

$$\left(\frac{\Delta}{r^2}Z'\right)' = \frac{r^2}{\Delta}(V-\omega^2)Z$$

we find then

$$\begin{aligned}
\Psi^{1'} &= \frac{3}{r}(r^3X) + r^3X' = r^3\left(\frac{3}{r}X + X'\right), \\
\Psi^{1''} &= \frac{3}{r}r^3\left(\frac{3}{r}X + X'\right) + r^3\left(-\frac{3}{r^2}X + \frac{3}{r}X' + X''\right) = r^3\left(\frac{6}{r^2}X + \frac{3}{r}X' + X''\right),
\end{aligned}$$

where

$$\begin{aligned}
X' &= V'Z + VZ' + W'(Z_{,r_*} + \mathrm{i}\omega Z) + +(W+2\mathrm{i}\omega)\frac{r^2}{\Delta}(V-\omega^2)Z + \mathrm{i}\omega(W+2\mathrm{i}\omega)Z' = \\
&= Z\left[V' + \mathrm{i}\omega W' + (W+2\mathrm{i}\omega)\frac{r^2}{\Delta}(V-\omega^2)\right] + Z_{,r_*}\left[\frac{r^2}{\Delta}V + W' + \mathrm{i}\omega\frac{r^2}{\Delta}(W+2\mathrm{i}\omega)\right],
\end{aligned}$$

and (remind that $\left(\frac{r^2}{\Delta}\right)' = -\frac{2Mr^2}{\Delta^2}$)

$$\begin{aligned}
X'' &= Z\left\{V'' + \mathrm{i}\omega W'' + W'\frac{r^2}{\Delta}(V-\omega^2) - \frac{2Mr^2}{\Delta^2}(W+2\mathrm{i}\omega)(V-\omega^2) + \right. \\
&\quad \left. +(W+2\mathrm{i}\omega)\frac{r^2}{\Delta}V' + \frac{r^2}{\Delta}(V-\omega^2)\left[\frac{r^2}{\Delta}V + W' + \mathrm{i}\omega\frac{r^2}{\Delta}(W+2\mathrm{i}\omega)\right]\right\} + \\
&\quad + Z_{,r_*}\left\{\frac{r^2}{\Delta}\left[V' + \mathrm{i}\omega W' + (W+2\mathrm{i}\omega)\frac{r^2}{\Delta}(V-\omega^2)\right] + \right. \\
&\quad \left. -\frac{2Mr^2}{\Delta^2}V + \frac{r^2}{\Delta}V' + W'' - \frac{2Mr^2}{\Delta^2}\mathrm{i}\omega(W+2\mathrm{i}\omega) + \mathrm{i}\omega\frac{r^2}{\Delta}W'\right\}.
\end{aligned}$$

The potentials V and the functions W to put in the previous formulas depend on the selection rules, and here we list the functions and their derivatives.

When $\ell+m$ is even

$$
\begin{aligned}
V &= V^{pol} = \frac{2\Delta}{r^5(nr+3M)^2}\left[n^2(n+1)r^3+3Mn^2r^2+9M^2nr+9M^3\right]\\
V' &= -\frac{2}{r^5\left(nr+3\,M\right)^3}\left(39\,M^2n^2r^3+99\,M^3nr^2-6\,Mn^4r^4-30\,M^2n^3r^3+\right.\\
&\quad \left.-126\,M^3n^2r^2-270\,M^4nr+3\,n^3r^4M+81\,rM^4-216\,M^5+2\,n^4r^5+2\,n^3r^5\right)\\
V'' &= \frac{12}{r^6\left(nr+3\,M\right)^4}\left(n^5r^6+162\,rM^5+n^4r^6-828\,rM^5n-540\,M^6+\right.\\
&\quad +138\,M^3n^2r^3+243\,M^4nr^2-4\,Mn^5r^5-28\,M^2n^4r^4-156\,M^3n^3r^3+\\
&\quad \left.-504\,M^4n^2r^2+2\,Mn^4r^5+34\,M^2n^3r^4\right)\\
W &= W^{pol} = 2\frac{nr^2-3Mnr-3M^2}{r^2(nr+3M)}\\
W' &= -2\,\frac{n^2r^3-6\,Mn^2r^2-18\,M^2nr-18\,M^3}{r^3\left(nr+3\,M\right)^2}\\
W'' &= 4\,\frac{n^3r^4-9\,n^3r^3M-45\,n^2r^2M^2-99\,nrM^3-81\,M^4}{r^4\left(nr+3\,M\right)^3}\,,
\end{aligned}
$$

while when $\ell+m$ is odd

$$
\begin{aligned}
V &= V^{ax} = \frac{2\Delta}{r^5}[(n+1)r-3M]\\
V' &= -\frac{2}{r^5}[2(n+1)r^2-15rM-6Mnr+24M^2]\\
V'' &= \frac{12}{r^6}[(n+1)r^2-10rM-4Mnr+20M^2]\\
W &= W^{ax} = \frac{2(r-3M)}{r^2}\\
W' &= -\frac{2(r-6M)}{r^3}\\
W'' &= \frac{4(r-9M)}{r^4}\,.
\end{aligned}
$$

We finally wish to make a point on the relative normalization of the functions in the two approaches. For definiteness, consider the polar case (analogous considerations, except for a factor ω, hold in the axial case). Given an outgoing solution Z^0 of the homogeneous Zerilli equation of unit amplitude, such that $Z^0(r\to\infty)=e^{\mathrm{i}\omega r_*}$, the corresponding BPT function is

$$
\Psi^0(r) = -\frac{\sqrt{n(n+1)}}{4}r^3\left[V^+(r)Z+(W^+(r)+2\mathrm{i}\omega)(\partial_{r_*}+\mathrm{i}\omega)Z\right],
$$

so that

$$
\Psi^0(r\to\infty) = -r^3\frac{\sqrt{n(n+1)}}{2}\mathrm{i}\omega(\partial_{r_*}+\mathrm{i}\omega)e^{\mathrm{i}\omega r_*} = \sqrt{n(n+1)}\omega^2r^3e^{\mathrm{i}\omega r_*}\,.
$$

It can be shown that the outgoing BPT function Ψ^0 behaves asymptotically as $\Psi^0(r\to\infty)=r^3e^{\mathrm{i}\omega r_*}$, so in order for Ψ^0 to have unit amplitude the corresponding (outgoing) Zerilli function has to be normalized in such a way that

$$
Z^0(r\to\infty) = \frac{1}{\sqrt{n(n+1)}\omega^2}e^{\mathrm{i}\omega r_*}\,.
$$

Appendix E

Radiation gauge

E.1 Polar perturbations

E.1.1 Asymptotic behaviour of the perturbation functions

Defining the tensor spherical harmonics as Zerilli does in [90], the general expression for the polar perturbation $h_{\mu\nu}^{(even)}$, prior to any choice of gauge, is ([90], p. 2143):

$$
\begin{aligned}
h_{\ell m}^{(even)} &= \left(1-\frac{2M}{r}\right) H_{0\ell m}(r,t)\, a_{\ell m}^{(0)} - i\sqrt{2} H_{1\ell m}(r,t)\, a_{\ell m}^{(1)} + \\
&+ \left(1-\frac{2M}{r}\right)^{-1} H_{2\ell m}(r,t)\, a_{\ell m} - i\frac{\sqrt{2}}{r} h_{0\ell m}(r,t)\sqrt{\ell(\ell+1)}\, b_{\ell m}^{(0)} + \\
&+ \frac{\sqrt{2\ell(\ell+1)}h_{1\ell m}(r,t)}{r}\, b_{\ell m} + G_{\ell m}(r,t)\frac{\sqrt{2\ell(\ell+1)(\ell-1)(\ell-2)}}{2}\, f_{\ell m} + \\
&+ \sqrt{2}\left(K_{\ell m}(r,t) - \frac{G_{\ell m}(r,t)\ell(\ell+1)}{2}\right) g_{\ell m}
\end{aligned}
\tag{E.1}
$$

or, explicitly,

$$
h_{\ell m}^{(even)} = \begin{pmatrix}
(t) & (\varphi) & (r) & (\vartheta) \\
(1-\frac{2M}{r})H_0(r,t)Y_{\ell m} & h_0\frac{\partial Y_{\ell m}}{\partial\varphi} & H_1 Y_{\ell m} & h_0\frac{\partial Y_{\ell m}}{\partial\vartheta} \\
Sym. & h_{\varphi\varphi} & h_1\frac{\partial Y_{\ell m}}{\partial\varphi} & r^2 G\left[\frac{\partial^2}{\partial\vartheta\partial\varphi} - \cot\vartheta\frac{\partial}{\partial\varphi}\right] Y_{\ell m} \\
Sym. & Sym. & \frac{H_2(r,t)}{(1-\frac{2M}{r})} Y_{\ell m} & h_1\frac{\partial Y_{\ell m}}{\partial\vartheta} \\
Sym. & Sym. & Sym. & r^2\left[K + G\frac{\partial^2}{\partial\vartheta^2}\right] Y_{\ell m}
\end{pmatrix}
\tag{E.2}
$$

where

$$
h_{\varphi\varphi} = r^2\left[K\sin^2\vartheta + G\left(\frac{\partial^2}{\partial\varphi^2} + \sin\vartheta\cos\vartheta\frac{\partial}{\partial\vartheta}\right)\right] Y_{\ell m}. \tag{E.3}
$$

Note that this expression is consistent with the notation used by Regge and Wheeler [71]. The perturbation variables in our gauge (see our internal notes on the spherical harmonics; in par-

ticular, compare formula (127) in the internal notes with the matrix we have just written down) are such that:

$$h_0 = h_1 = H_1 = 0 \tag{E.4}$$

$$H_0(r) = 2N(r), \qquad H_2(r) = -2L(r), \qquad K(r) = -2T(r), \qquad G(r) = -2V(r). \tag{E.5}$$

and $h^{(even)}_{\ell m}$ takes the form:

$$h^{(even)}_{\ell m} = 2\left(1-\frac{2M}{r}\right) N_{\ell m}(r,t)\, a^{(0)}_{\ell m} - 2\left(1-\frac{2M}{r}\right)^{-1} L_{\ell m}(r,t)\, a_{\ell m} -$$

$$-V_{\ell m}(r,t)\sqrt{2\ell(\ell+1)(\ell-1)(\ell-2)}\, f_{\ell m} - 2\sqrt{2}\left(T_{\ell m}(r,t) - \frac{\ell(\ell+1)}{2} V_{\ell m}(r,t)\right) g_{\ell m}$$

Once we know the asymptotic behaviour of the Zerilli function, from the Einstein equations we can determine the asymptotic behaviour of $L_{\ell m}(t,r)$, $N_{\ell m}(t,r)$, $T_{\ell m}(t,r)$ and $V_{\ell m}(t,r)$. In the gauge we are using to write down the equations, the asymptotic expansions can be written as:

$$L^{old} = \left[\frac{L_1}{r} + \frac{L_2}{r^2} + \mathcal{O}\left(\frac{1}{r^3}\right)\right] e^{i\epsilon\omega r^*}$$

$$V^{old} = \left[\frac{V_1}{r} + \frac{V_2}{r^2} + \mathcal{O}\left(\frac{1}{r^3}\right)\right] e^{i\epsilon\omega r^*}$$

$$N^{old} = \left[\frac{N_1}{r} + \frac{N_2}{r^2} + \mathcal{O}\left(\frac{1}{r^3}\right)\right] e^{i\epsilon\omega r^*}$$

$$T^{old} = \left[\frac{T_1}{r} + \frac{T_2}{r^2} + \mathcal{O}\left(\frac{1}{r^3}\right)\right] e^{i\epsilon\omega r^*}$$

where $\epsilon = \pm 1$ for outgoing or ingoing waves. $A_\epsilon(\omega)$ is the amplitude of the Zerilli function at infinity ($A_{\epsilon=+1}(\omega) = Z^{out}$, $A_{\epsilon=-1}(\omega) = Z^{in}$).
Since the time dependence is irrelevant for the present considerations, we shall omit a factor $e^{-i\omega t}$ common to all perturbation functions.
Substituting the preceding expressions in the Einstein equations we obtain (see the *Maple* code in Appendix H):

$$V_1 = A_\epsilon(\omega)$$

$$L_1 = -nA_\epsilon(\omega)$$

$$N_1 = -nA_\epsilon(\omega)$$

$$T_1 = (n+1)A_\epsilon(\omega)$$

Note that all the normalized tensor spherical harmonics, $a^{(0)}\,, a^{(1)}\,, a\,, b^{(0)}\,, b\,, f\,, g\,,$ when projected onto an orthonormal tetrad

$$\begin{aligned} e^{\mu}_{(t)} &= (1,0,0,0) \\ e^{\mu}_{(\varphi)} &= \left(0, -\frac{1}{r\sin\vartheta}, 0, 0\right) \\ e^{\mu}_{(r)} &= (0,0,-1,0) \\ e^{\mu}_{(\vartheta)} &= \left(0,0,0,-\frac{1}{r}\right) \end{aligned} \tag{E.6}$$

behave as *constants* in the limit $r \to \infty$; this means that the asymptotic behaviour of even perturbations projected onto the tetrad is determined by the asymptotic behaviour of the spherical harmonic *coefficients*. (Remember that the projection onto the tetrad (E.7) is simply obtained from the relations $h_{(\mu)(\nu)} = e^{\rho}_{(\mu)} e^{\sigma}_{(\nu)} h_{\rho\sigma}$).
Since $L_{\ell m}(t,r)$, $V_{\ell m}(t,r)$, $N_{\ell m}(t,r)$, and $T_{\ell m}(t,r)$ go asymptotically like $\frac{1}{r}$, from (E.6) it follows that $h^{even}_{(\mu)(\nu)}$ goes asymptotically like $\frac{1}{r}$, as it should (being a physical perturbation).

E.1.2 Gauge transformations

To compute the stress-energy pseudotensor we must use the radiation gauge. Under a change of coordinates

$$x^{i'} = x^i + \xi^i, \tag{E.7}$$

the vector ξ^i must behave as a polar vector, of the form

$$\xi^i_{\ell m} = \left[M_0(t,r) Y_{\ell m}, M_2(t,r) \frac{\partial Y_{\ell m}}{\partial \varphi}, M_1(t,r) Y_{\ell m}, M_2(t,r) \frac{\partial Y_{\ell m}}{\partial \vartheta} \right]. \tag{E.8}$$

The metric perturbation $h^{even}_{\mu\nu}$, due to the transformation (E.7), transforms in the following way:

$$h^{new}_{\mu\nu} = h^{old}_{\mu\nu} - \xi_{\mu;\nu} - \xi_{\nu;\mu} = h^{old}_{\mu\nu} - \xi_{\mu,\nu} - \xi_{\nu,\mu} + 2\Gamma^{\sigma}_{\mu\nu}\xi_{\sigma} \tag{E.9}$$

In particular, the single tensor components transform like this:

$$\begin{aligned}
h^{new}_{tt} &= h^{old}_{tt} - 2\xi_{t,t} + 2\Gamma^{\sigma}_{tt}\xi_{\sigma} = h^{old}_{tt} - 2\dot{M}_0 Y_{\ell m} + \frac{2M}{r^2}\left(1 - \frac{2M}{r}\right) M_1 Y_{\ell m} \\
h^{new}_{t\varphi} &= h^{old}_{t\varphi} - \xi_{t,\varphi} - \xi_{\varphi,t} + 2\Gamma^{\sigma}_{t\varphi}\xi_{\sigma} = h^{old}_{t\varphi} - M_0 \frac{\partial Y_{\ell m}}{\partial \varphi} - \dot{M}_2 \frac{\partial Y_{\ell m}}{\partial \varphi} \\
h^{new}_{tr} &= h^{old}_{tr} - \xi_{t,r} - \xi_{r,t} + 2\Gamma^{\sigma}_{tr}\xi_{\sigma} = h^{old}_{tr} - M_0' Y_{\ell m} - \dot{M}_1 Y_{\ell m} + \frac{2M}{r(r-2M)} M_0 Y_{\ell m} \\
h^{new}_{t\vartheta} &= h^{old}_{t\vartheta} - \xi_{t,\vartheta} - \xi_{\vartheta,t} + 2\Gamma^{\sigma}_{t\vartheta}\xi_{\sigma} = h^{old}_{t\vartheta} - M_0 \frac{\partial Y_{\ell m}}{\partial \vartheta} - \dot{M}_2 \frac{\partial Y_{\ell m}}{\partial \vartheta} \\
h^{new}_{\varphi\varphi} &= h^{old}_{\varphi\varphi} - 2\xi_{\varphi\varphi} + 2\Gamma^{\sigma}_{\varphi\varphi}\xi_{\sigma} = h^{old}_{\varphi\varphi} - 2M_2 \frac{\partial^2 Y_{\ell m}}{\partial \varphi^2} - \\
&\quad -2\left[(r-2M)\sin^2\vartheta M_1 Y_{\ell m} + \sin\vartheta\cos\vartheta M_2 \frac{\partial Y_{\ell m}}{\partial \vartheta} \right] \\
h^{new}_{\varphi r} &= h^{old}_{\varphi r} - \xi_{\varphi,r} - \xi_{r,\varphi} + 2\Gamma^{\sigma}_{\varphi r}\xi_{\sigma} = h^{old}_{\varphi r} - M_2' \frac{\partial Y_{\ell m}}{\partial \varphi} - M_1 \frac{\partial Y_{\ell m}}{\partial \varphi} + \frac{2}{r} M_2 \frac{\partial Y_{\ell m}}{\partial \varphi} \\
h^{new}_{\varphi\vartheta} &= h^{old}_{\varphi\vartheta} - \xi_{\varphi,\vartheta} - \xi_{\vartheta,\varphi} + 2\Gamma^{\sigma}_{\varphi\vartheta}\xi_{\sigma} = h^{old}_{\varphi\vartheta} - 2M_2 \frac{\partial^2 Y_{\ell m}}{\partial\vartheta\partial\varphi} + 2M_2 \cot\vartheta \frac{\partial Y_{\ell m}}{\partial \varphi}
\end{aligned}$$

This means that after the gauge transformation (E.7) the new perturbation variables will be related to the old ones by:

$$K^{new} = K^{old} - \frac{2}{r}\left(1 - \frac{2M}{r}\right) M_1 \tag{E.10}$$

$$H_2^{new} = H_2^{old} - 2\left(1 - \frac{2M}{r}\right) M_1' - \frac{2M}{r^2} M_1 \tag{E.11}$$

$$H_0^{new} = H_0^{old} - \frac{2r}{r-2M}\dot{M}_0 + \frac{2M}{r^2} M_1 \tag{E.12}$$

$$H_1^{new} = H_1^{old} - M_0' + \frac{2M\, M_0(r,t)}{r(r-2M)} - \dot{M}_1 \tag{E.13}$$

$$h_0^{new} = h_0^{old} - M_0 - \dot{M}_2 \tag{E.14}$$

$$h_1^{new} = h_1^{old} - M_2' + \frac{2}{r} M_2 - M_1 \tag{E.15}$$

$$G^{new} = G^{old} - \frac{2M_2}{r^2} \tag{E.16}$$

Taking into account that in our gauge relations (E.4) and (E.5) hold, we obtain:

$$T^{new} = T^{old} + \frac{1}{r}\left(1 - \frac{2M}{r}\right) M_1 \tag{E.17}$$

$$L^{new} = L^{old} + \left(1 - \frac{2M}{r}\right) M_1' + \frac{M}{r^2} M_1 \tag{E.18}$$

$$N^{new} = N^{old} - \frac{r}{r-2M}\dot{M}_0 + \frac{M}{r^2} M_1 \tag{E.19}$$

$$H_1^{new} = -M_0' + \frac{2M}{r(r-2M)} M_0 - \dot{M}_1 \tag{E.20}$$

$$h_0^{new} = -M_0 - \dot{M}_2 \tag{E.21}$$

$$h_1^{new} = -M_2' + \frac{2M_2}{r} - M_1 \tag{E.22}$$

$$V^{new} = V^{old} + \frac{M_2}{r^2} \tag{E.23}$$

E.1.3 Choice of the gauge functions

In the new gauge, the metric (E.1) will be given by:

$$
\begin{aligned}
h^{(even)}_{\ell m} = &\left\{ 2\left(1-\frac{2M}{r}\right) N^{new}(r)\, a^{(0)}_{\ell m} - i\sqrt{2} H^{new}_1(r)\, a^{(1)}_{\ell m} - \right. \\
&-2\left(1-\frac{2M}{r}\right)^{-1} L^{new}(r)\, a_{\ell m} - \frac{i\sqrt{2\ell(\ell+1)}}{r}\, h^{new}_0(r)\, b^{(0)}_{\ell m} + \\
&+\frac{\sqrt{2\ell(\ell+1)}}{r} h^{new}_1(r)\, b_{\ell m} - \sqrt{2\ell(\ell+1)(\ell-1)(\ell-2)} V^{new}(r)\, f_{\ell m} - \\
&\left. -2\sqrt{2}\left(T^{new}(r) - \frac{\ell(\ell+1)}{2} V^{new}(r)\right) g_{\ell m} \right\}
\end{aligned}
\tag{E.24}
$$

For the new gauge to be asymptotically *transverse* and *traceless*, we must require that:

- all the coefficients of the harmonics $a^{(0)}$, $a^{(1)}$, a , $b^{(0)}$, b , f , g , go *at least* as $1/r$, for the spacetime has to be asymptotically flat;
- V^{new} be the dominant term at infinity, since this coefficient multiplies $f_{\ell m}$, which is the only *even* harmonic to be tranverse and traceless. So we must require that $V^{new} \sim \frac{1}{r}$, and the remaining coefficients must go to zero at least as $\frac{1}{r^2}$.

We shall determine the functions M_0, M_1 and M_2 that specify the gauge transformation requiring that the *new* perturbation variables have the behaviour:

$$
\begin{aligned}
&T^{new} - \frac{\ell(\ell+1)}{2} V^{new} \sim \frac{1}{r^2} + \mathcal{O}\left(\frac{1}{r^3}\right) \\
&L^{new} \sim \frac{1}{r^2} + \mathcal{O}\left(\frac{1}{r^3}\right) \\
&N^{new} \sim \frac{1}{r^2} + \mathcal{O}\left(\frac{1}{r^3}\right) \\
&H^{new}_1 \sim \frac{1}{r^2} + \mathcal{O}\left(\frac{1}{r^3}\right) \\
&\frac{h^{new}_0}{r} \sim \frac{1}{r^2} + \mathcal{O}\left(\frac{1}{r^3}\right) \rightarrow\ h^{new}_0 \sim \frac{1}{r} + \mathcal{O}\left(\frac{1}{r^2}\right) \\
&\frac{h^{new}_1}{r} \sim \frac{1}{r^2} + \mathcal{O}\left(\frac{1}{r^3}\right) \rightarrow\ h^{new}_1 \sim \frac{1}{r} + \mathcal{O}\left(\frac{1}{r^2}\right) \\
&V^{new} \sim \frac{1}{r} + \mathcal{O}\left(\frac{1}{r^3}\right)
\end{aligned}
$$

We have seven asymptotic behaviours to determine, one for each perturbation function. We will now show, in seven steps, that the gauge functions can be chosen in such a way as to satisfy the asymptotic conditions we have just written down.

1. Let's start requiring $T^{new} \sim \frac{1}{r}$. We shall later verify that, even if $T^{new} \sim \frac{1}{r}$, the linear combination $T^{new} - \frac{l(l+1)}{2} V^{new} \sim \frac{1}{r^2}$ since the coefficients of order $\frac{1}{r}$ cancel out. From (E.17) and (E.6) it follows that we must impose the condition:

$$T^{new} = T^{old} + \frac{1}{r}\left(1 - \frac{2M}{r}\right) M_1 \sim$$
$$\sim e^{i\epsilon\omega r_*} \left(\frac{T_1}{r} + \frac{T_2}{r^2} + \mathcal{O}\left(\frac{1}{r^3}\right)\right) + \frac{1}{r}\left(1 - \frac{2M}{r}\right) M_1 \sim \mathcal{O}\left(\frac{1}{r}\right)$$

It follows that

$$M_1 = \frac{e^{i\epsilon\omega r_*}}{\left(1 - \frac{2m}{r}\right)} \left[c_0 + \frac{c_1}{r} + \mathcal{O}\left(\frac{1}{r^2}\right)\right] \tag{E.25}$$

where the costants c_0 and c_1 can still be freely chosen.

2. Let us now require that $L^{new} \sim \frac{1}{r^2}$.
Formulas (E.18) and (E.25) imply:

$$L^{new} = e^{i\epsilon\omega r_*} \left\{\frac{L_1}{r} + i\epsilon\omega \left(c_0 + \frac{c_1}{r} + \frac{2Mc_0}{r} + \mathcal{O}\left(\frac{1}{r^2}\right)\right)\right\}$$

and since this quantity has to be $\mathcal{O}\left(\frac{1}{r^2}\right)$ we can determine the coefficients appearing in (E.25):

$$c_0 = 0$$
$$c_1 = -\frac{L_1}{i\epsilon\omega}$$

So the first gauge function is determined to be:

$$M_1 = e^{i\epsilon\omega r_*} \left(1 - \frac{2M}{r}\right)^{-1} \left[-\frac{L_1}{i\epsilon\omega}\frac{1}{r} + \mathcal{O}\left(\frac{1}{r^2}\right)\right] \tag{E.26}$$

3. Let us require that $N^{new} \sim \frac{1}{r^2}$; from (E.19) and (E.6), considering that, according to our convention on the Fourier transform, every time derivative corresponds to a factor $(-i\omega)$, we get:

$$N^{new} = \left[\frac{N_1}{r} + \frac{N_2}{r^2} + \ldots\right] e^{i\epsilon\omega r_*} + \frac{i\omega}{\left(1 - \frac{2M}{r}\right)} M_0 + \frac{M}{r^2} M_1 \sim \mathcal{O}\left(\frac{1}{r^2}\right)$$

but from (E.26) it follows that $\frac{M}{r^2} M_1 \sim \frac{1}{r^3}$, so we shall impose

$$M_0 = -\frac{1}{i\omega}\left(1 - \frac{2M}{r}\right)\left[\frac{N_1}{r} + \frac{\mathcal{K}}{r^2} + \mathcal{O}\left(\frac{1}{r^3}\right)\right] e^{i\epsilon\omega r_*} \tag{E.27}$$

where K is an undetermined constant.

4. Consider now the asymptotic behaviour of H_1^{new}. From (E.27) we obtain:

$$\frac{dM_0}{dr} = \left[-\frac{\epsilon N_1}{r} - \frac{\epsilon \mathcal{K}}{r^2} + \frac{N_1}{i\omega}\frac{1}{r^2} + \mathcal{O}\left(\frac{1}{r^3}\right) \right] e^{i\epsilon\omega r_*}$$

Therefore, from (E.20):

$$H_1^{new} = e^{i\epsilon\omega r_*} \left[\frac{\epsilon N_1}{r} + \frac{\epsilon \mathcal{K}}{r^2} - \frac{N_1}{i\omega}\frac{1}{r^2} - \frac{i\omega}{1-\frac{2M}{r}}\frac{L_1}{i\epsilon\omega}\frac{1}{r} + \mathcal{O}\left(\frac{1}{r^3}\right) \right]$$

so that imposing $H_1^{new} \sim 1/r^2$ corresponds to the condition:

$$L_1 = N_1 \tag{E.28}$$

that we obtained from the asymptotic expansion of the metric functions!

5. We can choose the gauge functions imposing the condition $h_0^{new} = 0$.
From (E.21) we see that this request fixes M_2 as a function of M_0:

$$M_2 = \frac{1}{i\omega} M_0 = \frac{\left(1-\frac{2M}{r}\right)}{\omega^2} \left(\frac{N_1}{r} + \frac{\mathcal{K}}{r^2} + \mathcal{O}\left(\frac{1}{r^3}\right) \right) e^{i\epsilon\omega r_*} \tag{E.29}$$

where $\mathcal{K}$ is, of course, the same constant that appears in the expression for M_0.

6. Let's turn to h_1^{new}. From (E.29)

$$\begin{aligned} \frac{dM_2}{dr} &= \frac{2M}{\omega^2 r^2} \left(\frac{N_1}{r} + \frac{\mathcal{K}}{r^2} + \mathcal{O}\left(\frac{1}{r^3}\right) \right) e^{i\epsilon\omega r_*} + \\ &+ \frac{i\epsilon\omega}{\omega^2} \left(\frac{N_1}{r} + \frac{\mathcal{K}}{r^2} + \mathcal{O}\left(\frac{1}{r^3}\right) \right) e^{i\epsilon\omega r_*} + \\ &+ \left(1-\frac{2M}{r}\right) \frac{1}{\omega^2} \left(-\frac{N_1}{r^2} - \frac{2\mathcal{K}}{r^3} + \mathcal{O}\left(\frac{1}{r^4}\right) \right) e^{i\epsilon\omega r_*}. \end{aligned}$$

Since $\frac{M_2}{r} \sim \frac{1}{r^2}$, equation (E.22) implies

$$h_1^{new} \sim e^{i\epsilon\omega r_*} \left[\frac{L_1 + N_1}{i\epsilon\omega r} + \mathcal{O}\left(\frac{1}{r^2}\right) \right] \tag{E.30}$$

But $L_1 = N_1$, so that the coefficient $L_1 + N_1 \neq 0$, and asymptotically $h_1^{new} \sim \frac{1}{r}$ (as it should).

7. Finally, let us consider V^{new}. Since $\frac{1}{r^2}M_2 \sim \frac{1}{r^3}$, equation (E.6) implies

$$V^{new} = V^{old} + \frac{M_2}{r^2} = e^{i\epsilon\omega r_*}\left[\frac{V_1}{r} + \frac{V_2}{r^2} + \mathcal{O}\left(\frac{1}{r^3}\right)\right] \tag{E.31}$$

so that $V^{new} \sim \frac{1}{r}$. To complete the proof we only need to note that

$$T^{new} = e^{i\epsilon\omega r_*}\left\{\frac{T_1}{r} + \mathcal{O}\left(\frac{1}{r^2}\right)\right\} \tag{E.32}$$

and that, being $T_1 = (n+1)V_1$,

$$\begin{aligned} &T^{new} - \frac{\ell(\ell+1)}{2}V^{new} = \\ &= T^{new} - (n+1)V^{new} = e^{i\epsilon\omega r_*}\left[\frac{T_1 - (n+1)V_1}{r} + \mathcal{O}\left(\frac{1}{r^2}\right)\right] \sim \left(\frac{1}{r^2}\right) \end{aligned}$$

As anticipated, the coefficient multiplying $g_{\ell m}$ dies out asymptotically $\sim \frac{1}{r^2}$.

In summary, the transformation leading from our gauge to a TT-gauge is specified by:

$$\begin{aligned} M_1 &= \frac{e^{i\epsilon\omega r_*}}{\left(1-\frac{2M}{r}\right)}\left[\frac{n}{i\epsilon\omega r} + \mathcal{O}\left(\frac{1}{r^2}\right)\right] \\ M_2 &= e^{i\epsilon\omega r_*}\frac{\left(1-\frac{2M}{r}\right)}{\omega^2}\left[\frac{-n}{r} + \frac{\mathcal{K}}{r^2} + \mathcal{O}\left(\frac{1}{r^3}\right)\right] \\ M_0 &= -e^{i\epsilon\omega r_*}\frac{\left(1-\frac{2M}{r}\right)}{i\omega}\left[\frac{-n}{r} + \frac{\mathcal{K}}{r^2} + \mathcal{O}\left(\frac{1}{r^3}\right)\right] \end{aligned}$$

The asymptotic behaviour of $h^{even}_{\ell m}$ in the new gauge is determined by the harmonic $f_{\ell m}$:

$$h^{even}_{\ell m} \to \left\{-\sqrt{2\ell(\ell+1)(\ell-1)(\ell+2)}\, V^{new}\, f_{\ell m}\right\} + \mathcal{O}\left(\frac{1}{r^2}\right)$$

and the metric perturbation at infinity can be expressed in terms of the amplitude of the outgoing Zerilli function at infinity:

$$h^{even}_{\ell m} \to -\frac{e^{i\omega r_*}}{r}\left\{\sqrt{2\ell(\ell+1)(\ell-1)(\ell+2)}\, Z^{out}\, f_{\ell m}\right\} \tag{E.33}$$

E.1.4 Relation between $h_{\mu\nu}$ and the Zerilli function

The asymptotic form of the perturbed metric tensor in the radiative gauge, where all components have the correct dependency on the radial coordinate, can be written as:

$$h^{even}_{\ell m\ \mu\nu}(\omega, r, \varphi, \vartheta) = -\frac{e^{i\omega r^*}}{r}\sum_{\ell m} f_\ell Z^{out}_{\ell m}(\omega)\cdot f_{\ell m\ \mu\nu}, \tag{E.34}$$

where we have defined

$$f_\ell = \sqrt{2\ell(\ell+1)(\ell-1)(\ell+2)} \tag{E.35}$$

and

$$f_{\ell m\ \mu\nu} = \frac{r^2}{f_\ell} \begin{pmatrix} 0 & 0 & 0 & 0 \\ 0 & 0 & 0 & 0 \\ 0 & 0 & W_{\ell m} & X_{\ell m} \\ 0 & 0 & X_{\ell m} & -\sin\vartheta^2 W_{\ell m} \end{pmatrix},$$

is a tensor spherical harmonic, which satisfies the normalization condition

$$\int f^*_{\ell m\ \rho\sigma} f^{\rho\sigma}_{\ell m} d\Omega = 1. \tag{E.36}$$

The angular functions are given by

$$W_{\ell m} = \left[\partial^2_\vartheta - \cot\vartheta\partial_\vartheta - \frac{1}{\sin\vartheta^2}\partial^2_\varphi\right] Y_{\ell m}, \qquad X_{\ell m} = 2\partial_\varphi[\partial_\vartheta - \cot\vartheta] Y_{\ell m},$$

and r_* is the usual "tortoise" coordinate, $r_* = r + 2M\log(\frac{r}{2M} - 1)$. By projecting $h^{even}_{\mu\nu}$ onto the orthonormal tetrad

$$\begin{aligned} e_{(t)i} &= (1,0,0,0) \\ e_{(r)i} &= (0,0,-1,0) \\ e_{(\varphi)i} &= (0,-r\sin\vartheta,0,0) \\ e_{(\vartheta)i} &= (0,0,0,-r)\,, \end{aligned} \tag{E.37}$$

we find the transverse-traceless component of the perturbed metric tensor

$$\hat{h}^{even}_{\mu\nu} = -\frac{e^{i\omega r_*}}{r} f_\ell \sum_{\ell m} Z^{out}_{\ell m}(\omega)\cdot \hat{f}_{\ell m\ \mu\nu}, \tag{E.38}$$

where $\hat{f}_{\ell m\ \mu\nu}$ is now a *transverse, traceless* harmonic

$$\hat{f}_{\ell m\ \mu\nu} = \frac{1}{f_\ell} \begin{pmatrix} 0 & 0 & 0 & 0 \\ 0 & 0 & 0 & 0 \\ 0 & 0 & W_{\ell m} & \frac{1}{\sin\vartheta} X_{\ell m} \\ 0 & 0 & \frac{1}{\sin\vartheta} X_{\ell m} & -W_{\ell m} \end{pmatrix}. \tag{E.39}$$

(E.40)

This implies that:

$$\hat{h}^{even}_+ + i\hat{h}^{even}_\times = -\frac{e^{i\omega r_*}}{r} \sum_{\ell m} Z^{out}_{\ell m}(\omega) \left(W_{\ell m} + \frac{iX_{\ell m}}{\sin\vartheta}\right), \tag{E.41}$$

Now, using the definitions we obtain

$$W_{\ell m} + \frac{iX_{\ell m}}{\sin\vartheta} = Y_{\ell m,\vartheta\vartheta} - \cot\vartheta Y_{\ell m,\vartheta} + \frac{m^2}{\sin^2\vartheta} Y_{\ell m} - \frac{2m}{\sin\vartheta}\left(Y_{\ell m,\vartheta} - \cot\vartheta Y_{\ell m}\right) \tag{E.42}$$

so that, defining the spin-weighted spherical harmonic with spin weight 2 as:

$$
\begin{aligned}
{}_2Y_{\ell m} &= \frac{1}{\sqrt{\ell(\ell+1)(\ell-1)(\ell+2)}} \times \\
&\times \left\{ Y_{\ell m,\vartheta\vartheta} - \cot\vartheta Y_{\ell m,\vartheta} + \frac{m^2}{\sin^2\vartheta} Y_{\ell m} - \frac{2m}{\sin\vartheta}\left(Y_{\ell m,\vartheta} - \cot\vartheta Y_{\ell m}\right) \right\}
\end{aligned}
\tag{E.43}
$$

we finally have:

$$
\begin{aligned}
\hat{h}^{even}_{+} + i\hat{h}^{even}_{\times} &= -\frac{e^{i\omega r_*}}{r} \sum_{\ell m} \sqrt{\ell(\ell+1)(\ell-1)(\ell+2)} Z^{out}_{\ell m}(\omega)\ {}_2Y_{\ell m} \\
&= -\frac{e^{i\omega r_*}}{r} \sum_{\ell m} 2\sqrt{n(n+1)} Z^{out}_{\ell m}(\omega)\ {}_2Y_{\ell m}.
\end{aligned}
\tag{E.44}
$$

Note that, even correcting for a factor $\sqrt{2\pi}$ due to our different convention on the Fourier transform, this formula differs by a factor 2 from equation (39) in [45].

E.2 Radiation gauge for axial perturbations

A generic *axial* perturbation can be written as

$$
\begin{aligned}
h_{\ell m} &= -\frac{\sqrt{2\ell(\ell+1)}}{r} h_{0\ell m}(t,r) c^{(0)}_{\ell m} + \frac{i\sqrt{2\ell(\ell+1)}}{r} h_{1\ell m}(t,r) c_{\ell m} \\
&- \frac{i\sqrt{2\ell(\ell+1)(\ell-1)(\ell+2)}}{2r^2} h_{2\ell m}(t,r) d_{\ell m}
\end{aligned}
\tag{E.45}
$$

or, in matrix notation,

$$
h_{\ell m} = \begin{pmatrix}
0 & h_0 \sin\vartheta \frac{\partial Y_{\ell m}}{\partial\vartheta} & 0 & -h_0 \frac{1}{\sin\vartheta}\frac{\partial Y_{\ell m}}{\partial\varphi} \\
h_0 \sin\vartheta \frac{\partial Y_{\ell m}}{\partial\vartheta} & -\frac{1}{2}h_2 \sin\vartheta X_{\ell m} & h_1 \sin\vartheta \frac{\partial Y_{\ell m}}{\partial\vartheta} & -\frac{1}{2}h_2 \sin\vartheta W_{\ell m} \\
0 & h_1 \sin\vartheta \frac{\partial Y_{\ell m}}{\partial\vartheta} & 0 & -h_1 \frac{1}{\sin\vartheta}\frac{\partial Y_{\ell m}}{\partial\varphi} \\
-h_0 \frac{1}{\sin\vartheta}\frac{\partial Y_{\ell m}}{\partial\varphi} & -\frac{1}{2}h_2 \sin\vartheta W_{\ell m} & -h_1 \frac{1}{\sin\vartheta}\frac{\partial Y_{\ell m}}{\partial\varphi} & \frac{1}{2}h_2 \frac{1}{\sin\vartheta} X_{\ell m}
\end{pmatrix}.
\tag{E.46}
$$

Under an infinitesimal coordinate transformation of the form (E.7) the metric changes according to formula (E.9), so that, choosing an appropriate gauge, we can eliminate some components of $h^{old}_{\mu\nu}$.
The more general axial vector has the form

$$
\xi^{axial}_{\ell m} = ir\xi_3(r,t) \left[0,\ -\sin\vartheta \frac{\partial}{\partial\vartheta} Y_{\ell m},\ 0,\ \frac{1}{\sin\vartheta}\frac{\partial}{\partial\varphi} Y_{\ell m}\right],
\tag{E.47}
$$

or, defining $\xi_3(r,t) = -\frac{i}{r}\Lambda$,

$$
\xi^{axial}_{\ell m} = \Lambda(r,t) \left[0,\ -\sin\vartheta \frac{\partial}{\partial\vartheta} Y_{\ell m},\ 0,\ \frac{1}{\sin\vartheta}\frac{\partial}{\partial\varphi} Y_{\ell m}\right].
\tag{E.48}
$$

Under a gauge transformation the metric components change in the following way

$$h_{13}^{old} = -\frac{1}{2}h_2^{old}\sin\vartheta\, W_{\ell m} = \left[-\frac{1}{2}h_2(r,t)+\Lambda(r,t)\right]\sin\vartheta W_{\ell m} \tag{E.49}$$

$$h_{10}^{old} = h_0^{old}\sin\vartheta\, Y_{\ell m,\vartheta} = \left[h_0(r,t)+\dot{\Lambda}(r,t)\right]\sin\vartheta Y_{\ell m,\vartheta} \tag{E.50}$$

$$h_{21}^{old} = h_1^{old}\sin\vartheta\, Y_{\ell m,\vartheta} = \left[h_1(r,t)+\Lambda'(r,t)-\frac{2}{r}\Lambda\right]\sin\vartheta Y_{\ell m,\vartheta} \tag{E.51}$$

$$h_{33}^{old} = \frac{1}{2}h_2^{old}\,\frac{X_{\ell m,\vartheta}}{\sin\vartheta} = \left[\frac{1}{2}h_2(r,t)-\Lambda(r,t)\right]\frac{X_{\ell m}}{\sin\vartheta} \tag{E.52}$$

$$h_{11}^{old} = -\frac{1}{2}h_2^{old}\sin\vartheta\, X_{\ell m} = \left[-\frac{1}{2}h_2(r,t)+\Lambda(r,t)\right]\sin\vartheta X_{\ell m} \tag{E.53}$$

The Regge-Wheeler gauge corresponds to the choice $2\Lambda(r,t)=h_2(r,t)$. With this choice, the coefficient $h_{2\ell m}^{old}$ multiplying $d_{\ell m}$ is zero, so that

$$h_{\ell m}^{old} = -\frac{\sqrt{2\ell(\ell+1)}}{r}h_{0\ell m}^{old}(t,r)c_{\ell m}^{(0)}+\frac{i\sqrt{2\ell(\ell+1)}}{r}h_{1\ell m}^{old}(t,r)c_{\ell m} \tag{E.54}$$

Let us define a new function

$$Z^{ax}(r,t)=\frac{h_1^{old}}{r}e^{2\nu} \tag{E.55}$$

Then, since from the Einstein equations it follows that

$$\dot{h}_0=\left(1-\frac{2M}{r}\right)^2 h_1'+\frac{2M}{r^2}\left(1-\frac{2M}{r}\right)h_1 \tag{E.56}$$

and using our convention (1.40) on the Fourier transform:

$$h(t)=\int e^{-i\omega t}h(\omega)d\omega, \tag{E.57}$$

we have

$$-i\omega h_0^{old}=\frac{d}{dr_*}\left(rZ^{ax}\right). \tag{E.58}$$

At radial infinity the Regge-Wheeler function behaves as a pure outgoing wave:

$$\lim_{r_*\to\infty} Z^{ax}(\omega,r)=Z^{ax,out}(\omega)e^{i\omega r_*}$$

and therefore

$$h_1^{old} = \frac{rZ^{ax}}{\left(1-\frac{2M}{r}\right)}\sim rZ^{ax,out}(\omega)e^{i\omega r_*},$$

$$h_0^{old} = -\frac{1}{i\omega}\left[Z^{ax}+rZ'^{ax}\right]\sim -rZ^{ax,out}(\omega)e^{i\omega r_*}\ .$$

Since the perturbation functions go like r at radial infinity, the Regge-Wheeler gauge is not a radiation gauge, since at infinity the perturbations should die out as $1/r$. We can move to a radiative gauge by another coordinate transformation. Just like before,

$$h_{13}^{new} = -\frac{1}{2}h_2^{new}\sin\vartheta\, W_{\ell m} = \left[-\frac{1}{2}h_2^{old}(r,t) + \Lambda(r,t)\right]\sin\vartheta W_{\ell m} \tag{E.59}$$

$$h_{10}^{new} = h_0^{new}\sin\vartheta\, Y_{\ell m,\vartheta} = \left[h_0^{old}(r,t) + \dot{\Lambda}(r,t)\right]\sin\vartheta Y_{\ell m,\vartheta} \tag{E.60}$$

$$h_{21}^{new} = h_1^{new}\sin\vartheta\, Y_{\ell m,\vartheta} = \left[h_1^{old}(r,t) + \Lambda'(r,t) - \frac{2}{r}\Lambda\right]\sin\vartheta Y_{\ell m,\vartheta} \tag{E.61}$$

$$h_{33}^{new} = \frac{1}{2}h_2^{new}\,\frac{X_{\ell m,\vartheta}}{\sin\vartheta} = \left[\frac{1}{2}h_2^{old}(r,t) - \Lambda(r,t)\right]\frac{X_{\ell m}}{\sin\vartheta} \tag{E.62}$$

$$h_{11}^{new} = -\frac{1}{2}h_2^{new}\sin\vartheta\, X_{\ell m} = \left[-\frac{1}{2}h_2^{old}(r,t) + \Lambda(r,t)\right]\sin\vartheta X_{\ell m} \tag{E.63}$$

where $h_2^{old} = 0$. Let us choose the gauge function so that

$$h_0^{new} = h_0^{old} + \dot{\Lambda} = 0 \Rightarrow \dot{\Lambda} = -h_0^{old}.$$

In Fourier space

$$\Lambda = \frac{h_0^{old}}{i\omega}, \tag{E.64}$$

so that

$$h_0^{new} = 0, \tag{E.65}$$

$$h_2^{new} = h_2^{old} - 2\Lambda = -2\Lambda = -\frac{2h_0^{old}}{i\omega}, \tag{E.66}$$

$$h_1^{new} = h_1^{old} + \Lambda' - \frac{2}{r}\Lambda\,. \tag{E.67}$$

Being the Einstein equations gauge invariant, the equations written in the old gauge are still valid when we replace h^{old} by h^{new}. From the Einstein equations we have the relation

$$\ddot{h}_1 - \dot{h}_0' + \frac{2}{r}\dot{h}_0 + \left(1 - \frac{2M}{r}\right)\frac{2n}{r^2}h_1 = 0, \tag{E.68}$$

or, in Fourier space,

$$-\omega^2 h_1^{old} + i\omega h_0^{old\,\prime} - \frac{2i\omega}{r}h_0^{old} + \left(1 - \frac{2M}{r}\right)\frac{2n}{r^2}h_1^{old} = 0. \tag{E.69}$$

Using equation (E.64) we find

$$h_1^{old} + \Lambda' - \frac{2}{r}\Lambda = \frac{2n}{r^2\omega^2}\left(1 - \frac{2M}{r}\right)h_1^{old}\,. \tag{E.70}$$

But in this equation the left hand side is just h_1^{new}, so that

$$h_1^{new} = \frac{2n}{r^2\omega^2}\left(1-\frac{2M}{r}\right)h_1^{old} \sim \frac{2n}{r\omega^2}Z^{ax,out}(\omega)e^{i\omega r_*}, \tag{E.71}$$

$$h_2^{new} = -\frac{2h_0^{old}}{i\omega} \sim \frac{2r}{i\omega}Z^{ax,out}(\omega)e^{i\omega r_*}. \tag{E.72}$$

Substituting equations (E.71) and (E.72) in

$$h_{\ell m}^{new} = \frac{i\sqrt{2\ell(\ell+1)}}{r}h_1^{new}c_{\ell m} - \frac{i\sqrt{2\ell(\ell+1)(\ell-1)(\ell+2)}}{2r^2}h_2^{new}d_{\ell m} \tag{E.73}$$

and using the fact that, like the polar harmonics, the axial harmonics behave as constants in the limit $r \to \infty$ when projected on the tetrad, we find that the axial part of the metric at infinity is related to the Regge-Wheeler function, in radiation gauge, by:

$$\hat{h}^{odd}_{\ell m\ \mu\nu} \to -\frac{e^{i\omega r_*}}{r}\left\{\frac{\sqrt{2\ell(\ell+1)(\ell-1)(\ell+2)}}{\omega}Z^{ax,out}(\omega)\hat{d}_{\ell m\ \mu\nu}\right\} \tag{E.74}$$

Here $\hat{d}_{\ell m\ \mu\nu}$ is obtained projecting the tensor harmonic

$$d_{\ell m\ \mu\nu} = \frac{-ir^2}{f_\ell}\begin{pmatrix} 0 & 0 & 0 & 0 \\ 0 & 0 & 0 & 0 \\ 0 & 0 & +\sin\vartheta X_{\ell m} & \sin\vartheta W_{\ell m} \\ 0 & 0 & \sin\vartheta W_{\ell m} & -\frac{1}{\sin\vartheta}X_{\ell m} \end{pmatrix} \tag{E.75}$$

on the tetrad, and is given by

$$\hat{d}_{\ell m\ \mu\nu} = \frac{-i}{f_\ell}\begin{pmatrix} 0 & 0 & 0 & 0 \\ 0 & 0 & 0 & 0 \\ 0 & 0 & -\frac{1}{\sin\vartheta}X_{\ell m} & W_{\ell m} \\ 0 & 0 & W_{\ell m} & \frac{1}{\sin\vartheta}X_{\ell m} \end{pmatrix}, \tag{E.76}$$

where f_ℓ was defined in equation (E.35). Equations (E.74) and (E.38) can be combined to yield:

$$\hat{h}_{\ell m\ \mu\nu} = -\frac{e^{i\omega r_*}}{r}\sqrt{2\ell(\ell+1)(\ell-1)(\ell+2)}\left\{\frac{Z^{ax,out}(\omega)}{\omega}\hat{d}_{\ell m\ \mu\nu} + Z^{out}(\omega)\hat{f}_{\ell m\ \mu\nu}\right\}. \tag{E.77}$$

Appendix F

The Padé-approximants expansion

The Padé-approximants expansion tries to improve the convergence properties of the standard, Taylor-series Post-Newtonian expansion on the basis of a physical analysis of the behaviour of the energy function in the point-mass limit. The usually considered energy function E is related to the total relativistic energy E_{tot} (Bondi mass) of the binary system by

$$E_{tot} = M_{tot}(1 + E) \tag{F.1}$$

where $M_{tot} = M + m_0$ is the total mass of the binary. For a test particle m_0 moving in the background of a Schwarzschild black hole of mass M the total, conserved mass-energy reads

$$E_{tot} = M + \mathcal{E}_0, \tag{F.2}$$

where, if we denote by k_μ the time-translation Killing vector and by p^μ the 4-momentum of the test mass, $\mathcal{E}_0 = -k_\mu p^\mu$ is the conserved relativistic energy of the test particle. At infinity $k^\mu = P^\mu/M$, so $E_{tot} = M - P \cdot p/M$, which is clearly a very asymmetric expression. One should instead consider the Mandelstam variable $s = E_{tot}^2 = -(P + p)^2 = M^2 + m_0^2 - 2P \cdot p$, or better, a quantity which is very well suited to extend one-body-in-external-field results to two-body results, i.e.

$$\epsilon \equiv \frac{s - M^2 - m_0^2}{2Mm_0} = \frac{E_{tot}^2 - M^2 - m_0^2}{2Mm_0}, \tag{F.3}$$

which reduces to $\epsilon = -P \cdot p/Mm_0 = \mathcal{E}_0/m_0$ in the test-particle limit. For a test-mass orbiting a Schwarzschild black hole,

$$\epsilon = \frac{1 - 2\xi}{\sqrt{1 - 3\xi}}, \tag{F.4}$$

where $\xi = v^2$, and this suggests that the "true", two-body function ϵ will also have a square-root singularity in the complex ξ plane. This led Damour, Iyer and Sathyaprakash [28] to consider an energy function having a simple pole singularity, given by

$$e(\xi) \equiv \epsilon^2 - 1 \equiv \left(\frac{E_{tot}^2 - M^2 - m_0^2}{2Mm_0} \right)^2 - 1. \tag{F.5}$$

From this function one can easily obtain the "standard" energy $E(\xi)$:

$$E(\xi) = \left\{ 1 + 2\eta \left[\sqrt{1 + e(\xi)} - 1 \right] \right\}^{1/2} - 1. \tag{F.6}$$

Incidentally, we note that the v-derivative of this function reads

$$E'(v) = 2v \left.\frac{dE(\xi)}{d\xi}\right|_{\xi=v^2} = \frac{v\eta}{[1+E(\xi)]\sqrt{1+e(\xi)}} \left.\frac{de(\xi)}{d\xi}\right|_{\xi=v^2}. \tag{F.7}$$

In the test-mass limit, the "new" energy function is analytically given by

$$e(\xi, \eta = 0) = -\xi \frac{1-4\xi}{1-3\xi} = -\xi \left(1 - \xi - 3\xi^2 - 9\xi^3 - \ldots - 3^{n-1}\xi^n - \ldots\right). \tag{F.8}$$

In the equal-mass case, at present, we only know an expansion accurate up to the second Post-Newtonian order:

$$e_{2PN}(x, \eta) = -x \left[1 - \left(1 + \frac{\eta}{3}\right) x - \left(3 - \frac{35}{12}\eta\right) x^2\right]. \tag{F.9}$$

Now, an excellent tool to approximate rational functions, even when they have pole singularities, is the Padé-approximants technique.

A Padé approximant of a given function whose Taylor approximant to order n is

$$S_n(v) = \sum_{k=0}^{n} a_k v^k \tag{F.10}$$

is defined by two integers m, k such that $m + k = n$. If $T_n[\ldots]$ denotes the operation of expanding a function in a Taylor series and truncating the expansion at order n (included), the P_k^m Padé approximant of S_n is defined by

$$P_k^m(v) = \frac{N_m(v)}{D_k(v)}, \qquad T_n[P_m^k(v)] \equiv S_n(v), \tag{F.11}$$

where N_m and D_k are polynomials in v order m and k, respectively. If one assumes that $D_k(0) = 0$, then the last equation can be shown to uniquely define the Padé approximants. In many cases, the most useful Padé approximants turn out to be the ones near the diagonal $m = k$. In particular, we shall follow Damour, Iyer and Sathyaprakash in using diagonal Padé approximants, P_m^m, if $n = 2m$ is even, and subdiagonal approximants, P_{m+1}^m, if it is odd. These approximants can be conveniently expressed in a continued fraction form; for example, given

$$S_2(v) = a_0 + a_1 v + a_2 v^2 \tag{F.12}$$

one looks for

$$P_1^1(v) = \frac{c_0}{1 + \frac{c_1 v}{1 + c_2 v}} = c_0 \frac{1 + c_2 v}{1 + (c_1 + c_2) v}, \tag{F.13}$$

and given

$$S_3(v) = a_0 + a_1 v + a_2 v^2 + a_3 v^3 \tag{F.14}$$

one looks for

$$P_2^1(v) = \frac{c_0}{1 + \frac{c_1 v}{1 + \frac{c_2 v}{1 + c_3 v}}} = c_0 \frac{1 + (c_2 + c_3) v}{1 + (c_1 + c_2 + c_3) v + c_1 c_3 v^2}. \tag{F.15}$$

Using this approach one has the advantage that the lower order coefficients c_k remain unchanged as we increase the order of the polynomial we want to approximate, and that the c_k's are algorithmically obtainable from the coeffients a_j of the Taylor-series expansion with $j \leq k$.

As we said before, Padé approximants are excellent tools to approximate functions having pole singularities. For example, if we knew only the 2PN-accurate (i.e., $\mathcal{O}(v^4)$) approximation to the test-mass energy function, i.e.

$$e_{T_4}(\xi, \eta = 0) = -\xi(1 - \xi - 3\xi^2), \tag{F.16}$$

the corresponding Padé approximant would be uniquely defined as

$$e_{P_4}(\xi, \eta = 0) = -\xi \frac{1 - 4\xi}{1 - 3\xi}, \tag{F.17}$$

which is the exact result! This would also lead, already at this order, to a perfect location of the last stable orbit in the test mass case, since we would have

$$E'_{P_4}(v) = -\eta v \frac{1 - 6v^2}{(1 - 3v^2)^{3/2}}, \tag{F.18}$$

which has a zero for $v = v_{LSO} = 1/\sqrt{6}$. The idea is to consider η as a perturbation parameter, and use a sort of structural stability of the solution to locate the ISCO in the equal-mass case. Since the only known coefficients for the expansion of the energy function in the equal-mass case,

$$e_{T_{2n}} = -\xi \sum_{k=0}^{n} a_k \xi^k \tag{F.19}$$

are

$$a_0 = 1, \qquad a_1 = -1 - \eta/3, \qquad a_2 = -3 + 35\eta/12, \tag{F.20}$$

applying the diagonal Padé approximation as described before yields for the coefficients of the continued fraction:

$$c_0 = 1, \qquad c_1 = 1 + \frac{\eta}{3}, \qquad c_2 = -\frac{4 - 9\eta/4 + \eta^2/9}{1 + \eta/3}, \tag{F.21}$$

so that the best available Padé approximant is

$$e_{P_4}(x, \eta) = -\xi \frac{1 + \eta/3 - (4 - 9\eta/4 + \eta^2/9)\,\xi}{1 + \eta/3 - (3 - 35\eta/12)\,\xi}. \tag{F.22}$$

Now, from formula (F.7) it follows that the last stable circular orbit necessarily corresponds to a minimum of the function $e(x)$, while the last unstable circular orbit (or *light ring*) corresponds to a square-root singularity $\sim (x - x_{pole})^{-1/2}$ in $E(x)$, corresponding to a simple pole $\sim (x - x_{pole})^{-1}$ in $e(x)$. These considerations and formula (F.22) predict for the light ring

$$x_{LR}(\eta) = x_{pole}(\eta) = \frac{1}{3} \frac{1 + \eta/3}{1 - 35\eta/36}, \tag{F.23}$$

while for the last stable circular orbit we have

$$x_{LSO}(\eta) = \frac{1}{6} \frac{1 + \eta/3}{1 - 35\eta/36} \left[2 - \frac{1 + \eta/3}{\sqrt{1 - 9\eta/16 + \eta^2/36}} \right]. \tag{F.24}$$

In the equal-mass case, $\eta = 1/4$, this prediction yields

$$\nu_{GW}^{LSO} = 5719.4 \times (M_\odot/M_{tot}) \text{ Hz}. \tag{F.25}$$

For two neutron stars of mass equal to $1.4M_\odot$ the corresponding frequency is 2042.6 Hz, while for two 10-solar mass black holes it is of 286.0 Hz.

Of course, the main ingredient we need for the computation of the number of cycles and of the signal-to-noise reduction is not the energy function, but the flux function.

In the point-mass case, the flux function can be written as

$$\dot{E}(v, \eta = 0) = \frac{32}{5}\eta^2 v^{10}\left[\sum_{k=0}^{11} A_k v^k + \ln v \sum_{k=6}^{11} B_k v^k\right], \tag{F.26}$$

where the coefficients A_k and B_k can be read off from equation (4.55). In the equal-mass case, instead, only the firsty five coefficients are known,

$$\dot{E}(v, \eta) = \frac{32}{5}\eta^2 v^{10}\left[\sum_{k=0}^{5} A_k(\eta) v^k\right], \tag{F.27}$$

(no logarithmic corrections appear!) and they are given by

$$\begin{aligned} &A_0(\eta) = 1, \qquad A_1(\eta) = 0, \qquad A_2(\eta) = -\frac{1247}{336} - \frac{35\eta}{12}, \qquad A_3(\eta) = 4\pi, \\ &A_4(\eta) = -\left(\frac{44711}{9072} + \frac{9271\eta}{504} + \frac{65\eta^2}{18}\right), \qquad A_5(\eta) = -\left(\frac{8191}{672} + \frac{535\eta}{24}\right)\pi. \end{aligned} \tag{F.28}$$

In both cases, we the flux function can be reduced to a form allowing the application of the Padé procedure by the following steps:

- We introduce a "factored" flux function

  $$\dot{e}(v, \eta) = (1 - v/v_{pole}(\eta))\, \dot{E}(v, \eta), \tag{F.29}$$

  where, of course, $v_{pole}(\eta) = \sqrt{x_{pole}(\eta)}$. This operation "regularizes" the Taylor-series expansion introducing a linear term in v which is otherwise absent, both in the equal-mass and in the test-mass case, since $A_1(\eta) = 0$.

  In particular, notice that the pole velocity for the v^4 Padé approximant, in the equal mass case, is:

  $$v_{pole}^{P_4}(\eta) = \frac{1}{\sqrt{3}}\sqrt{\frac{1 + \eta/3}{1 - 35\eta/36}}, \tag{F.30}$$

  while in the test-mass case, since the v^4-accurate Padé approximant yields the correct result, all subsequent orders predict (correctly) $v_{pole}(\eta = 0) = 1/\sqrt{6}$.

- We factorize the logarithms by writing the new function as

  $$\dot{e}(v, \eta) = \frac{32}{5}\eta^2 v^{10}\left[1 + \ln\frac{v}{v_{LSO}(\eta)}\left(\sum_k \ell_k v^k\right)\right] \times \left[\sum_k f_k v^k\right]. \tag{F.31}$$

- We apply the Padé procedure:

$$\dot{e}_{P_n}(v,\eta) = \frac{32}{5}\eta^2 v^{10}\left[1+\ln\frac{v}{v_{LSO}(\eta)}\left(\sum_k \ell_k v^k\right)\right]\times P^m_{m+\epsilon}\left[\sum_k f_k v^k\right], \quad \text{(F.32)}$$

  where $\epsilon = 0$ when n is even, or $\epsilon = 1$ when n is odd.

- From the new function we go back to the old one, identifying the pole velocity $v^{P_n}_{pole}(\eta)$ defined by the v^n approximant of $e(x)$ and computing

$$\dot{E}_{P_n}(v,\eta) = \left(1-\frac{v}{v^{P_n}_{pole}(\eta)}\right)^{-1}\dot{e}_{P_n}(v,\eta). \quad \text{(F.33)}$$

In practice, the coefficients ℓ_k appearing in the definition (F.31) are related to the original coefficients by

$$\begin{aligned}&\ell_6 = B_6, \qquad \ell_7 = 0, \qquad \ell_8 = B_8 - A_2 B_6, \qquad \ell_9 = B_9 - A_3 B_6 \\ &\ell_{10} = B_{10} - A_2\ell_8 - A_4 B_6, \qquad \ell_{11} = B_{11} - A_2\ell_9 - A_3\ell_8 - A_5 B_6,\end{aligned} \quad \text{(F.34)}$$

and the f_k's are given numerically by

$$\begin{aligned}&f_0 = 1, \qquad f_1 = -1.732, \qquad f_2 = -3.711, \qquad f_3 = 18.99, \qquad f_4 = -26.69, \\ &f_5 = -29.76, \qquad f_6 = 196.66, \qquad f_7 = -327.26, \qquad f_8 = 11.06, \\ &f_9 = 1188.05, \qquad f_{10} = -2884.90, \qquad f_{11} = 2823.36.\end{aligned} \quad \text{(F.35)}$$

We have computed explicitly, both in the point-mass case and in the equal-mass case, the coefficients appearing in the continued-fraction form of the Padé expansion in equation (F.32).

Looking for the diagonal or subdiagonal Padé approximants in the point-mass case we find:

$$\begin{aligned}&c_0 = 1, \qquad c_1 = 1.732, \qquad c_2 = -3.875, \qquad c_3 = 4.015, \qquad c_4 = 0.629, \\ &c_5 = 0.590, \qquad c_6 = -0.345, \qquad c_7 = 5.560, \qquad c_8 = 2.035, \\ &c_9 = -31.576, \qquad c_{10} = 22.653, \qquad c_{11} = -0.101.\end{aligned}$$

Notice however that the Padé expansions at order v^7 and v^{10} show poles in the velocity region of interest for a binary coalescence. In principle, one can bypass this problem by using superdiagonal Padé approximants instead of subdiagonal ones, but we shall simply avoid using these irregular approximants.

In the equal-mass case, on the other hand, the series appearing in the flux function reads

$$\begin{aligned}\sum_{k=0}^{5} f_k v^k \;&=\; 1 - \frac{1}{v_{pole}}v + \left(-\frac{1247}{336} - \frac{35\eta}{12}\right)v^2 + \left(\frac{67338 + 52920\eta + 72576\pi v_{pole}}{18144 v_{pole}}\right)v^3 - \\ &- \left(\frac{72576\pi + (89422 - 333756\eta - 65520\eta^2)v_{pole}}{18144 v_{pole}}\right)v^4\end{aligned}$$

and the coefficients of the continued-fraction expansion are:

$$
\begin{aligned}
& c_0 = 1 \\
& c_1 = \frac{1}{v_{pole}} \\
& c_2 = -\frac{1}{336 v_{pole}}(336 + 1247 v_{pole}^2 + 980 \eta v_{pole}^2) \\
& c_3 = \frac{v_{pole}}{336}(418992 + 329280\eta + 1555009 v_{pole}^2 + 2444120 \eta v_{pole}^2 + 960400 \eta^2 v_{pole}^2 + \\
+ \quad & 451584 \pi v_{pole}) \times (336 + 1247 v_{pole}^2 + 980 \eta v_{pole}^2)^{-1} \\
& c_4 = \frac{1}{9}(1365590016\pi + 1111065984 v_{pole}\eta + 1671425280 v_{pole}\eta^2 + 6384911568 v_{pole} + \\
+ \quad & 3982970880 \pi v_{pole}^2 \eta + 22746168508 v_{pole}^3 \eta + 5068127232 \pi v_{pole}^2 + 9443785680 v_{pole}^3 \eta^2 - \\
- \quad & 5462360064 v_{pole}^3 \pi^2 + 4874990400 v_{pole}^3 \eta^3 + 23696383111 v_{pole}^3) \times \\
\times \quad & (336 + 1247 v_{pole}^2 + 980 \eta v_{pole}^2)^{-1} \times \\
\times \quad & (418992 + 329280\eta + 1555009 v_{pole}^2 + 2444120 \eta v_{pole}^2 + 960400 \eta^2 v_{pole}^2 + 451584 \pi v_{pole})^{-1}.
\end{aligned}
$$

In practice, to sum the continued fraction we use the algorithm developed by Teichroew and Gautschi [37]; given a continued fraction of the form

$$
\frac{a_1}{b_1 +}\frac{a_2}{b_2 +}\frac{a_3}{b_3 + \ldots} = \frac{a_1}{b_1 + \frac{a_2}{b_2 + \ldots}} \tag{F.36}
$$

with k terms, that we write as

$$
w_k = \frac{a_1}{b_1 +}\frac{a_2}{b_2 + \ldots}\frac{a_k}{b_k},
$$

its value can be obtained from the recursion relations (p=1,2,3...):

$$
u_{p+1} = \frac{1}{1 + \frac{a_{p+1}}{b_p b_{p+1}} u_p} \tag{F.37}
$$

$$
v_{p+1} = v_p(u_{p+1} - 1) \tag{F.38}
$$

$$
w_{p+1} = w_p + v_{p+1}, \tag{F.39}
$$

where the initial data to start the iteration are:

$$
u_1 = 1 \tag{F.40}
$$

$$
v_1 = w_1 = \frac{a_1}{b_1}. \tag{F.41}
$$

Appendix G

Spin-weighted spherical harmonics

This Appendix explains in detail how to compute the spin-weighted spherical harmonics ${}_sS^{lm}(\vartheta,\varphi)$. We shall follow the definition by Goldberg *et al.* [38]. The spin-weighted spherical harmonics are related to ordinary spherical harmonics $Y_{lm}(\vartheta,\varphi)$ by the relation:

$$\begin{aligned} {}_sS_{lm}(\vartheta,\varphi) &= (-)^s\sqrt{\frac{(l-s)!}{(l+s)!}}\,{}_{s+1}\bar{\partial}\,{}_{s+2}\bar{\partial}\ldots\,{}_0\bar{\partial}Y_{lm}(\vartheta,\varphi)\,, \qquad 0\le s\le l \\ {}_sS_{lm}(\vartheta,\varphi) &= \sqrt{\frac{(l+s)!}{(l-s)!}}\,{}_{s-1}\partial\,{}_{s-2}\partial\ldots\,{}_0\partial Y_{lm}(\vartheta,\varphi)\,, \qquad -l\le s\le 0 \end{aligned} \tag{G.1}$$

where the operators ${}_s\partial$ ed ${}_s\bar{\partial}$, acting on quantities η_s of spin-weight s, are defined as:

$$\begin{aligned} {}_s\partial\eta_s &= -(\sin\vartheta)^s\left[\frac{\partial}{\partial\vartheta}+\frac{i}{\sin\vartheta}\frac{\partial}{\partial\varphi}\right](\sin\vartheta)^{-s}\eta_s = -\left(\frac{\partial}{\partial\vartheta}+\frac{i}{\sin\vartheta}\frac{\partial}{\partial\varphi}-s\cot\vartheta\right)\eta_s = \\ &= -\left(\frac{\partial}{\partial\vartheta}-\frac{m}{\sin\vartheta}-s\cot\vartheta\right)\eta_s \\ {}_s\bar{\partial}\eta_s &= -(\sin\vartheta)^{-s}\left[\frac{\partial}{\partial\vartheta}-\frac{i}{\sin\vartheta}\frac{\partial}{\partial\varphi}\right](\sin\vartheta)^{s}\eta_s = -\left(\frac{\partial}{\partial\vartheta}-\frac{i}{\sin\vartheta}\frac{\partial}{\partial\varphi}+s\cot\vartheta\right)\eta_s \\ &= -\left(\frac{\partial}{\partial\vartheta}+\frac{m}{\sin\vartheta}+s\cot\vartheta\right)\eta_s \end{aligned}$$

From these definitions we have:

$$\begin{aligned} {}_{-2}S_{lm} &= \sqrt{\frac{(l-2)!}{(l+2)!}}\,{}_{-1}\bar{\partial}\,{}_0\bar{\partial}Y_{lm} \\ &= \sqrt{\frac{(l-2)!}{(l+2)!}}\left[Y_{lm,\vartheta\vartheta}-\cot\vartheta Y_{lm,\vartheta}+\frac{m^2}{\sin^2\vartheta}Y_{lm}+\frac{2m}{\sin\vartheta}\left(Y_{lm,\vartheta}-\cot\vartheta Y_{lm}\right)\right] \\ &= \sqrt{\frac{(l-2)!}{(l+2)!}}\sin^2\vartheta\left(\frac{1}{\sin\vartheta}\frac{\partial}{\partial\vartheta}+\frac{m}{\sin^2\vartheta}\right)\left(\frac{1}{\sin\vartheta}\frac{\partial}{\partial\vartheta}+\frac{m}{\sin^2\vartheta}\right)Y_{lm} \\ {}_{-1}S_{lm} &= (-1)\times\sqrt{\frac{(l-1)!}{(l+1)!}}\,{}_0\bar{\partial}Y_{lm} = \sqrt{\frac{(l-1)!}{(l+1)!}}\left[Y_{lm,\vartheta}+\frac{m}{\sin\vartheta}Y_{lm}\right] \end{aligned}$$

$$
\begin{aligned}
{}_0S_{lm} &= Y_{lm} \qquad\qquad (G.2)\\
{}_1S_{lm} &= \sqrt{\frac{(l-1)!}{(l+1)!}}\,{}_0\partial Y_{lm} = -\sqrt{\frac{(l-1)!}{(l+1)!}}\left[Y_{lm,\vartheta} - \frac{m}{\sin\vartheta}Y_{lm}\right]\\
{}_2S_{lm} &= \sqrt{\frac{(l-2)!}{(l+2)!}}\,{}_1\partial\,{}_0\partial Y_{lm}\\
&= \sqrt{\frac{(l-2)!}{(l+2)!}}\left[Y_{lm,\vartheta\vartheta} - \cot\vartheta Y_{lm,\vartheta} + \frac{m^2}{\sin^2\vartheta}Y_{lm} - \frac{2m}{\sin\vartheta}\left(Y_{lm,\vartheta} - \cot\vartheta Y_{lm}\right)\right]\\
&= \sqrt{\frac{(l-2)!}{(l+2)!}}\sin^2\vartheta\left(\frac{1}{\sin\vartheta}\frac{\partial}{\partial\vartheta} - \frac{m}{\sin^2\vartheta}\right)\left(\frac{1}{\sin\vartheta}\frac{\partial}{\partial\vartheta} - \frac{m}{\sin^2\vartheta}\right)Y_{lm}
\end{aligned}
$$

where the spherical harmonics for $m \geq 0$ can be obtained from the Legendre polynomials $P_l(x)$ through:

$$
Y_{lm}(\vartheta,\varphi) = \sqrt{\frac{2l+1}{4\pi}\frac{(l-m)!}{(l+m)!}}\,(\sin\vartheta)^m\left[\frac{1}{\sin\vartheta}\frac{\partial}{\partial\vartheta}\right]^m P_l(\cos\vartheta)e^{im\varphi}, \qquad (G.3)
$$

while those with $m < 0$ can be obtained from the harmonics with $m \geq 0$ using the relation

$$
Y_{l-m}(\vartheta,\varphi) = (-1)^m Y^\star_{lm}(\vartheta,\varphi). \qquad (G.4)
$$

The following **Maple** code computes the spin-weighted harmonics through these relations, and at the end it prints the values of the harmonics for ($\vartheta = \pi/2$, $\varphi = 0$):

```
restart:
with(orthopoly):
Digits:=20:
#
# Compute the spherical harmonics Y_{lm}(\theta,\phi), which
# are also spin-weighted harmonics of spin 0.
# Since Y_{lm}(\theta,\phi)=Y_{lm}(\theta,0)e^{im\phi}),
# the code computes only Y_{lm}(\theta,0),
# using different names in the cases m>=0 and m<0.
# If m>=0, call Y(l,m,theta)=Y_{lm}(\theta,0).
# If m<0, call Yb(l,m,theta)=Y_{lm}(\theta,0).
#
dz:=x->1/sin(theta)*diff(x,theta):
Y:=(l,m,theta)->sqrt((2*l+1)/(4*Pi)*(l-m)!/(l+m)!)*
sin(theta)^m*(dz@@m)(P(l,cos(theta))):
Yb:=(l,m,theta)->(-1)^m*Y(l,-m,theta):
#
# Compute the spin-weighted harmonics of spin s=-2,
# _{-2}S_{lm}(\theta,\phi).
# Even in this case, since
# _{-2}S_{lm}(\theta,\phi)=_{-2}S_{lm}(\theta,0)e^{im\phi},
# compute only _{-2}_S_{lm}(\theta,0),
# using different names in the cases m>=0 and m<0.
# If m>=0, call S2(l,m,theta)=_{-2}S_{lm}(\theta,\0).
```

```
# If m<0, call Sb2(l,-m,theta)=_{-2}S_{lm}(\theta,0).
#
dzz:=(m,x)->dz(x)+m/sin(theta)^2*x:
S2:=(l,m,theta)->sqrt((l-2)!/(l+2)!)*
sin(theta)^2*dzz(m,dzz(m,Y(l,m,theta))):
Sb2:=(l,m,theta)->sqrt((l-2)!/(l+2)!)*
sin(theta)^2*dzz(m,dzz(m,Yb(l,m,theta))):
#
# Compute the spin-weighted harmonics of spin s=-1,
# _{-1}S_{lm}(\theta,\phi), calling them S1 and Sb1
#
S1:=(l,m,theta)->sqrt((l-1)!/(l+1)!)*
(-diff(Y(l,m,theta),theta)-m*Y(l,m,theta)/sin(theta)):
Sb1:=(l,m,theta)->sqrt((l-1)!/(l+1)!)*
(-diff(Yb(l,m,theta),theta)-m*Yb(l,m,theta)/sin(theta)):
#
# Compute all the spin-weighted harmonics required in the source term
# and put them in an array.
#
fd:=fopen("c:/orbitechiuse/armonichespinMaple",WRITE);
for l from 2 to 4 do for m from -l to -1 do
fprintf(fd,"%d %d %d %16.10g\n",l,m,-2,
evalf(subs(theta=Pi/2,Sb2(l,m,theta))))
od od:
for l from 2 to 4 do for m from 0 to l do
fprintf(fd,"%d %d %d %16.10g\n",l,m,-2,
evalf(subs(theta=Pi/2,S2(l,m,theta))))
od od:
for l from 2 to 4 do for m from -l to -1 do
fprintf(fd,"%d %d %d %16.10g\n",l,m,-1,
evalf(subs(theta=Pi/2,Sb1(l,m,theta))))
od od:
for l from 2 to 4 do for m from 0 to l do
fprintf(fd,"%d %d %d %16.10g\n",l,m,-1,
evalf(subs(theta=Pi/2,S1(l,m,theta))))
od od:
for l from 2 to 4 do for m from -l to -1 do
fprintf(fd,"%d %d %d %16.10g\n",l,m,0,
evalf(subs(theta=Pi/2,Yb(l,m,theta))))
od od:
for l from 2 to 4 do for m from 0 to l do
fprintf(fd,"%d %d %d %16.10g\n",l,m,0,
evalf(subs(theta=Pi/2,Y(l,m,theta))))
od od:
#
# Compute the spin-weighted harmonics of spin s=2,
# _{-2}S_{lm}(\theta,\phi).
# Even in this case, since
# _{-2}S_{lm}(\theta,\phi)=_{-2}S_{lm}(\theta,0)e^{im\phi},
# compute only _{-2}_S_{lm}(\theta,0),
```

```
# using different names in the cases m>=0 and m<0.
# If m>=0, call S2p(l,m,theta)=_{-2}S_{lm}(\theta,\0).
# If m<0, call Sb2p(l,-m,theta)=_{-2}S_{lm}(\theta,0).
#
dzzp:=(m,x)->dz(x)-m/sin(theta)^2*x:
S2p:=(l,m,theta)->sqrt((l-2)!/(l+2)!)*
sin(theta)^2*dzzp(m,dzzp(m,Y(l,m,theta))):
Sb2p:=(l,m,theta)->sqrt((l-2)!/(l+2)!)*
sin(theta)^2*dzzp(m,dzzp(m,Yb(l,m,theta))):
#
# Compute the spin-weighted harmonics of spin s=-1,
# _{-1}S_{lm}(\theta,\phi), calling them S1p and Sb1p
#
S1p:=(l,m,theta)->sqrt((l-1)!/(l+1)!)*
(-diff(Y(l,m,theta),theta)+m*Y(l,m,theta)/sin(theta)):
Sb1p:=(l,m,theta)->sqrt((l-1)!/(l+1)!)*
(-diff(Yb(l,m,theta),theta)+m*Yb(l,m,theta)/sin(theta)):
for l from 2 to 4 do for m from -l to -1 do
fprintf(fd,"%d %d %d %16.10g\n",l,m,1,
evalf(subs(theta=Pi/2,Sb1p(l,m,theta))))
od od:
for l from 2 to 4 do for m from 0 to l do
fprintf(fd,"%d %d %d %16.10g\n",l,m,1,
evalf(subs(theta=Pi/2,S1p(l,m,theta))))
od od:
for l from 2 to 4 do for m from -l to -1 do
fprintf(fd,"%d %d %d %16.10g\n",l,m,2,
evalf(subs(theta=Pi/2,Sb2p(l,m,theta))))
od od:
for l from 2 to 4 do for m from 0 to l do
fprintf(fd,"%d %d %d %16.10g\n",l,m,2,
evalf(subs(theta=Pi/2,S2p(l,m,theta))))
od od:
fclose(fd);
```

The analytic formula for the spin-weighted spherical harmonics generalizing the one given by Poisson is

$$
\begin{aligned}
{}_sS_{lm}(\vartheta,\varphi) &= \frac{\sqrt{2l+1}}{2\sqrt{\pi}}\sqrt{(l+m)!(l-m)!(l+s)!(l-s)!}\left(\sin\frac{\vartheta}{2}\right)^{2l} e^{im\varphi}\times \\
&\times \sum_{p=p_0}^{p_1}\frac{(-1)^{s+l+m+p}\left(\cot\frac{\vartheta}{2}\right)^{2p+s-m}}{p!(l-s-p)!(p+s-m)!(l+m-p)!},
\end{aligned}
\tag{G.5}
$$

where $p_0 = max(0, m-s)$ e $p_1 = min(l-s, l+m)$. In writing the previous relation one should remind that the spin-weighted harmonics are not defined for $|s| > l$.

To check the computation of the harmonics one could verify, for example, the property

$$
{}_sS^{\star}_{lm}(\vartheta,\varphi) = (-1)^{m+s}\ {}_{-s}S_{lm}(\vartheta,\varphi), \tag{G.6}
$$

which, since

$$
{}_sS_{lm}(\vartheta,\varphi) = {}_sS_{lm}(\vartheta,0)e^{im\varphi} \tag{G.7}
$$

where ${}_sS_{lm}(\vartheta,0)$ contains *derivatives with respect to* φ of the orsinary spherical harmonics, is equivalent to

$$ {}_sS_{l-m}(\vartheta,0) = (-1)^{m+s}\ {}_{-s}S_{lm}(\vartheta,0). \tag{G.8}$$

We have checked that Poisson's relation (G.5) yields, for $\vartheta = \pi/2$ e $\varphi = 0$, numbers which agree with those obtained from formulas (G.2).

G.1 Ordinary spherical harmonics in analytic form

To evaluate analytically the spherical harmonics and their derivatives for general ℓ and m we can use the following procedure, which is also used as a check of the results in the **Maple** program **Flm**. We specialize the analytic expression for the spin-weighted spherical harmonics,

$$\begin{aligned} {}_sS_{lm}(\vartheta,\varphi) &= \frac{\sqrt{2l+1}}{2\sqrt{\pi}}\sqrt{(l+m)!(l-m)!(l+s)!(l-s)!}\left(\sin\frac{\vartheta}{2}\right)^{2l} e^{im\varphi}\times \\ &\times \sum_{p=p_0}^{p_1}\frac{(-1)^{s+l+m+p}\left(\cot\frac{\vartheta}{2}\right)^{2p+s-m}}{p!(l-s-p)!(p+s-m)!(l+m-p)!} \end{aligned} \tag{G.9}$$

where $p_0 = max(0, m-s)$ e $p_1 = min(l-s, l+m)$, to the case $s=0$ (corresponding to the ordinary spherical harmonics):

$$\begin{aligned} Y_{lm}(\vartheta,\varphi) &= \frac{\sqrt{2l+1}}{2\sqrt{\pi}}\sqrt{(l+m)!(l-m)!}\,l!\left(\sin\frac{\vartheta}{2}\right)^{2l} e^{im\varphi}\times \\ &\times \sum_{p=p_0}^{p_1}\frac{(-1)^{l+m+p}\left(\cot\frac{\vartheta}{2}\right)^{2p-m}}{p!(l-p)!(p-m)!(l+m-p)!} \end{aligned} \tag{G.10}$$

where $p_0 = max(0, m)$ e $p_1 = min(l, l+m)$. Then we differentiate this formula to get:

$$Y_{lm,\vartheta} = c_1^{lm}\sigma^{2l}e^{im\varphi}\left\{\sum_{p=p_0}^{p_1} c_2^{plm}\chi^{2p-m+1} - \frac{1}{\sigma^2}\sum_{p=p_0}^{p_1} c_2^{plm}(2p-m)\chi^{2p-m-1}\right\} \tag{G.11}$$

where

$$c_1^{lm} \equiv \frac{\sqrt{2l+1}}{2\sqrt{\pi}}\sqrt{(l+m)!(l-m)!}\,l!, \qquad c_2^{plm} \equiv \frac{(-1)^{l+m+p}}{p!(l-p)!(p-m)!(l+m-p)!}.$$

$$\sigma \equiv \sin(\vartheta/2), \qquad \chi \equiv \cot(\vartheta/2)$$

If we now decompose the spherical harmonics in a (real) $\vartheta-$dependent part times a (complex) $\varphi-$dependent part as follows

$$Y_{lm}(\vartheta,\varphi) = \Theta_{lm}(\vartheta)e^{im\varphi} \tag{G.12}$$

we can get the second $\vartheta-$derivative of $\Theta_{lm}(\vartheta) \equiv P_{lm}(\cos\vartheta)$ using the Legendre equation:

$$\Theta_{lm,\vartheta\vartheta} = -\cot\vartheta\,\Theta_{lm,\vartheta} + \left[\frac{m^2}{\sin^2\vartheta} - l(l+1)\right]\Theta_{lm} \tag{G.13}$$

Then we have:

$$X^*_{\ell m}(\vartheta,\varphi) = -2im\left[\Theta_{lm,\vartheta} - \cot\vartheta\Theta_{lm}\right]\left[\cos(m\varphi) - i\sin(m\varphi)\right] \tag{G.14}$$

$$W^*_{\ell m}(\vartheta,\varphi) = \left[\Theta_{lm,\vartheta\vartheta} - \cot\vartheta\Theta_{lm,\vartheta} + \frac{m^2}{\sin^2\vartheta}\Theta_{lm}\right]\left[\cos(m\varphi) - i\sin(m\varphi)\right] \tag{G.15}$$

Appendix H

MapleV

H.1 TetradWaveform

```
> # Given as an input the quadrupole moments matrix, project it
on the sphere. The Q_ij's are unspecified.
> restart:
> with(linalg):
> Q:=linalg[matrix](3,3,[Qxx,Qxy,0,Qxy,Qyy,0,0,0,Qzz]);
> P:=matrix(3,3,[1-sin(theta)^2*cos(phi)^2,-sin(theta)^2*sin(phi)*cos(phi),
-sin(theta)*cos(theta)*cos(phi),-sin(theta)^2*sin(phi)*cos(phi),
1-sin(theta)^2*sin(phi)^2,-sin(theta)*cos(theta)*sin(phi),
-sin(theta)*cos(theta)*cos(phi),-sin(theta)*cos(theta)*sin(phi),
sin(theta)^2]);
> PQ:=simplify(innerprod(P,Q)):
> H1:=innerprod(PQ,P):
> T:=simplify(trace(PQ)):
> H2:=-evalm(T*P)/2:
> H:=simplify(evalm(2*(H1+H2))):
> H11:=simplify(H[1,1]):
> H12:=H[1,2]:
> H13:=H[1,3]:
> H22:=H[2,2]:
> H23:=H[2,3]:
> H33:=H[3,3]:
> AT:=matrix(3,3,[sin(theta)*cos(phi),sin(theta)*sin(phi),cos(theta),
cos(theta)*cos(phi),cos(theta)*sin(phi),-sin(theta),-sin(phi),cos(phi),0]);
> A:=transpose(AT);
> QA:=simplify(innerprod(Q,A)):
> ATQA:=simplify(innerprod(AT,QA)):
> Pradial:=matrix(3,3,[0,0,0,0,1,0,0,0,1]);
> PradialQ:=simplify(innerprod(Pradial,ATQA)):
> H1:=innerprod(PradialQ,Pradial):
> T:=simplify(trace(PradialQ)):
> H2:=-evalm(T*Pradial)/2:
> H:=simplify(evalm(2*(H1+H2))):
> Hrr:=H[1,1]:
> Hrtheta:=H[1,2];
```

```
> Hrphi:=H[1,3];
> Hthetatheta:=factor(simplify(H[2,2]));
> Hthetaphi:=factor(simplify(H[2,3]));
> Hphiphi:=factor(simplify(H[3,3]));
```

H.2 Flm

```
# Given as an input the quadrupole moments matrix, project it
# on the sphere. The Q_ij's are unspecified.
> restart:
> with(linalg):
# Define K^* as the polar harmonic on which to make the projection,
# comment the others
# a_lm^(0)
> #Kstar:=linalg[matrix](4,4,[yylmstar,0,0,0,0,0,0,0,0,0,0,0,0,0,0,0]);
# a_lm
> #Kstar:=linalg[matrix](4,4,[0,0,-I/sqrt(2)*yylmstar,0,0,0,0,-I/sqrt(2)
> *yylmstar,0,0,0,0,0,0,0,0]);
# b_lm^(0)
> #Kstar:=linalg[matrix](4,4,[0,-I*nl*r*yylmphistar,0,-I*nl*r*yylmthetas
> tar,-I*nl*r*yylmphistar,0,0,0,0,0,0,0,-I*nl*r*yylmthetastar,0,0,0]);
# b_lm
> #Kstar:=linalg[matrix](4,4,[0,0,0,0,0,0,nl*r*yylmphistar,0,0,nl*r*yylm
> phistar,0,nl*r*yylmthetastar,0,0,nl*r*yylmthetastar,0]);
# g_lm
> #Kstar:=linalg[matrix](4,4,[0,0,0,0,0,r^2/sqrt(2)*sin(theta)^2*yylmsta
> r,0,0,0,0,0,0,0,0,0,0,r^2/sqrt(2)*yylmstar]);
# f_lm
> Kstar:=linalg[matrix](4,4,[0,0,0,0,0,-ml*r^2*sin(theta)^2*Wstar,0,ml*r
> ^2*Xstar,0,0,0,0,0,ml*r^2*Xstar,0,ml*r^2*Wstar]);
# Define the matrix e^{(\alpha)\mu}, where \alpha is the tetrad index
# and \mu the tensor index
> tetrad:=linalg[matrix](4,4,[1,-0,0,0,0,-1/(r*sin(theta)),0,0,0,0,-1,0,
> 0,0,0,-1/r]):
# Take the product e^{(\alpha)\mu}K^*_{\mu\nu}e^{\nu(\beta)}
> temp:=innerprod(Kstar,tetrad):
> Kstartetradup:=simplify(innerprod(tetrad,temp)):
> hplus:=((aa*cos(phi)^2+bb*sin(2*phi))*(1+cos(theta)^2)+cc*cos(theta)^2
> +dd)/r;
> hcross:=-cos(theta)*(aa*sin(2*phi)+2*bb*(1-2*cos(phi)^2))/r;
> H:=linalg[matrix](4,4,[0,0,0,0,0,-hplus,0,hcross,0,0,0,0,0,hcross,0,hp
> lus]):
> integrand:=sum(sum(Kstartetradup[i,j]*H[i,j],j=1..4),i=1..4);
# Define Xstar, Wstar and so on
> yylmstar:=ylm*(cos(m*phi)-I*sin(m*phi)):
> yylmphistar:=-I*m*ylm*(cos(m*phi)-I*sin(m*phi)):
> yylmthetastar:=ylmt*(cos(m*phi)-I*sin(m*phi)):
> Xstar:=-2*I*m*Xtheta*(cos(m*phi)-I*sin(m*phi)):
> Wstar:=Wtheta*(cos(m*phi)-I*sin(m*phi)):
```

```
#
# Project and find the components with l=2 and different m's
#
> l:=2:
> m:=2:
> ylm:=1/4*sqrt(15/(2*Pi))*sin(theta)^2;
> ylmt:=diff(ylm,theta):
> ylmtt:=-cot(theta)*ylmt+(m^2/(sin(theta))^2-l*(l+1))*ylm:
> Wtheta:=ylmtt-cot(theta)*ylmt+m^2/sin(theta)^2*ylm:
> Xtheta:=ylmt-cot(theta)*ylm:
> imag:=simplify(coeff(integrand,I));
> reale:=simplify(integrand-I*imag);
> realeth:=int(reale,phi=0..2*Pi);
> imagth:=int(imag,phi=0..2*Pi);
> K2R:=int(realeth*sin(theta),theta=0..Pi);
> K2I:=int(imagth*sin(theta),theta=0..Pi);
> l:=2:
> m:=1:
> ylm:=-sqrt(15/(8*Pi))*sin(theta)*cos(theta);
> ylmt:=diff(ylm,theta):
> ylmtt:=-cot(theta)*ylmt+(m^2/(sin(theta))^2-l*(l+1))*ylm:
> Wtheta:=ylmtt-cot(theta)*ylmt+m^2/sin(theta)^2*ylm:
> Xtheta:=ylmt-cot(theta)*ylm:
> imag:=simplify(coeff(integrand,I));
> reale:=simplify(integrand-I*imag);
> realeth:=int(reale,phi=0..2*Pi);
> imagth:=int(imag,phi=0..2*Pi);
> K1R:=int(realeth*sin(theta),theta=0..Pi);
> K1I:=int(imagth*sin(theta),theta=0..Pi);
> l:=2:
> m:=0:
> ylm:=sqrt(5/(4*Pi))*(3/2*cos(theta)^2-1/2);
> ylmt:=diff(ylm,theta):
> ylmtt:=-cot(theta)*ylmt+(m^2/(sin(theta))^2-l*(l+1))*ylm:
> Wtheta:=ylmtt-cot(theta)*ylmt+m^2/sin(theta)^2*ylm:
> Xtheta:=ylmt-cot(theta)*ylm:
> imag:=simplify(coeff(integrand,I));
> reale:=simplify(integrand-I*imag);
> realeth:=int(reale,phi=0..2*Pi);
> imagth:=int(imag,phi=0..2*Pi);
> K0R:=int(realeth*sin(theta),theta=0..Pi);
> K0I:=int(imagth*sin(theta),theta=0..Pi);
> l:=2:
> m:=-1:
> ylm:=sqrt(15/(8*Pi))*sin(theta)*cos(theta);
> ylmt:=diff(ylm,theta):
> ylmtt:=-cot(theta)*ylmt+(m^2/(sin(theta))^2-l*(l+1))*ylm:
> Wtheta:=ylmtt-cot(theta)*ylmt+m^2/sin(theta)^2*ylm:
> Xtheta:=ylmt-cot(theta)*ylm:
> imag:=simplify(coeff(integrand,I));
```

```
> reale:=simplify(integrand-I*imag);
> realeth:=int(reale,phi=0..2*Pi);
> imagth:=int(imag,phi=0..2*Pi);
> K1mR:=int(realeth*sin(theta),theta=0..Pi);
> K1mI:=int(imagth*sin(theta),theta=0..Pi);
> l:=2:
> m:=-2:
> ylm:=1/4*sqrt(15/(2*Pi))*sin(theta)^2;
> ylmt:=diff(ylm,theta):
> ylmtt:=-cot(theta)*ylmt+(m^2/(sin(theta))^2-l*(l+1))*ylm:
> Wtheta:=ylmtt-cot(theta)*ylmt+m^2/sin(theta)^2*ylm:
> Xtheta:=ylmt-cot(theta)*ylm:
> imag:=simplify(coeff(integrand,I));
> reale:=simplify(integrand-I*imag);
> realeth:=int(reale,phi=0..2*Pi);
> imagth:=int(imag,phi=0..2*Pi);
> K2mR:=int(realeth*sin(theta),theta=0..Pi);
> K2mI:=int(imagth*sin(theta),theta=0..Pi);
#
# Check the previous results using the analytic formula for the spherical
# harmonics obtained specializing that for tensor spherical harmonics.
# Before proceeding, unassign the harmonics, l and m
#
> ylm:='ylm':
> ylmt:='ylmt':
> ylmtt:='ylmtt':
> m:='m':
> l:='l':
> Wtheta:=ylmtt-cot(theta)*ylmt+m^2/sin(theta)^2*ylm:
> Xtheta:=ylmt-cot(theta)*ylm:
> yylmstar:=ylm*(cos(m*phi)-I*sin(m*phi)):
> yylmphistar:=-I*m*ylm*(cos(m*phi)-I*sin(m*phi)):
> yylmthetastar:=ylmt*(cos(m*phi)-I*sin(m*phi)):
> Xstar:=-2*I*m*Xtheta*(cos(m*phi)-I*sin(m*phi)):
> Wstar:=Wtheta*(cos(m*phi)-I*sin(m*phi)):
> integrand:
> imag:=simplify(coeff(integrand,I)):
> reale:=simplify(integrand-I*imag):
> realeth2:=simplify(int(subs(m=2,reale),phi=0..2*Pi));
> realeth1:=simplify(int(subs(m=1,reale),phi=0..2*Pi));
> realeth0:=simplify(int(subs(m=0,reale),phi=0..2*Pi));
> realeth1m:=simplify(int(subs(m=-1,reale),phi=0..2*Pi));
> realeth2m:=simplify(int(subs(m=-2,reale),phi=0..2*Pi));
> imagth2:=simplify(int(subs(m=2,imag),phi=0..2*Pi));
> imagth1:=simplify(int(subs(m=1,imag),phi=0..2*Pi));
> imagth0:=simplify(int(subs(m=0,imag),phi=0..2*Pi));
> imagth1m:=simplify(int(subs(m=-1,imag),phi=0..2*Pi));
> imagth2m:=simplify(int(subs(m=-2,imag),phi=0..2*Pi));
#
# Project and find the components with l=2 and different m's
```

```
#
> l:=2:
> m:=2:
> p0:=max(0,m):
> p1:=min(l,l+m):
> ylm:=sqrt((2*l+1)/Pi)/2*sqrt((l+m)!*(l-m)!)*l!*sin(theta/2)^(2*l)*sum(
> '(-1)^(l+m+p)*(cot(theta/2)^(2*p-m)/(p!*(l-p)!*(p-m)!*(l+m-p)!))',p=p0
> ..p1):
> ylmt:=diff(ylm,theta):
> ylmtt:=-cot(theta)*ylmt+(m^2/(sin(theta))^2-l*(l+1))*ylm:
> Wtheta:=ylmtt-cot(theta)*ylmt+m^2/sin(theta)^2*ylm:
> Xtheta:=ylmt-cot(theta)*ylm:
> K2R:=int(realeth2*sin(theta),theta=0..Pi);
> K2I:=int(imagth2*sin(theta),theta=0..Pi);
> l:=2:
> m:=1:
> p0:=max(0,m):
> p1:=min(l,l+m):
> ylm:=sqrt((2*l+1)/Pi)/2*sqrt((l+m)!*(l-m)!)*l!*sin(theta/2)^(2*l)*sum(
> '(-1)^(l+m+p)*(cot(theta/2)^(2*p-m)/(p!*(l-p)!*(p-m)!*(l+m-p)!))',p=p0
> ..p1):
> ylmt:=diff(ylm,theta):
> ylmtt:=-cot(theta)*ylmt+(m^2/(sin(theta))^2-l*(l+1))*ylm:
> Wtheta:=ylmtt-cot(theta)*ylmt+m^2/sin(theta)^2*ylm:
> Xtheta:=ylmt-cot(theta)*ylm:
> K1R:=int(realeth1m*sin(theta),theta=0..Pi);
> K1I:=int(imagth1m*sin(theta),theta=0..Pi);
> l:=2:
> m:=0:
> p0:=max(0,m):
> p1:=min(l,l+m):
> ylm:=sqrt((2*l+1)/Pi)/2*sqrt((l+m)!*(l-m)!)*l!*sin(theta/2)^(2*l)*sum(
> '(-1)^(l+m+p)*(cot(theta/2)^(2*p-m)/(p!*(l-p)!*(p-m)!*(l+m-p)!))',p=p0
> ..p1):
> ylmt:=diff(ylm,theta):
> ylmtt:=-cot(theta)*ylmt+(m^2/(sin(theta))^2-l*(l+1))*ylm:
> Wtheta:=ylmtt-cot(theta)*ylmt+m^2/sin(theta)^2*ylm:
> Xtheta:=ylmt-cot(theta)*ylm:
> K0R:=int(realeth0*sin(theta),theta=0..Pi);
> K0I:=int(imagth0*sin(theta),theta=0..Pi);
> l:=2:
> m:=-1:
> p0:=max(0,m):
> p1:=min(l,l+m):
> ylm:=sqrt((2*l+1)/Pi)/2*sqrt((l+m)!*(l-m)!)*l!*sin(theta/2)^(2*l)*sum(
> '(-1)^(l+m+p)*(cot(theta/2)^(2*p-m)/(p!*(l-p)!*(p-m)!*(l+m-p)!))',p=p0
> ..p1):
> ylmt:=diff(ylm,theta):
> ylmtt:=-cot(theta)*ylmt+(m^2/(sin(theta))^2-l*(l+1))*ylm:
> Wtheta:=ylmtt-cot(theta)*ylmt+m^2/sin(theta)^2*ylm:
```

```
> Xtheta:=ylmt-cot(theta)*ylm:
> K1mR:=int(realeth1m*sin(theta),theta=0..Pi);
> K1mI:=int(imagth1m*sin(theta),theta=0..Pi);
> l:=2:
> m:=-2:
> p0:=max(0,m):
> p1:=min(l,l+m):
> ylm:=sqrt((2*l+1)/Pi)/2*sqrt((l+m)!*(l-m)!)*l!*sin(theta/2)^(2*l)*sum(
> '(-1)^(l+m+p)*(cot(theta/2)^(2*p-m)/(p!*(l-p)!*(p-m)!*(l+m-p)!))',p=p0
> ..p1):
> ylmt:=diff(ylm,theta):
> ylmtt:=-cot(theta)*ylmt+(m^2/(sin(theta))^2-l*(l+1))*ylm:
> Wtheta:=ylmtt-cot(theta)*ylmt+m^2/sin(theta)^2*ylm:
> Xtheta:=ylmt-cot(theta)*ylm:
> K2mR:=int(realeth2m*sin(theta),theta=0..Pi);
> K2mI:=int(imagth2m*sin(theta),theta=0..Pi);
```

H.3 NewtonianQuadrupole

```
with(linalg);
%
% Build the matrix containing the reduced quadrupole moment
%
X[1]:=a*(cos(u)-e):
X[2]:=a*sqrt(1-e^2)*sin(u):
X[3]:=0:
f := (i,j) -> X[i]*X[j]:
M1:=matrix(3,3,f):
Xsq:=factor(simplify(sum('X[k]^2','k'=1..3))):
M2:=-1/3*matrix(3,3,[Xsq,0,0,0,Xsq,0,0,0,Xsq]):
Qreduced:=simplify(evalm(mu*(M1+M2)));
%
% Take the second time derivative (called ''Q'')
%
Qdot:=simplify(evalm(map(diff,Qreduced,u)*sqrt(G*M/a^3)/(1-e*cos(u)))):
Q:=simplify(evalm(map(diff,Qdot,u)*sqrt(G*M/a^3)/(1-e*cos(u)))):
%
% Take coefficients
%
Qxx:=factor(Q[1,1]);
Qxy:=factor(Q[1,2]);
Qxz:=factor(Q[1,3]);
Qyy:=factor(Q[2,2]);
Qyz:=factor(Q[2,3]);
Qzz:=factor(Q[3,3]);
%
% Take the projection and find the two independent components of h
%
AT:=matrix(3,3,[sin(theta)*cos(phi),sin(theta)*sin(phi),cos(theta),
```

```
cos(theta)*cos(phi),cos(theta)*sin(phi),-sin(theta),-sin(phi),cos(phi),0]):
A:=transpose(AT):
QA:=simplify(innerprod(Q,A)):
ATQA:=simplify(innerprod(AT,QA)):
Pradial:=matrix(3,3,[0,0,0,0,1,0,0,0,1]):
PradialQ:=simplify(innerprod(Pradial,ATQA)):
H1:=innerprod(PradialQ,Pradial):
T:=simplify(trace(PradialQ)):
H2:=-evalm(T*Pradial)/2:
H:=simplify(evalm(2*G*(H1+H2)/(c^4*r))):
Hthetatheta:=factor(simplify(H[2,2]));
Hthetaphi:=factor(simplify(H[2,3]));
%
% Verify the tensor is traceless!
%
Hphiphi:=factor(simplify(H[3,3]));
simplify(Hthetatheta+Hphiphi);
%
% Circular case: specialize to e=0
% Show explicitly that only functions of (2 omega0 t) appear
%
Hthetathetac:=factor(simplify(subs(e=0,cos(u)^2=(1+cos(2*u))/2,
sin(u)=sin(2*u)/(2*cos(u)),Hthetatheta)));
Hthetaphic:=simplify(subs(e=0,cos(u)^2=(1+cos(2*u))/2,
sin(u)=sin(2*u)/(2*cos(u)),Hthetaphi)):
Hthetathetac:=subs(u=omega0*t,Hthetathetac):
Hthetaphic:=subs(u=omega0*t,Hthetaphic):
%
% Take the Fourier component of H_{theta theta} at n=2
%
n:=2:
Htt:=simplify(omega0/(2*Pi)*int(Hthetathetac*exp(n*I*omega0*t),
t=0..(2*Pi)/omega0));
%
% Verify that the Fourier component yields the correct result
% in the time domain
%
simplify(evalc(Htt*exp(-2*I*omega0*t)+conjugate(Htt*exp(-2*I*omega0*t))
-Hthetathetac));
Htt2:=simplify(int(evalc(abs(Htt)^2*sin(theta)),theta=0..Pi)/(4*Pi)):
%
% Integrate over the solid angle
%
Htt2:=simplify(int(Htt2,phi=0..2*Pi));
%
% Do the same for H_{theta phi}
%
Htp:=simplify(omega0/(2*Pi)*int(Hthetaphic*exp(2*omega0*I*t),
t=0..(2*Pi)/omega0));
Htp2:=simplify(int(evalc(abs(Htp)^2*sin(theta)),theta=0..Pi)/(4*Pi)):
```

```
Htp2:=simplify(int(Htp2,phi=0..2*Pi));
%
% Compute flux and luminosity
%
flux:=2*c^3*(n*omega0)^2*(Htt2+Htp2)/(16*Pi*G);
lum:=simplify(flux*4*Pi*r^2);
```

H.4 RadiationGauge

```
readlib(mtaylor);
rstar(r):=r+2*M*ln(r/(2*M)-1);
nur:=M/(r*(r-2*M));
N(r):=exp(I*epsilon*sigma*rstar(r))*(N1/r+N2/r^2):
L(r):=exp(I*epsilon*sigma*rstar(r))*(L1/r+L2/r^2):
T(r):=exp(I*epsilon*sigma*rstar(r))*(T1/r+T2/r^2):
V(r):=exp(I*epsilon*sigma*rstar(r))*(V1/r+V2/r^2):
X(r):=n*V(r):
%
% Show that V1 is the amplitude of the Zerilli function at infinity
% (later we'll check that L1=-n*V1).
%
Z:=simplify(r^2/(n*r+3*M)*(3*M*X(r)/n/r-L(r))*exp(-I*epsilon*sigma*rstar(r)));
Z:=simplify(subs(r=1/rho,Z));
extrtaylor:=rho*simplify(mtaylor(Z,[rho],4));
Z1:=coeff(extrtaylor,rho);
%
% It turns out that Z1=-L1/n
%
eq1:=simplify(T(r)-V(r)+L(r)):
eq2:=simplify(diff(N(r),r)-diff(L(r),r)-(1/r-nur)*N(r)-(1/r+nur)*L(r)):
eq3:=simplify(diff(L(r),r)+(2/r-nur)*L(r)+(1/r-nur)*X(r)+diff(X(r),r)):
eq4:=simplify(2*diff(N(r),r)/r-2*(n+1)*N(r)/(r*(r-2*M))
-2*(1/r+2*nur)*L(r)/r-2*(1/r+nur)*(diff(L(r),r)+n*diff(V(r),r))-2*n*(V(r)
-L(r))/(r*(r-2*M))-2*sigma^2*(L(r)+n*V(r))/(1-2*M/r)^2):
eq2:=simplify(subs(r=1/rho,eq6*exp(-I*epsilon*sigma*rstar(r)))):
extrtaylor:=simplify(mtaylor(eq6,[rho],3));
e2_1:=coeff(extrtaylor,rho):
eq3:=simplify(subs(r=1/rho,eq7*exp(-I*epsilon*sigma*rstar(r)))):
extrtaylor:=simplify(mtaylor(eq7,[rho],3));
e3_1:=coeff(extrtaylor,rho):
eq4:=simplify(subs(r=1/rho,eq8*exp(-I*epsilon*sigma*rstar(r)))):
extrtaylor:=simplify(mtaylor(eq8,[rho],3));
e4_1:=coeff(extrtaylor,rho):
eq1:=simplify(subs(r=1/rho,eq4*exp(-I*epsilon*sigma*rstar(r)))):
extrtaylor:=simplify(mtaylor(eq4,[rho],3));
e1_1:=coeff(extrtaylor,rho):
solve({e1_1,e2_1,e3_1,e4_1},{N1,V1,L1,T1});
%
% The result is:
```

```
%   {T1 = V1 + n V1, L1 = -n V1, V1 = V1, N1 = -n V1}
%
```

H.5 SemiRelativisticSpectrum

```
restart:
#
# Define the factors H^+_j, H^-_j and H^0_j
# for h_{\theta\theta}
#
Hjp_thth:=(Iap+Ibp)*(cos(2*phi)+I*sin(2*phi))*(1+cos(theta)^2);
Hjm_thth:=(Iam-Ibm)*(cos(2*phi)-I*sin(2*phi))*(1+cos(theta)^2);
Hj0_thth:=3*K*(cos(theta)^2-1);
#
# Define the factors H^+_j and H^-_j
# for h_{\theta\phi}
#
Hjp_thph:=(Iap+Ibp)*2*cos(theta)*(sin(2*phi)-I*cos(2*phi));
Hjm_thph:=(Iam-Ibm)*2*cos(theta)*(sin(2*phi)+I*cos(2*phi));
#
# Evaluate the two square moduli and integrate over the solid angle
#
hththmodulus:=simplify(evalc(omp*Hjp_thth*conjugate(omp*Hjp_thth)
+omm*Hjm_thth*conjugate(omm*Hjm_thth)
+om0*Hj0_thth*conjugate(om0*Hj0_thth))):
hthth1:=int(emodulus*sin(theta),theta=0..Pi):
hthth2:=int(e1,phi=0..2*Pi);
hthphmodulus:=simplify(evalc(omp*Hjp_thph*conjugate(omp*Hjp_thph)
+omm*Hjm_thph*conjugate(omm*Hjm_thph))):
hthph1:=int(fmodulus*sin(theta),theta=0..Pi):
hthph2:=int(f1,phi=0..2*Pi);
#
# Sum over polarizations
#
final:=factor(simplify(hthth2+hthph2));
```

H.6 ABC

```
> restart;
> Omega0:=sqrt(AMASSA/r0^3):
Qui uso la convenzione G_\mu\nu=2T_\mu\nu, e nel programma moltiplico la
sorgente per 4\pi.
Definisco B0 e F (trasformate di Fourier!) ponendo m0=1 e non mettendo
la delta di omega.
> B0:=-I*sqrt(2)/sqrt(l*(l+1))*I*m*Omega0/sqrt(1-3*AMASSA/r0)*
(1-2*AMASSA/r)/r*Pl*delta(r):
> F:=(l*(l+1)-2*m^2)/sqrt(2*l*(l+1)*(l-1)*(l+2))*(AMASSA/(r0^3*
sqrt(1-3*AMASSA/r0)))*Pl*delta(r):
```

```
Definisco i fattori davanti a B0, B0', B0'' ed F nella sorgente
in gauge di Chandrasekhar-Ferrari.
> B0fact:=sqrt(2)*((r-2*AMASSA)*(n^2*r^2-12*AMASSA*r-3*AMASSA*n*r
+12*AMASSA^2)/r/(n*r+3*AMASSA)^2-r^3*(m*sqrt(AMASSA/r0^3))^2
/(n*r+3*AMASSA))/(m*sqrt(AMASSA/r0^3))/sqrt(l*(l+1)):
> B0rfact:=-(r-2*AMASSA)*(3*n*r^2+15*AMASSA*r-4*AMASSA*n*r-24*AMASSA^2)
/(n*r+3*AMASSA)^2*sqrt(2)/sqrt(l*(l+1))/m/sqrt(AMASSA/r0^3):
> B0rrfact:=-r*(r-2*AMASSA)^2*sqrt(2)/(n*r+3*AMASSA)/sqrt(l*(l+1))/m
/sqrt(AMASSA/r0^3):
> Ffact:=-2*sqrt(2)*(r-2*AMASSA)/sqrt(l*(l-1)*(l+1)*(l+2)):
Calcolo la sorgente
> n:=(l-1)*(l+2)/2:
> Ftot:=simplify(Ffact*F):
> B0tot:=simplify((B0fact*B0)):
> B0r:=simplify(diff(B0,r)):
> B0rtot:=simplify((B0rfact*B0r)):
> B0rr:=simplify(diff(B0r,r)):
> B0rrtot:=simplify((B0rrfact*B0rr)):
> B0pB0r:=simplify(B0tot+B0rtot+B0rrtot):
> B0pB0r:=subs(diff(delta(r),r)=deltar(r),B0pB0r):
> B0pB0r:=subs(diff(deltar(r),r)=deltarr,B0pB0r):
> sourceMia:=simplify(subs(deltar(r)=deltar,expand(B0pB0r+Ftot))):
> sourceMia:=simplify(subs(delta(r)=delta,sourceMia)):
Prendo i coefficienti della delta, della delta' e della delta''...
> C:=simplify(coeff(sourceMia,deltarr)):
> B:=simplify(coeff(sourceMia,deltar)):
> A:=factor(simplify(coeff(sourceMia,delta))):
...e li divido per (1-2M/r), poi calcolo le derivate.
> Astar:=simplify(A*r/(r-2*AMASSA)):
> Bstar:=B*r/(r-2*AMASSA):
> Bstarprime:=simplify(diff(Bstar,r)):
> Cstar:=simplify(C*r/(r-2*AMASSA)):
> Cstarprime:=simplify(diff(Cstar,r)):
> Cstarprimeprime:=simplify(diff(Cstarprime,r)):
Calcolo tutto in r0=r (raggio dell'orbita).
> r0:=r:
> Astar:=simplify(Astar);
> Bstar:=simplify(Bstar);
> Cstar:=simplify(Cstar);
> Bstarprime:=simplify(Bstarprime);
> Cstarprime:=simplify(Cstarprime);
> Cstarprimeprime:=simplify(Cstarprimeprime);
```

H.7 AsymptoticPolar

```
#
# Define the potential and write down the equation
#
V(r):=(2*n^2*(n+1)*r^3+6*n^2*M*r^2+18*n*M^2*r+18*M^3)
```

```
*(1-2*M/r)/(r^3*(n*r+3*M)^2);
rstar(r):=r+2*M*ln(r/(2*M)-1);
simplify(diff(rstar(r),r));
dZdrs:=(1-2*M/r)*diff(Z(r),r);
ddZdrs2:=(1-2*M/r)*diff(dZdrs,r);
eq:=ddZdrs2+(omega^2-V(r))*Z(r):
Z(r):=exp(-I*omega*rstar(r))*(1+a/r+b/r^2);
eq:=simplify(eq);
#
# We expand in rho=1/r !
#
eq:=simplify(subs(r=1/rho,eq));
#
# From ‘‘eq’’ we extract the coefficient multiplying the exponential:
#
extr:=-2*I*(12*I*a*M^2*n^2*rho^3-9*I*M^3*rho^3-omega*a*n^2+18*I*M^4*rho^4
-I*n^2-I*n^3+4*omega*M*b*n^2*rho^2+2*omega*M*a*n^2*rho+12*omega*M^2
*a*n*rho^2-12*omega*b*n*M*rho^2-6*omega*a*n*M*rho+24*omega*M^2*b*n*rho^3
-18*omega*b*M^2*rho^3+18*omega*M^3*a*rho^3-2*omega*b*n^2*rho-9*omega
*a*M^2*rho^2+36*omega*M^3*b*rho^4+2*I*b*n^2*rho^2+27*I*b*M^2*rho^4-54*
I*a*M^3*rho^4-9*I*M^2*n*rho^2+72*I*a*M^4*rho^5-135*I*b*M^3*rho^5+9*I*a
*M^2*rho^3+18*I*n*M^3*rho^3+2*I*n^3*M*rho+6*I*n^2*M^2*rho^2-I*n^3*a*rho
-I*M*n^2*rho-I*n^3*b*rho^2+162*I*b*M^4*rho^6+22*I*b*M^2*n^2*rho^4-6*I
*a*M*n^2*rho^2-39*I*a*M^2*n*rho^3+2*I*n^3*M*a*rho^2+2*I*n^3*M*b*rho^3
-15*I*b*M*n^2*rho^3-93*I*b*M^2*n*rho^4+54*I*a*M^3*n*rho^4+114*I*b*M^3*n
*rho^5+6*I*a*n*M*rho^2+18*I*b*n*M*rho^3)*rho^2/((n+3*M*rho)^2);
#
# Expand and take coefficients
#
readlib(mtaylor);
extrtaylor:=mtaylor(extr,[rho],4);
coeff(extrtaylor,rho^2);
a:=solve(%,a);
coeff(extrtaylor,rho^3);
b:=solve(%,b);
```

Bibliography

[1] M. E. Alexander, *Tidal resonances in binary star systems*, *MNRAS* **227**, 843 (1987).

[2] N. Andersson, K. D. Kokkotas, *Towards gravitational-wave asteroseismology*, *MNRAS* **299**, 1059 (1998).

[3] T. Apostolatos, D. Kennefick, A. Ori, E. Poisson, *Gravitational radiation from a particle in circular orbit around a black hole. III. Stability of circular orbits under radiation reaction*, *Phys. Rev. D* **47**, 12, 5376 (1993).

[4] J.M.Bardeen, W.H.Press, *Radiation fields in the Schwarzschild background*, *J. Math. Phys.* **14**, 7 (1973).

[5] T. W. Baumgarte, *The innermost stable circular orbit in compact binaries*, **gr-qc/0101045** (2001).

[6] T. W. Baumgarte, G. B. Cook, M. A. Scheel, S. L. Shapiro, S. A. Teukolsky, *Binary neutron stars in general relativity: quasiequilibrium models*, *Phys. Rev. Lett.* **79**, 7, 1182 (1997).

[7] O. Benhar, E. Berti, V. Ferrari, *The imprint of the equation of state on the axial w-modes of oscillating neutron stars*, *MNRAS* **310**, 797 (1999).

[8] E. Berti, *Studio delle frequenze di emissione gravitazionale da stelle di neutroni in relazione all'equazione di stato*, Laurea thesis, available as a postscript file at the URL `http://www.roma1.infn.it/~eberti/`.

[9] E. Berti, V. Ferrari, *Excitation of g-modes of solar type stars by an orbiting companion*, *Phys. Rev. D* **63**, 064031 (2001).

[10] L. Bildsten, C. Cutler, *Tidal interactions of inspiraling compact binaries*, *Ap. J.* **400**, 175 (1992).

[11] A. Buonanno, T. Damour, *Effective one-body approach to general relativistic two-body dynamics*, *Phys. Rev. D* **59**, 084006 (1999).

[12] A. Burrows, J. Liebert, *The science of brown dwarfs*, Rev. Mod. Phys. **65**, 301 (1993).

[13] J. W. Chamberlain, D. M. Hunten, *Theory of planetary atmospheres*, 2nd ed., Academic Press, Orlando (1987).

[14] S. Chandrasekhar, *The mathematical theory of black holes*, Clarendon Press, Oxford (1983).

[15] S. Chandrasekhar, S. L. Detweiler, *The quasi-normal modes of the Schwarzschild black-hole, Proc. R. Soc. London A* **344**, 441 (1975).

[16] S. Chandrasekhar, V. Ferrari, *The flux integral for axisymmetric perturbations of static space-times*, *Proc. R. Soc. London A* **428**, 325 (1990).

[17] S. Chandrasekhar, V. Ferrari, *On the non-radial oscillations of a star*, *Proc. R. Soc. London A* **432**, 247 (1991).

[18] J. Christensen-Dalsgaard, D. O. Gough, J. G. Morgan, *Dirty Solar Models*, *Astron. Astrophys.* **73**, 121-128 (1979).

[19] J. Christensen-Dalsgaard *et al.*, *The current state of solar modeling*, *Science* **272**, 1286 (1996).

[20] J. Christensen-Dalsgaard, private communication.

[21] J. P. A. Clark, D. M. Eardley, *Evolution of close neutron star binaries*, *Ap. J.* **215**, 311 (1977).

[22] G. H. A. Cole, *Physics of Planetary Interiors*, Adam Hilger (1984).

[23] T. G. Cowling, *The non-radial oscillations of polytropic stars*, *Mon. Not. R. Astr. Society* **101**, 367 (1941).

[24] K. P. Cox, *Theory of stellar pulsations*, Princeton University Press, Princeton (1980).

[25] C. Cutler, T. A. Apostolatos, L. Bildsten, L. S. Finn, E. E. Flanagan, D. Kennefick, D. M. Markovic, A. Ori, E. Poisson, G. J. Sussman, K. S. Thorne, *The last three minutes: issues in gravitational-wave measurements of coalescing compact binaries*, *Phys. Rev. Lett.* **70**, 2984 (1993).

[26] C. Cutler, L. S. Finn, E. Poisson, G. J. Sussman, *Gravitational radiation from a particle in circular orbit around a black hole. II. Numerical results for the nonrotating case*, *Phys. Rev. D* **47**, 4, 1511 (1993).

[27] C. Cutler, D. Kennefick, E. Poisson, *Gravitational radiation reaction for bound motion around a Schwarzschild black hole.*, *Phys. Rev. D* **50**, 6, 3816 (1994).

[28] T. Damour, B. R. Iyer, B. S. Sathyaprakash, *Improved filters for gravitational waves from inspiralling compact binaries*, *Phys. Rev. D* **57**, 885 (1998).

[29] S.L.Detweiler, *Black holes and gravitational waves. I. Circular orbits about a rotating hole*, *Ap. J* **225**, 687 (1978).

[30] A. Duquennoy, M. Mayor, *Multiplicity among solar-type stars in the solar neighbourhood. II. Distribution of the orbital elements in an unbiased sample*, *Astron. Astrophys.* **248**, 485 (1991).

[31] V. Ferrari, M. D'Andrea, E. Berti, *Gravitational waves emitted by extrasolar planetary systems*, *Int. J. Mod. Phys. D***9**, n.5, 495 (2000).

[32] V. Ferrari, M. Germano, *Scattering of gravitational waves by Newtonian stars*, *Proc. R. Soc. London A* **444**, 389 (1994).

[33] V. Ferrari, L. Gualtieri, A. Borrelli, *Stellar pulsations excited by a scattered mass*, *Phys. Rev. D* **59**, 124020 (1999).

[34] V. Ferrari, K. D. Kokkotas, *Scattering of particles by neutron stars: time-evolution for axial perturbations*, *Phys. Rev. D* **62**, 107504 (2000).

[35] L. G. Fishbone, *The relativistic Roche problem. I. Equilibrium theory for a body in equatorial, circular orbit around a Kerr black hole*, *Ap. J.* **185**, 43 (1973).

[36] E. B. Ford, F. A. Rasio, A. Sills, *Structure and Evolution of Nearby Stars with Planets. I. Short-Period Systems*, *Ap. J.* **514**, 411 (1999).

[37] W. Gautschi, *Computational aspects of three-term recurrence relations*, *SIAM Rev.* **9**, 24 (1967).

[38] J. N. Goldberg, A. J. MacFarlane, E. T. Newman, F. Rohrlich, E. C. G. Sudarshan, *Spin-s spherical harmonics and ∂*, *J. Math. Phys.* **8**, 2155 (1967).

[39] L. P. Grishchuk, V. M. Lipunov, K. A. Postnov, M. E. Prokhorov, B. S. Sathyaprakash, *Gravitational wave astronomy: in anticipation of first sources to be detected*, *Phys. Usp.* **44**, 1 (2001); *Usp. Fiz. Nauk* **171**, 3 (2001).

[40] L.Gualtieri, E. Berti, J.A. Pons, G.Miniutti,V. Ferrari, *Gravitational signals emitted by a point mass orbiting a neutron star: a perturbative approach*, *Phys. Rev. D* **64**, 104007 (2001).

[41] T. Guillot, A. Burrows, W. B. Hubbard, J. I. Lunine, D. Saumon, *Giant planets at small orbital distances*, *Ap. J.* **459**, L35 (1996).

[42] R. A. Hulse, J. H. Taylor, *Discovery of a pulsar in a binary system*, *Ap. J.* **195**, L51 (1975).

[43] L. E. Kidder, C. M. Will, A. G. Wiseman, *Class. Quantum Grav.* **9**, L125 (1992); *Coalescing binary systems of compact objects to (post)$^{5/2}$-Newtonian order. III. Transition from inspiral to plunge*, Phys. Rev. D **47**, 3281 (1993).

[44] C. S. Kochanek, *Coalescing binary neutron stars*, *Ap. J.* **398**, 234 (1992).

[45] Y. Kojima, *Stellar resonant oscillations coupled to gravitational waves*, *Prog. Theor. Phys.* **77**, 297, (1987).

[46] K. D. Kokkotas, G. Schäfer, *Tidal and tidal-resonant effects in coalescing binaries*, *MNRAS*, **275**, 301 (1995).

[47] K.D. Kokkotas, B.F. Schutz, *W–modes: a new family of normal modes of pulsating relativistic stars*, *MNRAS*, **255**, 119 (1992).

[48] D. Lai, *Resonant tidal excitations of rotating neutron stars in coalescing binaries*, *MNRAS* **308**, 153 (1999).

[49] D. Lai, *Resonant oscillations and tidal heating in coalescing binary neutron stars*, *MNRAS* **270**, 611 (1994).

[50] K. R. Lang, *Astrophysical Data: Stars and Planets*, Springer-Verlag, New York (1992).

[51] U. Lee, *Acoustic oscillations of Jupiter*, *Ap. J.* **405**, 359 (1993).

[52] L. Lindblom, S. L. Detweiler, *The quadrupole oscillations of neutron stars, Ap. J. Suppl.* **53**, 73 (1983).

[53] D. R. Lorimer, *Binary and millisecond pulsars at th new millennium*, in *Living reviews in relativity*, `http://www.livingreviews.org/Articles/Volume4/2001-5lorimer` (2001).

[54] G. M. Marcy, P. Butler, S. Vogt, D. Fischer and J. Lissauer, *A Planetary Companion to a Nearby M4 Dwarf, Gliese 876*, *Ap. J.* **505**, L147 (1998).

[55] K. Martel, E. Poisson, *Gravitational waves from eccentric compact binaries: Reduction in signal-to-noise ratio due to nonoptimal signal processing*, *Phys. Rev. D* **60**, 124008.

[56] M. Mayor, D. Queloz, S. Udry, J. L. Halbwachs, in *Bioastronomy 96, Astronomical and Biochemical Origins and the Search for Life in the Universe*, ed. C. B. Cosmovici, S. Bowyer and D. Werthimer (1997).

[57] T. Mazeh, S. Zucker, *Comparison Between Extrasolar Planets and Low-Mass Secondaries*, in *Proceedings of IAU Symp. 2000, "Birth and Evolution of Binary Stars"*, astro-ph/0008087.

[58] E. D. Miner, *Uranus*, Wiley (1998).

[59] T. Nakamura, K. Oohara, Y. Kojima, *General relativistic collapse to black holes and gravitational waves from black holes*, *Prog. Theor. Phys. Suppl.* **90**, 1 (1987).

[60] H. P. Nollert, *Quasinormal modes of Schwarzschild black holes: The determination of quasinormal frequencies with very large imaginary parts*, *Phys. Rev. D* **47**, 5253 (1993).

[61] K. Oohara, T.Nakamura, *Prog. Theor. Phys. Suppl.* **136** , 270, (1999); M. Ruffert, H.T. Janka, *Prog. Theor. Phys. Suppl.* **136** , 287, (1999) ; F.A. Rasio, S.L. Shapiro, *Class. Quant. Grav.* **16**, 1, (1999); T.W. Baumgarte, S.A. Hughes, S.L. Shapiro, *Phys. Rev. D* **60**, 87501, (1999); M. Shibata, T.W. Baumgarte, S.L. Shapiro, *Ap. J.* **542**, 453, (2000); K. Uryu, M. Shibata, Y. Eriguchi, *Phys. Rev. D* **62**, 104015, (2000); J.A. Faber, F.A. Rasio, J.B. Manor, *Phys. Rev. D* **63**, 044012, (2001).

[62] V.R. Pandharipande, *Dense neutron matter with realistic interactions*, *Nucl. Phys.* **A174**, 641 (1971).

[63] V.R. Pandharipande, R.A. Smith, *Nuclear matter calculations with mean scalar fields*, *Phys. Lett.* **59B**, n. 1, 15 (1975).

[64] M. A. C. Perryman, *Extra-Solar Planets*, *Inst. of Physics*, *Report on Progress in Physics* (2000).

[65] P. C. Peters, J. Mathews, *Gravitational radiation from point masses in a Keplerian orbit*, *Phys. Rev.* **131**, 435 (1963).

[66] E. Poisson, *Gravitational radiation from a particle in circular orbit around a black hole. I. Analytical results for the nonrotating case*, *Phys. Rev. D* **47**, 4, 1497 (1993).

[67] E. Poisson, *Gravitational radiation from a particle in circular orbit around a black hole. VI. Accuracy of the Post-Newtonian expansion*, *Phys. Rev. D* **52**, 10, 5719 (1995). See also the Erratum and Addendum in *Phys. Rev. D* **55**, 12, 7980 (1997).

[68] J. A. Pons, F. M. Walter, J. M. Lattimer, M. Prakash, R. Neuhauser, P. An, *Towards a mass and radius determination of the nearby isolated neutron star RXJ185635-3754.*, astro-ph/0107404, *Ap. J.* in press (2001).

[69] W. H. Press, S. A. Teukolsky, *On formation of close binaries by two-body tidal capture*, *Ap. J.* **213**, 183 (1977).

[70] W. H. Press, S. A. Teukolsky, W. T. Vetterling, B. P. Flannery, *Numerical Recipes*, Cambridge University Press, Cambridge, England (1992).

[71] T. Regge, J. A. Wheeler, *Stability of a Schwarzschild singularity*, *Phys. Rev.* **108**, 1063 (1957).

[72] A. Reisenegger, P. Goldreich, *Excitation of neutron star normal modes during binary inspiral*, *Ap. J.* **395**, 240 (1992).

[73] J. Ruoff, P. Laguna, J. Pullin, *Excitation of neutron star oscillations by an orbiting particle*, *Phys. Rev. D* **63**, 064019 (2001).

[74] M. Sasaki, T. Nakamura, *The Regge-Wheeler equation with sources for both even and odd parity perturbations of the Schwarzschild geometry*, *Phys. Lett.* **87A**, 85 (1981).

[75] D. Saumon, W.B. Hubbard, A. Burrows, T. Guillot, J.I. Lunine and G. Chabrier, *A theory of extrasolar giant planets*, *Ap. J.* **460**, 993 (1996).

[76] J. Schneider, *Extrasolar Planets Catalog*, `http://www.obspm.fr/encycl/catalog`.

[77] B. F. Schutz, *A first course in general relativity*, Cambridge University Press (1985).

[78] T. Tanaka, H. Tagoshi, M. Sasaki, *Gravitational Waves by a Particle in Circular Orbits around a Schwarzschild black hole -5.5 Post-Newtonian Formula-*, *Prog.Theor.Phys.* **96**, 1087 (1996).

[79] T. Tanaka, H. Tagoshi, M. Sasaki, *Black Hole Perturbation*, in *Prog.Theor.Phys.Suppl.* **128**, 1 (1997).

[80] T. Tanaka, M. Shibata, M. Sasaki, H. Tagoshi, T. Nakamura, *Gravitational wave induced by a particle orbiting around a Schwarzschild black hole*, *Progr. Theor. Phys.* **90**, 1, 65 (1993).

[81] J. H. Taylor, J. M. Weisberg, *A new test of general relativity: gravitational radiation and the binary pulsar PSR1913+16*, *Ap. J.* **253**, 908 (1982).

[82] C. Terquem, J. C. B. Papaloizou, R. P. Nelson and D. N. C. Lin, *On the tidal interaction of a solar-type star with an orbiting companion: excitation of g-mode oscillation and orbital evolution*, *Ap.J.* **502**, 788 (1998).

[83] S.A.Teukolsky, *Perturbations of a rotating black hole. I. Fundamental equations for gravitational, electromagnetic and neutrino-field perturbations*, *Ap. J.*, **185**, 635 (1973).

[84] K. S. Thorne, in *300 Years of Gravitation*, ed. S. Hawking and W. Israel, Cambridge University Press, Cambridge (1987).

[85] K. S. Thorne, A. Campolattaro, *Non-Radial Pulsation of General-Relativistic Stellar Models. I. Analytic Analysis for* $\ell \geq 2$, *Ap. J.* **149**, n. 3, 591 (1967).

[86] S. E. Thorsett and D. Chakrabarty, *Neutron star mass measurements. I. Radio pulsars*, *Ap. J.* **512**, 288 (1999).

[87] K. Uryu, M. Shibata, Y. Eriguchi, *Properties of general relativistic, irrotational binary neutron stars in close quasiequilibrium orbits: Polytropic equations of state*, *Phys. Rev. D* **62**, 104015.

[88] Wiringa R.B., Fiks V., Fabrocini A., *Equation of state for dense nucleon matter*, *Phys. Rev. C* **32**, 1057 (1988).

[89] A. Wolsczan and D. A. Frail, *A planetary system around the millisecond pulsar PSR1257+12*, *Nature*, **355**, 145 (1992).

[90] F. J. Zerilli, *Gravitational field of a particle falling in a Schwarzschild geometry analyzed in tensor harmonics*, *Phys. Rev. D* **2**, 2141 (1970).

[91] F. J. Zerilli, *Effective potential for even-parity Regge-Wheeler gravitational perturbation equations*, *Phys. Rev. Lett.* **24**, 737 (1970).

[92] `http://obswww.unige.ch/ udry/planet/hd75289.html`